Neurotransmitter receptors

in mouse models of Alzheimer's disease

Dissertation

zur

Erlangung des Doktorgrades (Dr.rer.nat.)

der

Mathematisch-Naturwissenschaftlichen Fakultät

der

Rheinischen Friedrich-Wilhelms-Universität Bonn

vorgelegt von

Elena von Staden

aus Münster

Bonn, Januar 2014

Angefertigt mit Genehmigung der Mathematisch-Naturwissenschaftlichen Fakultät der Rheinischen Friedrich-Wilhelms-Universität Bonn

1. Gutachter: Prof. Dr. Karl Zilles

2. Gutachter: Prof. Dr. Gerhard von der Emde

Tag der Promotion:
15. 05. 2014

Erscheinungsjahr:
2014

Für meine Mutter und Großmutter

Table of content

Abbreviations

Aβ	β-amyloid
AD	Alzheimer's disease
AICD	APP-intracellular domain
α2M	α2-macroglobulin
AMPA	α-amino-3-hydroxy-5-methyl-4-isoxazolepropionic acid
ANOVA	analysis of variance
APP	amyloid precursor protein
apoE	apolipoprotein E
tgArcAβ mice	mice that overexpress APP containing the Swedish, Florida and London mutation and PS1 containing M146L and L286V mutations
BZ	benzodiazepine
CaMKII	Ca(2+)/calmodulin-dependent protein kinase II
cAMP	cyclic adenosine monophosphate
CCD	charge-coupled device
ChAT	acetyltransferase
CNS	central nervous system
CPu	caudatus-putamen (striatum)
αCTF	C-terminal fragment of APP
ER	endoplasmic reticulum
FAD	familiar AD
tg5xFAD mice	mice that overexpress APP containing the Swedish, Florida and London mutation and PS1 containing two FAD mutations
tg5xFAD/LRP1 mice	mice that overexpress APP containing the Swedish, Florida and London mutation and PS1 containing M146L and L286V mutations
GABA	γ-amino butyric acid
hil	hilus fasciae dentatae
LC	locus coeruleus
LRP1	low density lipoprotein receptor-related protein 1

LRP1 mice	LRP1 knockout mice
LTP	long-term potentiation
M1	motor cortex
MBN	basalis magnocellularis
mf	mossy fiber
mRNA	messenger ribonucleic acid
NMDA	N-methyl-D-aspartate
NMDAR	N-methyl-D-aspartate receptor
OB	olfactory bulb
P3	cleavage product of APP
PET	positron emission tomography
Pir	piriform cortex
PS	presenilin
ROI	region of interest
RT	room temperature
S1	somatosensory cortex
SA	specific activity
SD	standard deviation
MGr	stratum moleculare/granulosum
WT	wild type
5-HT	serotonin

I. Introduction

1 Alzheimer's disease

Alzheimer's disease (AD) is most common form of dementia (Selkoe, 2001a). It was first described by the psychiatrist and neuropathologist Alois Alzheimer (1864-1915), who observed the symptoms of memory disorder in Auguste Deter in 1901. After her death in 1906, he examined her brain and found amyloid plaques and loss of neurons

The disease occurs in a common sporadic and a familiar form (FAD). Both forms show a very similar clinical and pathological picture. Most patients developing sporadic AD are 65 years or older and have no family record of AD. For this reason, it is also called late-onset AD. Patients suffering from FAD are commonly much younger (early-onset AD) and show mutations on the *APP*-, *PS1*- and *PS2*-gene. Neither the cause nor the pathogenesis have been understood completely till today, although several risk factors have been described, such as age, trisomy 21, stress and genetic predisposition. Such a possible genetic risk factor for sporadic AD is the apolipoprotein E4 (apoE-ε4) (Corder et al., 1993), a component of lipoproteins which plays an important role in the lipoprotein metabolism (Andersen and Willnow, 2006). Since the pathological and clinical picture is very similar in both forms, there are good chances that the analysis of genetic components may help to understand the sporadic form as well.

Being mostly a disease of older age and having a continuing exponential increase in the aged population worldwide (Hynd et al., 2004), the number of persons affected by this disease is rising. Nursing and medical care cause immense costs, and AD is among the most expensive diseases. Therefore, without effective therapy, AD will present significant social, ethical and socio-economic demands in the years to come.

2 Pathological condition

AD is characterized by cortical atrophy, neuron and synapse loss, neuritic plaques (chapter 4.1), and neurofibrillary tangles (Terry et al., 1991; Twamley et al., 2006) which consist mainly of the protein tau. Especially the cholinergic neurons in the cortex and hippocampus

are affected (Price et al., 1998). The neuropathological changes of AD start well before the disease becomes clinically apparent (Braak and Braak, 1991). The brain may initially compensate for such changes until cognitive decline becomes obvious.

AD frequently takes a typical clinical course which reflects the underlying expanding neuropathology (Förstl and Kurz, 1999). The disease course is divided into four phases, the pre-dementia, the mild dementia, the moderate dementia and the severe dementia stage. From the diagnosis till death it takes five to eight years generally (Bracco et al., 1994).

In the beginning, patients show non-specific symptoms as learning disability, headache and reduced short term memory. Later on the long term memory gets affected as well. As the disease progresses, speech and cognitive performance as well as spatial and temporal orientation are impaired. During this process, changes in mood can occur, often accompanied by depression and anxiety. Motor symptoms are rigidity, taking very small steps and stereotypical movements.

3 APP and the generation of plaques

3.1 Plaques

Plaques mainly consist of a peptide with the size of 4 kDa, the so called β-amyloid (Aβ) (Glenner and Wong, 1984), which is generated by proteolytic cleavage of the amyloid precursor protein (APP). Additional plaque components are for example laminin, glycosaminoglycans and apolipoproteins. The generation of plaques occurs in the extracellular space.

One can discriminate between two forms of plaques, namely diffuse and senile plaques. Senile plaques are largely observed in the gray matter of the brain and have a core of β-amyloid. They are surrounded by dystrophic neurites. Reactive astrocytes and microglia can be observed. In contrast to senile plaques, diffuse plaques also consist of Aβ but do not possess a core. Furthermore, there are no or only few neuritic alterations visible. Diffuse plaques represent the earliest visible structural change and can be observed in older people without dementia as well (Price and Morris, 1999).

3.2 Amyloid Precursor Protein (APP)

APP is an ubiquitously expressed integral membrane protein (Wolfe and Guenette, 2007), which exists in multiple isoforms due to alternative splicing (Sandbrink et al., 1994; Selkoe, 1994). The most common transcripts are APP695, APP751 and APP770, with APP695 being the predominant form in neuronal tissue (Ling et al., 2003). APP is coded by a gene of 19 exons, which in humans is located on chromosome 21 and has a length of 400kb (Goldgaber et al., 1987; Kang et al., 1987; Lamb et al., 1993). The protein itself is made of a large extramembranous N-terminal region, a single transmembrane domain and a small cytoplasmic C-terminal tail (Kang et al., 1987). During its processing, it is trafficking through the endocytic pathway (4.2.3), thereby taking two possible pathways, the non-amyloidogenic and the amyloidogenic way.

3.2.1 Non-amyloidogenic pathway

A large number of newly synthesized APP molecules are processed at the cell surface by α-secretase (Lee et al., 2008), a member of the ADAM (*A disintegrin and metalloprotease*) family. Because α-secretase cleaves within the Aβ sequence between the amino acid 16 and 17 (Anderson et al., 1991; Sisodia, 1992), it prevents generation of Aβ (Figure 1). This step results in the soluble N-terminal APP fragment sAPPα (100-120 kDa) and the C-terminal fragment αCTF (10 kDa), the latter one still remaining anchored in the membrane (Weidemann et al., 1989). sAPPα is released in the extracellular space (Racchi and Govoni, 2003). There is growing evidence that sAPP is involved in many physiological processes, such as neuroprotection, neurite outgrowth, the modulation of ion channels and synaptic plasticity and neurogenesis (Mattson et al., 1993; Furukawa et al., 1996; Mattson and Furukawa, 1998; Caille et al., 2004; Ring et al., 2007; Gakhar-Koppole et al., 2008; Taylor et al., 2008). In early endosomes and the plasma membrane the αCTF fragment is cleaved within the transmembrane domain by γ-secretase (Kaether et al., 2006). The γ-secretase is a protease complex consisting of the transmembrane proteins presenilin 1 (PS1) or presenilin 2 (PS2), as well as nicastrin, Aph-1 (anterior pharynx-defective 1) and Pen-2 (presenilin enhancer 2) as accessory proteins. PS1 or PS2 are the catalytic subunits (Kimberly et al.,

2003). Hereby the peptide P3 and the APP-intracellular domain (AICD, 6 kDa) are generated (Haass and Selkoe, 1993; Kimberly et al., 2003) (Figure 1).

3.2.2 Amyloidogenic pathway

Not all APP molecules are processed at the cell surface. Part of APP is internalized from the plasma membrane and delivered to the endocytic compartments. Here, they are processed by a β-secretase, also referred to as BACE1, β-site APP-cleaving enzyme 1 (Kinoshita et al., 2003), which cleaves the extracellular domain at the N-terminus of the Aβ sequence. This leads to the soluble sAPPβ and the C-terminal fragment βCTF (C99, 12 kDa), which is attached to the membrane. The latter one gets cleaved in the transmembrane domain by γ-secretase, forming Aβ peptides of different lengths (39-43 amino acids) as well as the APP intracellular domain AICD (LaFerla et al., 2007) (Figure 1). Aβ is released in the extracellular space (Haass et al., 1993; Haass and Selkoe, 1993). The most important forms of Aβ in AD are considered Aβ40 and Aβ42.

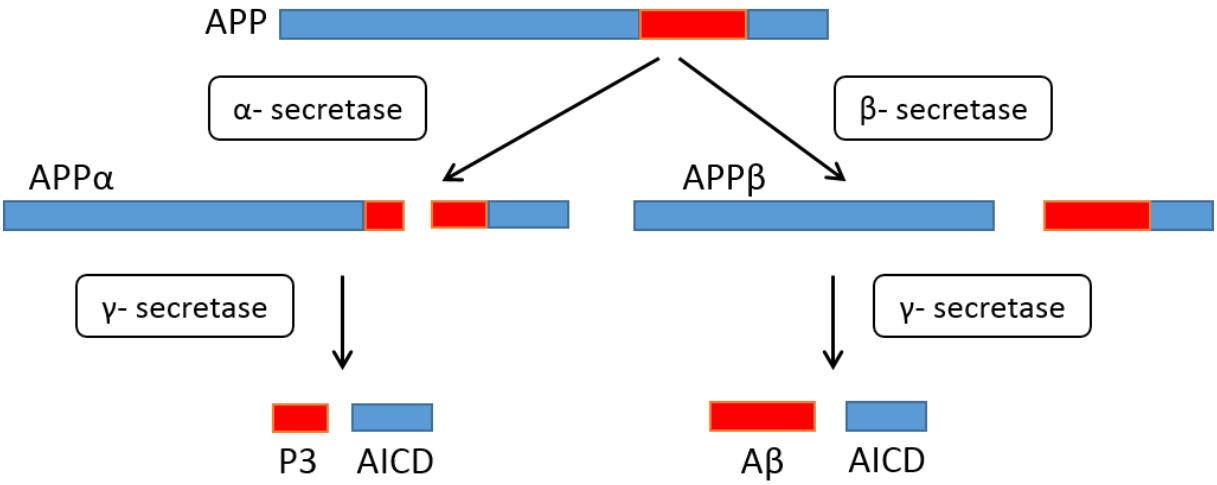

Figure 1: Proteolytic cleavage of APP, demonstrating both possible pathways. Taking the non-amyloidogenic pathway, APP is processed by α-secretase, cleaving within the Aβ sequence. This pathway results in the fragments sAPPα, P3 and AICD. Taking the amyloidogenic pathway, APP is processed by β-secretase, leading to APPβ, AICD and Aβ, which accumulates to plaques.

3.2.3 Endocytic transport of APP

APP is synthesized in the rough endoplasmic reticulum (ER) and delivered to the cell membrane using the secretory pathway (Haass and Selkoe, 1993). Alternatively it may also be transported to an endosomal compartment (Haass et al., 2012). During its transit through the Golgi apparatus, major posttranslational modifications such as glycosylation, phosphorylation and sulfation take place (Rajendran and Annaert, 2012). At the cell membrane, APP can be processed directly by α- and γ-secretase, as outlined above. The part of APP which is not processed by α-secretase is reinternalized into endosomal compartments (Haass et al., 2012). Thereby, the low density lipoprotein receptor-related protein 1 (LRP1) plays an important role. LRP1 belongs to the LDL receptor gene family (Herz and Strickland, 2001) and is expressed in all neurons in the brain (Herz and Strickland, 2001; Ling et al., 2003). It interacts with APP at the cell membrane and in the Golgi apparatus and therefore enhances the endocytosis and modifies its metabolism. LRP1 seems to interact with all secretases, too, thus manipulating the access of APP to proteolytic cleavage. Furthermore, it mediates the clearance of Aβ, either alone or in complexes of Aβ with apoE (Andersen and Willnow, 2006; Cam and Bu, 2006) as well as the transport of Aβ across the blood-brain barrier (Shibata et al., 2000; Deane et al., 2004). Cleavage by β-secretases occurs in the early and late endosomes. γ-secretases activity is present in endosomes and at the cell surface (O'Brien and Wong, 2011) (Figure 2).

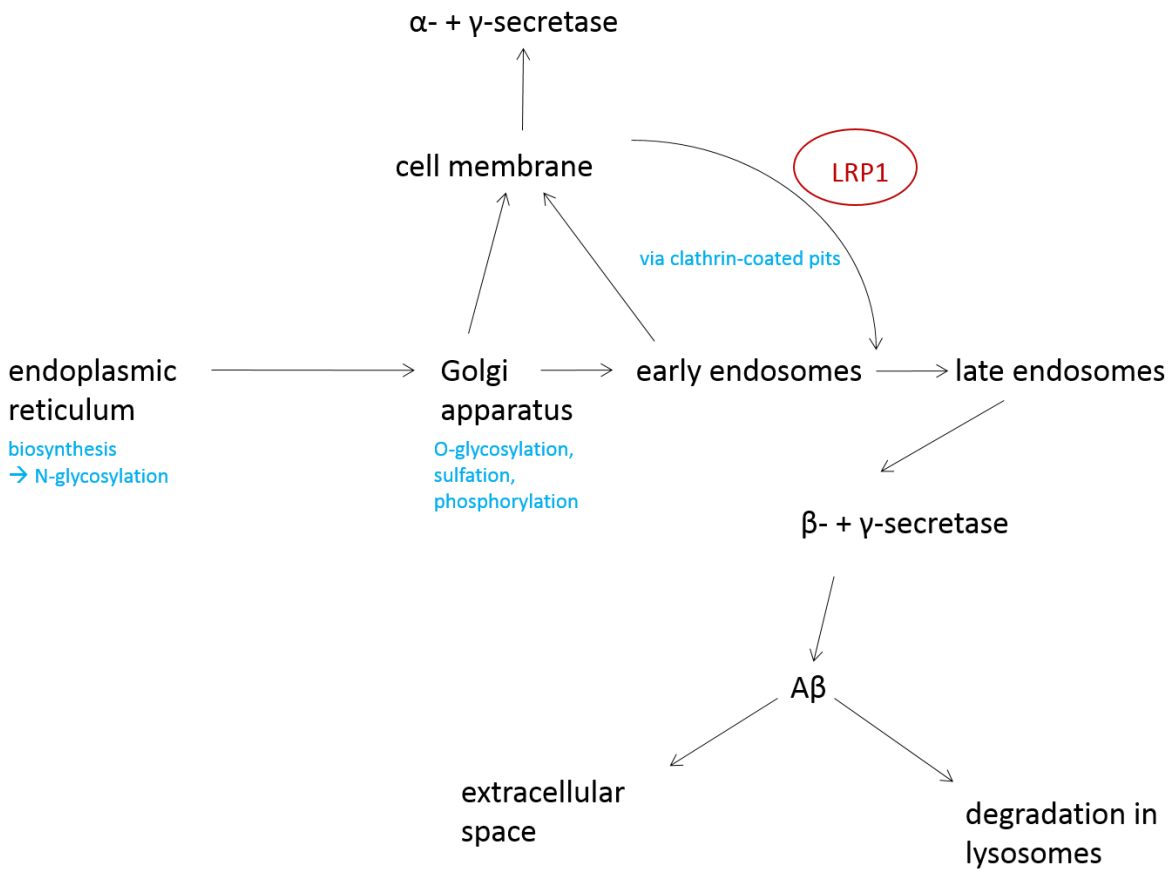

Figure 2: Schematic overview of the endocytic trafficking of APP. It is synthesized and modified in the ER, further modifications take place in the Golgi apparatus. Parts of APP molecules are transported to the plasma membrane, followed by cleavage by α- and γ-secretases. Unprocessed molecules are internalized and processed by β- and γ-secretases in endosomal compartments.

3.2.4 Neurotoxicity of Aβ

For the pathogenic effect, the ratio between Aβ40 and Aβ42 seems to play an important role. Aβ42 is hydrophobic and therefore aggregates faster than Aβ40. Due to this, it forms stable Aβ oligomers at an early stage of AD (Burdick et al., 1992; Bitan et al., 2003; Chen and Glabe, 2006) and tends to generate stable trimeric and tetrameric oligomers (Chen and Glabe, 2006; Haass and Selkoe, 2007). Especially oligomers seem to disturb learning (Cleary et al., 2005). The resulting oligomers and fibrils are a possible cause of the neurotoxic effect (Haass and Selkoe, 2007).

There are several theories concerning the neurotoxic effect of Aβ. One of them is the amyloid cascade hypothesis. According to this theory increased generation of Aβ leads to more insoluble Aβ and therefore more plaques are formed. These plaques are the cause for

neurodegeneration in the brain and symptoms like neurofibrillary tangles and degeneration of neurons are the consequence of plaque generation (Hardy and Selkoe, 2002). Reasons for an increased level of plaques may be changes in the processing of APP or a shift in Aβ40/Aβ42 ratio. During transition from the soluble to insoluble form Aβ undergoes a conformational change from α-helix to β- sheet (Zagorski and Barrow, 1992). This transformation starts from the carboxyterminal end, therefore Aβ with an extended C-terminal end accumulates faster than those with a truncated C-terminal end (Jarrett et al., 1993b, a). Furthermore, Aβ42 is more resistant to degeneration (Selkoe, 1999; Glabe, 2001). As Aβ42 is found in diffuse plaques, it is assumed that Aβ40 and fibril Aβ42 are enclaved in diffuse plaques, which causes senile plaques (Selkoe, 2001b). The amyloid cascade theory is supported by the fact that mutations in the *tau* gene alone cause no condition comparable to AD (Hardy et al., 1998). However, there are some arguments against the amyloid cascade hypothesis. The most important point is the weak correlation of plaques and early cognitive decline (Terry et al., 1991; McLean et al., 1999). Furthermore, in brains of some elderly people without AD, diffuse plaques can be observed (Price and Morris, 1999). These plaques have no associated neuritic alterations and do not seem to be toxic (Selkoe, 1996). Taken together, these facts indicate that plaques play an important role in the generation of AD, but are not the exclusive cause.

Alternatively soluble Aβ42 oligomers are discussed as the primary cause of AD (Lambert et al., 1998; Selkoe, 2002). Recent studies have shown impairment of the cognitive function provoked by Aβ oligomers (Walsh et al., 2002; Cleary et al., 2005; Shankar et al., 2008). Furthermore, they are able to bind at the surface of synapses and dendrites which can lead to synaptic dysfunction (Lacor et al., 2004). Since they can be generated with only few monomers, formation of oligomers is an early event in the course of the disease.

There is also increasing evidence that Aβ, besides the formation of plaque deposition, accumulates intracellularly which is initially involved in AD (Wirths et al., 2004). Recent studies have shown that Aβ exists not only as insoluble extracellular plaques, but also intracellularly as soluble oligomers. One theory is that Aβ monomers and oligomers first accumulate intracellularly and are secreted afterwards in the extracellular space. There, oligomers can further aggregate into plaques (LaFerla et al., 2007). Due to this theory, accumulation of intracellular Aβ could be a cause of AD. It occurs earlier than the generation of extracellular plaques and correlates well with the appearance of cognitive decline in

patients (McLean et al., 1999) and mouse models (Oddo et al., 2003). The toxic effect of Aβ is summarized in Figure 3.

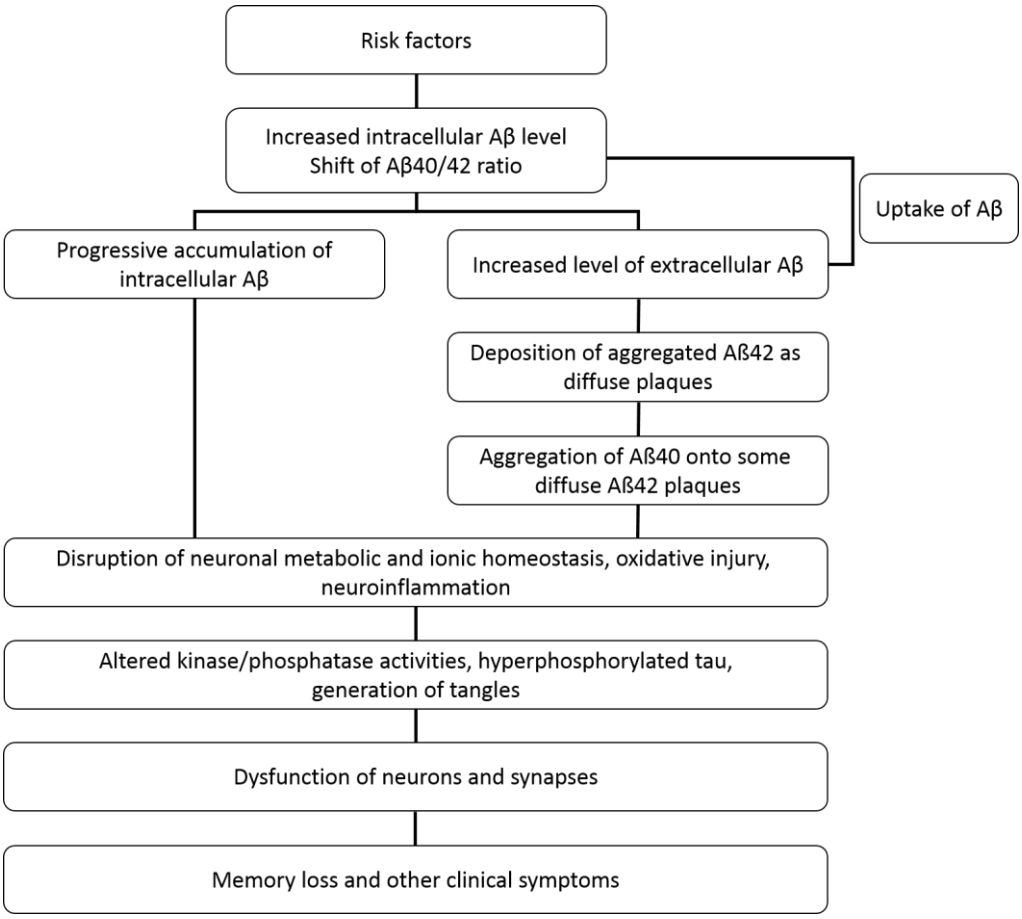

Figure 3: Simplified schematic overview of the toxic effect of Aβ. Due to risk factors, intracellular levels of Aβ increase and/or ratio of Aβ40/42 shifts, leading to accumulation of intracellular Aβ. In parallel, extracellular Aβ deposition increases, thus forming extracellular plaques. Uptake of Aβ increases the intracellular level of Aβ, thereby increasing the neurotoxic effects.

4 Genetics of AD

As mentioned before, AD is subdivided in sporadic AD and FAD. FAD is an autosomal dominant inherited variant. For most of the cases of FAD, the genes responsible for the disease have been identified. The ones which are known to be important in the etiology of FAD are the APP gene on chromosome 21 (Goate et al., 1991), the presenilin 1 (PS1) gene on chromosome 14 (Sherrington et al., 1996) and the presenilin 2 (PS2) gene on chromosome 1 (Levy-Lahad et al., 1995). All mutations linked to FAD known so far lead to a higher secretion of all forms of Aβ or to a specific raise of Aβ42 (Citron et al., 1992; Cai et al., 1993; Suzuki et

al., 1994; Tamaoka et al., 1994; Borchelt et al., 1996; Duff et al., 1996; Scheuner et al., 1996; Citron et al., 1997; Haass and Steiner, 2002). In PS1, more than 100 mutations, spread throughout the molecule, are known. All of these mutations lead to an increased ratio of Aβ42 to Aβ40, increased plaque deposition and early age of onset (Berezovska et al., 2005).
The generation of Aβ also occurs in persons without cognitive impairment. Here, Aβ can be found in the cerebrospinal fluid (Seubert et al., 1992). It is also found in the supernatant of mixed-brain cell culture and human kidney 293 cells transfected with APP (Haass et al., 1992; Seubert et al., 1992). All processing products seem to play a physiological role. Under normal conditions, intracellular Aβ is efficiently secreted. But certain mutations, like the Artic and Swedish mutation of APP, cause an enhancement of the intracellular retention (Rajendran et al., 2007). All these alterations cause impaired Aβ processing, leading to increased plaque deposition. The consequence is an early onset of the disease, usually between 50 and 65 years of age, though it can occur much earlier.

5 Mouse models

For this study, well established mouse models of AD were used. The mouse models displayed some neuropathological and behavioral features of AD, such as enhanced levels of Aβ or plaque deposition and cognitive impairment. However, no model did reflect the disease completely, since they generate no tau tangles and in *tgArcAβ* mice no neurodegeneration occurs. However, animal models mirror some aspects of the pathology, therefore, they prove to be a useful tool to investigate the pathogenesis of AD.

5.1 TgArcAβ

The transgenic (tg) *ArcAβ* mouse model overexpresses human APP with the Swedish and the Arctic mutation combined in a single construct (Knobloch et al., 2007). The Swedish mutation is a double mutation, which is located right before the N-terminus of the Aβ domain of APP. Lysine is substituted to asparagine at codon 670 and methionine to leucine at codon 671 (K670N, M671L) (Mullan et al., 1992). This causes a three to six times increase in the production of total Aβ (Citron et al., 1992; Cai et al., 1993; Oakley et al., 2006).

Furthermore, P3 is decreased by several times in the supernatant of cultured cells (Citron et al., 1992). The Arctic mutation is located at codon 693 within the Aβ region of APP, where glutamic acid is replaced by glycine (E693G) (Nilsberth et al., 2001). This mutation causes reduced extracellular Aβ levels (Nilsberth et al., 2001). Aβarc40 has been shown to aggregate faster than wild type Aβ40 (Murakami et al., 2002) and to form soluble protofibrils more rapidly (Nilsberth et al., 2001). The same holds true for Aβarc42 (Johansson et al., 2006).

The *tgArcAβ* model shows age-dependent increases in Aβ levels in neuronal tissues and develops strong intraneuronal Aβ aggregation at three months of age, prior to extracellular plaque formation (Lord et al., 2006). The maximum of intracellular deposits attains between 7 and 15 months (Knobloch et al., 2007). Plaque deposition starts around 7 months of age, with a dramatic increase between 9 and 15 months. Memory is impaired from the age of 6 months on (Knobloch et al., 2007).

5.2 Tg5xFAD

Tg5xFAD is a transgenic mouse line that co-overexpresses human APP695 harboring the Swedish, Florida and London mutation in the same APP molecule and human PS1 containing two FAD mutations (M146L and L286V). The Swedish mutation was described above (chapter 5.1).

In the Florida mutation isoleucine is changed to valine at codon 716. This mutation causes about a 2-fold increase in the ratio of Aβ42 to Aβ40 (Eckman et al., 1997). The London mutation causes an amino-acid substitution as well. At codon 717, valine is changed to isoleucine. This takes place within the transmembrane domain, two residues apart from the carboxy terminus of the β-amyloid peptide (Goate et al., 1991).

Previous studies have suggested that mutations which elevate the Aβ42 level, act in an additive manner to increase Aβ42 generation when integrated within the same molecule (Oakley et al., 2006). In the *tg5xFAD* mouse model, the combination of the London and the Florida mutation within APP doubled Aβ42 production when compared to each mutation alone (Oakley et al., 2006). The same is true for the two PS1 mutations when introduced together into the PS1 gene (Citron et al., 1998). Moreover, the combination of mutations in APP and PS1 also add to each other to increase the Aβ42 generation (Citron et al., 1998).

Due to this effect, *tg5xFAD* mice show a very high level of Aβ42 and develop cerebral amyloid plaques and gliosis at the age of two months. Furthermore, synaptic markers are reduced and neuron loss as well as memory impairment in the Y-maze can be observed (Oakley et al., 2006).

5.3 LRP1 knockout mice

The low density lipoprotein receptor related protein (LRP1) is highly expressed in neurons of the central nervous system (CNS) (Bu et al., 1994; Andersen and Willnow, 2006).

An essential component of neuronal membrane is cholesterol, therefore having a great importance for synaptic integrity and neuronal function (Liu et al., 2010). Efficacy of synapses requires interaction of cholesterol with apolipoprotein (apoE) and its receptors (Mauch et al., 2001), thus, depletion of cholesterol/sphingolipid causes gradual loss of synapses and dendritic spines (Hering et al., 2003; Liu et al., 2010). Cholesterol and other lipids are transported to neurons via apoE receptors. The presence of the ε4 allele apoE gene has been identified as a strong risk factor for sporadic AD (Corder et al., 1993). It is likely, that apoE4 promotes Aβ fibrillogenesis and amyloid plaque formation (Liu et al., 2007).

Another risk factor found for sporadic AD is α2-macroglobulin (α2M), a plasma protein which is part of the innate immune system (Blacker et al., 1998). Besides the ability to bind APP, Aβ and secretases, as described in chapter 3.2.3, LRP1 interacts with both apoE and α2M.

Moreover, LRP1 mediates the clearance of Aβ, which for example involves cellular uptake and degradation and clearance through the blood brain barrier (Bu, 2009; Kanekiyo et al., 2011). Furthermore, γ-secretases-dependent APP processing seems to be involved in the regulation of brain cholesterol via transcriptional repression of LRP1 (Liu et al., 2007; Bu, 2009). Increasing evidence point towards a role of abnormal cholesterol metabolism in AD, such as reduced level of cholesterol and LRP1 in the brain of AD patients (Kang et al., 2000; Vance et al., 2006).

Since LRP1 full knockout mice (*LRP1* mice) are embryonic lethal, neuronal conditional *LRP1 knockout* mice were used. Initially, they have the same size and weight compared to wt mice, but fall behind in their growth rate eventually. *LRP1* mice show increased voluntary movement and a constant muscle tremor. At the age of 18 months, *LRP1* mice traveled longer distances compared to control animal, indicating hyperactivity in *LRP1* mice.

Furthermore, behavioral test showed memory impairment at 24 months of age as well as LTP deficiency measured in slices (Liu et al., 2010).

6 Aims of the study

In this work, the density and distribution of neurotransmitter receptor binding sites was analyzed in four mouse models of AD using quantitative receptor autoradiography in unfixed frozen brain tissue (Zilles et al., 2002b; Zilles et al., 2004). Since receptors interact with each other, alterations of a single receptor often affect other receptors as well. For that reason, 17 to 19 different receptors, relevant for seven different neurotransmitter systems, were investigated in eight brain regions.

The aim of the present study is the characterization of the neurotransmitter receptor expression in the brain of four mouse models of AD. Two models (*tgArcAβ, tg5xFAD*) reflect mutations associated with FAD. These models express enhanced levels of Aβ, a crucial hallmark of AD. LRP1 knockout mice are analyzed, which show a reduced clearance of Aβ and an impaired cholesterol metabolism as a possible risk factors of AD. Finally, the density and distribution of receptors are investigated in a mouse model (*tg5xFAD/LRP1*), which combines both factors, enhanced Aβ levels and LRP1 knockout. The correlation between alterations of receptor and neuropathological changes (i.e., presence of Aβ and plaque deposition) in AD will be discussed.

II. Material and Methods

1 Animals

All animals were kept under standard conditions with free access to food and water. The experiments were carried out according to the German animal welfare guidelines and approved by the responsible government agency (Landesamt für Natur, Umwelt und Verbraucherschutz). All mice used were adult males.

Transgene ArcAβ (*tgArcAβ*) and the corresponding control mice (C57Bl/6) were kindly provided by Dr. Jan Deussing, Molecular Neurogenetics, Max Planck Institute of Psychiatry, Munich. Their age was 8 months.

Transgene 5xFAD (*tg5xFAD*), LRP1 knock out (*LRP1* mice) and *tg5xFAD/ LRP1* as well as corresponding control mice (129xBl/6) were kindly provided by the group of Prof. Dr. Thomas Willnow, Molecular Physiology, Max Delbrück Center for Molecular Medicine (MDC). *LRP1, tg5xFAD* and *tg5xFAD/LRP1* mice were between 4 and 6 months old.

Mice were anesthetized with CO_2 and sacrificed by decapitation. Brains were removed from the skull and frozen in isopentane at -50°C for 2 minutes. For storage, brains were packed in plastic bags and kept at -80°C.

2 Preparations of slices

2.1 Receptor autoradiography and histological staining

Brains were kept for 30 minutes at -15°C in the cryostat microtome (Leica Instruments GmbH, Germany), and fixed for sectioning using a tissue freezing medium (Tissue Tec, Jung). Coronal serial sections were prepared at -15°C. In case of the *tgArcAβ* mice, 20μm slices were thaw-mounted on pre-cooled gelatin-coated glass slides. The sections of *LRP1*, *tg5xFAD* and *tg5xFAD/LRP1* mice were 10μm thick and thaw-mounted on pre-cooled silanized glass slides. Sections were dried on a heating plate at 37°C for 20 minutes, packed in freezer bags, vacuum sealed and stored at -80°C.

2.2 Immunohistochemistry

Preparation of sections for immunohistochemistry was done according to the same protocol as described in chapter 2.1. Sections were shortly thawed and stored in plastic boxes at -15°C during preparation, immersion-fixed in 4% ($^{w}/_{v}$) paraformaldehyde for 10 minutes, dried at room temperature for 10 minutes, vacuum sealed and stored at -80°C.

3 Receptor autoradiography

3.1 Binding experiments

One hour before binding experiments started, sections were defrosted on a heating plate at 37°C.

Receptor labeling using autoradiography was carried out according to previously described standardized protocols (Zilles et al., 2002; Palomero-Gallagher et al., 2003). Each protocol consists of three steps, pre-washing, main incubation and rinsing. During the first step, the sections are incubated in the respective buffer, to rehydrate the slices, to wash out endogenous ligands and to adapt pH value.

In a second step (main incubation), sections were incubated either in a buffer solution containing a [^{3}H]-labeled ligand in nM concentrations (total binding), or a [^{3}H]-ligand together with μM concentrations of a respective non-radioactive displacer (non-specific binding). Concentrations of the respective radioactive ligand in buffer solution were measured by three-fold liquid scintillation. The specific binding is the difference between total binding and non-specific binding, identified in alternating sections. In general, the non-specific binding was lower than 10%. Therefore, the total binding is a good measure of the specific binding.

The third step (rinsing in water) terminated the incubation, and eliminated the non-bound ligands and buffer salts. The specific protocols of each binding experiment are listed in Table 1.

The sections were air-dried under a cold-air fan and stored on wooden tables at room temperature.

Table 1: Summary of the used [^{3}H]-ligands with corresponding displacer and incubation buffer

Receptor/ [^{3}H]-ligand	**Displacer**	**Incubation buffer**	**Preincubation**	**Main incubation**	**Rinsing**
AMPA/ AMPA [10nM] *only tgArcAβ*	Quisqualate [10µM]	50mM Tris-acetate [pH 7.2] + 100mM KSCN*	3 x 10min, 4°C	45min, 4°C	4 x 4sec, 4°C 2 x2 sec in 2.5% glutaraldehyde in acetone
Kainate/ Kainate [9.4nM]	SYM 2081 [100µM]	50mM Tris-citrate (pH 7.1) + 10mM Ca-acetate	3 x 10min, 4°C	45min, 4°C	3 x 4sec, 4°C 2 x2 sec in 2.5% glutaraldehyde in acetone
NMDA/ MK 801 [3.3nM]	MK 801 [100µM]	50mM Tris-HCl (pH 7.2) + 50µM Glutamate + 30µM Glycine + 50µM Spermidine	15 x 10min, 4°C	60min, 22°C	2 x 5min, 4°C 1sec in distilled water
mGlu2/3/ LY 341,495 [1nM]	L-Glutamate [1mM]	Phosphate buffer (pH 7.6): 137mM NaCl; 2.7mM KCl; 4.3mM Na_2HPO_4 x H_2O; 1.4mM KH_2PO_4 + 100mM KBr*	2 x 5min, 22°C	60min, 4°C	2 x 5min, 4°C 1sec in distilled water
$GABA_A$/ Muscimol [7.7]	GABA [10µM]	50mM Tris-citrate (pH 7.0)	3 x 5min, 4°C	40min, 4°C	3 x 3sec, 4°C 1sec in distilled water
$GABA_A$/ SR 95531 [3nM]	GABA [1mM]	50mM Tris-citrate (pH 7.0)	3 x 5min, 4°C	40min, 4°C	3 x 3sec, 4°C 1sec in distilled water
$GABA_B$/ CGP 54626 [2nM]	CGP 55845 [100µM]	50mM Tris-HCl (pH 7.2) + 2.5mM $CaCl_2$	3 x 5min, 4°C	60min, 4°C	3 x 2sec, 4°C 1sec in distilled water

BZ ($GABA_A$ associated benzodiazepine binding sites)/ Flumazenil [1nM]	Clonazepam [2µM]	170mM Tris-HCl (pH 7.4)	1 x 15min,4°C	60min, 4°C	3 x 1min, 4°C 1sec in distilled water
M_1/ Pirenzepine [10nM]	Pirenzepine dehydrate [2µM]	Modified Krebs-buffer (pH7.4): 5.6mM KCl; 30.6mM NaCl; 1.2mM $MgSO_4$; 1.4mM KH_2PO_4; 5.6mM D-Glucose; 5.2mM $NaHCO_3$; 2.5mM $CaCl_2$	1 x 15min,4°C	60min, 4°C	3 x 1min, 4°C 1sec in distilled water
M_2/ Oxotremorine-M [1.7nM]	Carbachol [10µM]	20mM Hepes-Tris (pH 7.5) + 10mM $MgCl_2$	1 x 20min,22 °C	60min, 22°C	2 x 2min, 4°C 1sec in distilled water
M_2/ AF-DX 384 [5nM] *only tg5xFAD, LRP1 , tg5xFAD/LRP1*	Atropine sulphate [100µM]	Modified Krebs-buffer (pH7.4): 4.7mM KCl; 120mM NaCl; 1.2mM $MgSO_4$; 1.4mM KH_2PO_4; 5.6mM D-Glucose; 25mM $NaHCO_3$; 2.5mM $CaCl_2$	1 x 15min,22 °C	60min, 22°C	3 x 4min, 4°C 1sec in distilled water
M_3/ 4-DAMP [1nM	Atropine sulphate [10µM]	50mM Tris-HCl (pH 7.4) +0.1mM PMSF + 1mM EDTA	1 x 15min,22 °C	45min, 22°C	2 x 5min, 4°C 1sec in distilled water
α_1/ Prazosin [0.09nM]	Phentolamine mesylate [10µM]	50mM Na/K-phosphate buffer (pH 7.4)	1 x 15min,22 °C	60min, 22°C	2 x 5min, 4°C 1sec in distilled water

α_2/ UK14,304 [0.64nM]	Phentolamine mesylate [10µM]	50mM Tris-HCl (pH 7.7) + 100µM $MnCl_2$	1 x 15min,22 °C	90min, 22°C	1 x 5min, 4°C 1sec in distilled water
5-HT_{1A}/ 8-OH-DPAT [0.3nM]	5-HT [1µM]	170mM Tris-HCl (pH 7.7) + 0.01% Ascorbate* + 4mM $CaCl_2$*	1 x 30min,22 °C	60min, 22°C	1 x 5min, 4°C 3 x 1sec in distilled water
5-HT_{2A}/ Ketanserin [1.14nM]	Mianserin [10µM]	170mM Tris-HCl (pH 7.7)	1 x 30min,22 °C	120min, 22°C	2 x 10min, 4°C 3 x 1sec in distilled water
D_1/ SCH 23390 [1.67nM]	SKF 83566 [1µM]	50mM Tris-HCl (pH 7.4) + 120mM NaCl + 5mM KCl + 2mM $CaCl_2$ + 1mM $MgCl_2$ + 1µM Mianserin*	1 x 20min,22 °C	90min, 22°C	2 x 10min, 4°C 1sec in distilled water
D_2/ Raclopride [0.55nM]	Butaclamol [1µM]	50mM Tris-HCl (pH 7.4) + 150mM NaCl + 0.1% Ascorbate	1 x 20min,22 °C	45min, 22°C	6 x 1min, 4°C 1sec in distilled water
D_2/D_3 Fallypride [4nM]	Haloperidol [10µM]	50mM Tris-HCl (pH 7.4) + 5mM KCl + 120mM NaCl	1 x 30min,22 °C	60min, 37°C	2 x 2min, 4°C 1sec in distilled water
A_{2A}/ ZM 241 385 [0.42nM]	2-Chloroadenosine [2[10µM]0µM]	120mM Tris-HCl (pH 7.4) + 1mM EDTA (only preincubation) +2U/L adenosine deaminase (only pre- and main incubation) + 10mM $MgCl_2$ (only prerinsing and main incubation)	1 x 30min,37 °C Prerinsing 2 x 10min, 22°C	120min, 22°C	2 x 5min, 4°C 1sec in distilled water

* Only added to main incubation

3.2 Film exposure

Glass slides with the labeled sections were fixed on paper sheets with double-sided adhesive tape and co-exposed to tritium-sensitive film (Kodak, PerkinElmer LAS GmbH, Germany) together with either plastic or tissue ^{3}[H]-standards with increasing concentrations of radioactivity. Sheets were fixed between plastic plates, and hold together with several metal clips. Depending on the ligand, slices were exposed to the film 9 to 15 weeks. Exposure time of each ligand used is listed in Table 2. During exposure, the plates were stored in wooden boxes, thus ensuring that the films were not exposed to light. Finally, films were developed under red light using a Hyperprocessor Automatic Film Processor (Amersham Biosciences, Europe).

Table 2: List of exposure times of all used [^{3}H]-ligands

[^{3}H]-ligand	Exposure times [weeks]
AF-DX 384	10
AMPA	15
CGP 54626	10
4-DAMP	9
Fallyprid	15
Flumazenil	9
Kainate	12
Ketanserin	15
LY 341,495	10
MK 801	12
Muscimol	12
8-OH-DPAT	15
Oxotremorine-M	15
Pirenzepine	12
Prazosin	15
Raclopride	15
SCH 23390	15
SR 95531	12
UK 14,304	15
ZM 241 385	15

3.3 Digitization and analysis of the autoradiographic images

The autoradiographic images were digitized and analyzed using a video based technique (Zilles and Schleicher, 1991). Images were placed on a homogenously illuminated table, and digital images were taken using a fixed CCD-camera (Zeiss, Carl Zeiss Mikro Imaging GmbH, Germany), and the AxioVision-Software system, Version 4.8 (Zeiss, Carl Zeiss Mikro Imaging GmbH, Germany). Images were saved 8-bit coded in 256 gray values, at which 0 means black and 256 white, having a resolution of 4164x3120 pixels. To avoid diffuse and uneven illumination, shading correction was done each day. Furthermore, at the beginning of digitization of each series of images, the intensity of the light source and the aperture of the macro lens were adjusted measuring a blank area of the exposed film. Additional steps were reduction of stray light and sufficient warm-up of the light source and the camera to avoid shifts in the system (Zilles et al., 2002).

3.4 Calibration, analysis and color coding

The standards with known concentrations were used to calculate a non-linear transformation curve, respectively, to define the correlation between the measured gray values of the autoradiograph and the receptor concentration (Zilles et al., 2004).

Based on the transformation curve, the autoradiograph itself was converted into images with pixel values representing concentrations of radioactivity, given in fmol/mg protein (Zilles and Schleicher, 1995; Zilles et al., 2002a). The consequence is an image in which the gray values are a linear function of the concentration of radioactivity.

Eight brain regions, the regions of interest (ROI), were defined. ROIs were the olfactory bulb, the motor, somatosensory and piriform cortex, striatum (caudatus-putamen), as well as CA1 region, mossy fiber termination fields/hilus and stratum moleculare/granulosum in the hippocampus (Figure 4). The receptor density was analyzed in each of these ROIs using the AxioVision software. Per ROI and animal, three sections were measured.

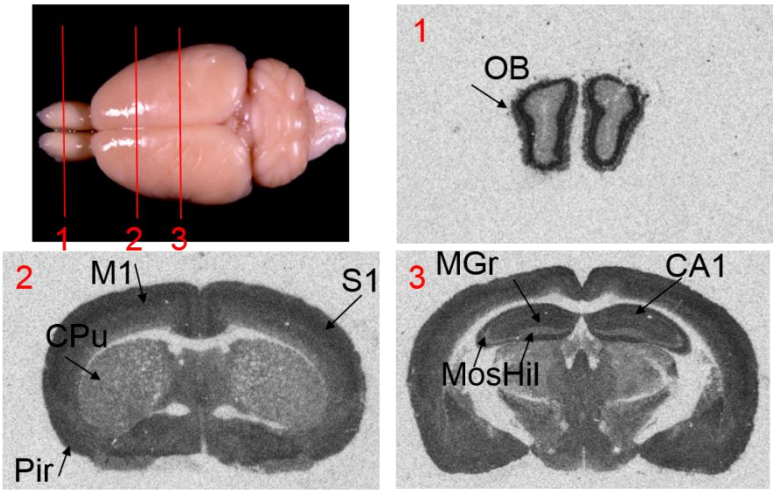

Figure 4: Overview of the brain regions investigated.
B: olfactory bulb, M1: motor cortex, S1: somatosensory cortex, Pir: piriform cortex, CPu: caudatus-putamen (striatum), CA1: CA1 region of the hippocampus, MGr: stratum moleculare/granulosum, MosHil: mossy fiber termination fields.

To provide a clear impression of the regional distribution of receptor density, linearized images were color coded. The full range of 256 gray values is color coded, at which the gray values are assigned to a scale of eleven colors to equally spaced density ranges (Figure 5). These contrast-enhanced images were used only for illustration, not for the measurement of the receptor densities.

4 Statistical analysis

Data are indicated as means and standard deviations. For each ligand, differences between the two groups *control* and *experimental model* were tested applying analysis of variance (ANOVA) using SYSTAT®Version 13. Each ligand was tested for group differences using a repeated measures design, the within factor set to *brain region* and the response factor to *density* of the receptor tested. If a group effect was found to be significant ($P \leq 0.05$), each brain region of that compartment was subjected to a one way, univariate post hoc test.
The dopamine receptor ligands [^{3}H]-Fallypride, [^{3}H]-Raclopride, [^{3}H]-SCH 23390 and [^{3}H]-ZM 241 385 were tested with univariate, one way ANOVA and subsequent Bonferroni correction, since their densities were above the detection limit of receptor autoradiography only in the striatum.

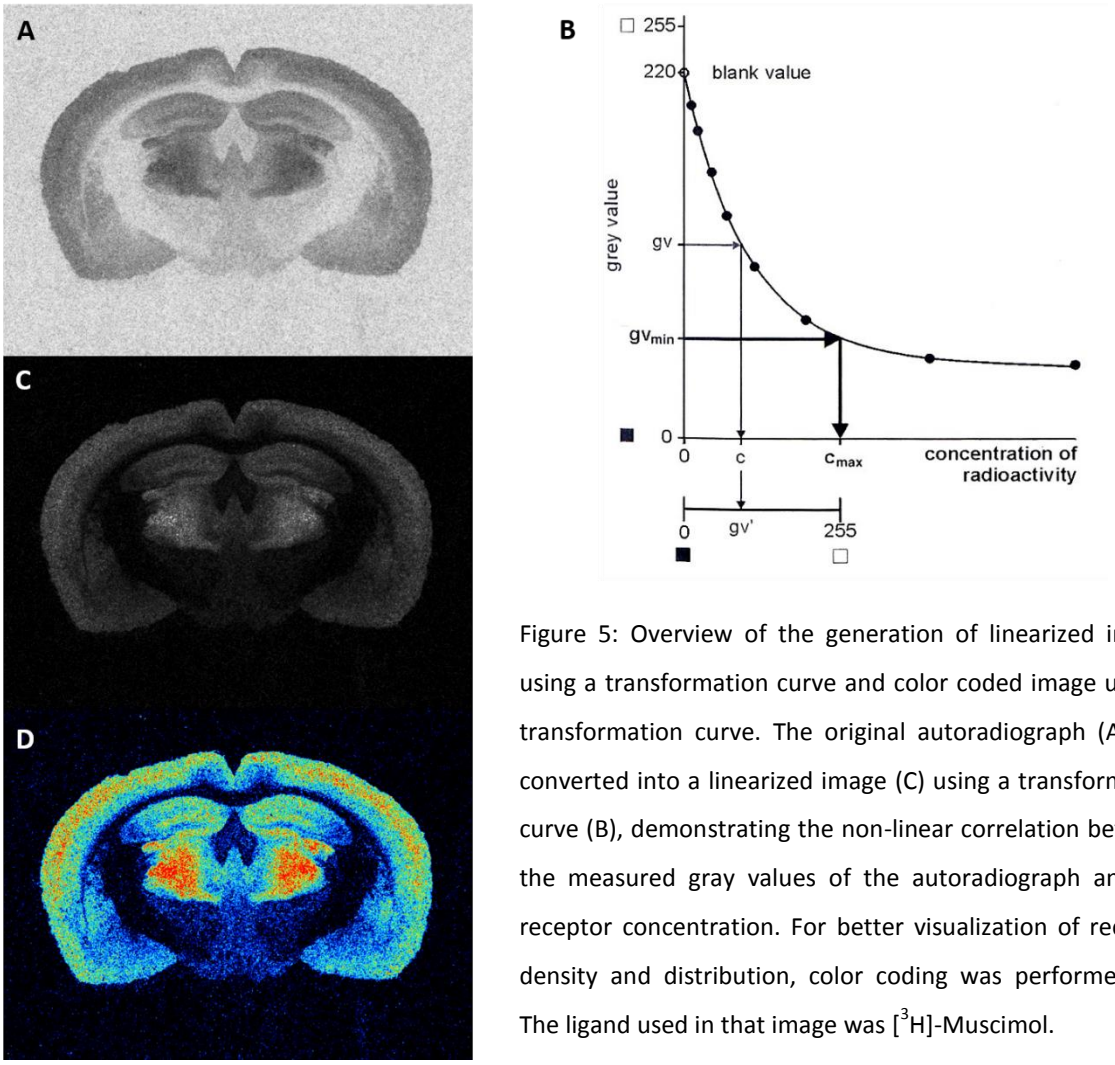

Figure 5: Overview of the generation of linearized images using a transformation curve and color coded image using a transformation curve. The original autoradiograph (A) was converted into a linearized image (C) using a transformation curve (B), demonstrating the non-linear correlation between the measured gray values of the autoradiograph and the receptor concentration. For better visualization of receptor density and distribution, color coding was performed (D). The ligand used in that image was [^{3}H]-Muscimol.

5 Histological staining

Silver staining was performed (Merker, 1983) to visualize cell bodies and cytoarchitecture. Alternating cryostat sections of the same brains, in which the receptor binding was performed, were defrosted for one hour using a heating plate at 37°C and fixated in 4% buffered formalin for 30 minutes. After fixation, sections were washed in purified water for 30 minutes, put into 4% formic acid for three hours and in formic acid/hydrogen peroxide mixture over night. For the formic acid/hydrogen peroxide mixture, 60 vol% purified water, 30 vol% hydrogen peroxide and 10 vol% concentrated formic acid were mixed together. The next day, slices were washed in purified water for 30 minutes and rinsed with acetic acid (1 vol%) two times for five minutes. During this step, the three components of the developer

solution were mixed together, and sections were incubated directly after mixing. The substances used for the developer solution are listed in Table 3. The cell body staining was checked using a microscope and stopped with 1 vol% acetic acid. Afterwards, slices were rinsed with purified water for five minutes, fixated with T-MAX for 2 minutes and rinsed with purified water again. Using increasing isopropanol concentrations (70%, 80%, 97% and 100%), followed by incubation in xylol, slices were dehydrated. Finally, slices were coverslipped with DPX.

Table 3: Amount of substances used for the developer solution in histological Nissl staining

Amount	Solution
Developer solution A	
1000 ml	purified water
50 g	absolute sodium carbonate
Developer solution B	
500 ml	purified water
1 g	ammonium nitrate
1 g	silver nitrate
5 g	tungstosilicic acid
Developer solution C	
1000 ml	purified water
2 g	ammonium nitrate
2 g	silver nitrate
10 g	tungstosilicic acid
7.3ml	Formaldehyde

6 Immunohistochemical staining

To analyze the presence of Aβ plaques, immunohistochemical staining was performed. For immunohistochemical staining, frozen brain sections were immersion-fix in 4% ($^{w}/_{v}$) paraformaldehyde for 10 minutes, dried at room temperature for 10 minutes and stored at -80°C. For antigen retrieval, frozen sections were incubated in 70% formic acid for five

minutes. Afterwards, sections were equilibrated in three changes of ice cold (1 vol%) TBS-Triton for one minutes each and permeabilized in TBS-Triton solution (1 vol%) at room temperature for 10 minutes. Subsequently, sections were washed in TBS-Triton three times for one minute each. The sections were surrounded with PAP pen and the glass slides were stored in plastic boxes. Blocking of the staining took place using M.O.M. (Mouse on Mouse; Vector Labs, Burlingame, USA; one drop in 1.25µl TBS-Triton) for 30 minutes. Sections were probed with a primary antibody which is diluted in 1 vol% BSA/TBS-Triton one hour at room temperature, then over night at 8°C. Sections were double stained with G2-10 (Millipore, Schwalbach, Germany; 1:100) for Aβ40 and 1-11-3 (Covance, Munich, Germany; 1:200) for Aβ42.

The next morning, sections were washed in TBS-Triton three times for four minutes and incubated with the secondary antibodies G-M A488 (Life Technologies GmbH, Darmstadt, Germany; 1:500) and G-R A568 (Life Technologies GmbH, Darmstadt, Germany; 1:150) in 1 vol% BSA/TBS-Triton for four hours at room temperature. Next, washing took place in TBS-Triton two times for 4 minutes. Nuclei were stained by adding 0.5µg/ml DAPI (Sigma-Aldrich Chemie GmbH, Steinheim, Germany) for three minutes, and sections were washed with TBS-Triton for four minutes. The tissue was coverslip-mounted with Aqua Poly/Mont (DAKO, Agilant Technologies, Hamburg, Germany).

III. Results

1 Neurotransmitter receptor densities in brains of *tg5xFAD*, *LRP1* and *tg5xFAD/LRP1* mice

The principal regional receptor distribution patterns were similar between control mice and all three models of AD. However, the absolute receptor densities differed between controls and transgenic mice in various, but not all brain regions.

1.1 Glutamate receptors

Ionotropic and metabotropic glutamate receptors were present throughout all areas investigated. Kainate receptors showed the lowest mean density in the CA1 region of the hippocampus and highest in the mossy fiber termination fields, with intermediate densities in the olfactory bulb, motor cortex, somatosensory and piriform cortex, hilus and stratum moleculare/granulosum. NMDA receptors had a very similar distribution within the brain, with the notable exception of the hippocampus area, especially the CA1 region. Here the mean density was higher. The density of the metabotropic Glu2/3 (mGlu2/3) receptors was higher in the neocortical areas, striatum and the stratum moleculare/granulosum than in the olfactoric bulb and the remaining areas of the hippocampus. In the following chapters, changes of the receptor density between AD mouse models and control mice, respectively, are described in detail (compare Figure 6 - Figure 9).

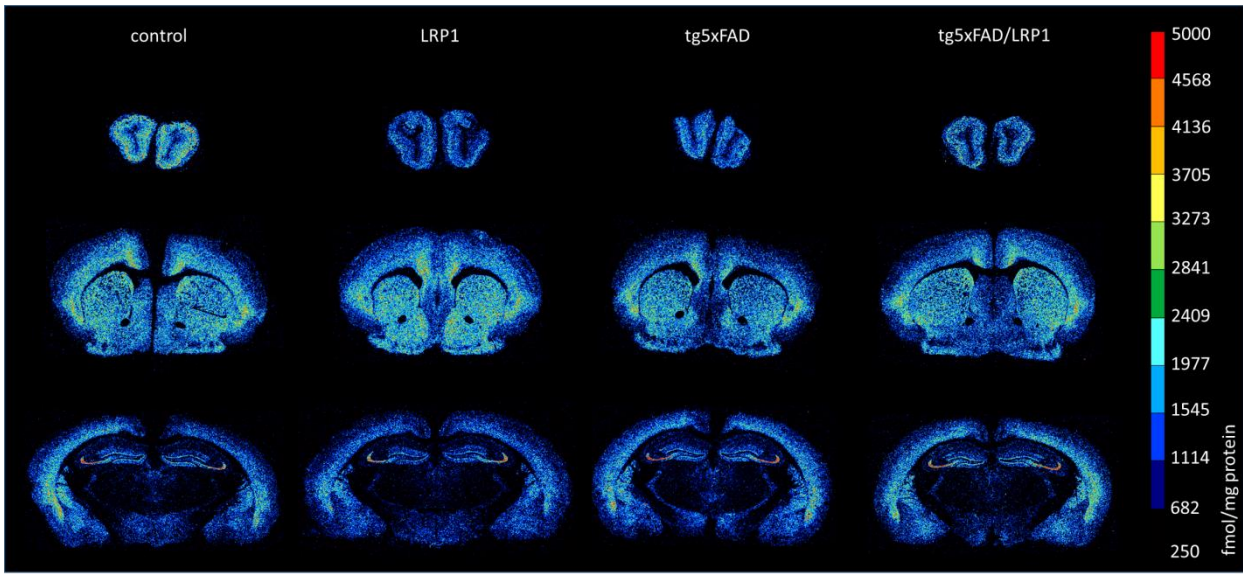

Figure 6: Color coded image of kainate receptor densities (fmol/mg protein) in the brains of *tg5xFAD*, *LRP1* and *tg5xFAD/LRP1* mice compared to control mice. The images show a similar regional distribution of this receptor in all strains but differences in absolute receptor densities (see text).

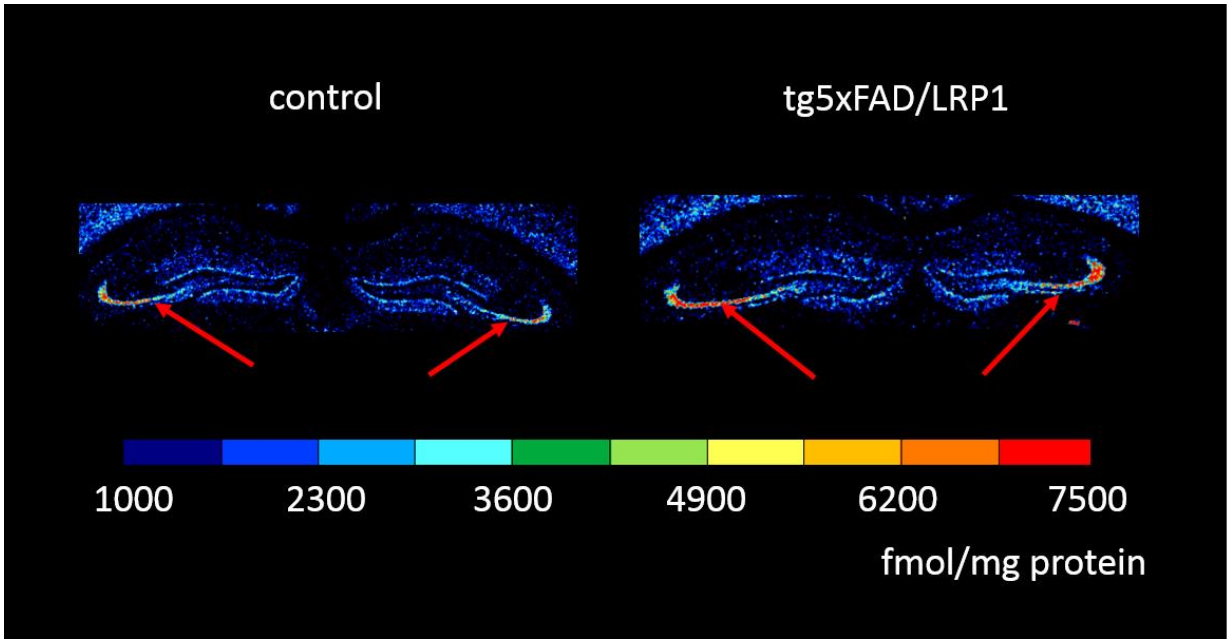

Figure 7: Color coded image of kainate receptor density (fmol/mg protein) in the hippocampus of *tg5xFAD/LRP1* mice in detail. Mossy fibers can clearly be distinguished and are increased in tg5xFAD/LRP1 mice compared to control.

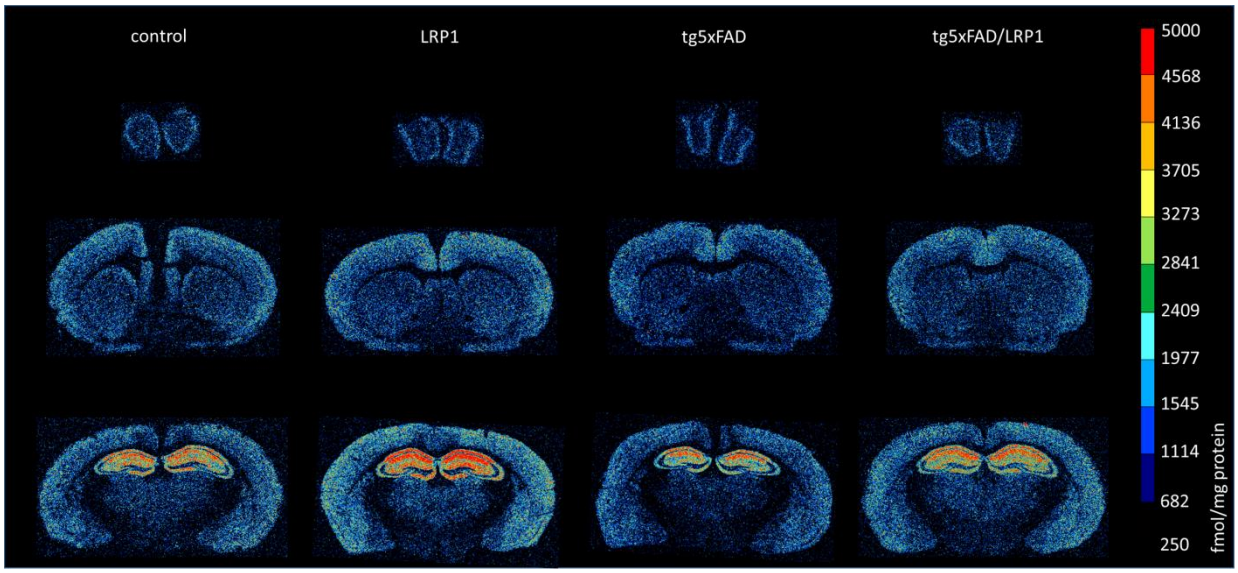

Figure 8: Color coded image of NMDA receptor densities (fmol/mg protein) in the brains of *tg5xFAD*, *LRP1* and *tg5xFAD/LRP1* mice compared to control mice. The images show a similar regional distribution of this receptor in all strains but differences in absolute receptor densities (see text).

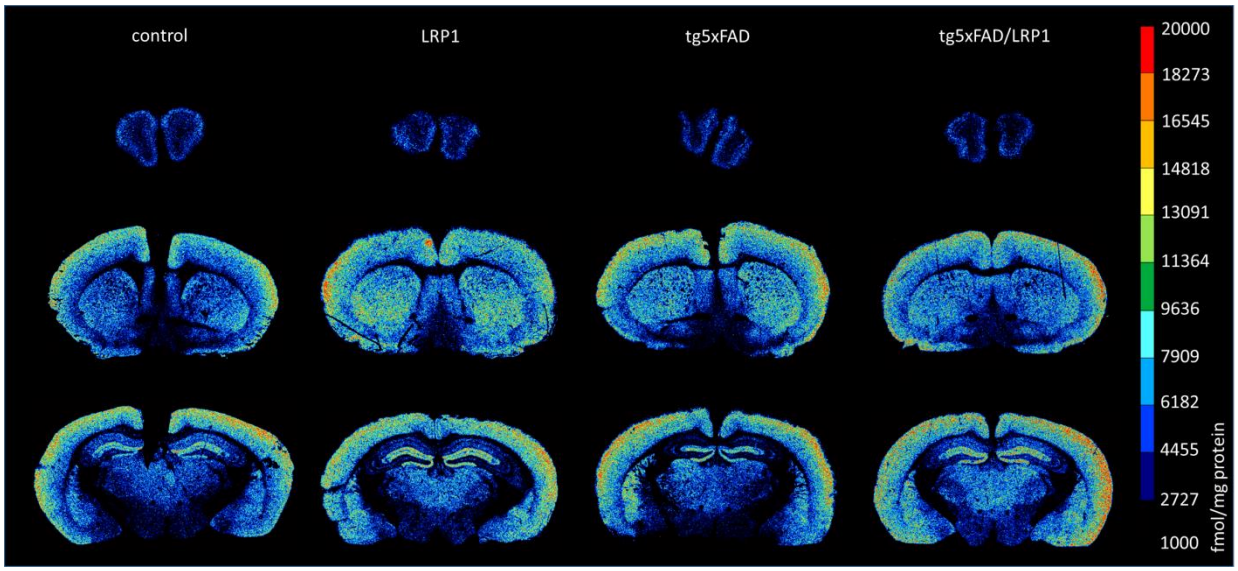

Figure 9: Color coded image of mGlu2/3 receptor densities (fmol/mg protein) in the brains of *tg5xFAD*, *LRP1* and *tg5xFAD/LRP1* mice compared to control mice. The images show a similar regional distribution of this receptor in all strains but differences in absolute receptor densities (see text).

1.1.1 Kainate receptor

The densities of kainate receptors of ***LRP1*** mice compared to controls were decreased in all brain regions investigated. Differences were statistically significant in the olfactory bulb

(28%; p=0.0005), the piriform cortex (24%; p=0.01) and in the hippocampal regions CA1 (17%; p=0.02) and stratum moleculare/granulosum (22%; p=0.004).

The ***tg5xFAD*** model revealed a reduced density in the olfactory bulb (23%; p=0.02) and the piriform cortex (17%; p=0.03), compared to the corresponding control.

Between ***tg5xFAD/LRP1*** and control mice, down- as well as upregulation in three regions could be observed. In two regions, the mean density of kainate receptors was significant lower in *tg5xFAD/LRP1* than in control mice, i.e. in the olfactory bulb (15%; p=0.02) and the piriform cortex (15%; p=0.03). In termination regions of the mossy fibers/hilus, it was increased by 15% (p=0.03, compare Figure 7). Figure 10 summarizes the kainate receptor data.

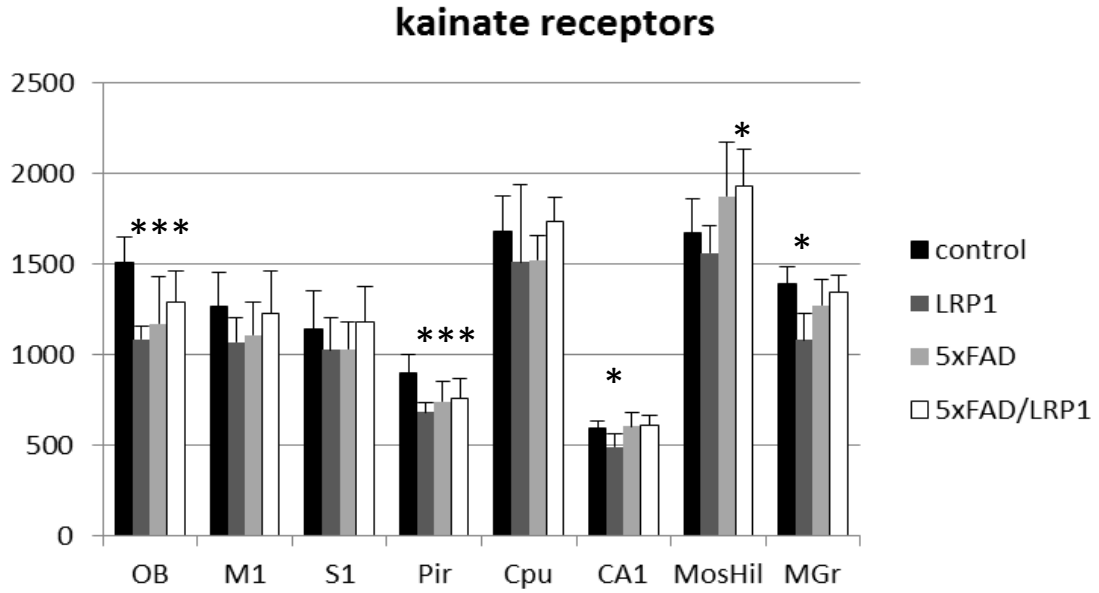

Figure 10: Bar charts demonstrating mean kainate receptor density together with standard deviation in all brain regions investigated of control (black), *LRP1* (dark grey), *tg5xFAD* (light grey) and *tg5xFAD/LRP1* (white) mice. Significant differences are shown by *, p<0.05.

1.1.2 NMDA receptor

In comparison to wild type mice, NMDA receptor densities of ***LRP1*** mice were increased in the CA1 region by 16% (p=0.03) and in the stratum moleculare/granulosum by 12% (p=0.04).

In ***tg5xFAD*** mice, a trend towards decrease was observed in the olfactory bulb, somatosensory and piriform cortex, but did not reach significance.

In ***tg5xFAD/LRP1*** mice, the olfactory bulb showed a significant reduction by 12% (p=0.04). In the mossy fiber termination fields/hilus, however, an upregulation by 14% (p=0.02) was observed (Figure 11).

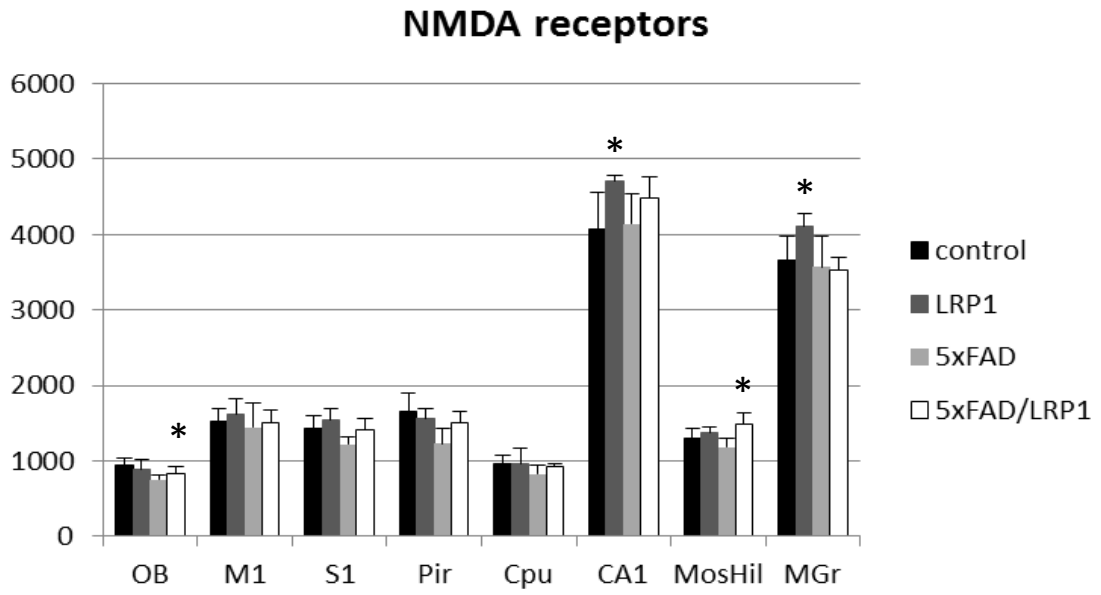

Figure 11: Bar charts demonstrating mean NMDA receptor density together with standard deviation in all brain regions investigated of control (black), *LRP1*(dark grey), *tg5xFAD* (light grey) and *tg5xFAD/LRP1*(white) mice. Significant differences are shown by *, p<0.05.

1.1.3 mGlu2/3 receptor

In the brains of ***LRP1*** mice, only one significant difference could be observed. The mGlu2/3 receptor was downregulated by 35% (p=0.02) in the CA1 region.

The same regional preference could be observed in ***tg5xFAD/LRP1*** mice. Here, a significant lower mean receptor density was shown (31%; p=0.003) in the hippocampal CA1 region.

In ***tg5xFAD*** mice, the mGlu2/3 receptor density of the olfactory bulb was reduced by 38% (p=0.03). Furthermore, the CA1 region showed lower mean receptor density by 29% (p=0.02).

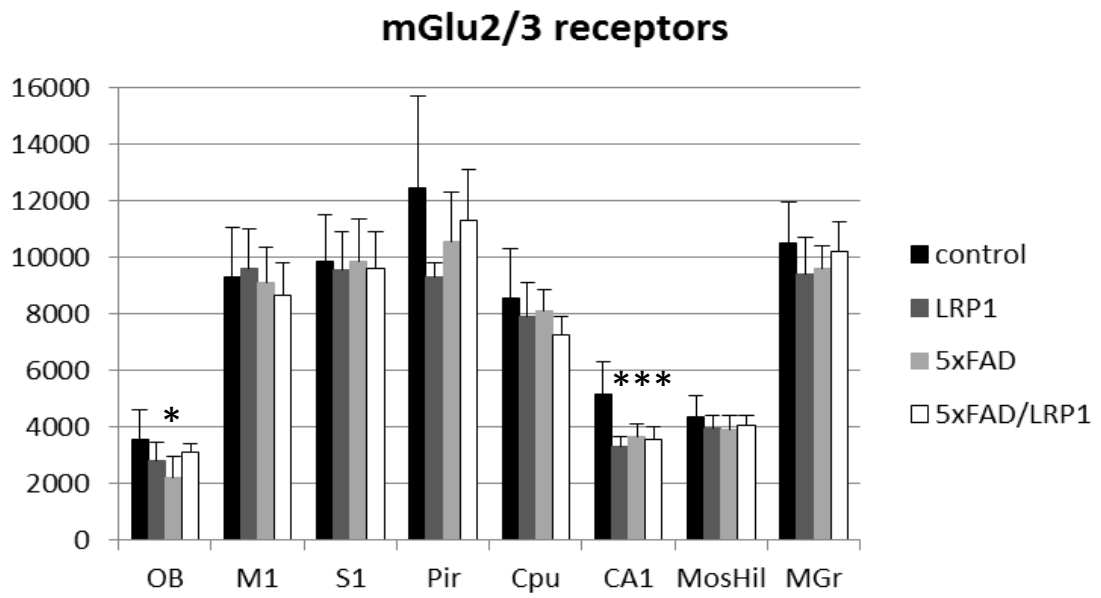

Figure 12: Bar charts demonstrating mean mGlu2/3 receptor density together with standard deviation in all brain regions investigated of control (black), *LRP1* (dark grey), *tg5xFAD* (light grey) and *tg5xFAD/LRP1* (white) mice. Significant differences are shown by *, $p<0.05$.

1.2 Cholinergic receptors

The receptors of the cholinergic system, $\mathbf{M_1}$, $\mathbf{M_2}$ and $\mathbf{M_3}$ receptors, demonstrated different regional distribution patterns. $\mathbf{M_1}$ receptor density was lowest in the olfactory bulb and the termination fields of mossy fibers. Highest density was seen in the striatum and the CA1 region, with intermediate density in the motor, somatosensory and piriform cortices, the hilus and stratum moleculare/granulosum.

$\mathbf{M_2}$ receptor density revealed by agonist and antagonist binding was high in the olfactory bulb, the striatum and the somatosensory cortex. Intermediate levels were found in the piriform cortex and the termination fields of mossy fibers. The lowest density was observed in the hippocampal regions CA1, hilus and stratum moleculare/granulosum.

$\mathbf{M_3}$ receptors showed the lowest mean density in the olfactory bulb, the hilus and the mossy fiber regions (600-4,700 fmol/mg protein), and intermediate densities in most of the other cortical areas. The highest density could be found in the striatum, the CA1 region and the stratum moleculare/granulosum, with concentrations ranging between 8,900 and 12,000 fmol/mg protein (see Figure 13 - Figure 16).

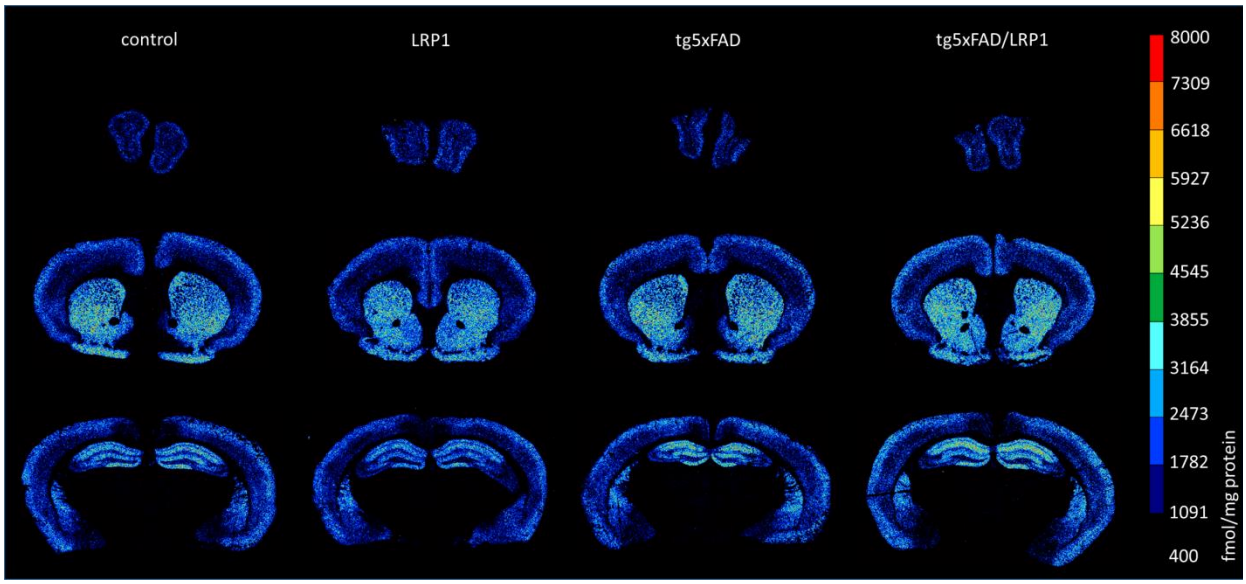

Figure 13: Color coded image of M_1 receptor densities (fmol/mg protein) in the brains of *tg5xFAD*, *LRP1* and *tg5xFAD/LRP1* mice compared to control mice. The images show a similar distribution of this receptor in all strains.

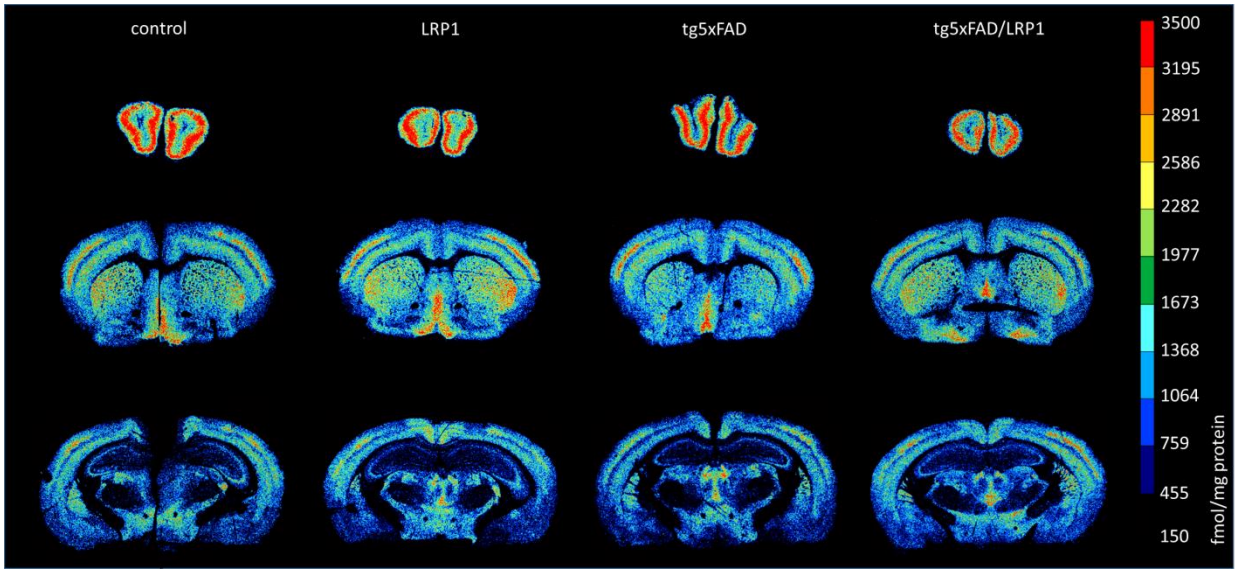

Figure 14: Color coded image of M_2 ([^{3}H]-Oxotremorine-M) receptor densities (fmol/mg protein) in the brains of *tg5xFAD*, *LRP1* and *tg5xFAD/LRP1* mice compared to control mice. The images show a similar regional distribution of this receptor in all strains but differences in absolute receptor densities (see text).

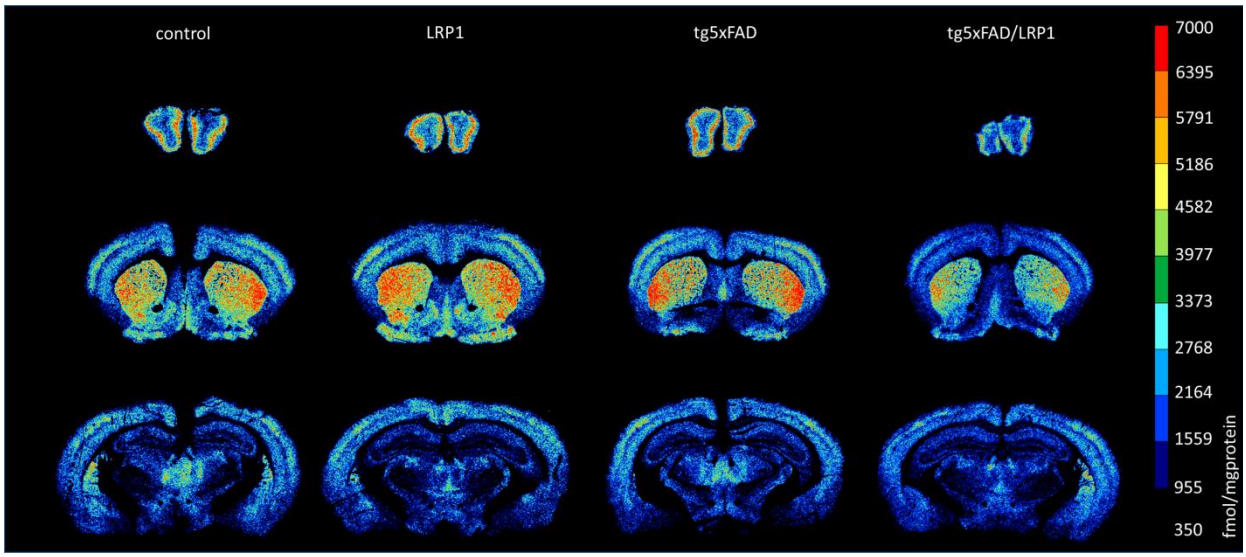

Figure 15: Color coded image of M_2 ([^{3}H]-AF-DX 384) receptor densities (fmol/mg protein) in the brains of *tg5xFAD*, *LRP1* and *tg5xFAD/LRP1* mice compared to control mice. The images show a similar regional distribution of this receptor in all strains but differences in absolute receptor densities (see text).

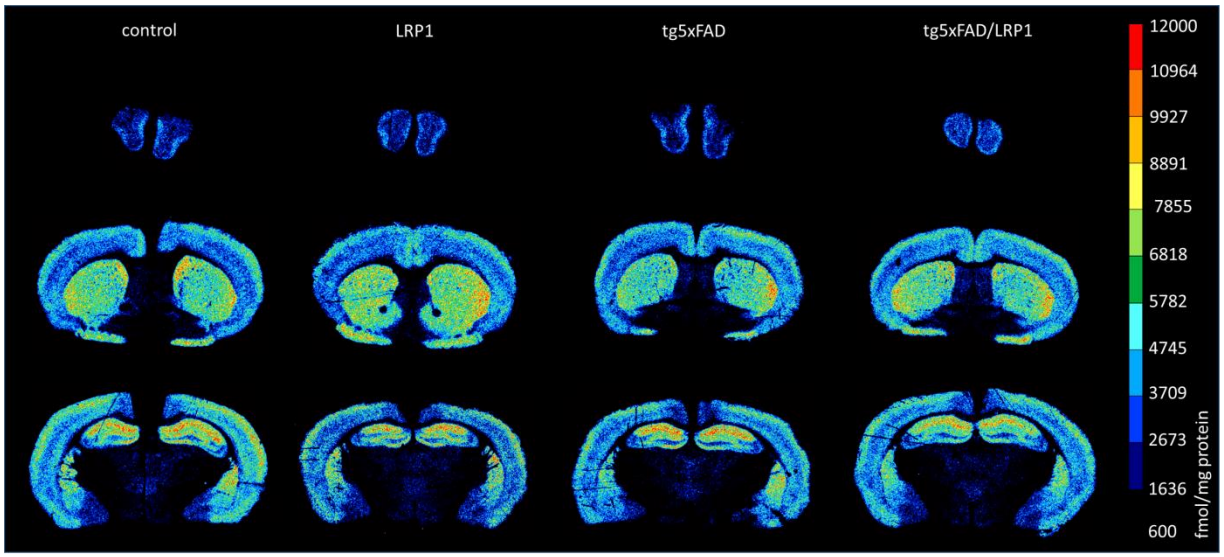

Figure 16: Color coded image of M_3 receptor densities (fmol/mg protein) in the brains of *tg5xFAD*, *LRP1* and *tg5xFAD/LRP1* mice compared to control mice. The images show a similar distribution of this receptor in all strains.

1.2.1 Muscarinic acetylcholine receptor M_1

No significant differences could be observed in any area between ***LRP1, tg5xFAD***, ***tg5xFAD/LRP1*** and control mice (Figure 17).

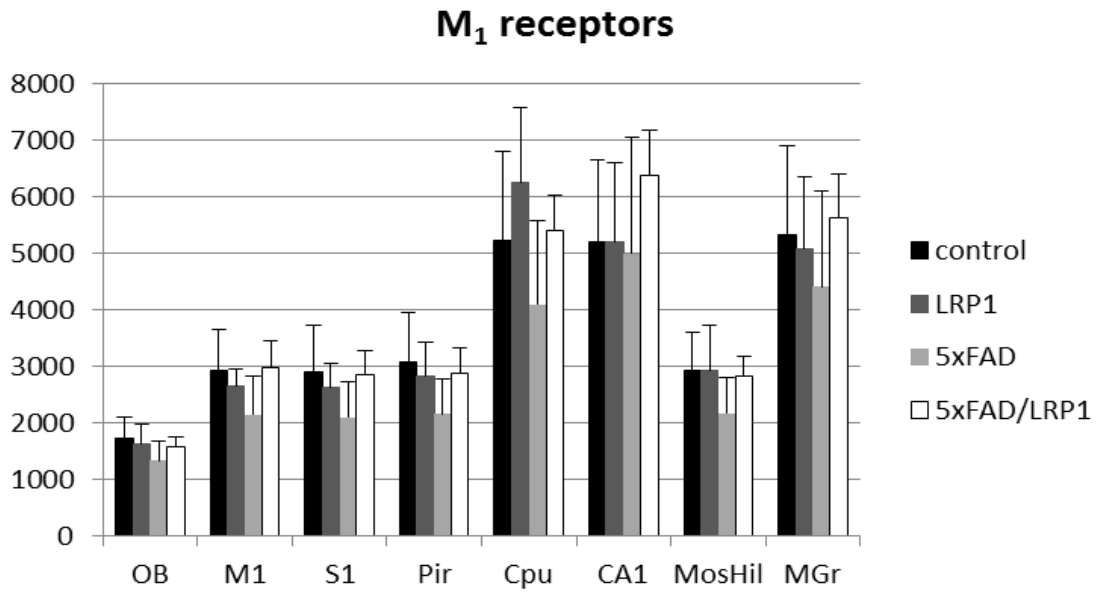

Figure 17: Bar charts demonstrating mean M_1 receptor density together with standard deviation in all brain regions investigated of control (black), *LRP1* (dark grey), *tg5xFAD* (light grey) and *tg5xFAD/LRP1* (white) mice.

1.2.2 Muscarinic acetylcholine receptor M_2

Binding of the agonist [^{3}H]-Oxotremorine-M showed a significant downregulation in all hippocampal regions of ***LRP1***. Receptor density was lower in CA1 by 35% (p=0.005), in mossy fiber termination fields/hilus by 31% (p=0.002) and in the stratum moleculare/granulosum by 40% (p=0.02). Binding of the antagonist of the M_2 receptor, [^{3}H]-AF-DX 384, revealed reduced receptor density in the CA1 region (17%; p=0.02) and the stratum moleculare/granulosum (16%; p=0.02). An upregulation was observed in the striatum (17%; p=0.01).

In the ***tg5xFAD*** model, binding of the agonist [^{3}H]-Oxotremorine-M to the M_2 receptors was decreased by 22% (p=0.05) in the mossy fiber termination fields/hilus and by 24% (p=0.03) in

the stratum moleculare/granulosum, respectively. Using the antagonist [^{3}H]-AF-DX 384, no differences were seen.

Reduced density was observed in the ***tg5xFAD/LRP1*** mice by binding of the agonist as well as the antagonist. Binding of [^{3}H]-Oxotremorine-M revealed a downregulation in the olfactory bulb by 17% (p=0.02). The M_2 receptor densities appeared downregulated when using the antagonist of the M_2 receptor, [^{3}H]-AF-DX 384 in the olfactory bulb (21%; p=0.02), the motor (14%; p=0.01) and the somatosensory cortex (12%; p=0.02) as well as the striatum (12%; p=0.01). See Figure 18 and Figure 19.

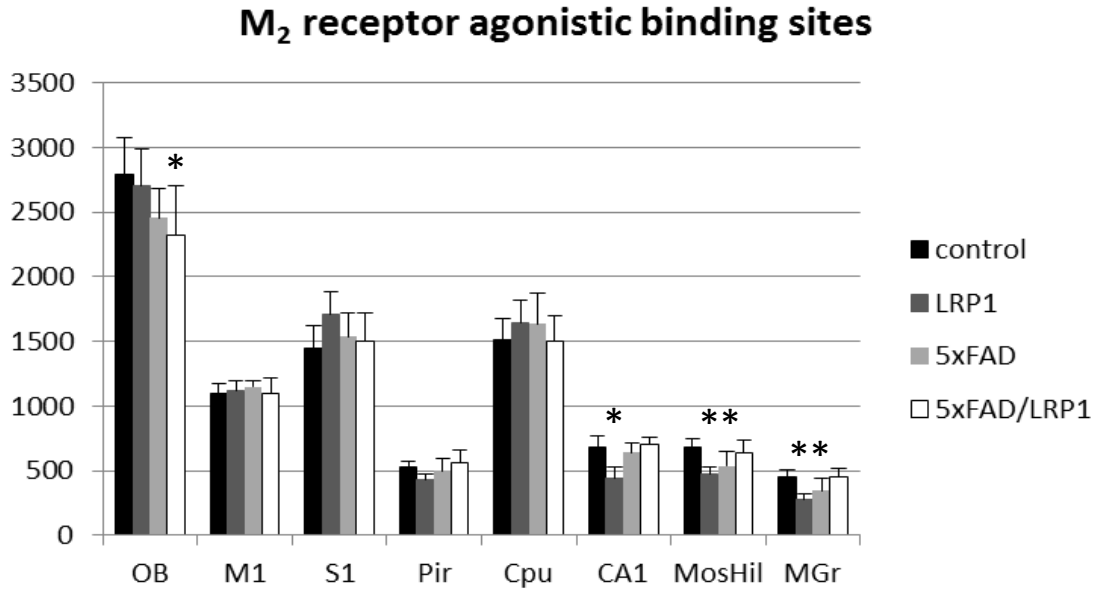

Figure 18: Bar charts demonstrating mean M_2 receptor density ([^{3}H]-Oxotremorine-M binding) together with standard deviation in all brain regions investigated of control (black), *LRP1* (dark grey), *tg5xFAD* (light grey) and *tg5xFAD/LRP1* (white) mice. Significant differences are shown by *, p<0.05.

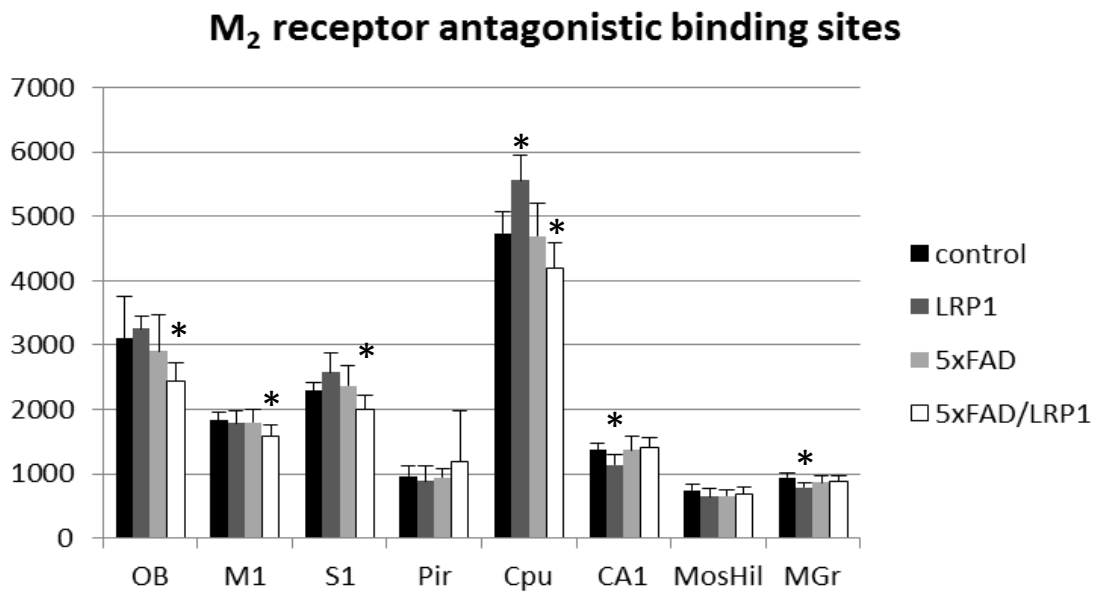

Figure 19: Bar charts demonstrating mean M_2 receptor density ([^{3}H]-AF-DX 384 binding) together with standard deviation in all brain regions investigated of control (black), *LRP1*(dark grey), *tg5xFAD* (light grey) and *tg5xFAD/LRP1* (white) mice. Significant differences are shown by *, p<0.05.

1.2.3 Muscarinic acetylcholine receptor M_3

The receptor densities of ***LRP1*** and ***tg5xFAD/LRP1*** mice did not show any significant differences compared to control mice (Figure 20). In ***tg5xFAD*** mice, M_3 receptor density was enhanced in the CA1 region by 15% (p=0.03).

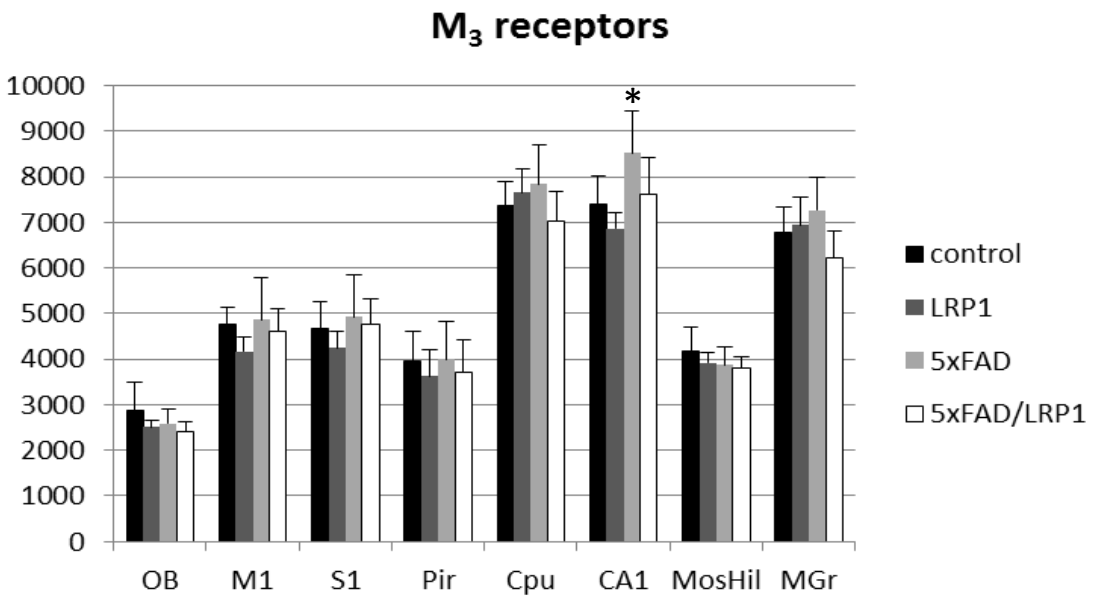

Figure 20: Bar charts demonstrating mean M_3 receptor density together with standard deviation in all brain regions investigated of control (black), LRP1 (dark grey), tg5xFAD (light grey) and tg5xFAD/LRP1 (white) mice. Significant differences are shown by *, $p<0.05$.

1.3 Serotonin receptors

5-HT_{2A} receptors reached their highest density in the striatum, the motor cortex and the somatosensory cortex. Intermediate concentrations were observed in the CA1 region of the hippocampus. The lowest concentration could be seen in the olfactory bulb. Comparison between control and models of AD showed a similar regional receptor distribution in all brains (Figure 21) but differences in absolute densities in some brain regions (see below).

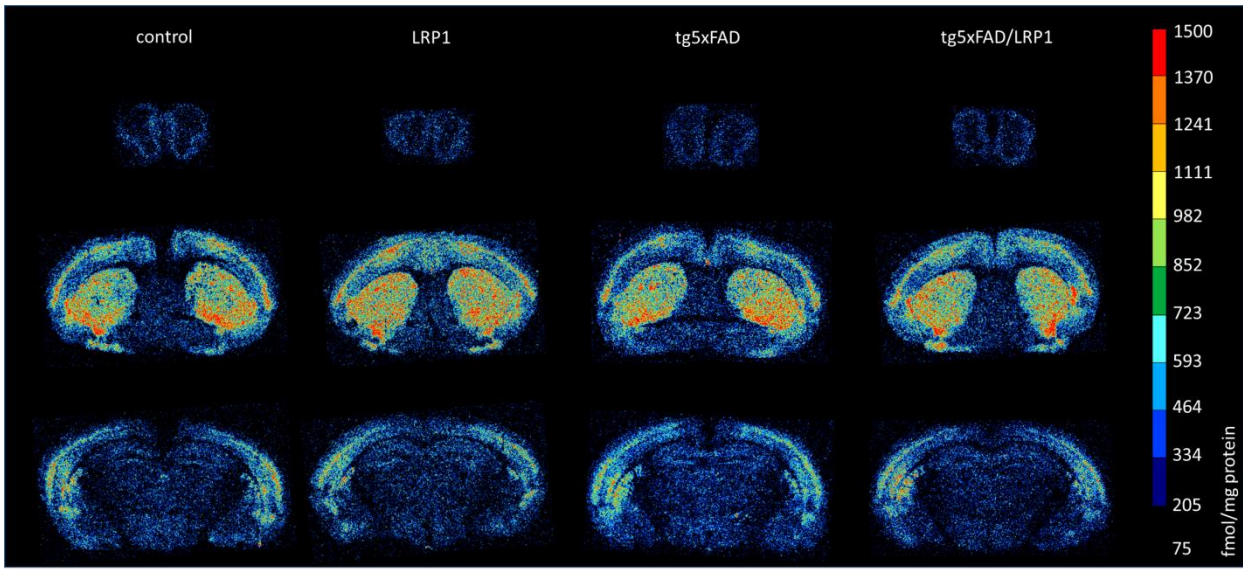

Figure 21: Color coded image of 5-HT_{2A} receptor densities (fmol/mg protein) in the brains of *tg5xFAD*, *LRP1* and *tg5xFAD/LRP1* mice compared to control mice. The images show a similar regional distribution of this receptor in all strains but differences in absolute receptor densities (see text).

1.3.1 5-HT_{2A} receptor

Significant differences in receptor densities could not be observed by comparing ***LRP1*** and ***tg5xFAD*** with control mice in any area.

In ***tg5xFAD/LRP1*** mice, higher mean receptor densities were observed in the striatum (18%; p=0.04) and in the CA1 region (31%; p=0.02). See Figure 22.

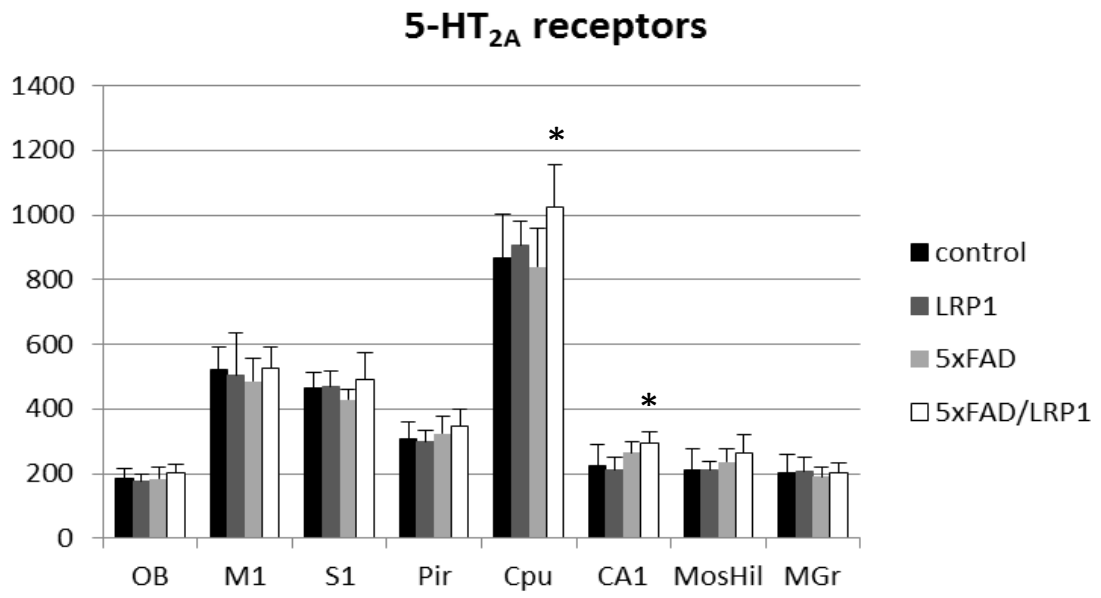

Figure 22: Bar charts demonstrating mean 5-HT_{2A} receptor density together with standard deviation in all brain regions investigated of control (black), *LRP1* (dark grey), *tg5xFAD* (light grey) and *tg5xFAD/LRP1* (white) mice. Significant differences are shown by *, $p<0.05$.

1.4 GABA receptors

GABA receptors had a similar regional distribution in all mice strains. **$GABA_A$** receptor density was lowest in the striatum, both by binding of [^{3}H]-Muscimol and [^{3}H]-SR 95531. [^{3}H]-Muscimol binding revealed the highest receptor concentration in the olfactory bulb and the somatosensory cortex. Intermediate concentrations were present in the hippocampus. The highest $GABA_A$ receptor density was found by [^{3}H]-SR 95531 binding in the hippocampal areas CA1 and stratum moleculare/granulosum.

The lowest density of **BZ** binding sites of the $GABA_A$ receptors was found in the striatum, mossy fiber termination fields and hilus, the highest in the motor, somatosensory and piriform cortices, CA1 region and stratum moleculare/granulosum. **$GABA_B$** receptors showed the lowest mean density in the olfactory bulb, followed by mossy fiber termination fields, striatum and CA1 region. The highest concentrations were found in the motor, somatosensory and piriform cortices and the stratum moleculare/granulosum (see Figure 23 - Figure 26).

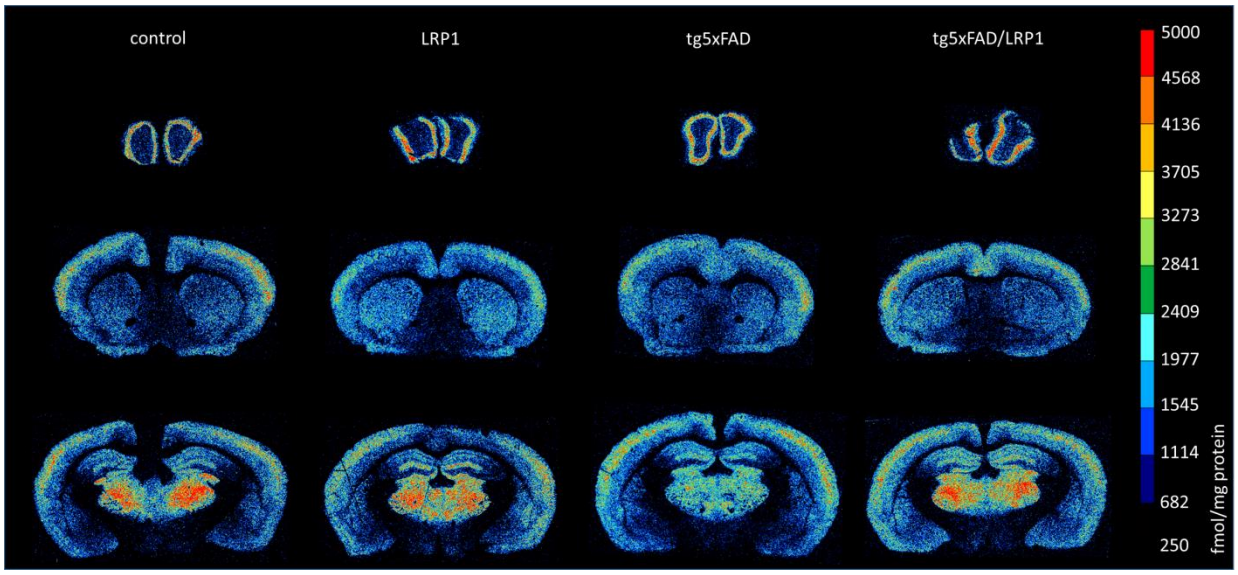

Figure 23: Color coded image of $GABA_A$ ([^{3}H]-Muscimol) receptor densities (fmol/mg protein) in the brains of *tg5xFAD*, *LRP1* and *tg5xFAD/LRP1* mice compared to control mice. The images show a similar regional distribution of this receptor in all strains but differences in absolute receptor densities (see text).

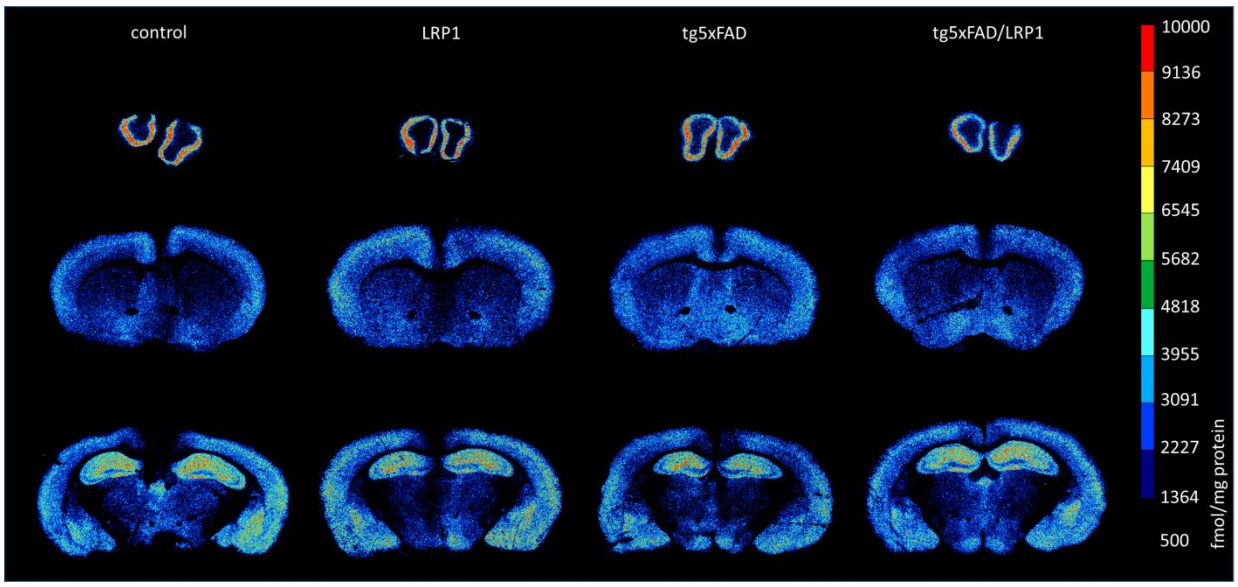

Figure 24: Color coded image of $GABA_A$ ([^{3}H]-SR 95531) receptor densities (fmol/mg protein) in the brains of *tg5xFAD*, *LRP1* and *tg5xFAD/LRP1* mice compared to control mice. The images show a similar regional distribution of this receptor in all strains but differences in absolute receptor densities (see text).

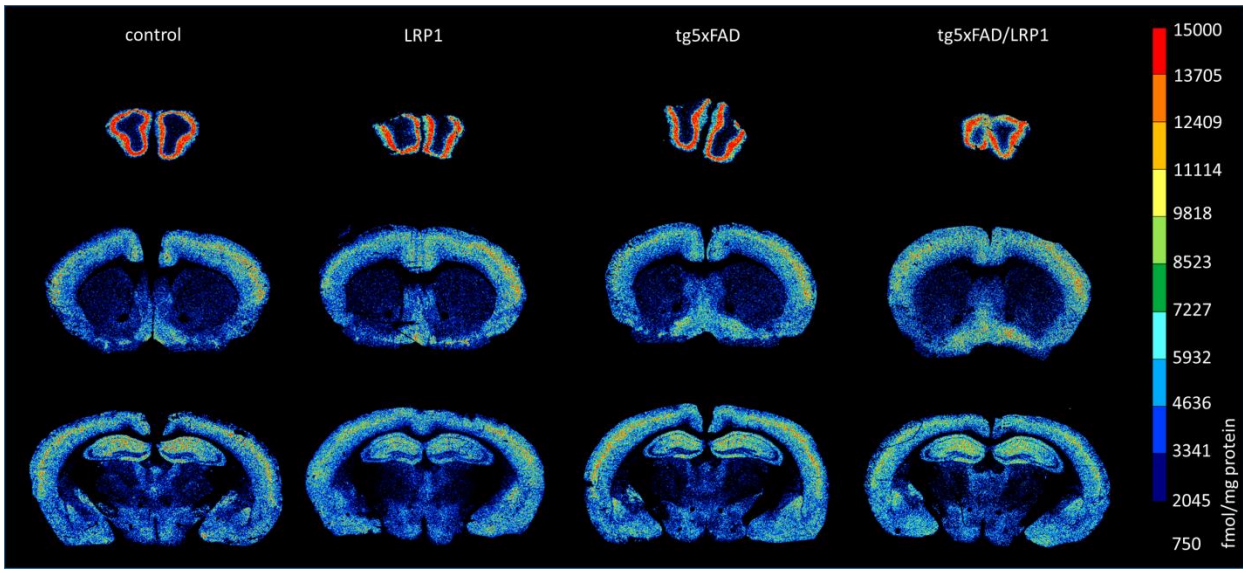

Figure 25: Color coded image of BZ receptor densities (fmol/mg protein) in the brains of *tg5xFAD*, *LRP1* and *tg5xFAD/LRP1* mice compared to control mice. The images show a similar regional distribution of this receptor in all strains but differences in absolute receptor densities (see text).

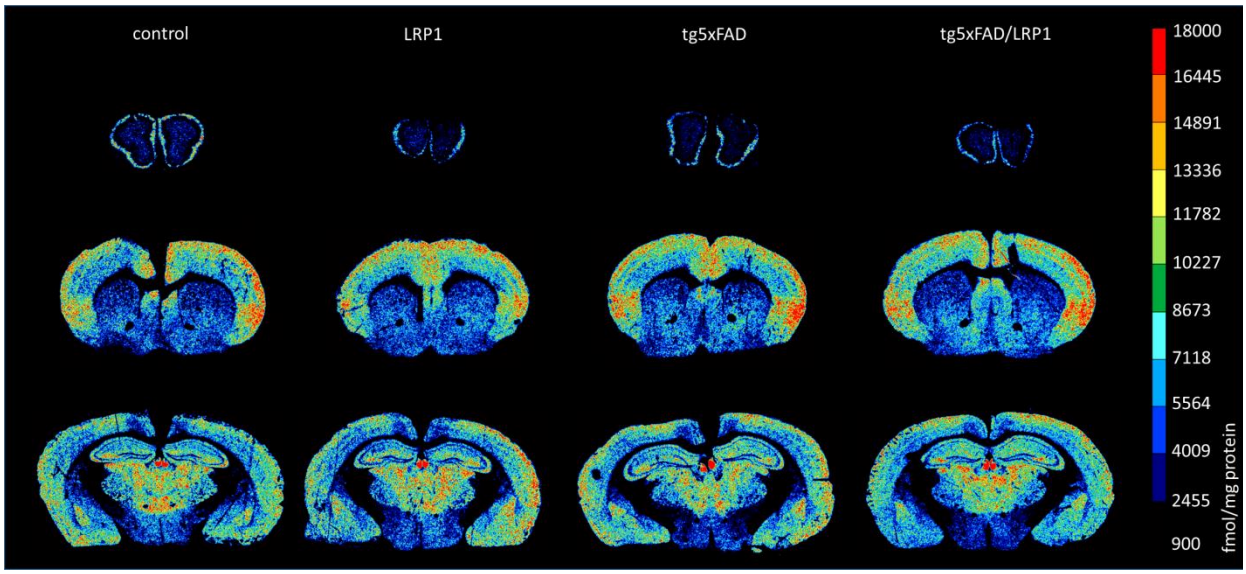

Figure 26: Color coded image of $GABA_B$ receptor densities (fmol/mg protein) in the brains of *tg5xFAD*, *LRP1* and *tg5xFAD/LRP1* mice compared to control mice. The images show a similar regional distribution of this receptor in all strains but differences in absolute receptor densities (see text).

1.4.1 $GABA_A$ receptor

The binding of the $GABA_A$ receptor agonist [^{3}H]-Muscimol as well as the antagonist [^{3}H]-SR 95531 showed no significant differences between ***LRP1*** and controls in all areas analyzed.

Binding of the antagonist [^{3}H]-SR 95531 revealed no difference in either ***tg5xFAD***, ***tg5xFAD/LRP1*** mice compared to control mice. [^{3}H]-Muscimol binding, on the other hand, revealed a lower mean receptor density in the stratum moleculare/granulosum by 24% (p=0.003) in ***tg5xFAD*** mice, and by 19% (p=0.01) in ***tg5xFAD/LRP1*** mice (see Figure 27 and Figure 28).

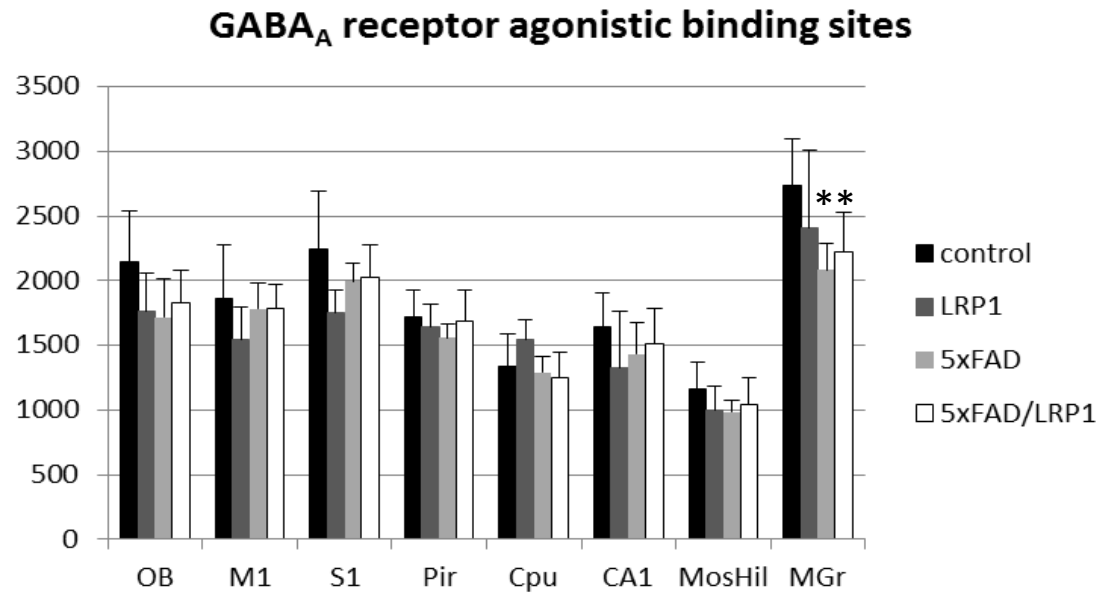

Figure 27: Bar charts demonstrating mean $GABA_A$ receptor density (agonist) together with standard deviation in all brain regions investigated of control (black), *LRP1* (dark grey), *tg5xFAD* (light grey) and *tg5xFAD/LRP1* (white) mice. Significant differences are shown by *, p<0.05.

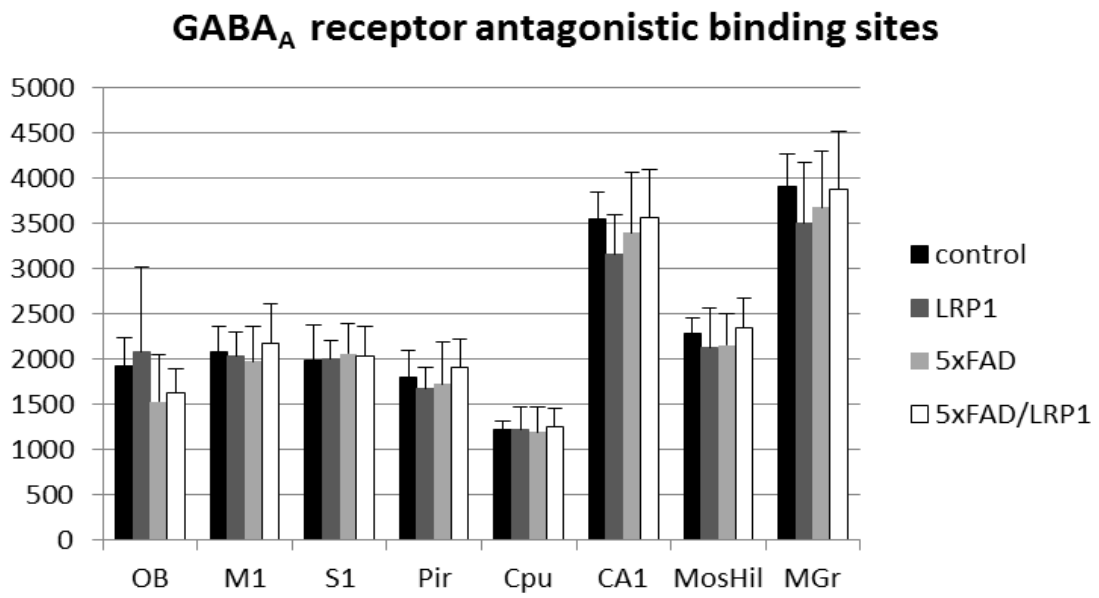

Figure 28: Bar charts demonstrating mean $GABA_{A\ ANT}$ receptor density (antagonist) together with standard deviation in all brain regions investigated of control (black), *LRP1* (dark grey), *tg5xFAD* (light grey) and *tg5xFAD/LRP1* (white) mice.

1.4.2 $GABA_A$ associated benzodiazepine binding sites (BZ)

Neither in the ***LRP1*** nor in the ***tg5xFAD*** or ***tg5xFAD/LRP1*** mice, any up- or downregulation was observed in any brain region (Figure 29).

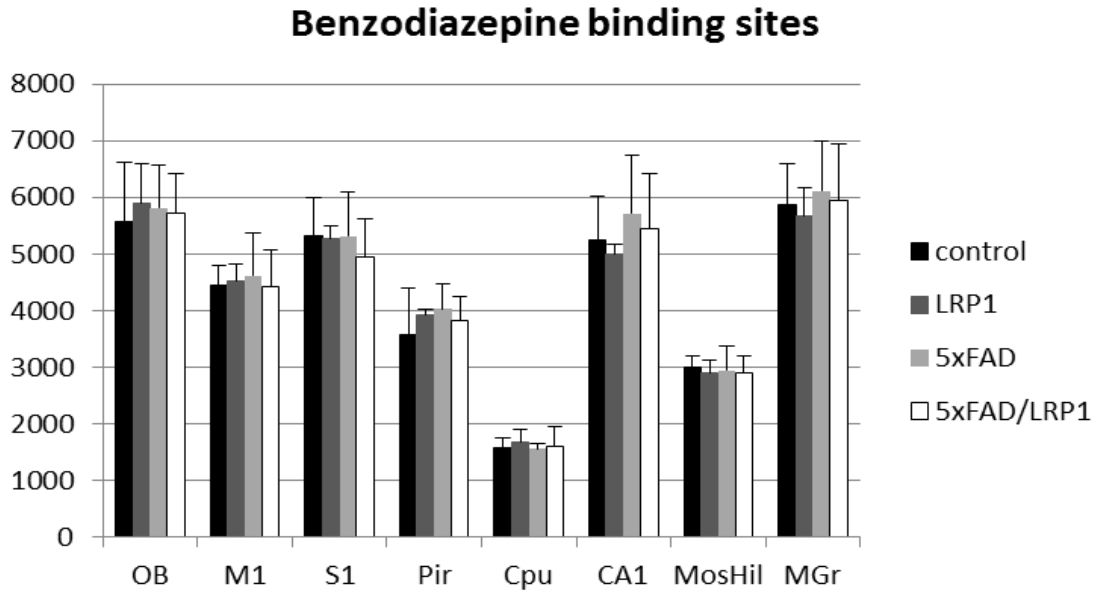

Figure 29: Bar charts demonstrating mean BZ receptor density together with standard deviation in all brain regions investigated of control (black), *LRP1* (dark grey), *tg5xFAD* (light grey) and *tg5xFAD/LRP1* (white) mice.

1.4.3 $GABA_B$ receptors

Statistical tests revealed a lower mean receptor density (21%; p=0.03) in the olfactory bulb of the ***LRP1*** compared to control mice. In the other regions, no changes could be observed.

Analyzing ***tg5xFAD*** mice, only a non-significant trend towards downregulation in the olfactory bulb could be observed.

In the ***tg5xFAD/LRP1*** mice, no decrease or increase of the mean receptor densities could be shown in any brain region, compare Figure 30.

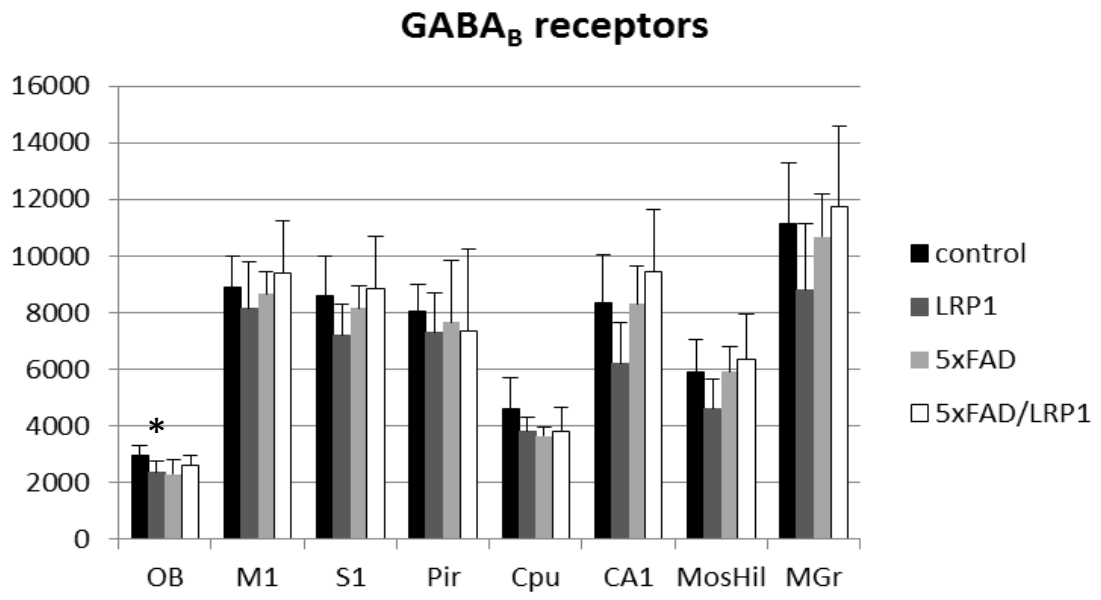

Figure 30: Bar charts demonstrating mean $GABA_B$ receptor density together with standard deviation in all brain regions investigated of control (black), *LRP1* (dark grey), *tg5xFAD* (light grey) and *tg5xFAD/LRP1* (white) mice. Significant differences are shown by *, p<0.05.

1.5 Adrenergic receptors

A Comparison of the two adrenergic receptors α_1 und α_2 revealed different regional distributions (Figure 31, Figure 32).

α_1 receptors showed the lowest mean density in the striatum and hippocampus, whereas piriform and somatosensory cortices showed intermediate densities. The highest density was found in the motor cortex and the olfactory bulb.

The highest density of α_2 receptors was observed in the stratum moleculare/granulosum and the piriform cortex. The lowest concentration was revealed in the striatum. Intermediate densities were observed in the CA1 region, hilus and mossy fiber termination fields and all other cortical areas (Figs. 30-31).

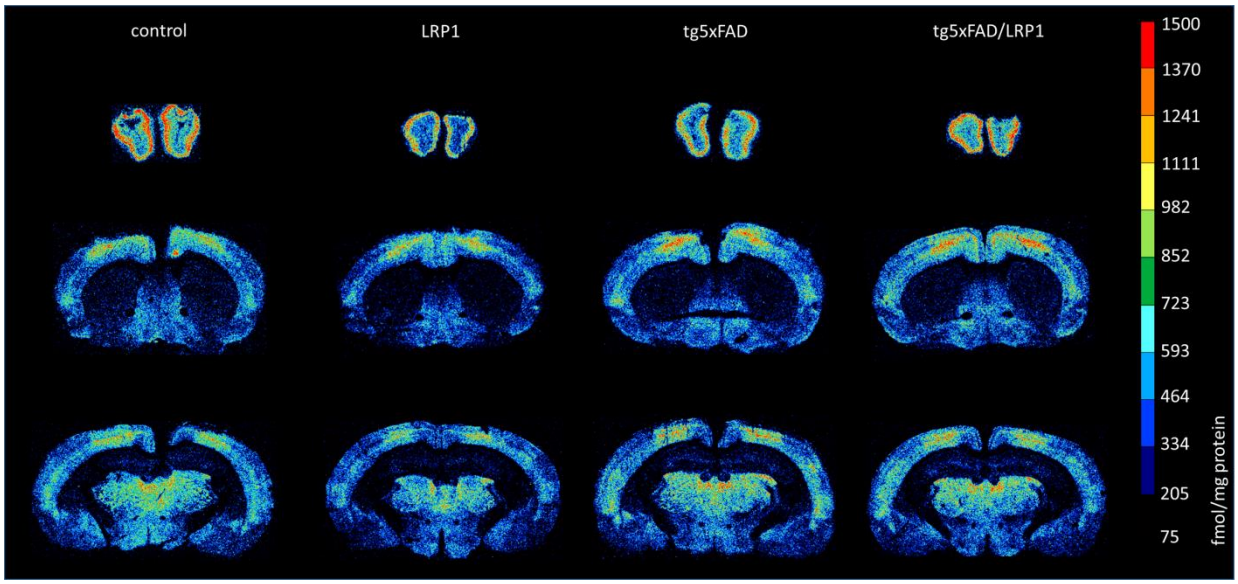

Figure 31: Color coded image of α_1 receptor densities (fmol/mg protein) in the brains of *tg5xFAD*, *LRP1* and *tg5xFAD/LRP1* mice compared to control mice. The images show a similar regional distribution of this receptor in all strains but differences in absolute receptor densities (see text).

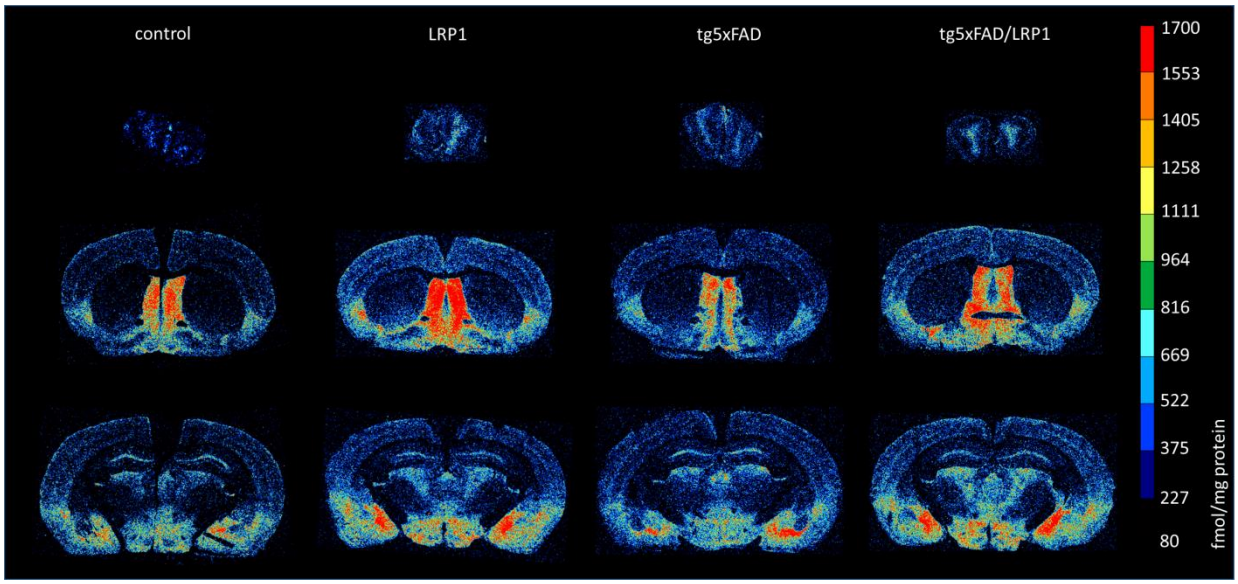

Figure 32: Color coded image of α_2 receptor densities (fmol/mg protein) in the brains of *tg5xFAD*, *LRP1* and *tg5xFAD/LRP1* mice compared to control mice. The images show a similar regional distribution of this receptor in all strains but differences in absolute receptor densities (see text).

1.5.1 α_1 receptor

In several regions of the brain of the ***LRP1*** mouse, the α_1 receptor was significantly downregulated, i.e. the olfactory bulb (23%; p=0.03), piriform (31%; p=0.05) and somatosensory (26%; p=0.05). A generally but not significantly lower mean density could be observed in all other regions of the ***LRP1*** model.

In neither of the other two models, ***tg5xFAD*** and ***tg5xFAD/LRP1***, significant differences were found compared to control mice, although a generally lower mean density was visible in all regions analyzed (Figure 33).

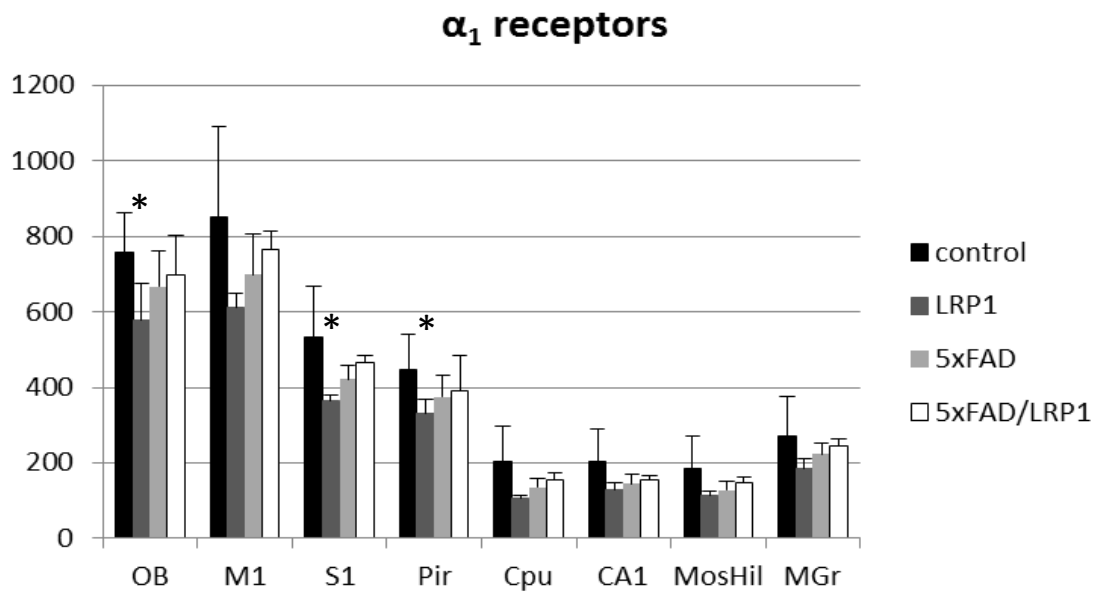

Figure 33: Bar charts demonstrating mean α_1 receptor density together with standard deviation in all brain regions investigated of control (black), *LRP1* (dark grey), *tg5xFAD* (light grey) and *tg5xFAD/LRP1* (white) mice. Significant differences are shown by *, p<0.05.

1.5.2 α_2 receptor

The mean densities of α_2 receptors were increased in all brain regions of the ***LRP1*** mouse. All differences were significant, with exception of the piriform cortex and stratum moleculare/granulosum of the fascia dentata. In the olfactory bulb α_2 receptor density was upregulated by 57% (p=0.02), in the motor cortex by 33% (p=0.05), in the somatosensory cortex by 47% (p=0.01) and in the striatum by 89% (p=0.0002). The receptor density was also increased in the hippocampal areas CA1 by 36% (p=0.01), in the mossy fiber termination fields/hilus by 41% (p=0.01).

The ***tg5xFAD*** mouse revealed a significant receptor upregulation in all brain regions. In the olfactory bulb, the mean receptor density was higher by 27% (p=0.01), in the motor cortex by 36% (p=0.004), in the somatosensory cortex by 31% (p=0.001), in the piriform cortex by 42% (p=0.04) and in the striatum by 55% (p=0.000004). In the hippocampal areas α_2 receptors were increased by 55% (p=0.0001) in CA1, by 49% (p=0.00002) in the mossy fiber termination fields/hilus and in the stratum moleculare/granulosum by 28% (p=0.005).

With exception of the stratum moleculare/granulosum of FD, all investigated brain regions in ***tg5xFAD/LRP1*** mice showed significant upregulations as well. The cortical areas revealed an

upregulation by 50% (p=0.0009) in the motor cortex, by 54% (p=0.0007) in the somatosensory cortex and by 57% (p=0.002) in the piriform cortex. In the olfactory bulb mean densities of α_2 receptors were increased by 38% (p=0.0001), in the striatum by 81% (p=0.00001), in CA1 by 53% (p=0.00002), in the mossy fiber termination fields/hilus by 61% (p=0.0001). The mean receptor density of the stratum moleculare/granulosum was not significantly different from controls, but showed a higher density as well (Figure 34).

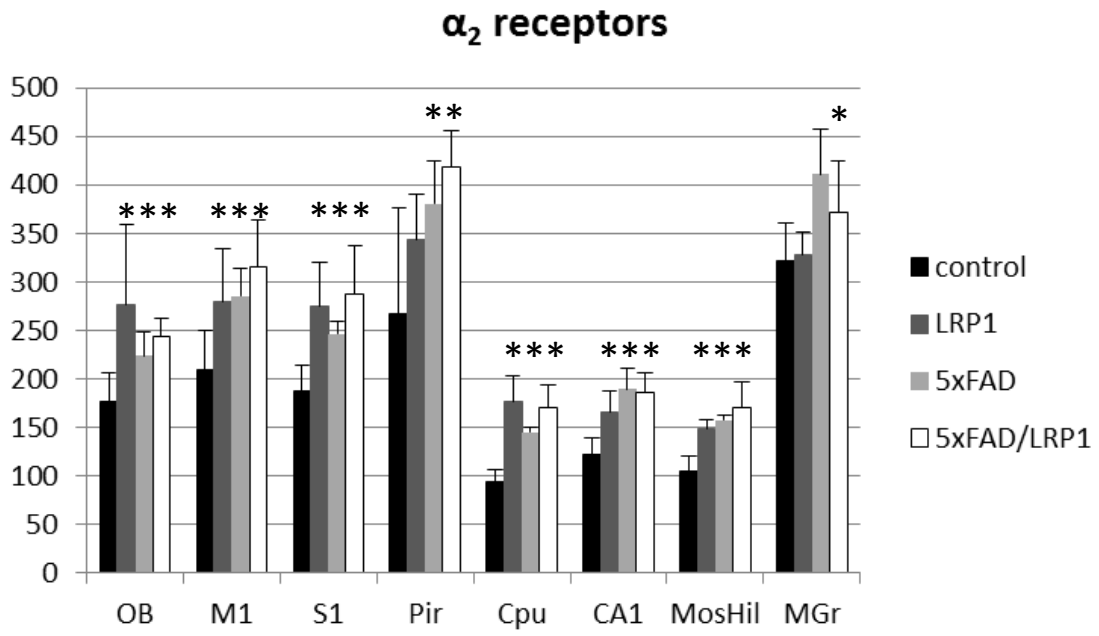

Figure 34: Bar charts demonstrating mean α_2 receptor density together with standard deviation in all brain regions investigated of control (black), *LRP1* (dark grey), *tg5xFAD* (light grey) and *tg5xFAD/LRP1* (white) mice. Significant differences are shown by *, p<0.05.

1.6 Dopamine receptors

Dopamine receptor densities were below detection limit in most of the analyzed brain regions with exception of the striatum (**D1, D2** and **D2/3** receptors), respectively (Figure 35 - Figure 37).

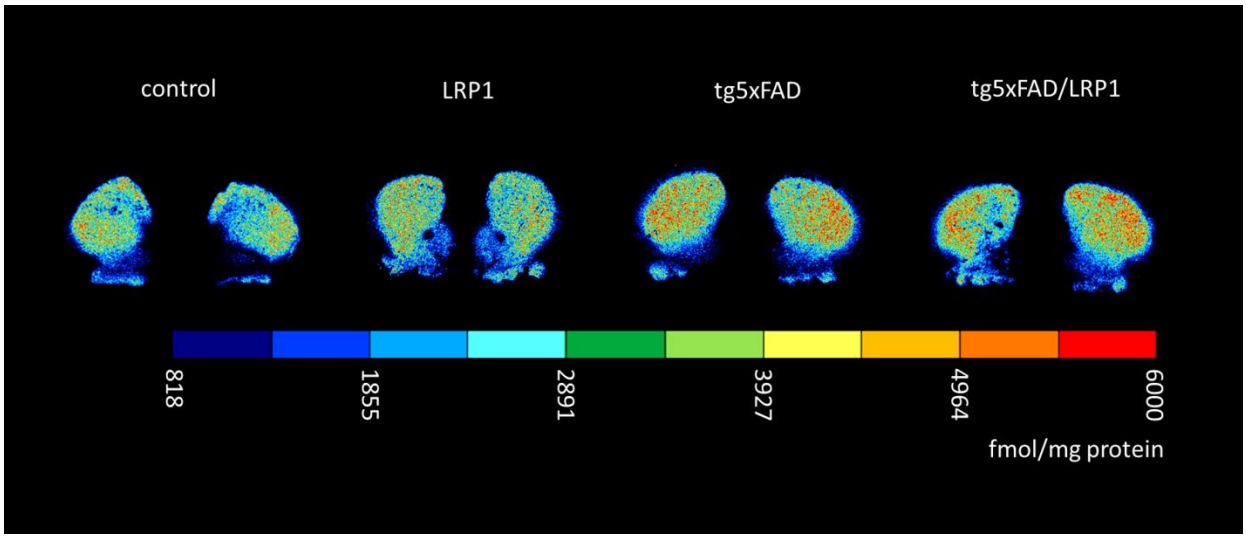

Figure 35: Color coded image of D_1 receptor densities (fmol/mg protein) in the brains of *tg5xFAD*, *LRP1* and *tg5xFAD/LRP1* mice compared to control mice. The images show a similar regional distribution of this receptor in all strains (see text).

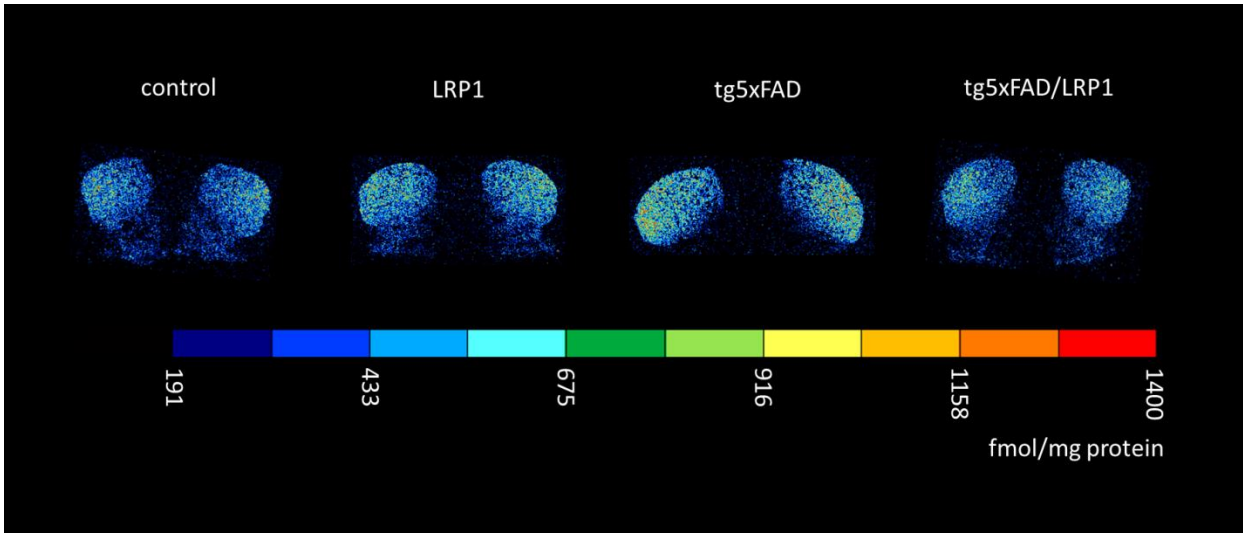

Figure 36: Color coded image of D_2 receptor densities (fmol/mg protein) in the brains of *tg5xFAD*, *LRP1* and *tg5xFAD/LRP1* mice compared to control mice. The images show a similar regional distribution of this receptor in all strains but differences in absolute receptor densities (see text).

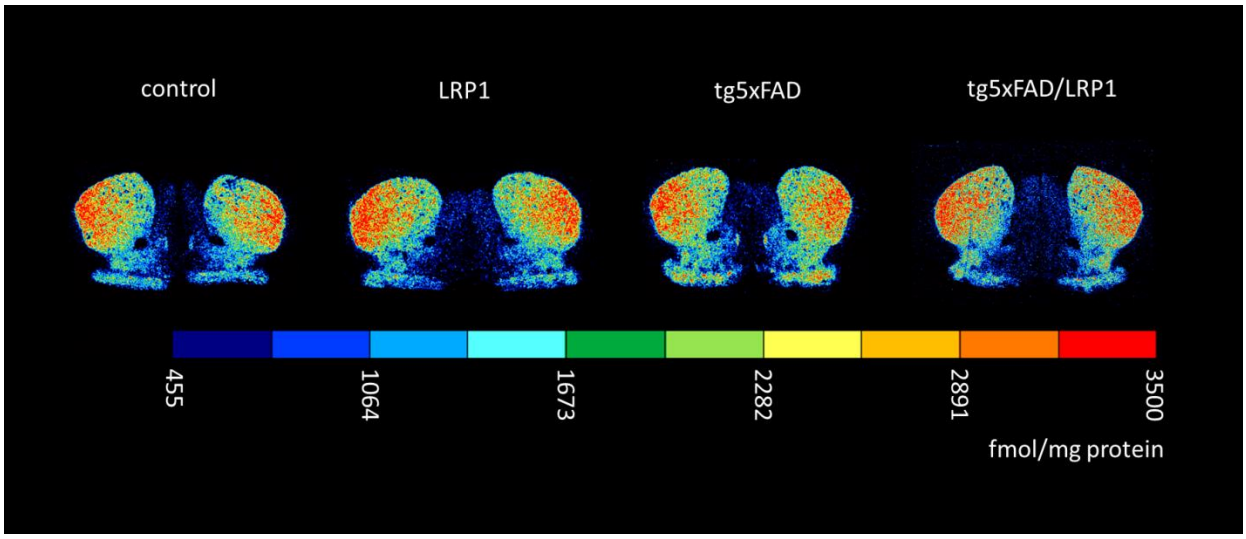

Figure 37: Color coded image of $D_{2/3}$ receptor densities (fmol/mg protein) in the brains of *tg5xFAD*, *LRP1* and *tg5xFAD/LRP1* mice compared to control mice. The images show a similar regional distribution of these receptors in all strains (see text).

1.6.1 D_1 receptor

No significant differences were observed in the striatum of ***LRP1, tg5xFAD/LRP1*** and ***tg5xFAD*** compared to control mice (Figure 38).

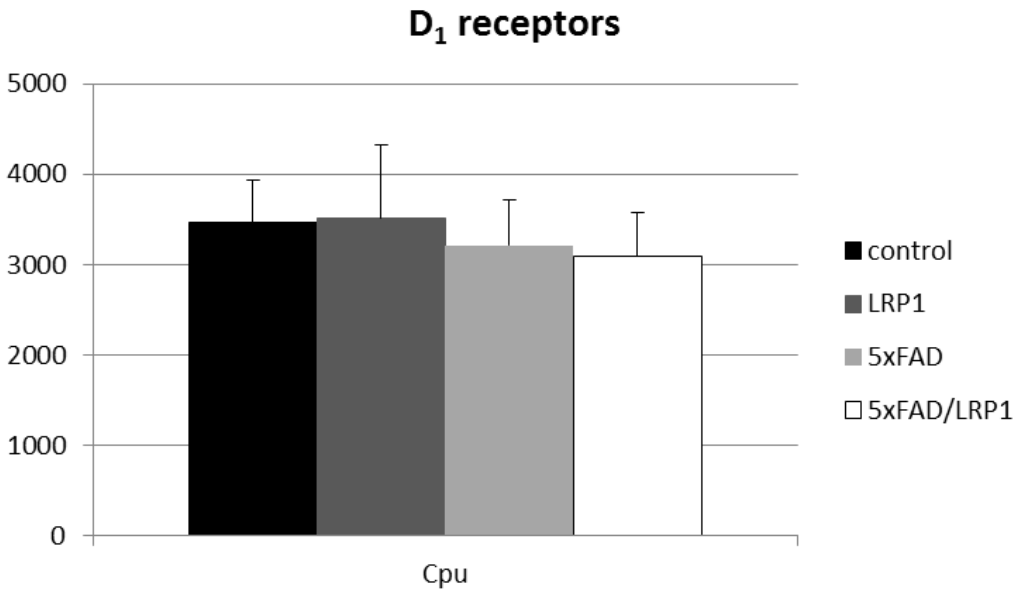

Figure 38: Bar charts demonstrating mean D_1 receptor density together with standard deviation in the striatum of control (black), *LRP1* (dark grey), *tg5xFAD* (light grey) and *tg5xFAD/LRP1* (white) mice. CPu caudatus-putamen (striatum).

1.6.2 D_2 receptor

In the ***LRP1*** and ***tg5xFAD/LRP1*** mice, no decrease or increase of the mean receptor density could be shown in the striatum. In all other brain regions, receptor density was below detection limit using receptor autoradiography. The comparison of ***tg5xFAD*** and control mice revealed an upregulation in the striatum of ***tg5xFAD*** mice (Figure 39).

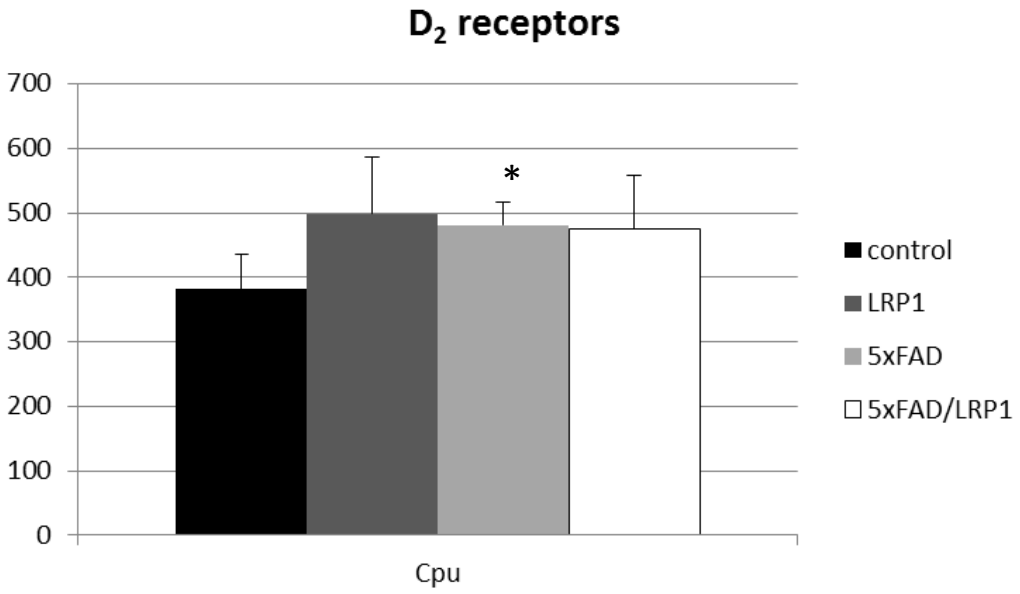

Figure 39: Bar charts demonstrating mean D_2 receptor density together with standard deviation in the striatum of control (black), *LRP1* (dark grey), *tg5xFAD* (light grey) and *tg5xFAD/LRP1* (white) mice. Significant differences are shown by *, $p<0.05$.

1.6.3 $D_{2/3}$ receptor

$D_{2/3}$ receptor density was not significantly different in any region analyzed in the ***LRP1***, ***tg5xFAD/LRP1,*** and ***tg5xFAD*** mice compared to control mice (Figure 40).

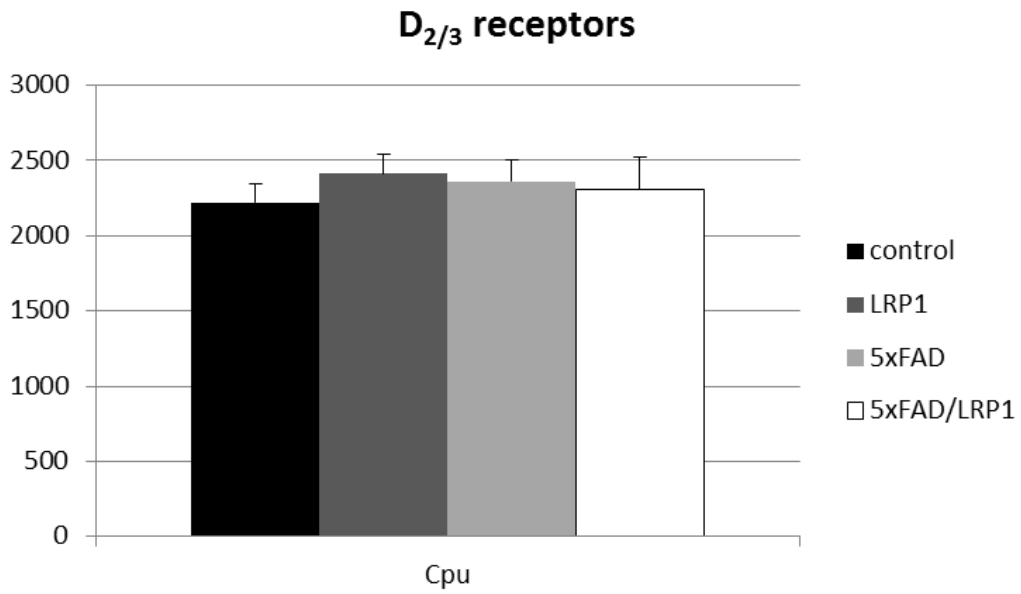

Figure 40: Bar charts demonstrating mean $D_{2/3}$ receptor density together with standard deviation in the striatum of control (black), *LRP1* (dark grey), *tg5xFAD* (light grey) and *tg5xFAD/LRP1* (white) mice.

1.7 Adenosine receptor A_2

As seen in dopamine receptors, adenosine A_2 receptors were only detectable in the striatum.

All other analyzed brain regions were below detection limit (Figure 41).

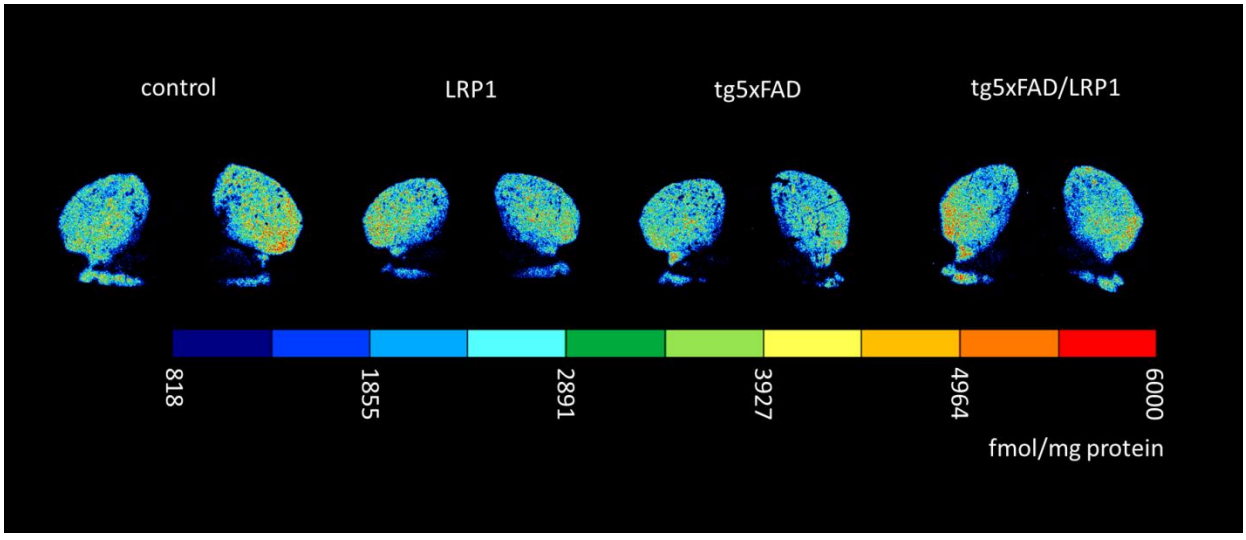

Figure 41: Color coded image of A_2 receptor densities (fmol/mg protein) in the brains of *tg5xFAD*, *LRP1* and *tg5xFAD/LRP1* mice compared to control mice. The images show a similar regional distribution of this receptor in all strains (see text).

1.7.1 A_2 receptor

The ***LRP1, tg5xFAD/LRP1*** and ***tg5xFAD*** mice did not show significant differences of the mean receptor densities when compared to controls in the striatum (Figure 42).

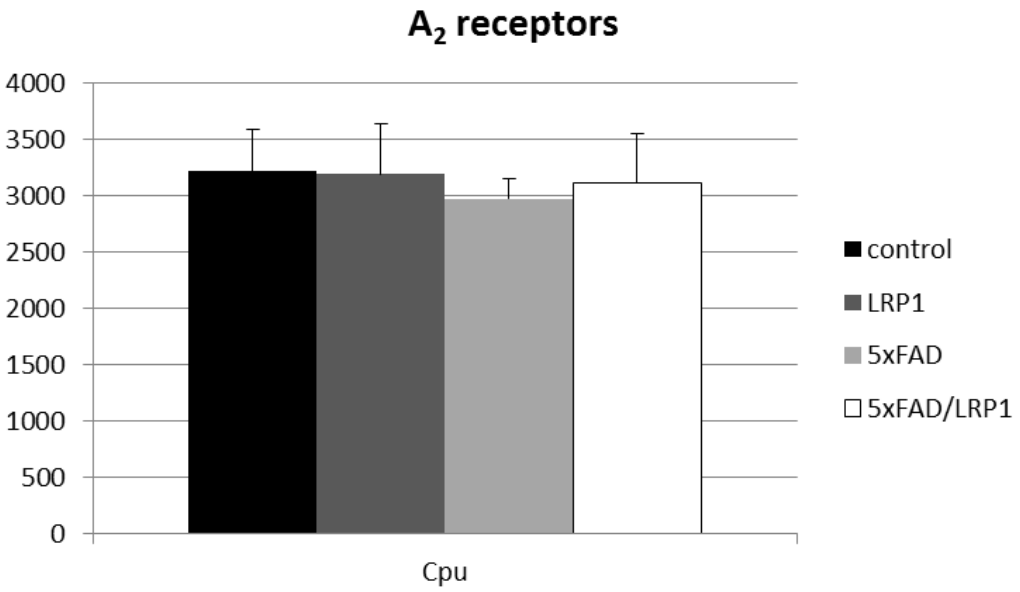

Figure 42: Bar charts demonstrating mean A_2 receptor density together with standard deviation in the striatum of control (black), *LRP1* (dark grey), *tg5xFAD* (light grey) and *tg5xFAD/LRP1* (white) mice.

Summary of all significant differences between *LRP1*, *tg5xFAD* and *tg5xFAD/LRP1* mice compared to controls

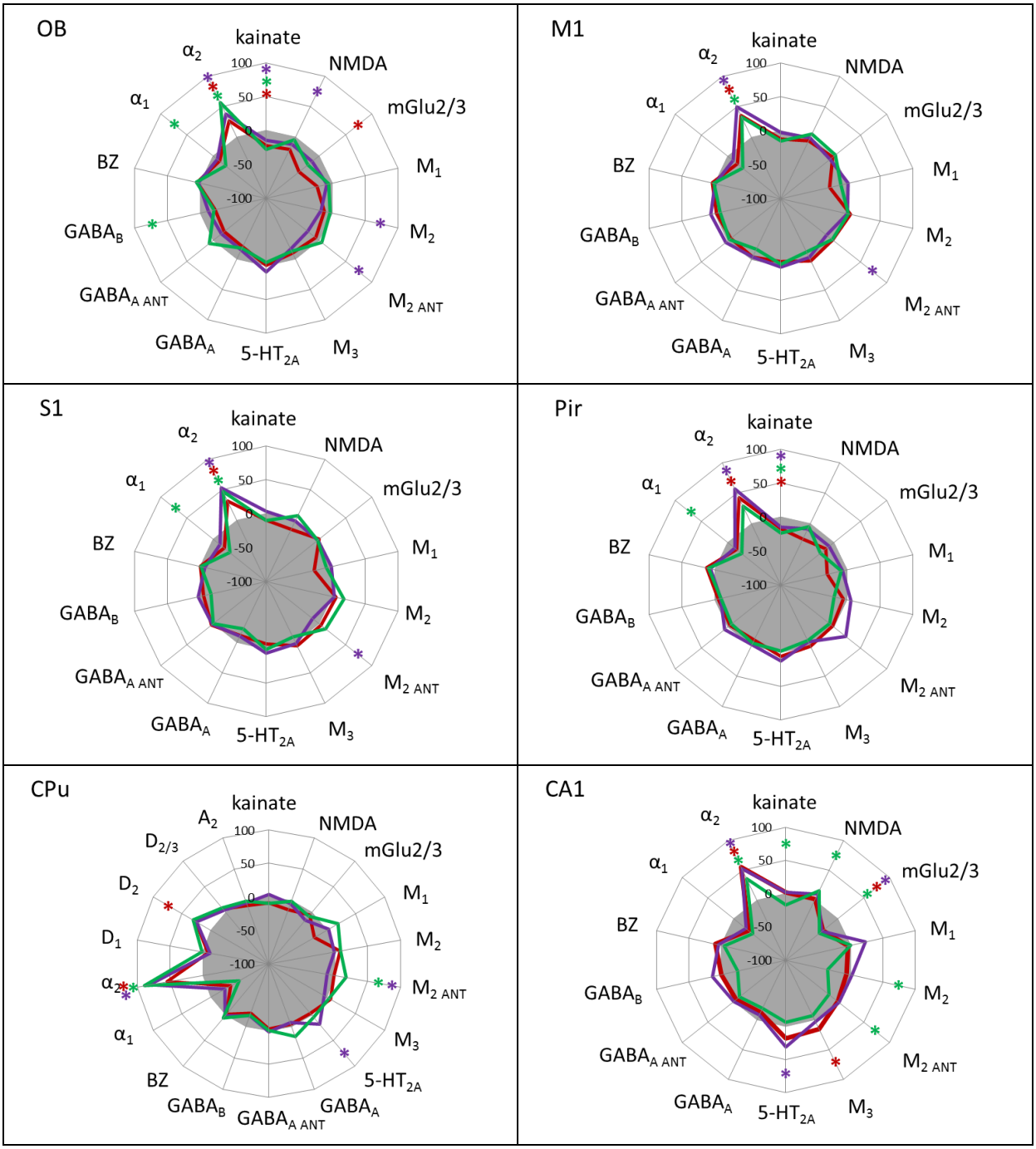

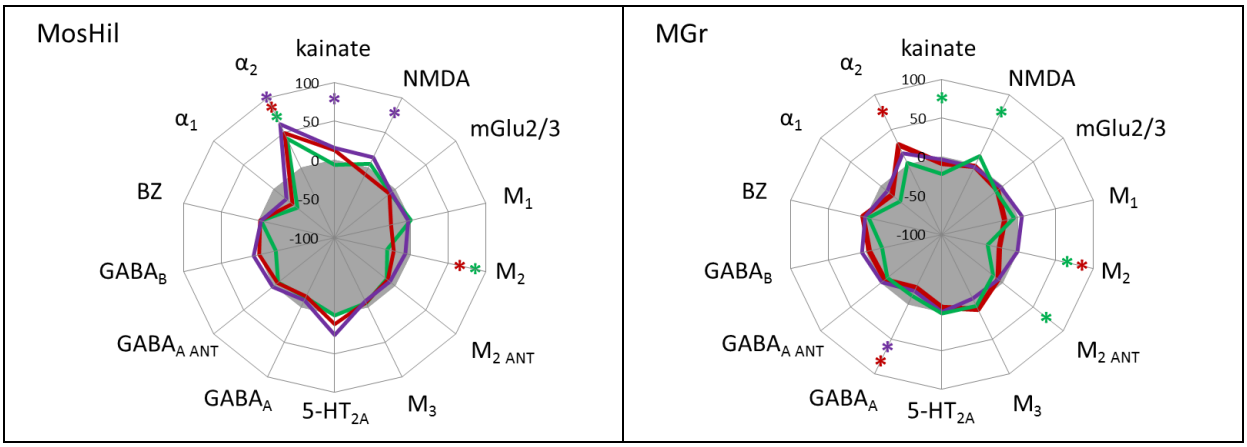

Figure 43: Polar plots of mean receptor densities in 8 different brain regions of control (grey), *LRP1* (green), *tg5xFAD* (red) and *tg5xFAD/LRP1* mice (purple). Values were normalized to the mean value of control animals, respectively. Significant differences are indicated by *.

2 Neurotransmitter receptor densities in brains of *tgArcAβ* mice

2.1 Glutamate receptors

The principal regional distribution patterns of AMPA, NMDA, kainate and mGlu2/3 receptors were similar between control mice and ***tgArcAβ*** mice (Figure 44).

The lowest mean density of **AMPA** receptors was found in the olfactory bulb, followed by the striatum and cortical regions. The highest concentration was found in the hippocampus. **Kainate** receptors showed the lowest mean density in the CA1 region of the hippocampus and highest values in the mossy fiber termination fields, the olfactory bulb, motor, somatosensory and piriform cortices, hilus and stratum moleculare/granulosum. **NMDA** receptors had a regional distribution within the brain similar to that of kainate receptors. Only the hippocampal area differed, with a higher density of NMDA receptors in the CA1 region. Furthermore, the mossy fiber termination fields showed a lower density compared to kainate receptors. The density of the metabotropic Glu2/3 (**mGlu2/3**) receptors is higher in the cortical areas, the striatum and the stratum moleculare/granulosum than in the olfactory bulb and the remaining areas of the hippocampus.

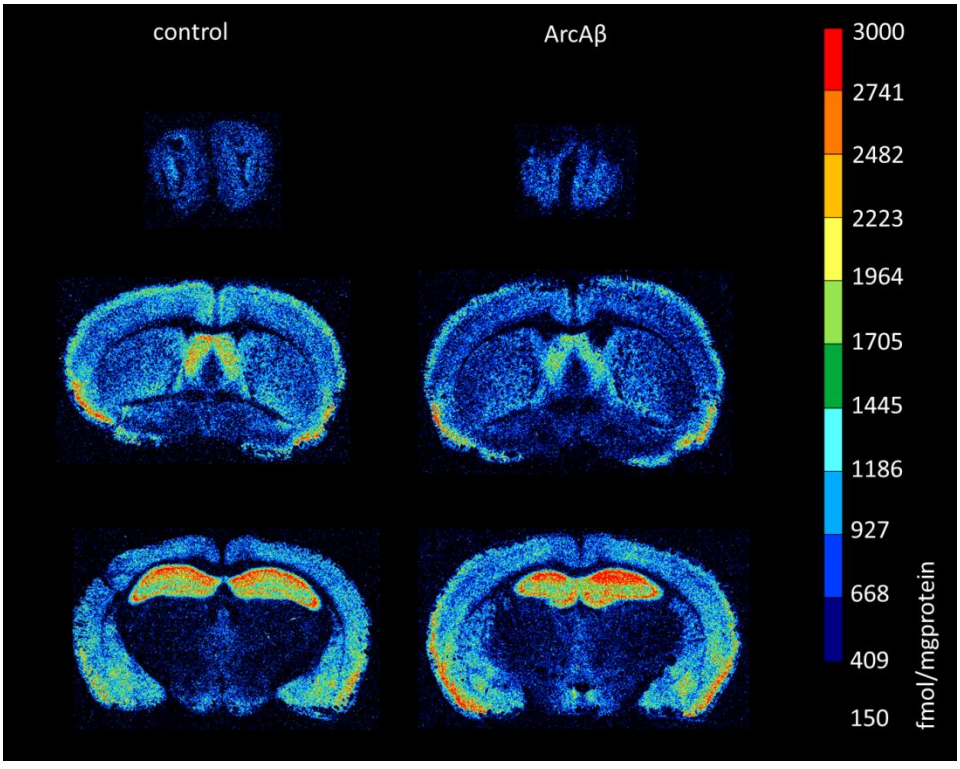

Figure 44: Color coded image of AMPA receptor densities (fmol/mg protein) in the brains of *tgArcAβ* compared to control mice. The images show a similar regional distribution of this receptor in both strains.

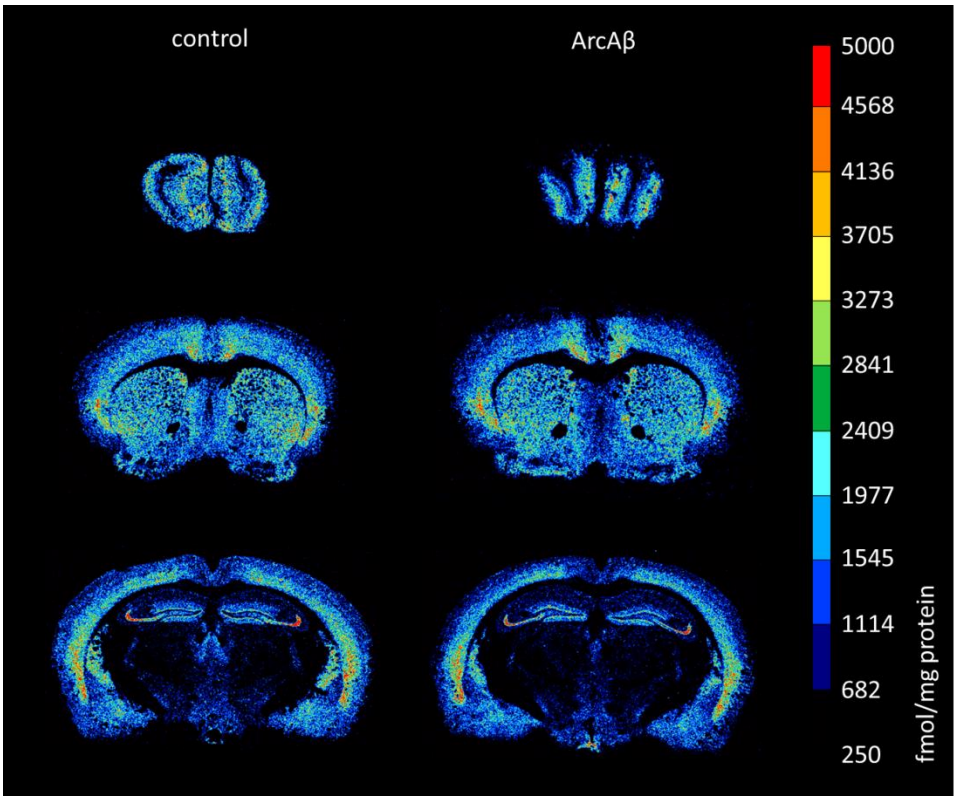

Figure 45: Color coded image of kainate receptor densities (fmol/mg protein) in the brains of *tgArcAβ* compared to control mice. The images show a similar regional distribution of this receptor in both strains but differences in absolute receptor densities (see text).

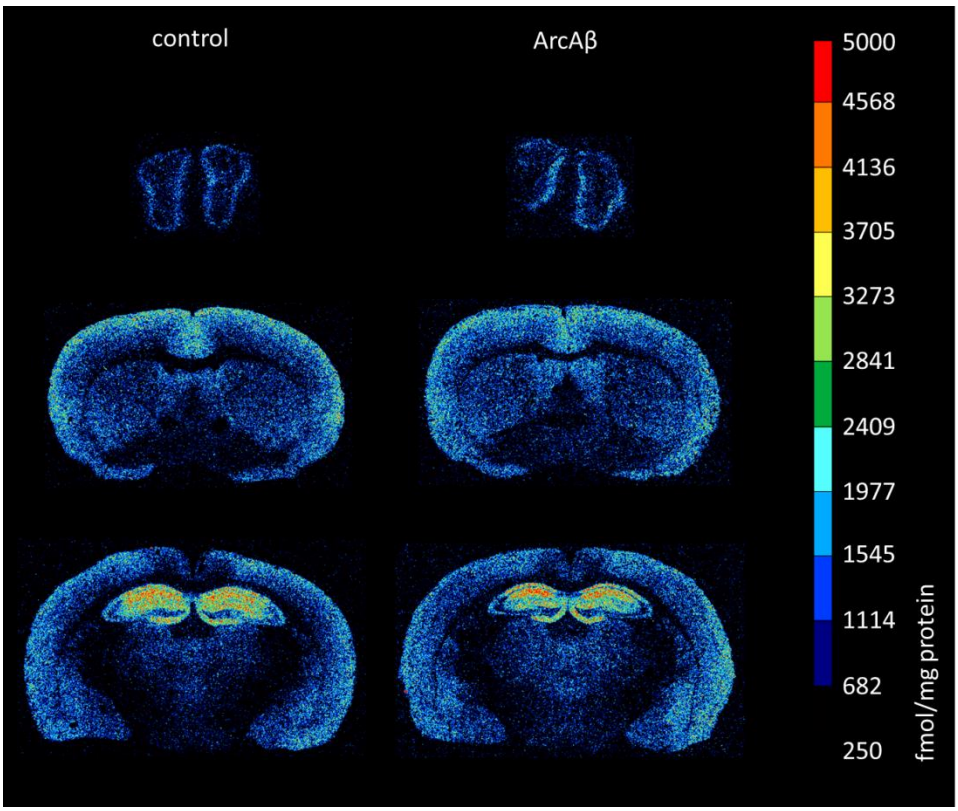

Figure 46: Color coded image of NMDA receptor densities (fmol/mg protein) in the brains of *tgArcAβ* compared to control mice. The images show a similar regional distribution of this receptor in both strains but differences in absolute receptor densities (see text).

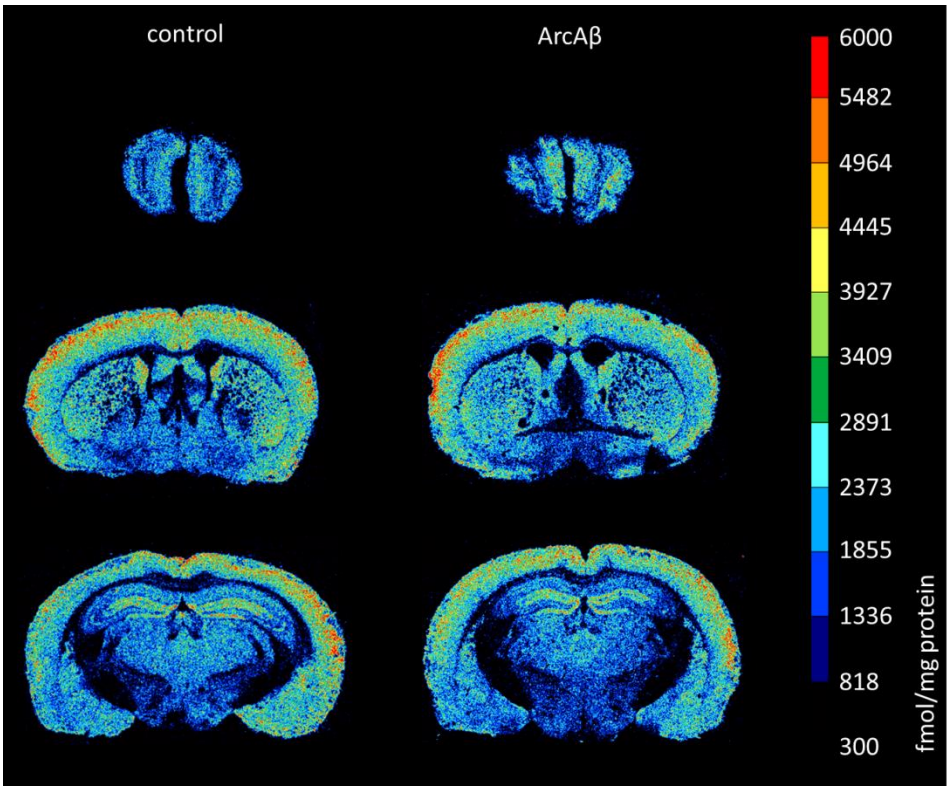

Figure 47: Color coded image of mGlu2/3 receptor densities (fmol/mg protein) in the brains of *tgArcAβ* compared to control mice. The images show a similar regional distribution of this receptor in both strains.

2.1.1 AMPA receptor

No significant differences could be observed in any brain region between ***tgArcAβ*** and control mice (Figure 48).

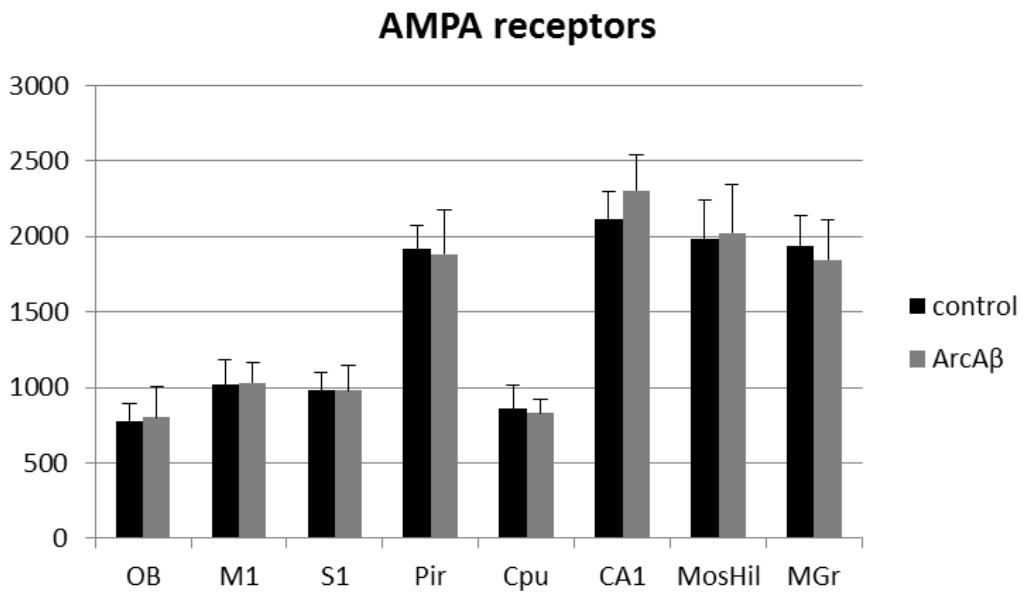

Figure 48: Bar charts demonstrating mean AMPA receptor density together with standard deviation in all brain regions investigated of control (black) and *tgArcAβ* (grey) mice.

2.1.2 Kainate receptor

In the motor cortex of ***tgArcAβ*** mice, the mean density of kainate receptors was significantly lower by 15% (p=0.02) when compared to controls. In the striatum, kainate receptors were downregulated by 14% (p= 0.0006) (Figure 49). Significant differences were not found in any other brain region.

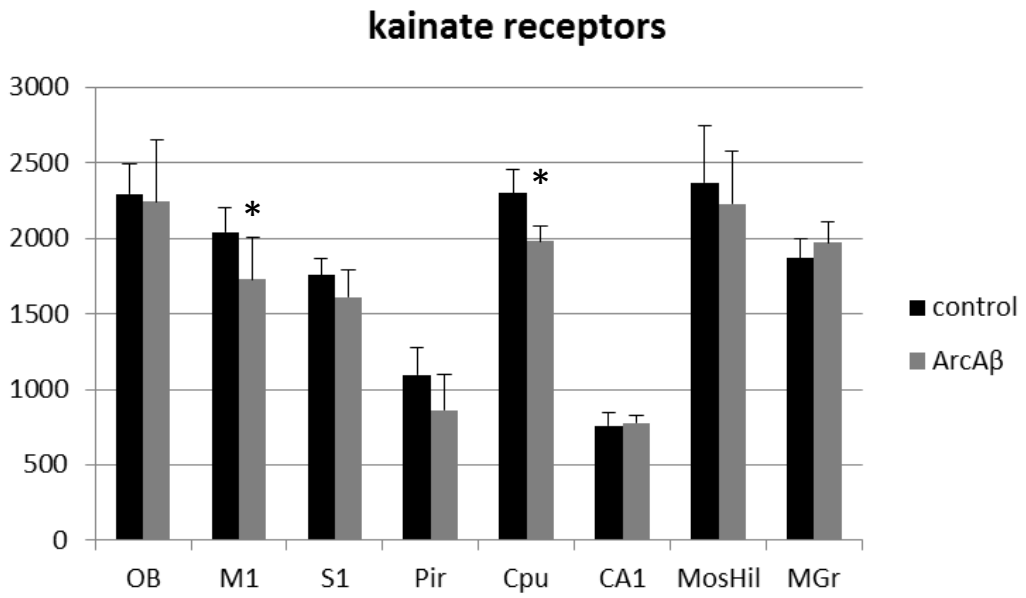

Figure 49: Bar charts demonstrating mean kainate receptor density together with standard deviation in all brain regions investigated of control (black) and *tgArcAβ* (grey) mice. Significant differences are shown by *, $p<0.05$.

2.1.3 NMDA receptor

Comparison of the mean density of ***tgArcAβ*** and control mice revealed an upregulation of the NMDA receptors in several cortical areas. The mean density in the motor cortex was increased by 22% ($p=0.04$) and in the piriform cortex by 26% ($p=0.02$; Figure 50).

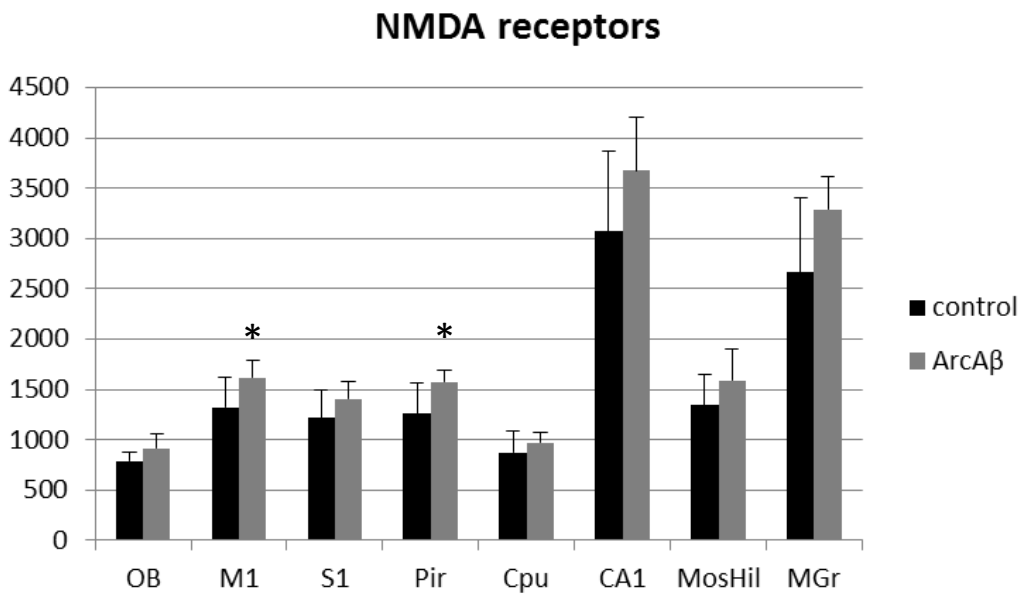

Figure 50: Bar charts demonstrating mean NMDA receptor density together with standard deviation in all brain regions investigated of control (black) and *tgArcAβ* (grey) mice. Significant differences are shown by *, $p<0.05$.

2.1.4 mGlu2/3 receptor

In all brain regions, no significant differences in mGlu2/3 receptor density between ***tgArcAβ*** and control mice were found (Figure 51).

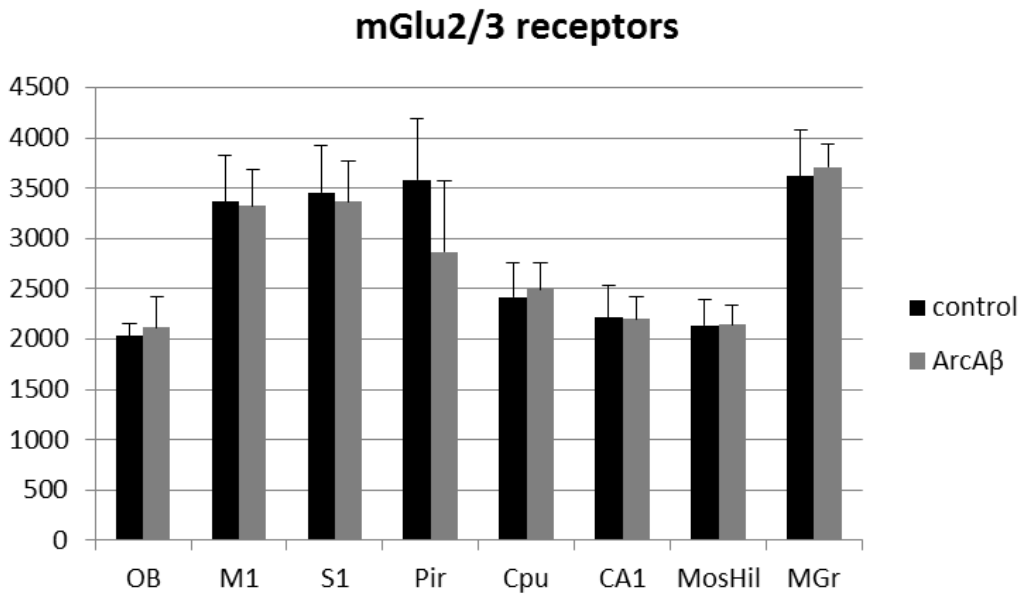

Figure 51: Bar charts demonstrating mean mGlu2/3 receptor density together with standard deviation in all brain regions investigated of control (black) and *tgArcAβ* (grey) mice.

2.2 Cholinergic receptors

The **M_1** receptor density reached lowest levels in the olfactory bulb, mossy fiber terminal fields and hilus. Highest densities were found in the striatum, stratum moleculare/granulosum and the CA1 region, and intermediate values in the other cortical areas.

M_2 receptor density reached highest values in the olfactory bulb, striatum, and somatosensory cortex. Intermediate values were observed in the piriform cortex and mossy fiber termination fields. The density was lowest in the hippocampal regions CA1, hilus and stratum moleculare/granulosum (Figure 52 - 52).

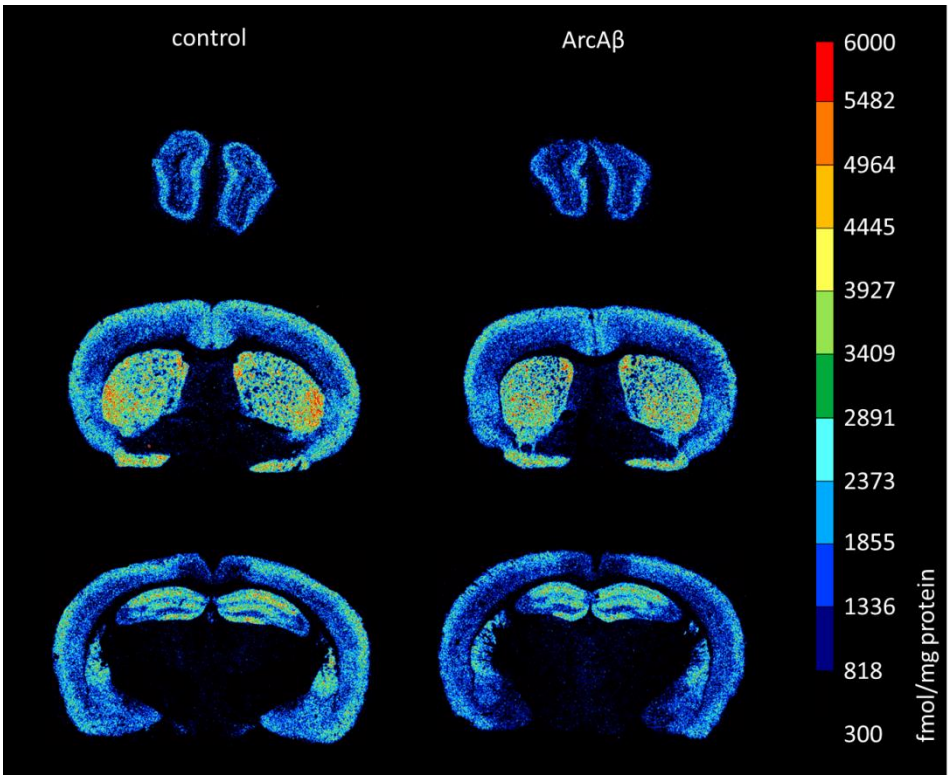

Figure 52: Color coded image of M_1 receptor densities (fmol/mg protein) in the brains of *tgArcAβ* compared to control mice. The images show a similar distribution of these receptors in both strains.

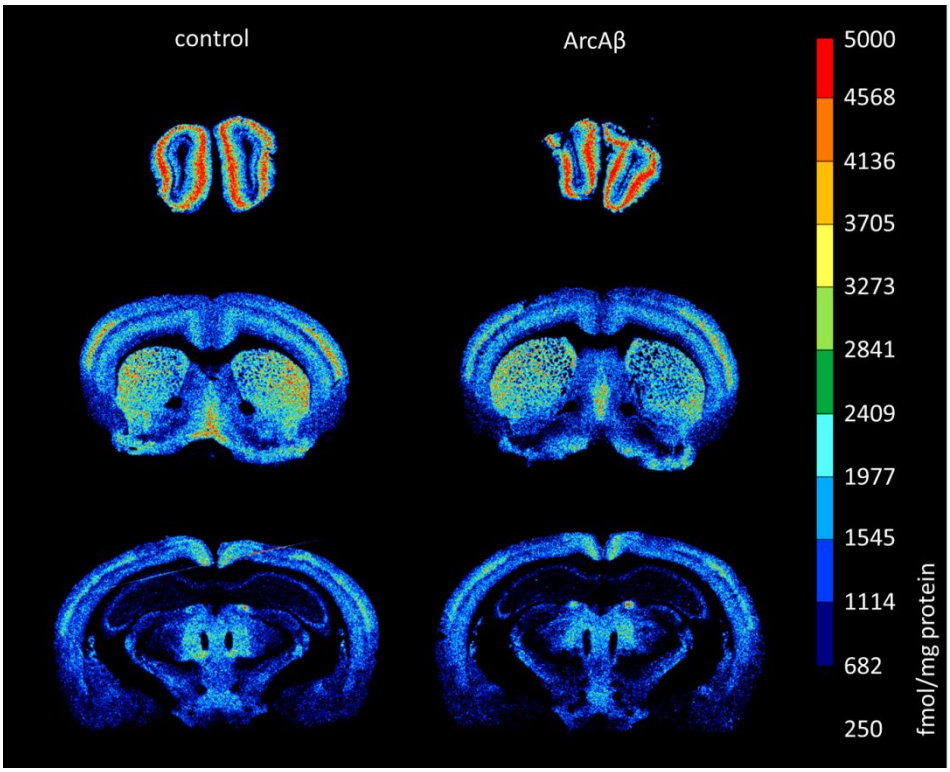

Figure 53: Color coded image of M_2 receptor densities (fmol/mg protein) in the brains of *tgArcAβ* compared to control mice. The images show a similar distribution of these receptors in both strains but differences in absolute receptor densities (see text).

2.2.1 Muscarinic acetylcholine receptor M_1

In a comparison of ***tgArcAβ*** with control mice, no significant differences could be observed in any area (Figure 54).

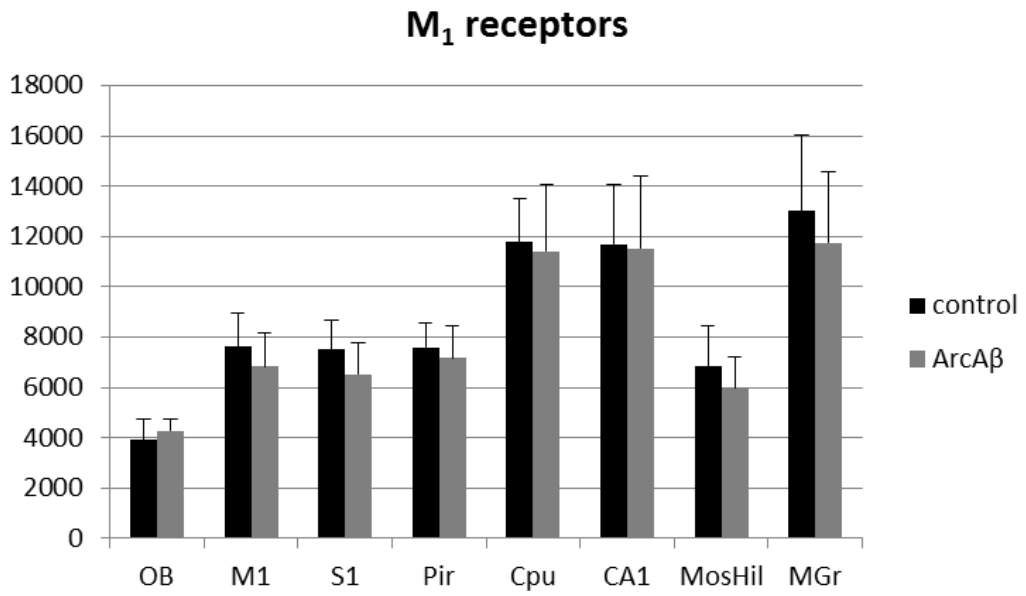

Figure 54: Bar charts demonstrating mean M_1 receptor density together with standard deviation in all brain regions investigated of control (black) and *tgArcAβ* (grey) mice.

2.2.2 Muscarinic acetylcholine receptor M_2

Analyzing the mean receptor density of the acetylcholine receptor M_2 between ***tgArcAβ*** and control mice a higher density was found in the somatosensory cortex of ***tgArcAβ*** (16%; p=0.02) In the CA1 region, M_2 receptors were decreased by 10% (p=0.03; Figure 55).

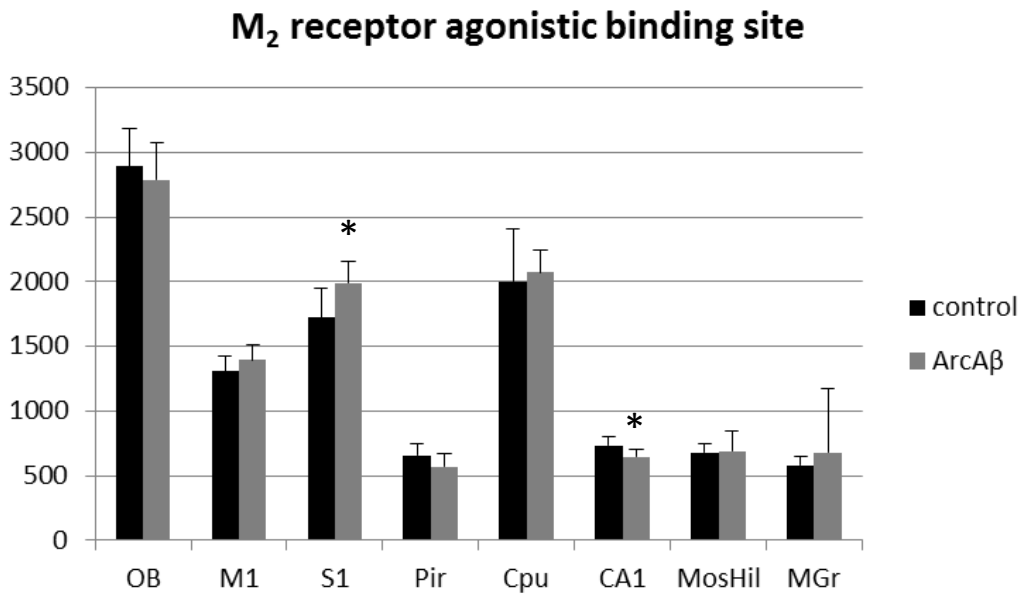

Figure 55: Bar charts demonstrating mean M_2 receptor density ([^{3}H]-Oxotremorine-M) together with standard deviation in all brain regions investigated of control (black) and *tgArcAβ* (grey) mice. Significant differences are shown by *.

2.3 Serotonin receptors

The 5-HT_{1A} und 5-HT_{2A} receptors showed a considerably different regional distribution (Figure 56 - Figure 57). 5-HT_{1A} receptors had their lowest mean density in the olfactory bulb, whereas cortical areas showed intermediate values. The highest density could be found in the CA1 region of the hippocampus. In the striatum, the density was close to the detection limit (Figure 56).

The 5-HT_{2A} receptor had a higher mean density than the 5-HT_{1A} receptor throughout the whole brain, with its highest density in the striatum and intermediate values in cortical areas.

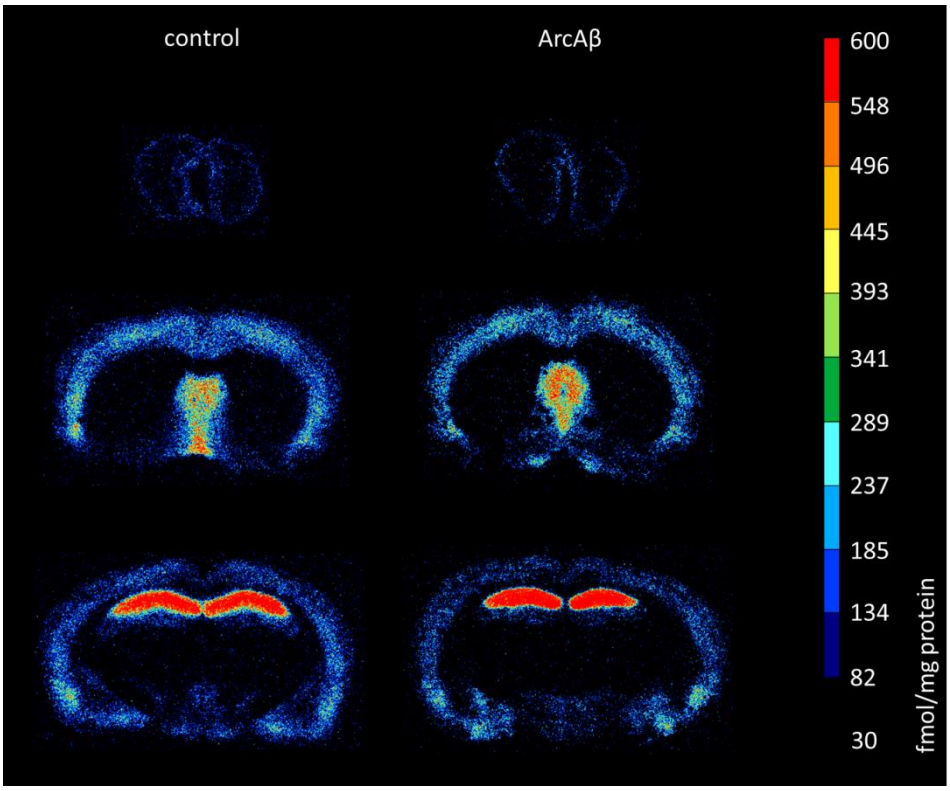

Figure 56: Color coded image of 5-HT_{1A} receptor densities (fmol/mg protein) in the brains of *tgArcAβ* compared to control mice. The images show a similar distribution of these receptors in both strains but differences in absolute receptor densities (see text).

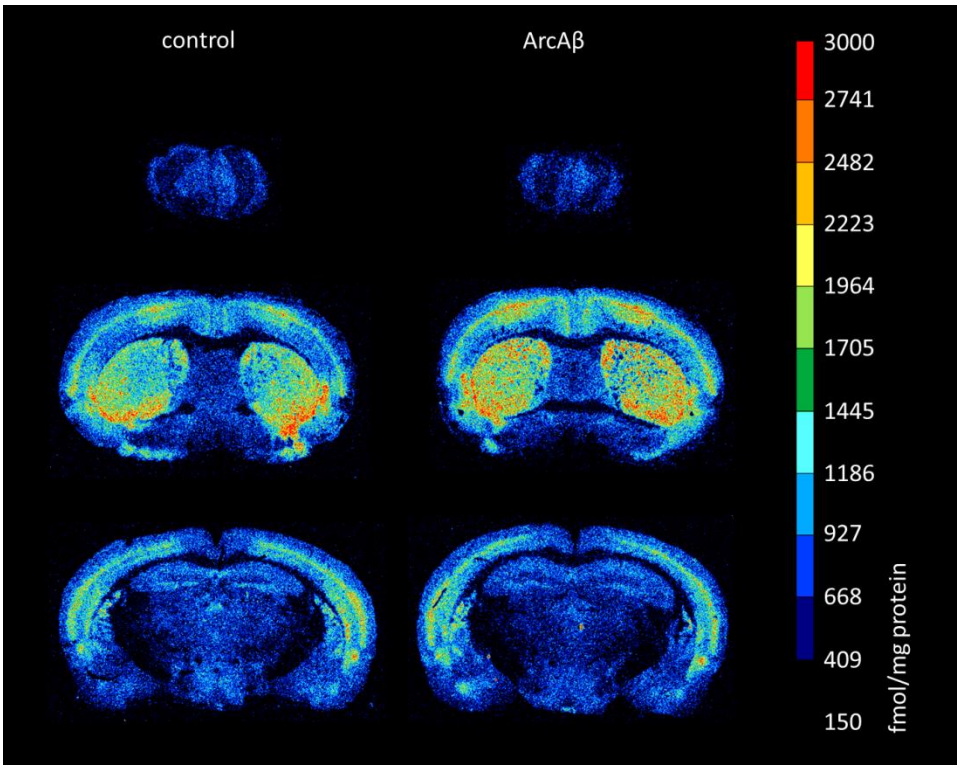

Figure 57: Color coded image of 5-HT_{2A} receptor densities (fmol/mg protein) in the brains of *tgArcAβ* compared to control mice. The images show a similar distribution of these receptors in both strains but differences in absolute receptor densities (see text).

2.3.1 5-HT$_{1A}$ receptor

No significant differences were observed in the brains of ***tgArcAβ*** compared to control mice, except for the CA1 region. The mean receptor density of 5-HT$_{1A}$ receptors is upregulated by 13% (p=0.03; Figure 58).

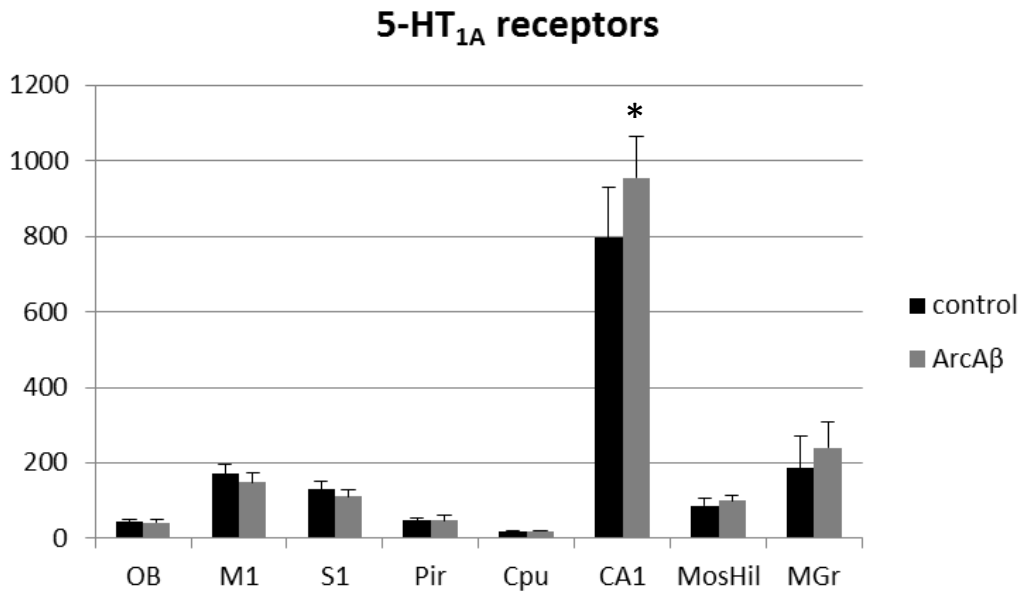

Figure 58: Bar charts demonstrating mean 5-HT$_{1A}$ receptor density together with standard deviation in all brain regions investigated of control (black) and *tgArcAβ* (grey) mice. Significant differences are shown by *.

2.3.2 5-HT$_{2A}$ receptor

5-HT$_{2A}$ receptors were upregulated in several regions. The motor (10%; p=0.02) and somatosensory cortices (10%; p=0.01) reached slightly higher densities in ***tgArcAβ*** compared to control mice. In the striatum, a significantly higher density could also be observed (12%; p=0.002; Figure 59).

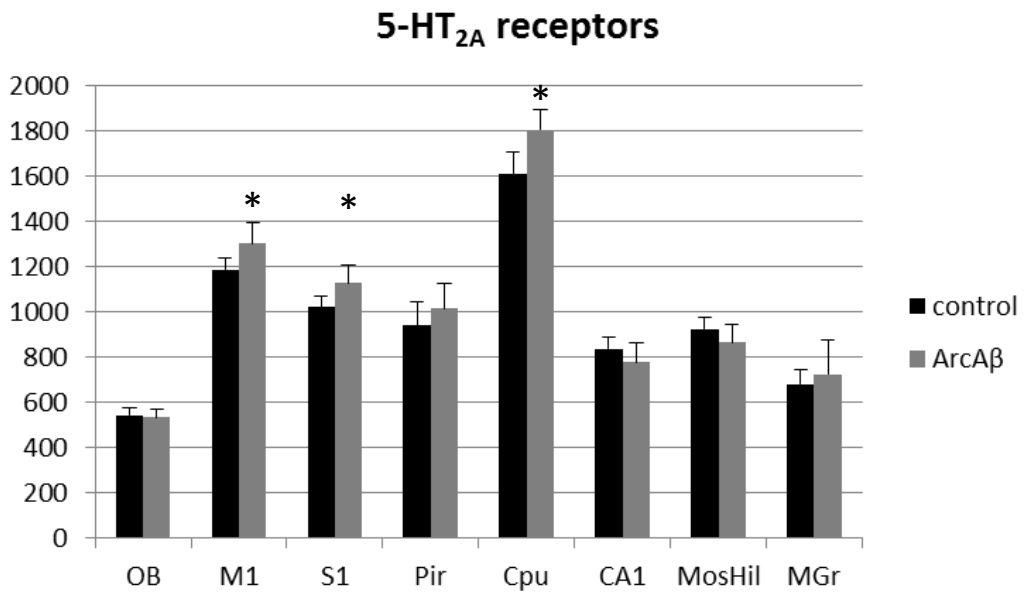

Figure 59: Bar charts demonstrating mean 5-HT_{2A} receptor density together with standard deviation in all brain regions investigated of control (black) and *tgArcAβ* (grey) mice. Significant differences are shown by *.

2.4 GABA receptors

All receptors of the GABAergic system showed a similar regional distribution throughout the brain, as demonstrated in Figure 60 - Figure 62. An exception is the mean density of BZ receptor binding sites in the olfactory bulb, which is higher than $GABA_A$ and $GABA_B$ receptors. $GABA_A$ and $GABA_B$ receptors showed the highest mean densities in the olfactory bulb, and in the cortical areas including the hippocampal regions CA1 and stratum moleculare/granulosum. The mossy fiber termination fields showed the lowest values. Highest densities of BZ receptor binding sites were found in the olfactory bulb.

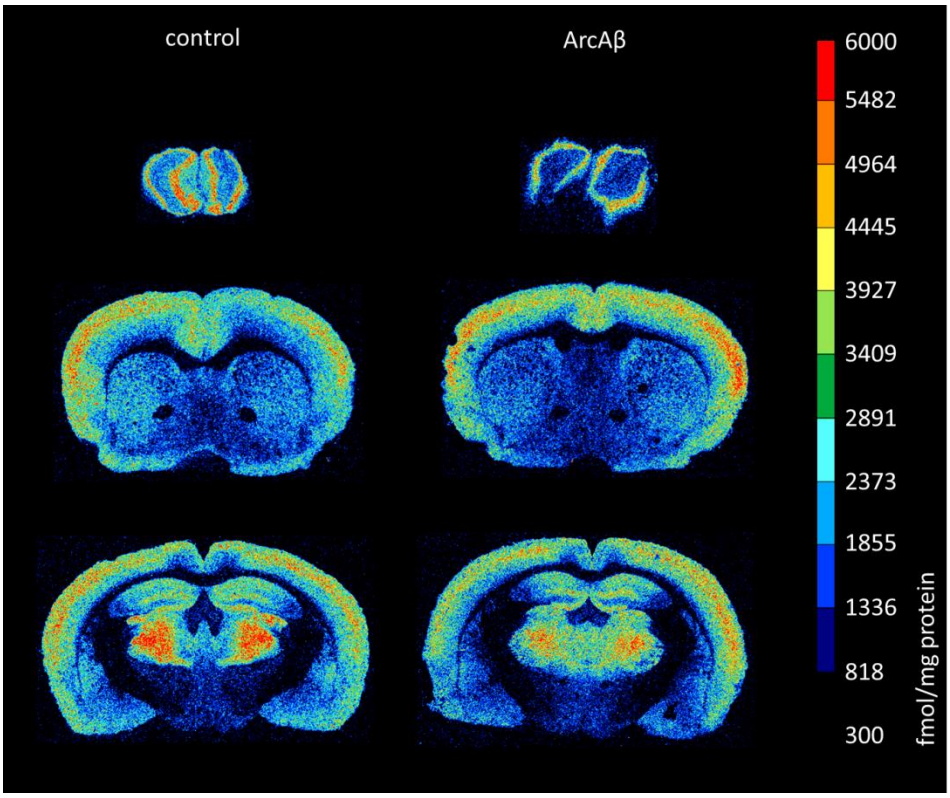

Figure 60: Color coded image of $GABA_A$ receptor densities (fmol/mg protein) in the brains of *tgArcAβ* compared to control mice. The images show a similar distribution of these receptors in both strains but differences in absolute receptor densities (see text).

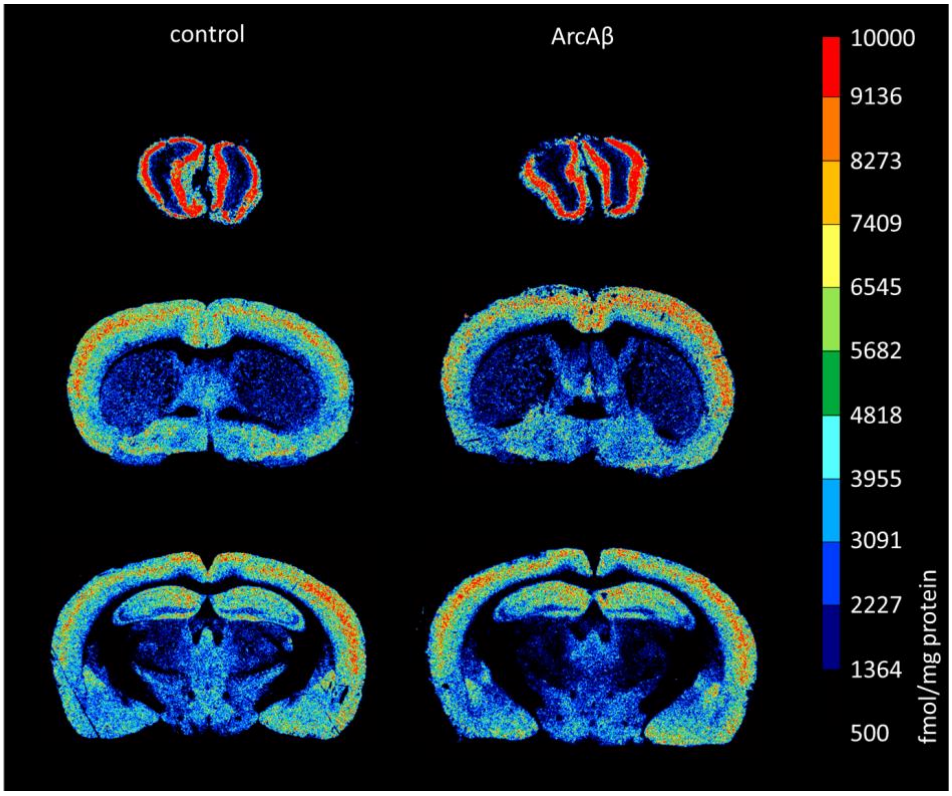

Figure 61: Color coded image of BZ receptor densities (fmol/mg protein) in the brains of *tgArcAβ* compared to control mice. The images show a similar distribution of these receptors in both strains.

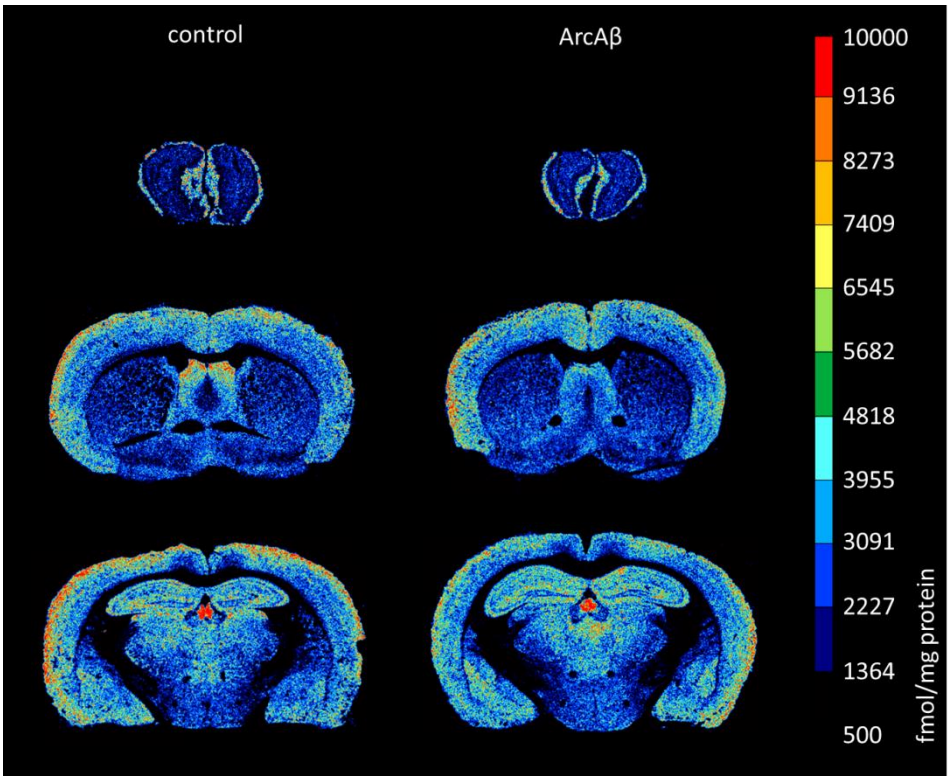

Figure 62: Color coded image of $GABA_B$ receptor densities (fmol/mg protein) in the brains of *tgArcAβ* compared to control mice. The images show a similar distribution of these receptors in both strains but differences in absolute receptor densities (see text).

2.4.1 $GABA_A$ receptor

Statistical tests revealed a significant reduction of $GABA_A$ receptor densities in the olfactory bulb (19%; p=0.01), the striatum (12%; p=0.01) and the hippocampal region mossy fiber terminal field/hilus (10%; p=0.007), compare Figure 63.

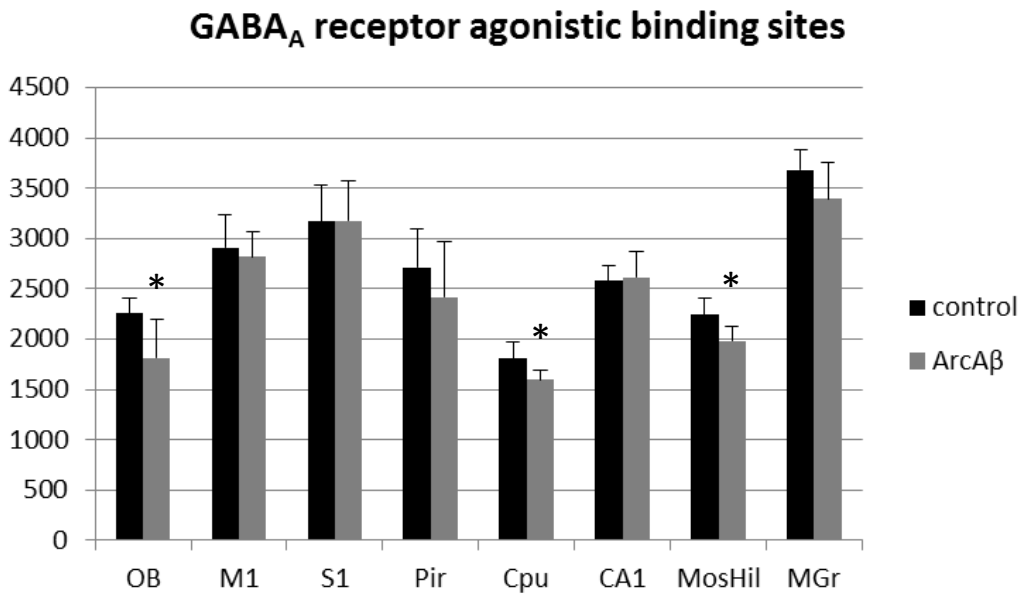

Figure 63: Bar charts demonstrating mean $GABA_A$ receptor density together with standard deviation in all brain regions investigated of control (black) and *tgArcAβ* (grey) mice. Significant differences are shown by *.

2.4.2 $GABA_A$ associated benzodiazepine binding sites (BZ)

The comparison of ***tgArcAβ*** and control mice revealed no up- or downregulation of $GABA_A$ associated benzodiazepine binding sites in any of the brain areas (Figure 64).

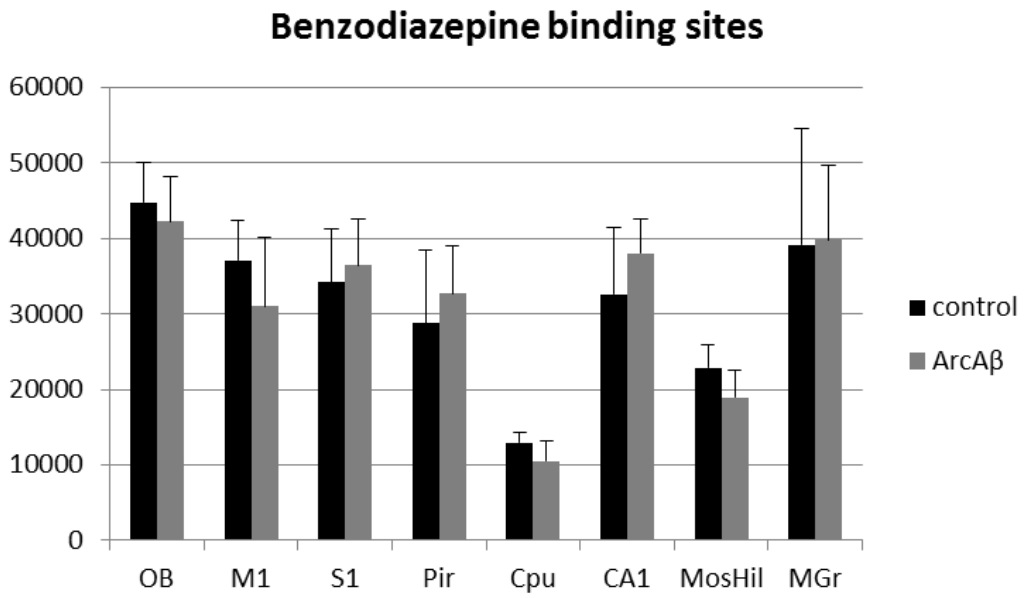

Figure 64: Bar charts demonstrating mean BZ receptor density together with standard deviation in all brain regions investigated of control (black) and *tgArcAβ* (grey) mice.

2.4.3 $GABA_B$ receptor

In ***tgArcAβ*** mice the receptor density was not significantly different in any region analyzed compared to control mice (Figure 65).

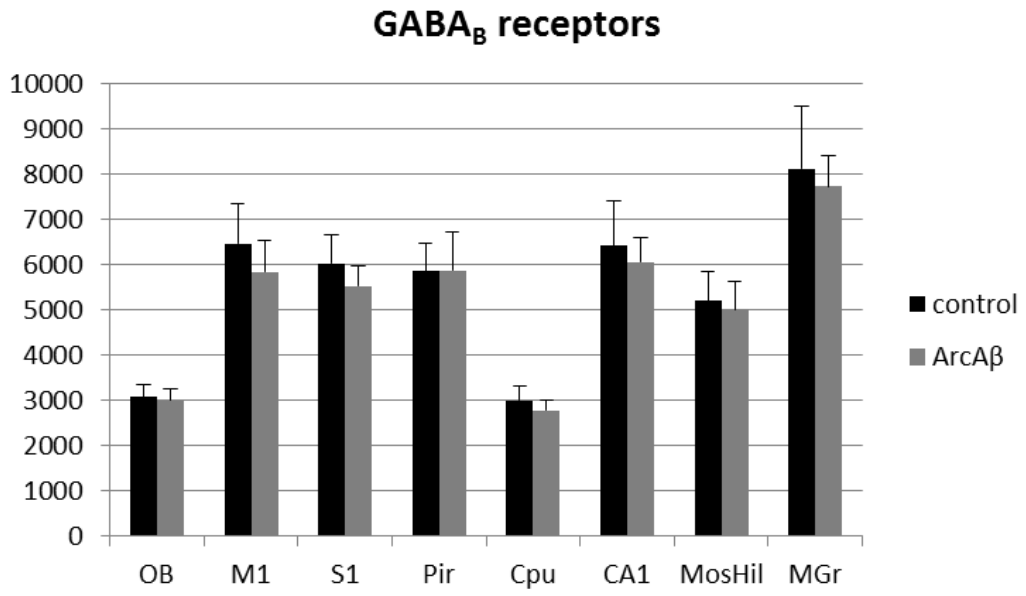

Figure 65: Bar charts demonstrating mean $GABA_B$ receptor density together with standard deviation in all brain regions investigated of control (black) and *tgArcAβ* (grey) mice. Significant differences are shown by *.

2.5 Adrenergic receptors

The **α_1** and **α_2** receptors had a different regional distribution. **α_1** receptors reached the highest densities in the olfactory bulb and motor cortex. Striatum, piriform cortex and hippocampus showed the lowest mean α_1 receptor densities.

Contrastingly, the highest density of **α_2** receptors was found in the piriform cortex. Cortical areas, striatum and hippocampus showed lowest mean receptor densities, with exception of the stratum moleculare/granulosum. This region had intermediate values. Density in the cortical areas and striatum was similar compared to **α_1** receptors (Figure 66 - Figure 67).

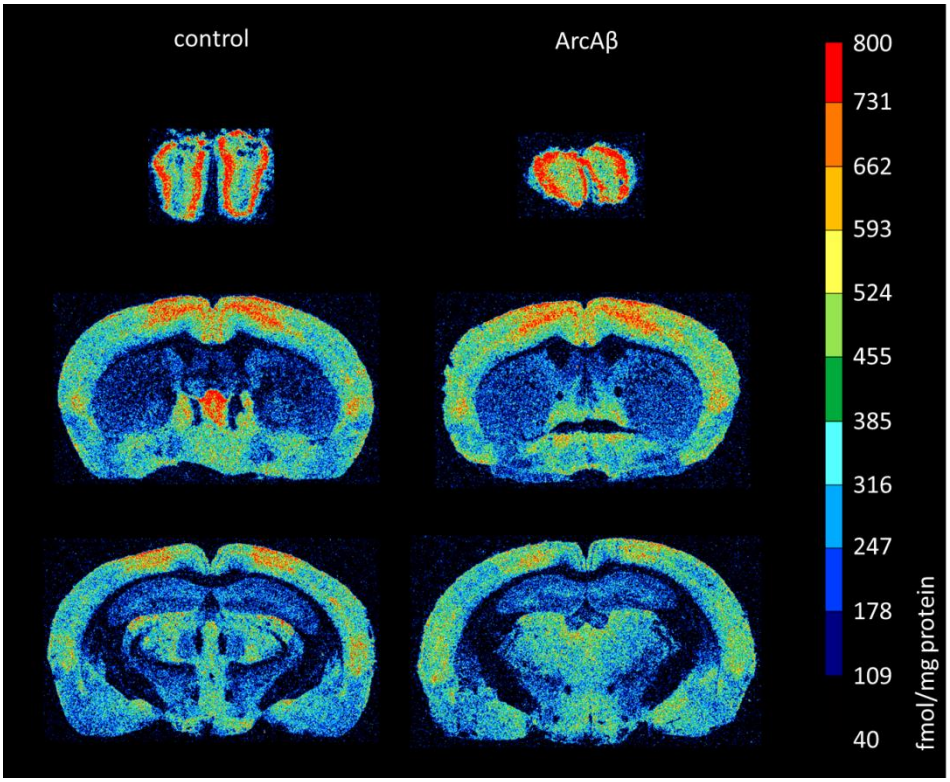

Figure 66: Color coded image of α_1 receptor densities (fmol/mg protein) in the brains of *tgArcAβ* compared to control mice. The images show a similar distribution of these receptors in both strains.

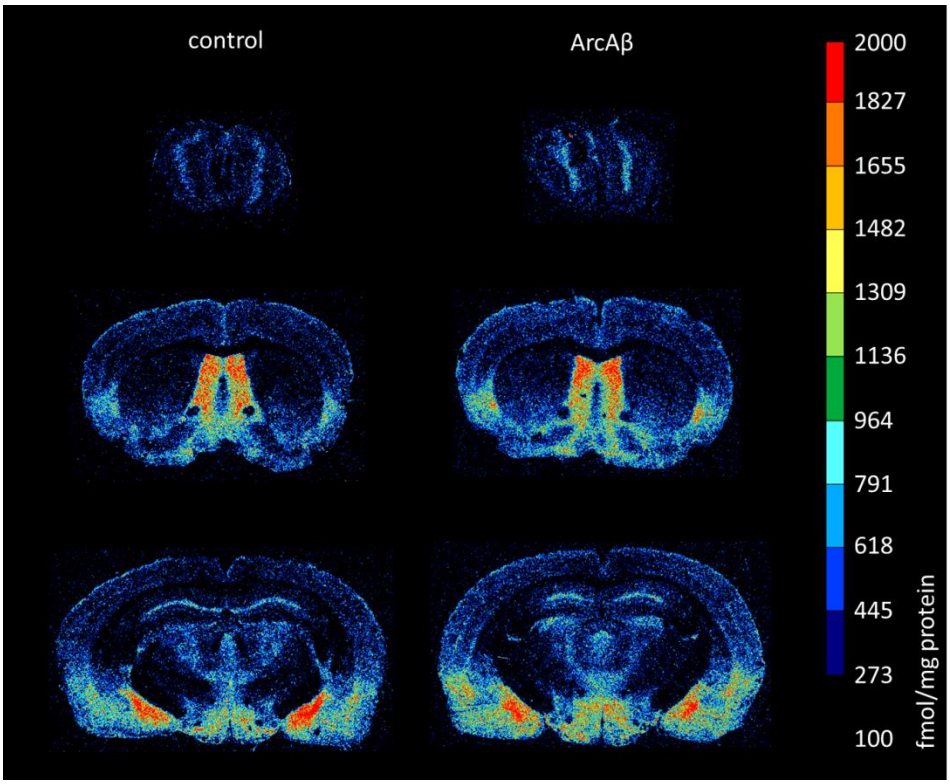

Figure 67: Color coded image of α_2 receptor densities (fmol/mg protein) in the brains of *tgArcAβ* compared to control mice. The images show a similar distribution of these receptors in both strains but differences in absolute receptor densities (see text).

2.5.1 α_1 receptor

The α_1 receptor density was significantly increased by 14% in the striatum of the ***tgArcAβ*** model compared to control mice (p=0.0005; Figure 68).

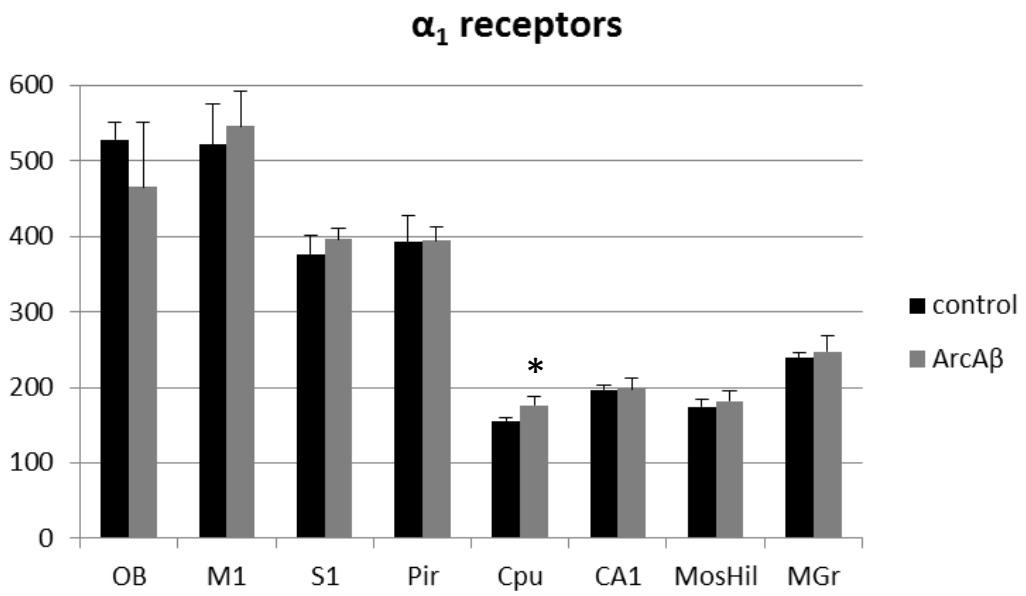

Figure 68: Bar charts demonstrating mean α_1 receptor density together with standard deviation in all brain regions investigated of control (black) and *tgArcAβ* (grey).

2.5.2 α_2 receptor

The mean densities of α_2 receptors of ***tgArcAβ*** were increased in several brain regions when compared to control mice. Differences were statistically significant in the olfactory bulb (16%; p=0.02), the piriform cortex (32%; p=0.002) and in the hippocampal region stratum moleculare/granulosum (17%; p=0.01), see Figure 69.

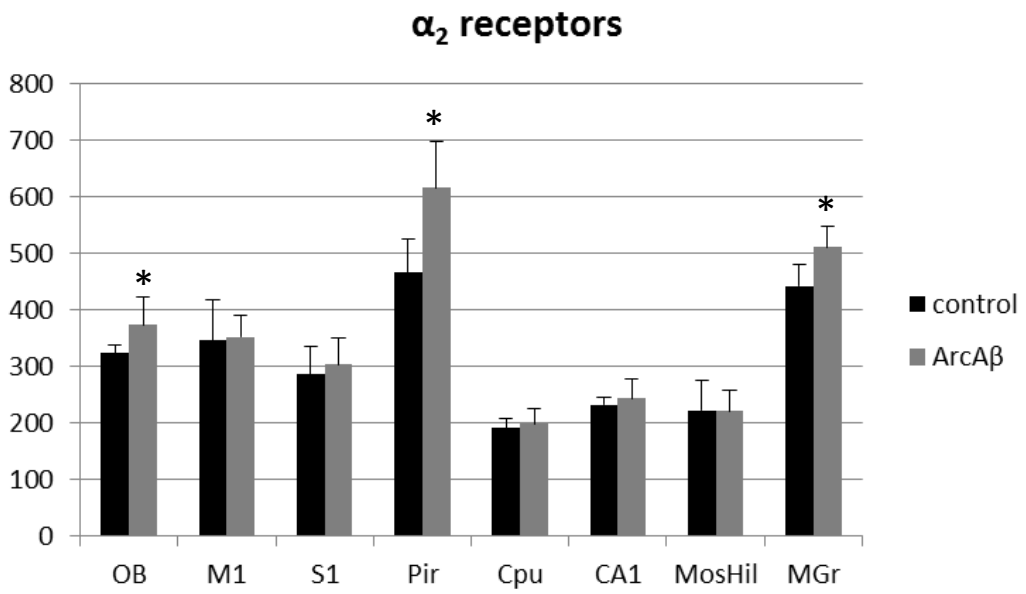

Figure 69: Bar charts demonstrating mean α_2 receptor density together with standard deviation in all brain regions investigated of control (black) and *tgArcAβ* (grey). Significant differences are shown by *.

2.6 Dopamine receptors

Dopamine receptor densities were below detection limit in most of the analyzed brain regions with exception of the striatum (**D1, D2** and **D2/3** receptors). See Figure 70 - Figure 72).

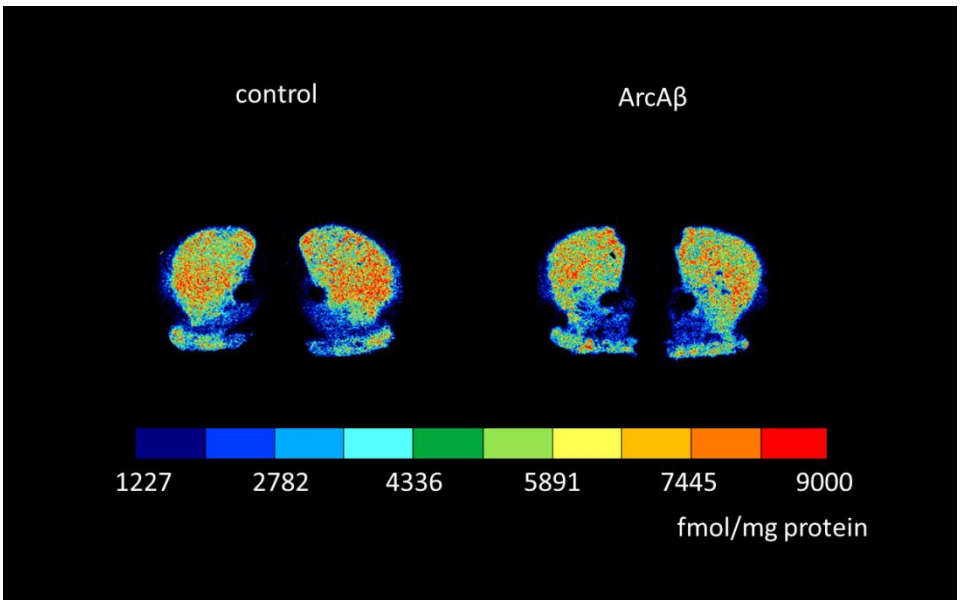

Figure 70: Color coded image of D_1 receptor densities (fmol/mg protein) in the brains of *tgArcAβ* compared to control mice. The images show a similar distribution of these receptors in both strains.

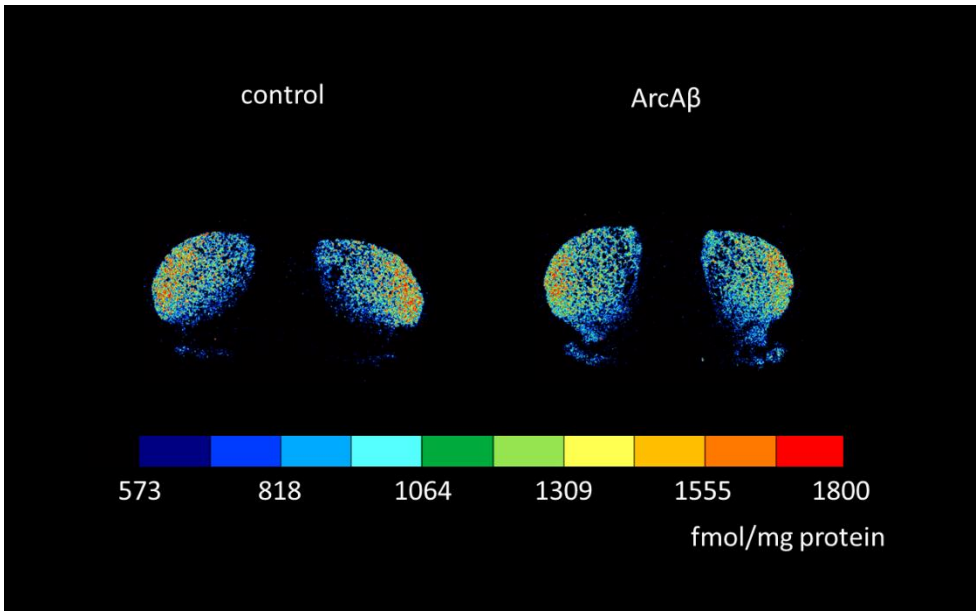

Figure 71: Color coded image of D_2 receptor densities (fmol/mg protein) in the brains of *tgArcAβ* compared to control mice. The images show a similar distribution of these receptors in both strains.

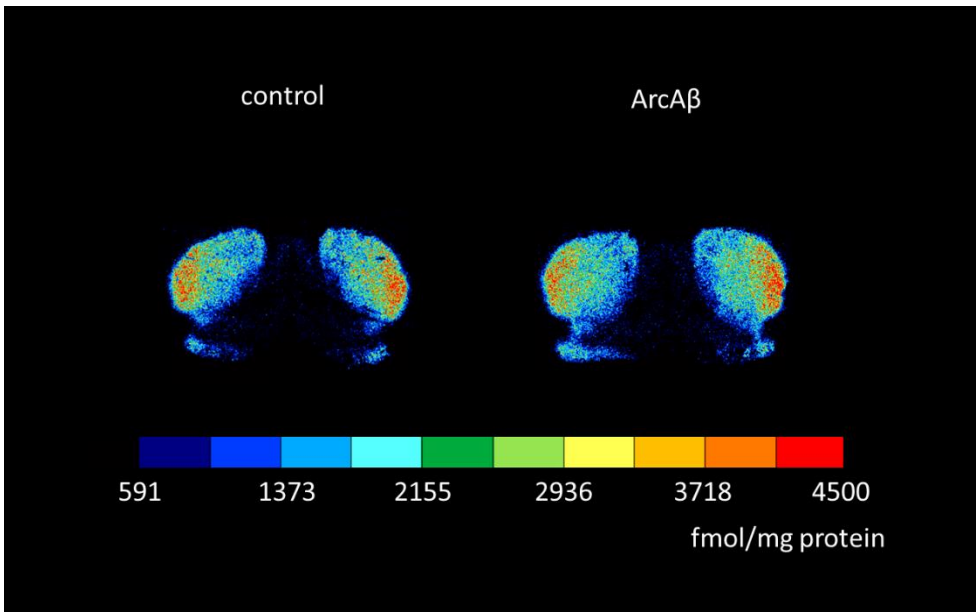

Figure 72: Color coded image of $D_{2/3}$ receptor densities (fmol/mg protein) in the brains of *tgArcAβ* compared to control mice. The images show a similar distribution of these receptors in both strains.

2.6.1 D_1 receptor

No significant differences were observed in the brains of ***tgArcAβ*** compared to control mice (Figure 73). Only a trend towards downregulation was seen.

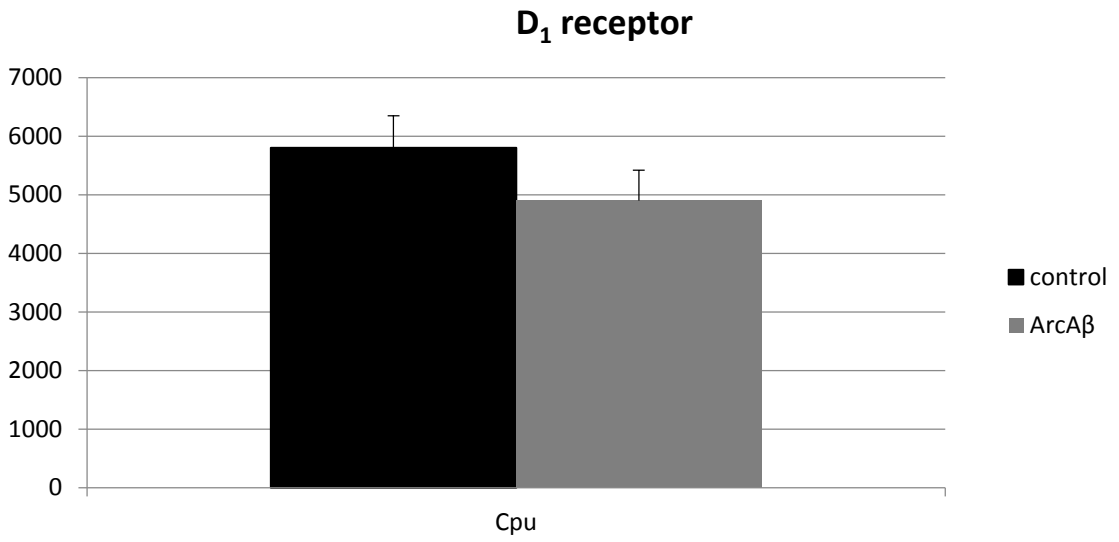

Figure 73: Bar charts demonstrating mean D_1 receptor density together with standard deviation in the striatum of control (black) and *tgArcAβ* (grey).

2.6.2 D_2 receptor

In ***tgArcAβ*** mice compared to control mice, the mean density of D_2 receptors was not altered in the striatum (Figure 74).

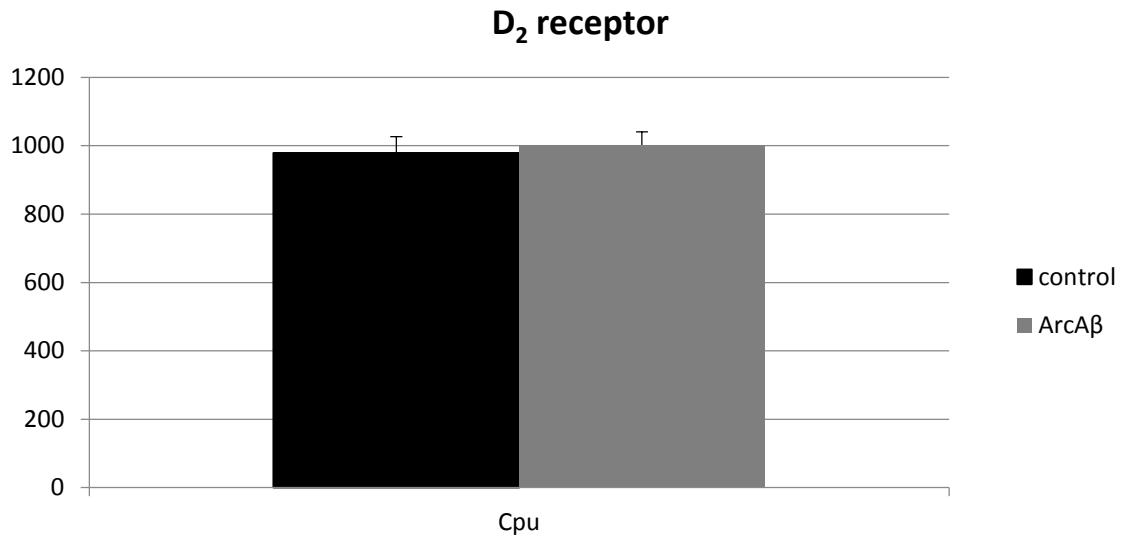

Figure 74: Bar charts demonstrating mean D_2 receptor density together with standard deviation in the striatum of control (black) and *tgArcAβ* (grey).

2.6.3 $D_{2/3}$ receptor

In the ***tgArcAβ*** mouse compared to controls, no decrease or increase of the mean receptor density could be shown in the striatum (Figure 75).

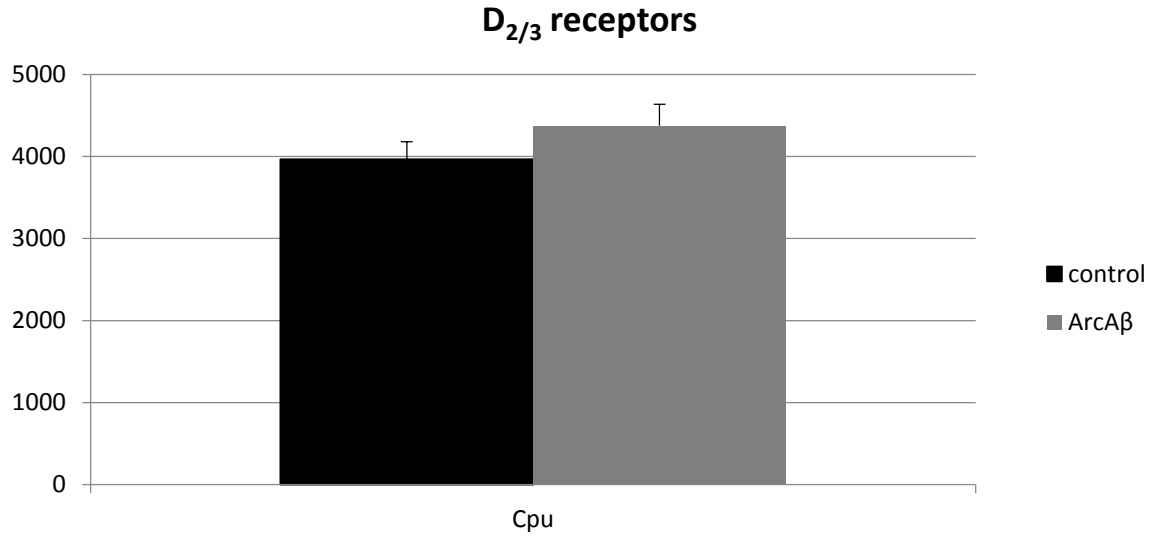

Figure 75: Bar charts demonstrating mean $D_{2/3}$ receptor density together with standard deviation in the striatum of control (black) and *tgArcAβ* (grey).

2.7 Adenosine A_2 receptor

As described for dopamine receptors, A_2 adenosine receptor densities were only detectable in the striatum. All other analyzed brain regions were below the detection limit (Figure 76).

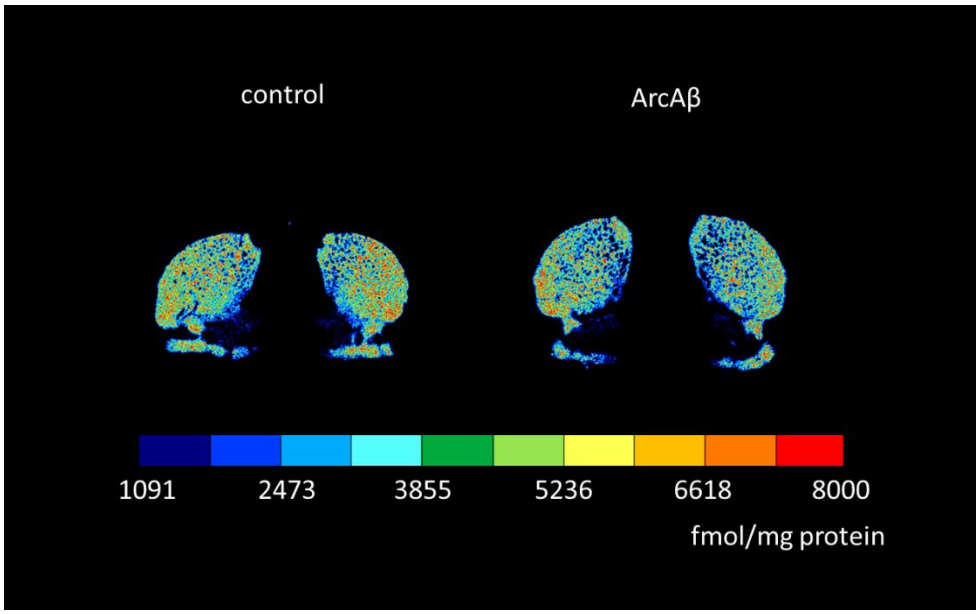

Figure 76: Color coded image of A_2 receptor densities (fmol/mg protein) in the striatum of *tgArcAβ* compared to control mice. The images show a similar distribution of these receptors in both strains.

2.7.1 A_2 receptors

The A_2 receptor density was not significantly different in any region analyzed in the ***tgArcAβ*** mouse compared to control mice (Figure 77).

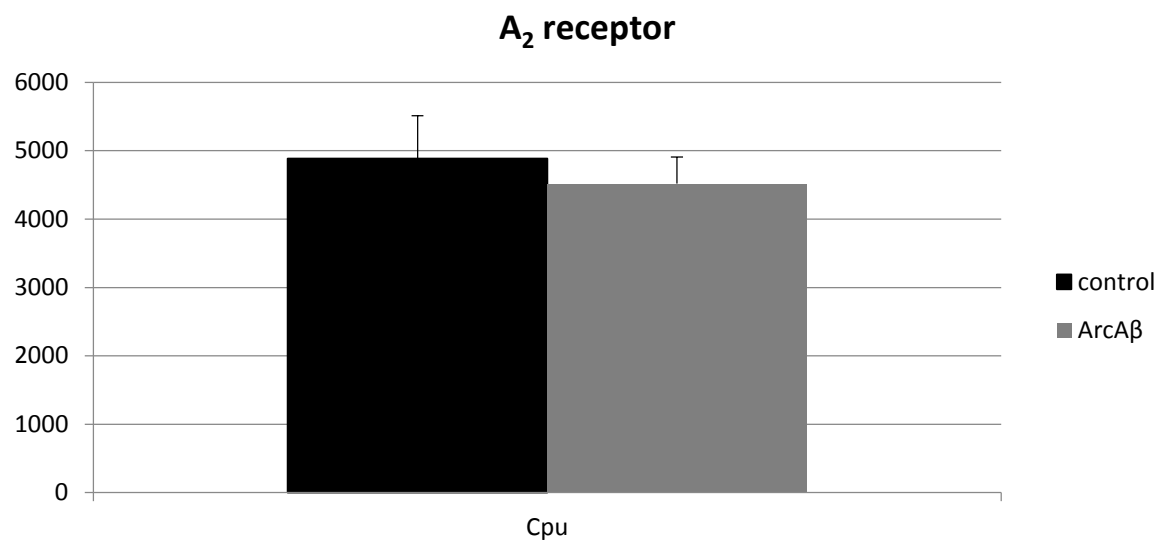

Figure 77: Bar charts demonstrating mean A_2 receptor density together with standard deviation in the striatum of control (black) and *tgArcAβ* (grey).

2.8 Summary of all significant differences in *tgArcAβ* mice compared to controls

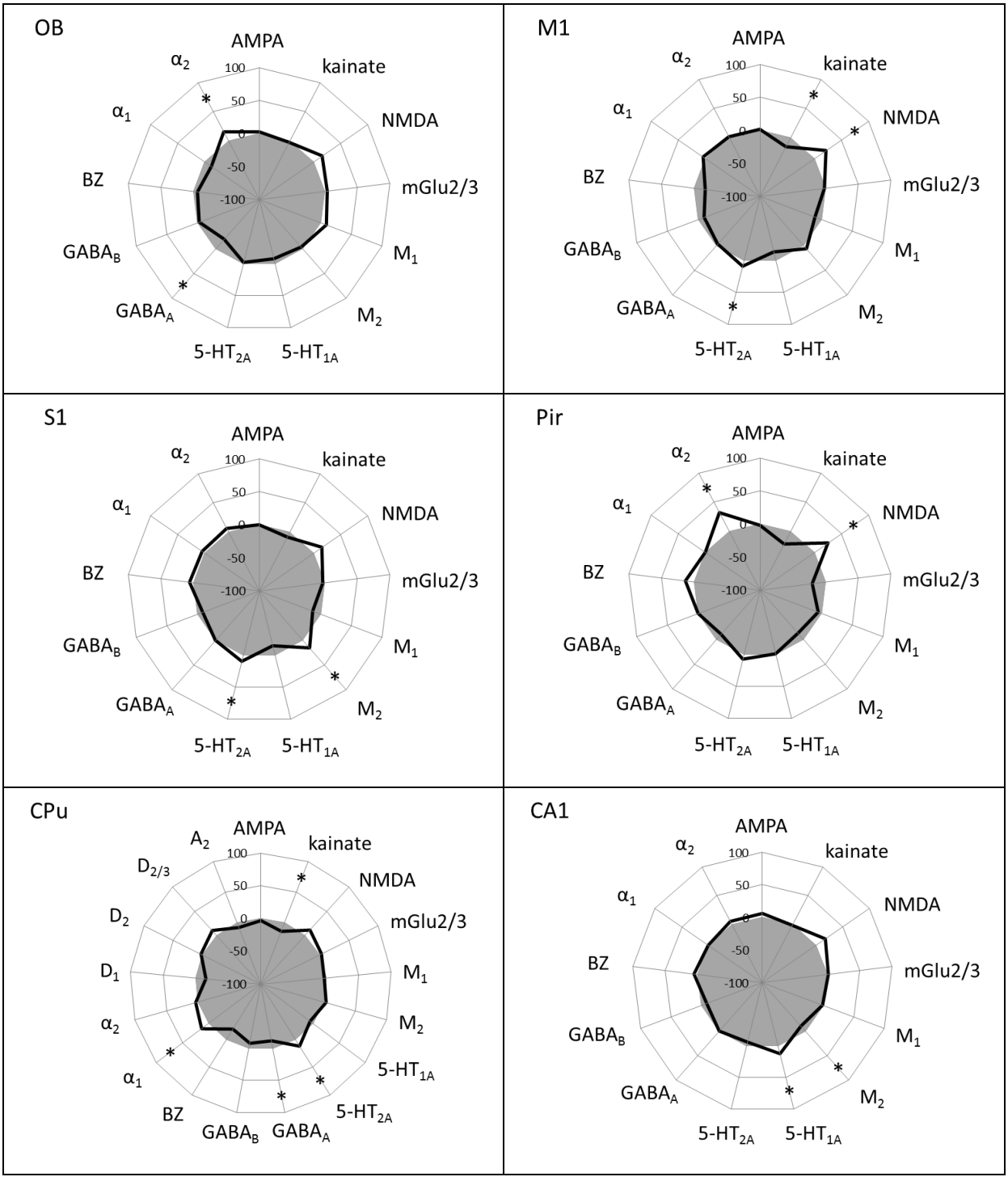

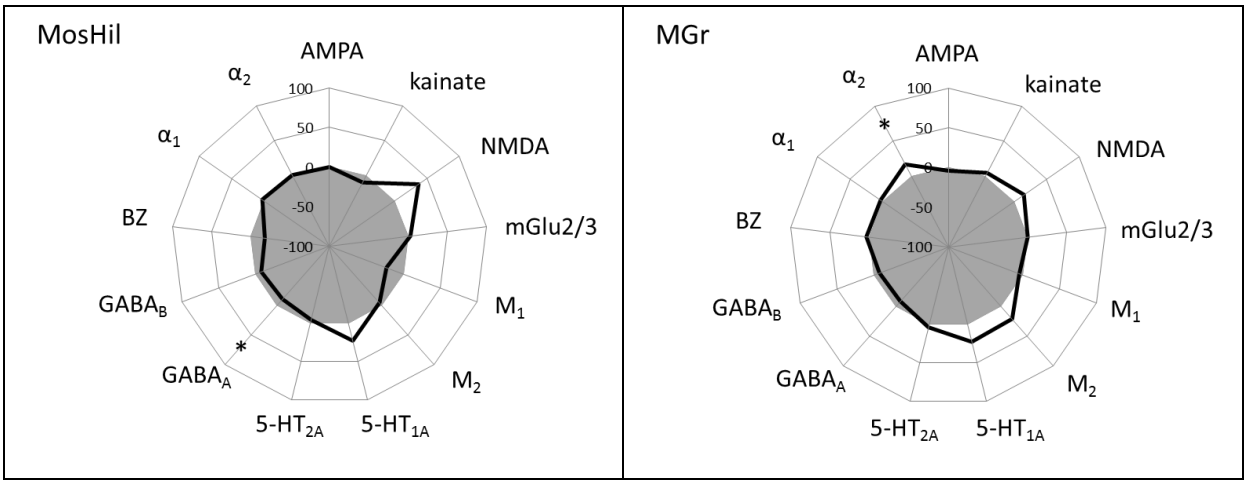

Figure 78: Polar plots of mean receptor densities in 8 different brain regions of control (grey) and *tgArcAβ* (black) mice. Values were normalized to the mean value of control animals, respectively. Significant differences are indicated by *****.

3 Immunohistochemical staining

3.1 *LRP1*, *tg5xFAD* and *tg5xFAD/LRP1* mice

Brain sections were double stained with antibodies against Aβ40 and Aβ42 (Figure 79 - Figure 82). In LRP1 mice, no plaques were observed in any of the areas investigated (Figure 80). However, immunohistochemical staining indicated a beginning aggregation of Aβ. The greatest plaque generation was observed in *tg5xFAD* mice. Figure 81 demonstrates plaques in the motor cortex and the hippocampus of this strain. *tg5xFAD/LRP1* mice showed plaque generation in the motor cortex and the hippocampus as shown in Figure 82. Aβ40 and Aβ42 were found to be co-localized to a great extent in these two mouse models, with Aβ42 being more conspicuous. Plaques together with aggregated Aβ were not present in any of the mouse models.

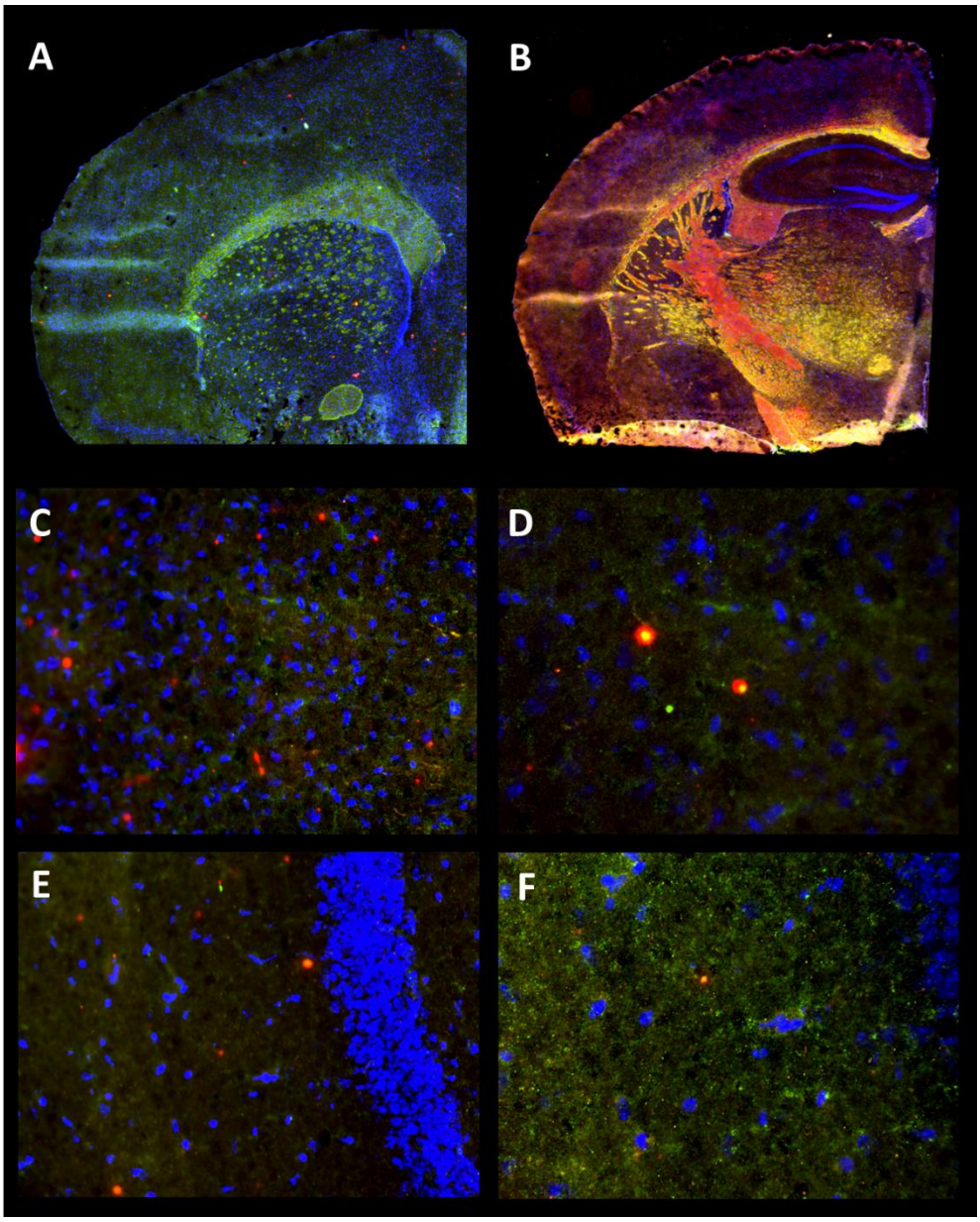

Figure 79: Double immunofluorescence staining against Aβ40 and Aβ42 in control mice. No specific staining of Aβ40 and Aβ42 is visible. The round red dots are caused by non-specific staining, and differ from the specific staining of red-stained plaques containing Aβ42 in shape and size (see Figs. 81-82). Cell nuclei are stained blue. An overview of the staining is given in A-B. M1 (C-D), hippocampus (E-F). Left column in C and E: 20x magnification; right column in D and F: 40x magnification.

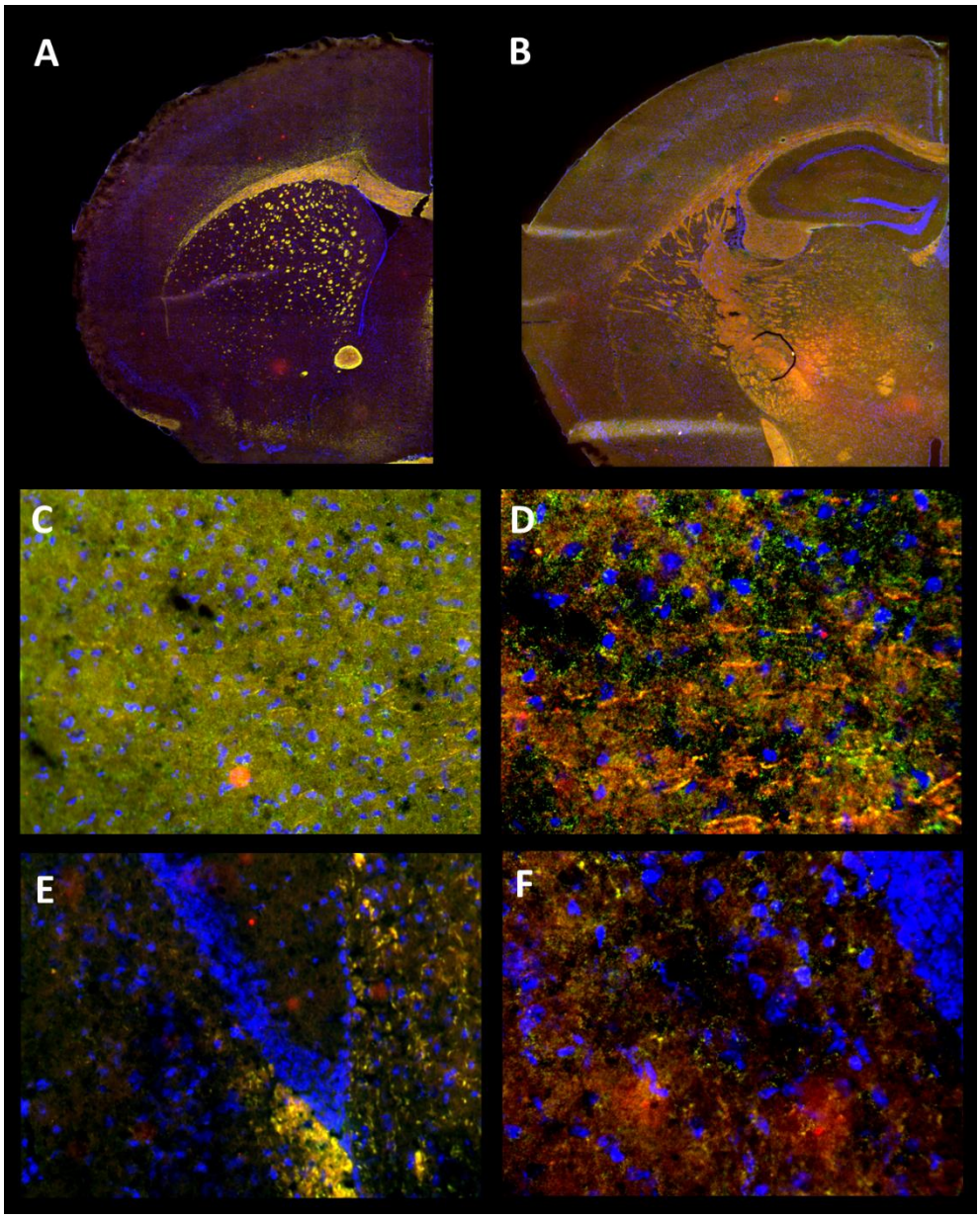

Figure 80: Double immunofluorescence staining against Aβ40 (green) and Aβ42 (red) in *LRP1* mice. Cell nuclei are stained blue. Green and red background is unspecific staining. An overview of the staining is given in A-B. M1 (C-D), hippocampus (E-F). Left column in C and E: 20x magnification; right column in D and F: 40x magnification. No plaques are present in any of the regions, though there seems to be some aggregation of Aβ.

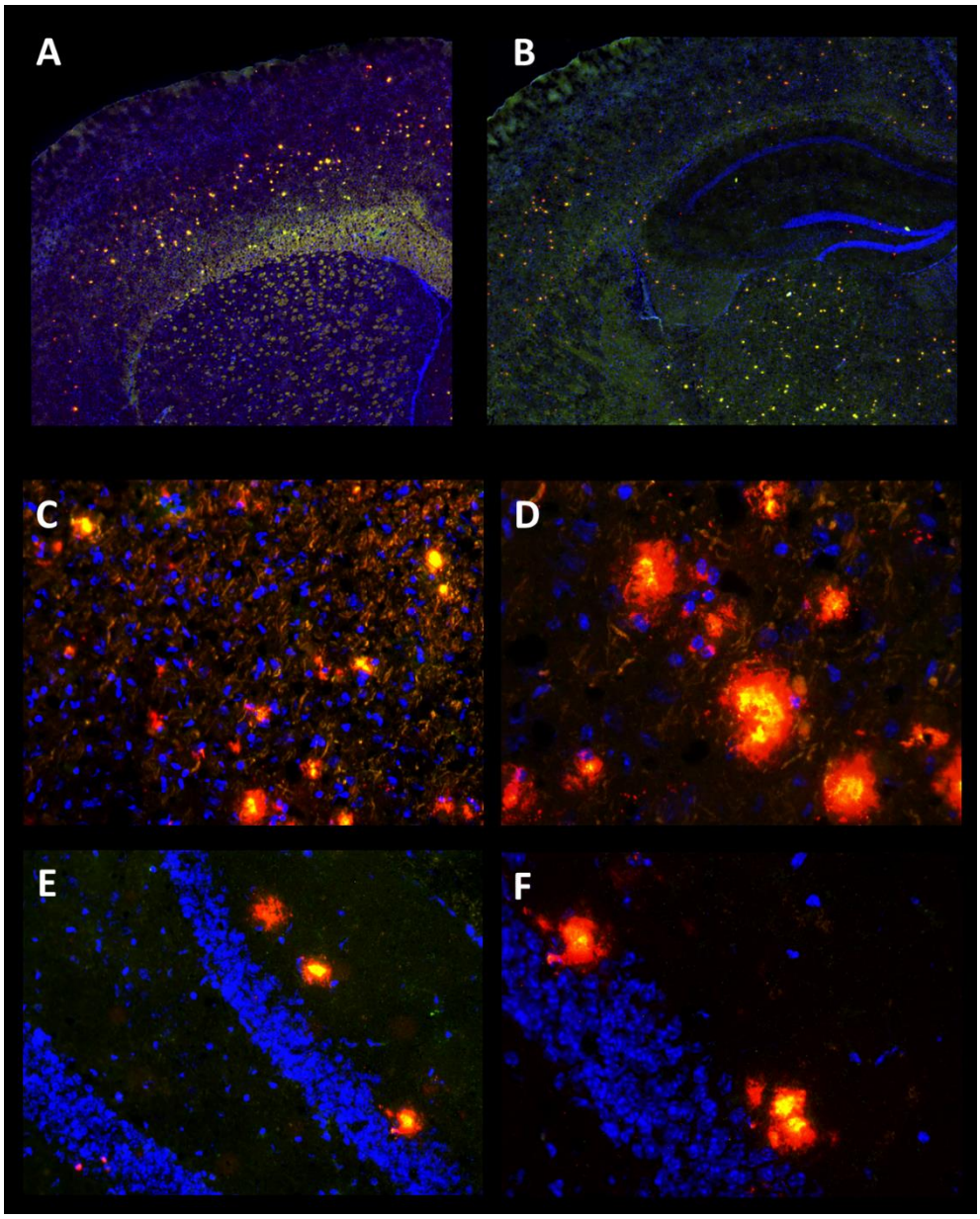

Figure 81: Double immunofluorescence staining against Aβ40 (green) and Aβ42 (red) in *tg5xFAD* mice. Cell nuclei are stained blue. An overview of the staining is given in A-B. M1 (C-D), hippocampus (E-F). Left column in C and E: 20x magnification; right column in D and F: 40x magnification. Plaques are shown in the motor cortex and the hippocampus. A co-localization of Aβ40 and Aβ42 can be observed (yellow), with Aβ42 being more conspicuous.

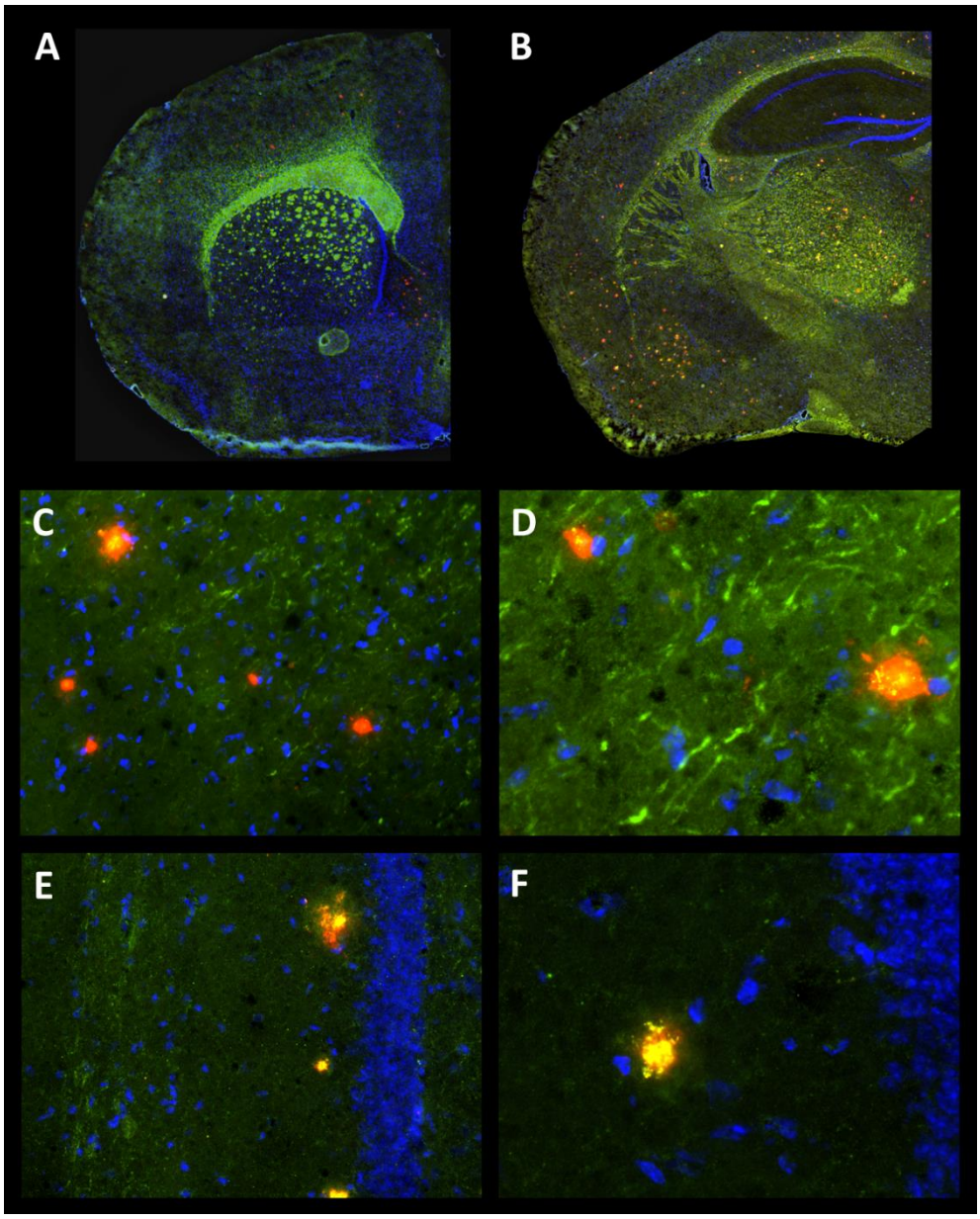

Figure 82: Double immunofluorescence staining against Aβ40 and Aβ42 in *tg5xFAD/LRP1* mice. Cell nuclei are stained blue. Green background is unspecific staining. An overview of the staining is given in A-B. M1 (C-D), hippocampus (E-F). Left column in C and E: 20x magnification; right column in D and F: 40x magnification. Plaques are shown in the motor cortex and the hippocampus (Aβ40 green, Aβ42 red). Co-localization of Aβ40 and Aβ42 can be observed (yellow) in C-F, with Aβ42 being more conspicuous, especially in the motor cortex.

3.2 *tgArcAβ* mice

In *tgArcAβ* mice, intracellular Aβ was observed in the motor cortex and the hippocampus (Figure 84). In control mice no intracellular Aβ was observed (Figure 83). No accumulation of Aβ was observed in the olfactory bulb and piriform cortex.

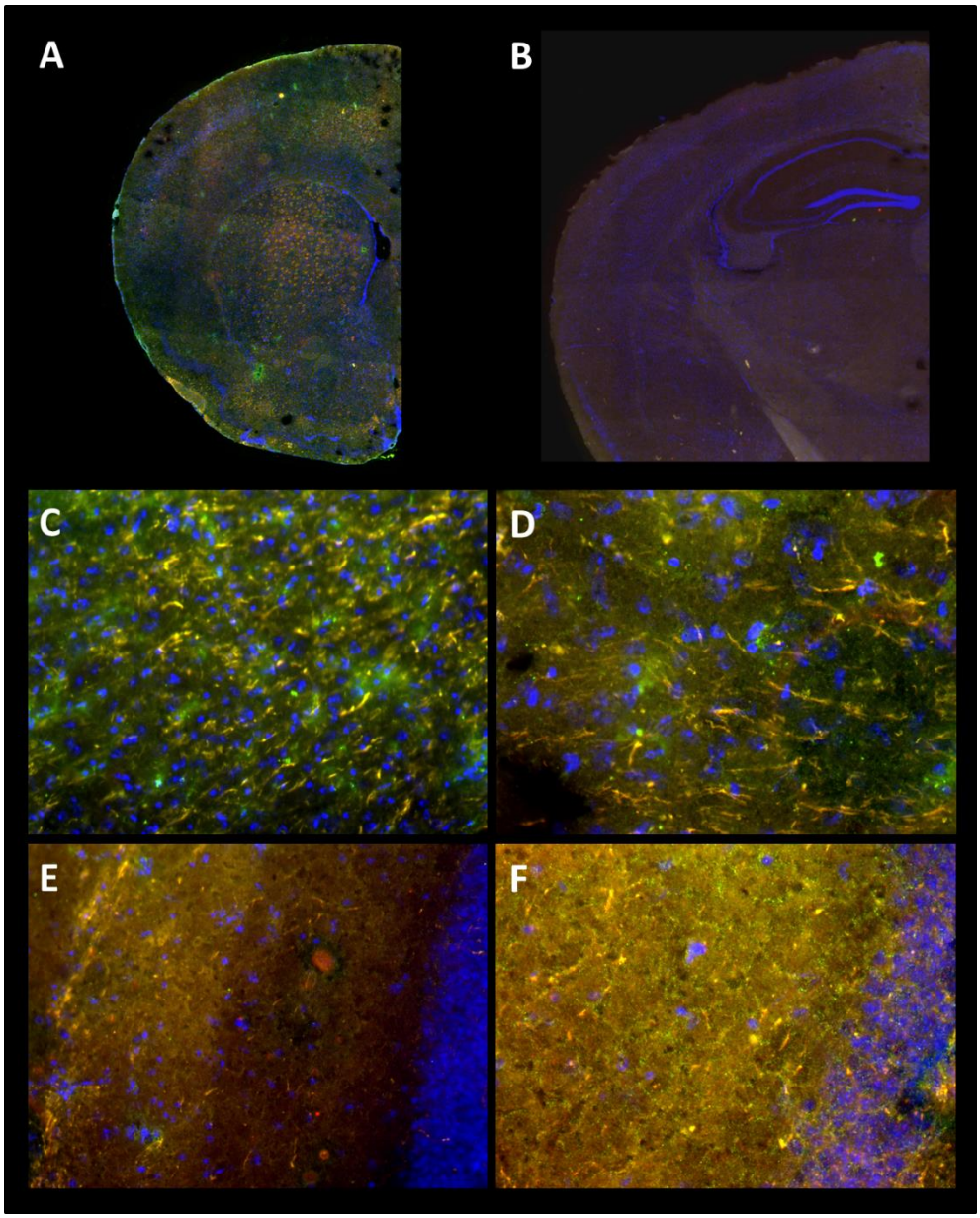

Figure 83: Double immunofluorescence staining against Aβ40 (green) and Aβ42 (red) in control mice. Cell nuclei are stained blue. Green and yellow background is unspecific staining. An overview of the staining is given in A-B. M1 (C-D), hippocampus (E-F). Left column in C and E: 20x magnification; right column in D and F: 40x magnification.

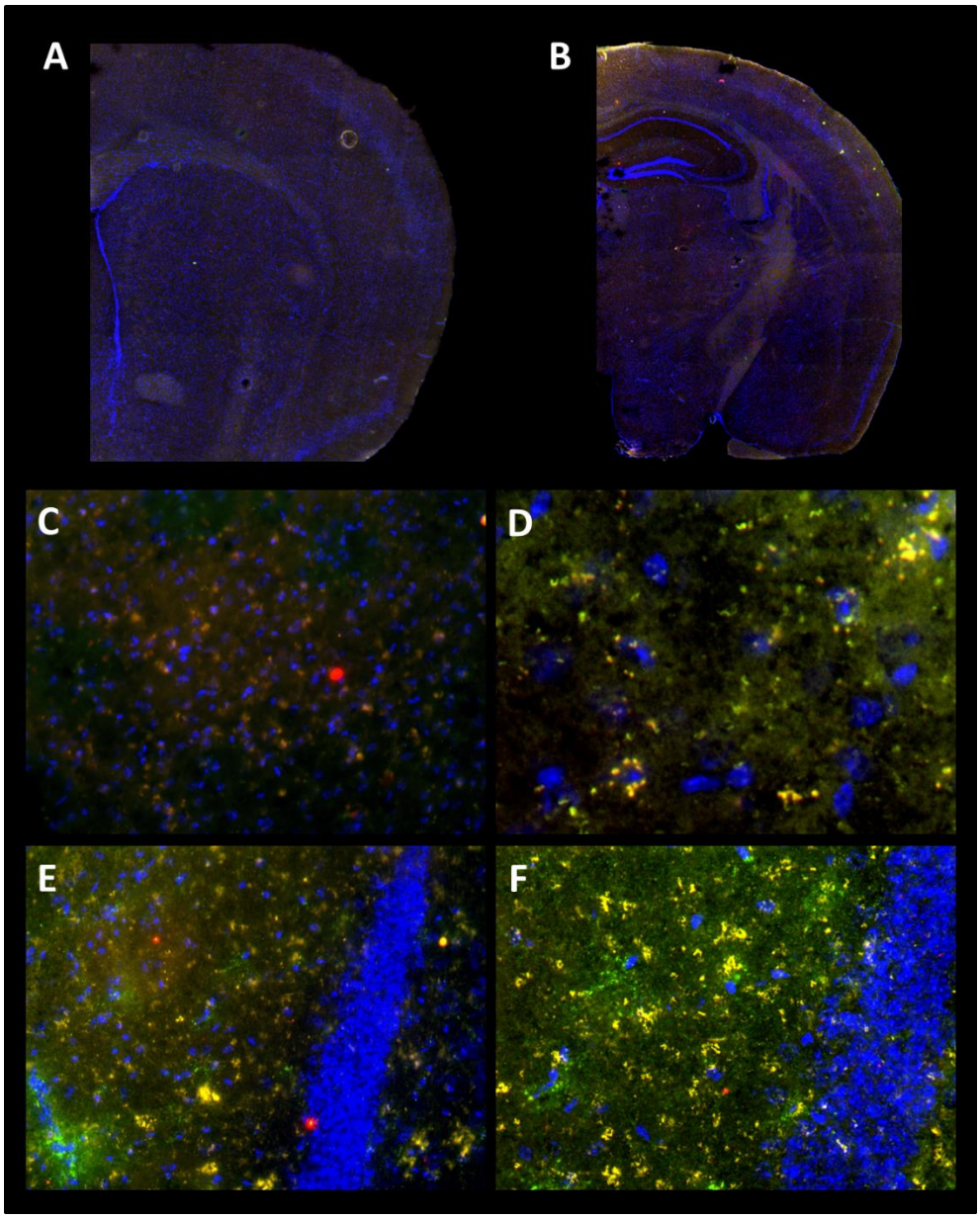

Figure 84: Double immunofluorescence staining against Aβ40 (green) and Aβ42 (red) in *tgArcAβ* mice. Cell nuclei are stained blue. Green background is unspecific staining. An overview of the staining is given in in A-B. M1 (C-D), hippocampus (E-F). Left column in C and E: 20x magnification; right column in D and F: 40x magnification. Aβ aggregation can be observed in the motor cortex and hippocampus with co-localization of Aβ40 and Aβ42 (yellow).

IV. Discussion

Alterations in several neurotransmitter systems were demonstrated in all mouse models. Raw data and corresponding mean values ± standard deviation are demonstrated in the Appendix.

1 Glutamate receptors

The excitatory neurotransmitter glutamate is found in more than 80% of all neurons in the brain (Gao and Bao, 2011). Glutamate passes through the blood brain barrier via amino acid transporters, and is synthetized in neurons and glial cells. Glutamate plays an essential role in synaptic plasticity, learning and memory. Furthermore, glutamate concentrations in temporal areas showed a significant reduction in AD patients (Ellison et al., 1986). Glutamate induced signaling is mediated through ionotropic and metabotropic glutamate receptors (Frisardi et al., 2011). The ionotropic AMPA, kainate and NMDA receptors contain ligand gated ion channels, whereas mGlu2/3 receptors are metabotropic receptors, which are coupled to second messenger systems. Eight different types of mGlu receptor exist, which are divided into three main groups, group I (mGlu1 and mGlu5), group II (mGlu2 and mGlu3) and group III (mGlu4 and mGlu7-8).

NMDA receptor:

***LRP1* mice:** The NMDA receptor density was increased in the CA1 region and the stratum moleculare/granulosum of *LRP1* mice. The present results of an increased NMDA receptor density correspond well with a previous report by Qiu et al. (2002). One of the numerous ligands for LRP1 is the macroglobulin α2M*, which is associated with neurodegeneration and glutamate signaling. α2M* is able to bind a variety of small molecules, such as endogenous, soluble Aβ peptides, and is a ligand for binding and clearance by LRP1. Moreover, calcium signaling, which was induced by NMDA stimulation, can be reduced by treatment with α2M*. It seems that α2M* alters calcium signaling via the LRP1-mediated mechanism (Qiu et al., 2002). Thus, knockout of LRP1 can impair glutamate induced neurotransmission.

Contrastingly, Liu et al. (2010) found a decrease of the receptor subunit NMDAR1 in the forebrain of a LRP1 KO mouse. Since NMDA is a heteromeric complex consisting of the obligatory subunit NMDAR1 and several, cell type specific NNMDAR2 subunits, the reduction

of NMDAR1 may not affect the binding of the antagonist MK801. Moreover, mice tested in the study of Liu et al. (2010) were 18 months old, while in the present study, mice were significantly younger (between four and six months of age).

Furthermore, recent studies have shown that an increase in the intracellular calcium level, either induced by mutations or depolarization, leads to an elevation of intracellular Aβ42 (Pierrot et al., 2004). Moreover, Aβ oligomers co-immunoprecipitate NMDA receptors, i.e. they interact with each other. Blocking of the subunit NMDAR1 reduces oligomer binding (De Felice et al., 2007). Furthermore, Aβ is known to accumulate extracellular glutamate. Glutamate gives rise to increased receptor activation, which leads to even more Aβ (Paula-Lima et al., 2005). Due to the enhanced number of NMDA receptors, an increasing toxic effect may lead to neurodegeneration.

***tgArcAβ* mice:** In *tgArcAβ* mice, increased NMDA receptor density was found in the primary motor and piriform cortex. These findings are in agreement with LRP1 mice and were discussed above.

***tg5xFAD* mice:** In *tg5xFAD* mice, NMDA receptors only show a trend towards decrease in the olfactory bulb, the somatosensory and piriform cortices. The results will be discussed together with the findings for *tg5xFAD/LRP1* mice.

***tg5xFAD/LRP1* mice:** In *tg5xFAD/LRP1* mice, a significant decrease of NMDA receptor density was found in the olfactory bulb. In the mossy fiber termination fields/hilus, NMDA receptor density was increased. Mutations in PS1 linked to FAD were shown to increase Aβ42 production, and reduce calcium influx across the plasma membrane (Yoo et al., 2000). Since both the *tg5xFAD* and *tg5xFAD/LRP1* mice contain two PS1 mutations, the decrease is in agreement with the study described above.

A study of AMPA receptors found that Aβ induces loss of the AMPA subunit GluR1 in cultured primary neurons of APP transgenic mice (Almeida et al., 2005). There is evidence that the loss of the subunit is caused by the reduction of Ca(2+)/calmodulin-dependent protein kinase II (CaMKII), a signaling molecule critical for AMPA receptor trafficking and function. The experiment was performed on cortical neurons from APP transgenic mice (Gu et al, 2009). However, in the current study, a decrease in the NMDA receptor density was found. It seems plausible, that NMDA receptors are affected in a similar way. CaMKII is activated by calcium entry and translocates to the synapse. Here it binds to NMDA receptors. Therefore a reduction of CaMKII caused by Aβ might cause a reduction of NMDA

receptors as well. The Aβ induced loss of receptors might explain both the increase and decrease of NMDA receptors in the current study. The increase of NMDA receptors leads to enhanced calcium influx, causing increased Aβ42. This in turn causes a reduction of CaMKII, leading to reduced NMDA receptors. In *tg5xFAD* and *tg5xFAD/LRP1* mice, plaques were observed (see Figure 81, 82). Therefore, more Aβ42 was present. In *LRP1* and *tgArcAβ* mice, no plaques were observed (see Figure 80, 84). It might be that as the disease progresses, NMDA receptor density decreases.

In the pathogenesis of AD, pathological changes occur in the hippocampus as well as in entorhinal, frontal and temporal cortices. Glutamate is the main excitatory neurotransmitter in these brain regions, which are involved in higher cognitive functions (Bernareggi et al., 2007). Therefore, a reduction of NMDA receptors may cause memory impairment, which was described in *tg5xFAD* and *LRP1* mice (Oakley et al., 2006; Liu et al., 2010).

In the hilus of ***tg5xFAD/LRP1*** mice, NMDA receptor density was increased. This is interesting, since it provides two prominent features of *LRP1* and *tg5xFAD* mice; these are reduced density of NMDA receptors in the olfactory bulb and increased density in the hippocampus. It is possible, that some regions are more prone to the Aβ induced effect on glutamate receptors than others.

Kainate receptor: In the past, kainate receptors have only rarely been studied in AD models, although there is evidence, that kainate receptors are affected in AD. Electrophysiological observations on glutamate receptors transplanted from human AD and non-AD-brains to frog oocytes reported essentially the same functional properties in both cases with the notable finding that the amplitudes of the currents elicited by glutamate were consistently larger in case of glutamate receptors from non-AD samples compared to those of AD samples (Bernareggi et al., 2007). Quantification of mRNA coding for the kainate subunit GluR5 revealed a smaller amount in the AD brain. Thus, a diminished number of corresponding receptors seemed likely (Bernareggi et al., 2007).

***LRP1* mice:** The most conspicuous changes were revealed in *LRP1* mice, where the olfactory bulb, piriform cortex and most hippocampal regions were affected. Behavioral test showed memory impairment at 24 months of age as well as LTP deficiency measured in slices (Liu et al., 2010). Since the trisynaptic pathway of the hippocampus (Henze et al., 2000) with an exceptionally high density of kainate receptors at the mossy fiber termination fields is known

to play a major role in learning and memory (Squire, 1992), the reduction of kainate receptors might contribute to the memory impairment. Although LTP is mainly dependent on NMDA receptors, there is evidence that altered kainate receptor availability also contributes to LTP impairment (Boer et al., 2010). It is interesting that *LRP1* mice show the most conspicuous changes, since plaque generation was not observed at this age (compare Figure 80). Impaired synaptic plasticity might contribute to this effect. LRP1 mediates the uptake of cholesterol into neurons by apoE (Spuch et al., 2012). Cholesterol, however, is important for synaptic plasticity (Frank et al., 2008). Moreover, a former study found kainate receptors to be involved in synaptic transmission and to interact with cholesterol (Frank et al., 2008). In *LRP1* mice, uptake of cholesterol is impaired due to the knockout of LRP1.

***tgArcAβ* mice:** In *tgArcAβ* mice, kainate receptor density was reduced in the motor cortex and the striatum, while in mossy fibers only a trend towards downregulation was revealed. These results are in agreement with behavioral findings by Knobloch et al. (2007). From the age of six months on, *tgArcAβ* mice are cognitively impaired in the Morris Water Maze, the Y-maze and active avoidance behavior (Knobloch et al., 2007). The described reductions in kainate receptors might underlie these behavioral alterations.

Szegedi et al. (2005) investigated the effect of Aβ on neuronal firing evoked by agonist for AMPA, NMDA and kainate in CA1 neurons of Wistar rats. While NMDA elicited firing was increased, the response mediated by AMPA and kainate was reduced. In both the LRP1 and *tgArcAβ* mice, the density of NMDA receptors was increased. Kainate receptor density was decreased, which fits well with the findings of Szegedi et al. (2005). AMPA was not affected in *tgArcAβ* mice. This might be due to their relatively young age (8 months). In *LRP1* mice, AMPA was not investigated.

***tg5xFAD* and *tg5xFAD/LRP1* mice:** Kainate receptors are significantly reduced in the olfactory bulb and the piriform cortex of *tg5xFAD* and *tg5xFAD/LRP1* mice (see chapter 10). However, in contrast to *LRP1* mice, the mossy fiber termination fields of *tg5xFAD/LRP1* mice had a significant higher density of kainate receptors compared to controls. No significant receptor changes were found in the *tg5xFAD* mouse, but a trend towards increase was shown in the mossy fiber termination fields. In studies of rats, where the perforant path was lesioned by destroying the angular bundle, a redistribution and spreading of kainate receptors was found in the stratum moleculare (Geddes et al., 1985). This is in agreement

with the findings in *tg5xFAD* and *tg5xFAD/LRP1* mice. Furthermore, plaques were found in the hippocampus of *tg5xFAD* and *tg5xFAD/LRP1* mice (see Figure 81,Figure 82). In mice without extracellular plaques in the hippocampus (*tgArcAβ* and *LRP1* mice; see Figure 80Figure 84), the kainate receptor density in the mossy fiber termination fields was not enhanced. This may indicate a disturbance of the synaptic transmission caused by plaques. Plaques were also found in neocortical areas of *tg5xFAD* and *tg5xFAD/LRP1* mice (see Figure 81, Figure 82). It is possible, that the increase was only observed in the mossy fiber terminal fields/hilus, because here the density of kainate receptors is exceptionally high. Since in *tg5xFAD* mice only a trend can be observed, it might be that the additional knockout of LRP1 aggravates the effect.

However, as described above, the density of kainate receptors was significantly lower in numerous other brain regions of all AD models compared to controls. Apparently, the lower kainate receptor density of the transgenic mice is the result of a more complex adaptation, which cannot be mirrored by a surgical removal of the perforant path inducing plastic changes in the hippocampus.

mGlu2/3:

The metabotropic glutamate receptors mGlu2/3 were downregulated in the CA1 region of ***LRP1*** and ***tg5xFAD/LRP1*** mice. In ***tg5xFAD*** mice, mGlu2/3 receptors were decreased in the CA1 region and the olfactory bulb. ***tgArcAβ*** mice were not affected in any region. mGlu2/3 metabotropic glutamate receptor was found to be neuroprotective in cortical neurons against neuronal toxicity induced by a brief NMDA pulse or by a prolonged exposure to kainic acid (Bruno et al., 1995). A possible mechanism of neuroprotection is reduced glutamate release. mGlu2/3 receptors belong to group II. mGlu receptors of group II/III reduce the vesicular release of glutamate by inhibition of presynaptic calcium influx, thereby optimizing synaptic transmission (Coutinho and Knopfel, 2002; Parameshwaran et al., 2008). However, receptors of group III are more important for glutamate release than mGlu2/3 receptors (Bruno et al., 2001). Therefore, another mechanism has to contribute to the neuroprotective effect.

It was shown that agonists of mGlu2/3 receptors enhance the production of TGF-β1 in the mouse brain (D'Onofrio et al., 2001). Former studies have demonstrated a role for TGF-β1 in

neuroprotection (Brionne et al., 2003; Vivien and Ali, 2006). TGF-β1 is a member of the TGF-β family, whose members have an important role as modulators of cell survival, inflammation and apoptosis, as well as in immune suppression and post-lesional repair (Taipale et al., 1998; Li et al., 2006). TGF-β1 is only expressed in specific brain regions, such as the hippocampus and the cortex (Vivien and Ali, 2006). In mouse models of AD, disturbance of TGF-β signaling promoted Aβ deposition and lead to neuritic dystrophy and increased levels of secreted Aβ and β-secretase-cleaved soluble amyloid precursor protein (Tesseur et al., 2006). Taken together, TGF-β1 seems to reduce Aβ accumulation in the brain. Furthermore, the TGF-β1 signaling pathway has been demonstrated to be impaired particularly in the early phase of the disease (Caraci et al., 2012; Krieglstein et al., 2012). Since D'Onofrio showed that activation of mGlu2/3 receptors enhance the production of TGF-β1 in the mouse brain (D'Onofrio et al., 2001), the results of the present study fit well to this finding. Less activation of mGlu2/3 receptors due to their reduced expression might cause reduced production of TGF-β1.

Furthermore, Lee et al. (1995) found that the activation of mGlu receptors accelerate non-amyloidogenic processing of APP in hippocampal neurons of fetal rats by stimulation of PKC. Hence, the downregulation of mGlu2/3 receptors found in *LRP1*, *tg5xFAD* and *tg5xFAD/LRP1* mice might favor Aβ production.

2 Acetylcholine receptors

Acetylcholine receptors are integral membrane proteins, which can be divided into either muscarinic (mACh) or nicotinic (nACh) receptors, according to their affinities and sensitivities (Xu et al., 2012). Cholinergic neurons, which project to all layers of cortical regions, including the olfactory bulb, hippocampal areas and the amygdala, are found in the basal forebrain (Struble et al., 1982; Whitehouse et al., 1982; Nyakas et al., 2011). The nucleus basalis Meynert (MBN) is part of the basal forebrain. Under physiological conditions, the cholinergic system is critically involved - beside other functions - in the control of cognition (Everitt and Robbins, 1997) and memory. In the pathogenesis of AD, dysfunction and severe loss of MBN cholinergic neurons and cortical projections are one of the earliest hallmarks observed (Nyakas et al., 2011). Likewise, drugs which potentiate central cholinergic functions have so far proven to be one of the most effective therapeutic treatments (Auld et al., 2002).

***LRP1* mice:** In the present study, only the M_2 receptor expression was found to differ significantly from that of controls in various brain regions in *LRP1* mice. Agonist binding of the M_2 receptor revealed reduced density in all hippocampal regions. Binding of M_2 antagonist showed decreased density in the CA1 and stratum moleculare/granulosum and an increase the striatum. M_1 receptors were not affected.

The signaling mechanism of the M_2 receptor differs from M_1 and M_3 receptors. The M_2 receptor is bound to a G protein, which activates potassium channels. Due to the increased conductance for potassium, hyperpolarization is induced. Reduced density of M_2 receptors causes less hyperpolarization; hence, depolarization may occur more easily. As has been discussed (see glutamate receptors), that increased influx of calcium through NMDA receptors leads to increased Aβ formation. In *LRP1* mice, NMDA receptor density was increased in two hippocampal areas, i.e. the CA1 region and stratum moleculare/granulosum. Likewise, M_2 density revealed by *agonist* binding was found to be reduced in the CA1 region and stratum moleculare/granulosum. Thus, the decreased density of M_2 receptors could further increase the calcium influx via the depolarization together with the increased density of NMDA receptors and their effect on calcium influx. Furthermore, it is striking that cholinergic reduction in *LRP1* mice occurs in the hippocampus. Cognitive function and short-term memory are disrupted when mACh receptors are blocked (Coyle et al., 1983), while drugs increasing cholinergic function improve short-term memory (Sitaram et al., 1978). Thus, cholinergic receptor reduction, which was found in *LRP1* mice, might contribute to the LTP and memory impairment found (Liu et al., 2010)

Binding studies using an antagonist revealed increased M_2 receptor density only in the striatum. This increase might be a compensatory mechanism, a trial to compensate reduced acetylcholine level in the brain, as was described in Hoshi et al. (1997). Alternatively, the regionally specific de- or increase of M_2 receptors (decrease with agonist binding and increase with antagonist binding) may be caused by different receptor affinities of the used ligands with the antagonist preferring low affinity and the agonist high affinity binding sites, and also by different relations between high- and low affinity binding sites of this receptor in the different brain regions.

***tg5xFAD/LRP1* mice:** In *tg5xFAD/LRP1* mice, M_2 receptor density revealed by antagonist binding was reduced in the olfactory bulb, the motor and somatosensory cortex as well as

the striatum. Agonist binding of the M_2 receptor showed downregulation in the olfactory bulb. In *tg5xFAD/LRP1* mice, plaques were observed in the neocortex and hippocampus (see Figure 81). Former studies found evidence that the cholinergic system is affected by the presence of Aβ. Due to the formation of plaques, it can be assumed, that the Aβ level is high in *tg5xFAD/LRP1* mice. Therefore, it is plausible that Aβ influences cholinergic receptors. However, plaques do not seem to be the exclusive cause, since *LRP1* mice show reductions in the cholinergic system as well, but did not display any plaques (see Figure 80). Therefore, the impairment of synaptic transmission (discussed for kainate receptors) might contribute to alterations in the cholinergic system. Furthermore, acetylcholine synthesis is suppressed in the presence of Aβ in primary cultures of MBN neurons (Hoshi et al., 1997), and its release is reduced in the neocortex of humans (Nilsson et al., 1986) as well as in the hippocampus of rats (Kar et al., 1996). Therefore, the reduced density of M_2 receptors may be a response to lower levels of acetylcholine. In transgenic mice carrying combined mutations in APP and PS1, which is also the case for *tg5xFAD/LRP1* mice, a decline in size and density of cholinergic synapses was reported in the frontal cortex (Wong et al., 1999).

Cholinergic markers are altered as well, e.g. acetyltransferase (ChAT). Araujo et al. (1988) found a significant decrease in the ChAT level in several brain regions, i.e. various neocortical areas, hippocampus and the MBN. Furthermore, the density of M_2 receptors in patients was lowered in all cortical areas and in the hippocampus (Araujo et al., 1988). This is in agreement with the finding of the current study. In ***tg5xFAD/LRP1*** mice, the M_2 receptors are reduced in the motor and somatosensory cortex. In ***LRP1*** mice, the CA1 region and stratum moleculare/granulosum revealed decreased M_2 density (see discussion above). Differences between the affected areas described by Araujo et al. (1988) may be caused by the less specific ligands and the human brain tissue used by these authors.

***tg5xFAD* mice:** In *tg5xFAD* mice, the M_2 receptor density was decreased in the mossy fiber terminal fields/hilus and the stratum moleculare/granulosum. A reduction of M_2 receptors was already discussed in the discussion of *LRP1* mice. Moreover, M_3 receptors were increased in the striatum. In addition to the impact of Aβ peptides on the cholinergic system described above, the cholinergic system also seems to affect Aβ signaling. Activation of muscarinic receptors causes modification of APP processing, thus inhibiting amyloidogenic Aβ production and promoting the non-amyloidogenic pathway (Nitsch et al., 1992; Hung et al., 1993). Additionally, in healthy as well as cholinergic denervated rats, treatment with a

muscarinic agonist lowers APP levels (Lin et al., 1999). Taken all this together, an interaction of Aβ and muscarinic receptors can be assumed. Thus, the enhanced M_3 receptor density might be a compensatory mechanism to reduce the Aβ level. This effect is only observed in *tg5xFAD* mice. A possible cause is that they generated the most numerous plaques of all AD models (see Figure 81).

***tgArcAβ* mice:** Only the M_2 receptor density analyzed by agonist binding was significantly decreased in the CA1 region of *tgArcAβ* mice, as well as increased in the somatosensory cortex. The reduction of this receptor was already discussed in the discussion of *LRP1* mice. The increase, however, may be a regionally specific compensatory mechanism caused by the reduced acetylcholine level (Hoshi et al., 1997).

In summary, *LRP1* and *tg5xFAD/LRP1* mice revealed the strongest alterations in the cholinergic system of all mouse models investigated. Since LRP1 is missing in both mouse lines, LRP1 seems to play a major role in the cholinergic system. Given the fact that no plaques were observed in the *LRP1* mouse model (see Figure 80), degeneration of the cholinergic systems may start well before plaque generation (see discussion above). This supports the hypothesis that the alteration of the cholinergic system is an early event in the generation of AD with regard to sporadic AD.

3 Serotonin receptors

Sixteen different types of serotonin receptors are known. Based on their primary physiological mechanism, they can be divided into 7 sub-families (Hoyer and Martin, 1997; Xu et al., 2012), 5-HT_1 to 5-HT_7. The receptor groups investigated in this study, 5-HT_{1A} and 5-HT_{2A} are G protein coupled receptors (Gerhardt and van Heerikhuizen, 1997).

Serotonergic neurons of the dorsal and median raphe nuclei innervate regions of the neocortex and the limbic system (Siever et al., 1991; Lanctot et al., 2001). They influence aggression, anxiety, mood, feeding, sleep, temperature and motor behavior (Siever et al., 1991; Lanctot et al., 2001).

No alterations of serotonin receptors were observed in the ***LRP1*** and ***tg5xFAD*** mice. ***tg5xFAD/LRP1*** mice revealed increased 5-HT_{2A} receptor density in the striatum and the CA1

region of the hippocampus. This indicates that the mutations associated with FAD together with knockout of LRP1 might further aggravate the effects on the serotonergic system.

In *tgArcAβ* mice, an enhanced level of 5-HT_{2A} receptors was seen in the motor and somatosensory cortex, and in the striatum. In addition, increased 5-HT_{1A} receptor density was found in the CA1 region.

The results of *tg5xFAD/LRP1* and *tgArcAβ* mice support the finding of former studies. Enhanced serotonin fiber sprouting was observed in the striatum and the hippocampus after accumulation of Aβ (Harkany et al., 2000; Harkany et al., 2001; Noristani et al., 2011). Moreover, the serotonin transporter (SERT) as well as the density of SERT axons and terminals was increased in the hippocampus of a mouse model of AD (Noristani et al., 2011). Serotonergic neurons are associated with neurotrophic factors, such as brain-derived neurotrophic factor, somatostatin and neuropeptide Y (Lanctot et al., 2001). In addition, serotonin has been shown to be a co-transmitter of noradrenaline. Noradrenergic α_2 receptors were increased in *tg5xFAD/LRP1* and *tgArcAβ* mice (see chapter 5), implying lower adrenaline level. Thus, the increased density of 5-HT_{2A} receptors might reflect a compensatory mechanism.

However, a reduction of 5-HT_{2A} receptors was found in former studies, both in rodents and in humans. PET studies showed reduced 5-HT_{2A} binding in patients with AD (Blin et al., 1993; Meltzer et al., 1998). In a rodent model of FAD, intrahippocampal injection of aggregated Aβ caused reduced 5-HT_{2A} receptor level and, moreover, impairment in memory (Holm et al., 2010). An explanation for the controversial results found by Holm et al. (2010) and in the current study might be the age of the mice. Mice used in this study were between four to six months or eight months old, while Holm investigated groups of mice being four, eight and eleven months old. A reduction was only found in the mice being eleven months old. Another study found increase of the 5-HT_{1A} receptor in patients with mild cognitive impairment. In patients with AD, the receptor was reduced (Truchot et al., 2007). This might indicate that the serotonergic system decreases as the disease progresses. The same might be true for 5-HT_{2A} receptors. Another explanation might be different radioactive ligand used by Holm et al. (2010). The affinity for their 5-HT_{2A} receptor differs from the one used in the current study (Lopez-Gimenez et al., 1998). Furthermore, the *PS1* gene was partly deleted. The mice in the current study carried mutated PS1 (*tg5xFAD/LRP1* mice) or wt PS1 (*tgArcAβ* mice).

Additionally, serotonergic neurons interact with dopaminergic neurons. For example, neurons emerging from the raphe nuclei control dopamine release in the midbrain, striatum and nucleus accumbens (Meltzer, 1992; Lanctot et al., 2001). Moreover, serotonergic neurons are able to enhance the release of dopamine (Lanctot et al., 2001). In *tg5xFAD/LRP1* mice, a trend towards increase was observed in dopaminergic D_2 receptors (compare chapter 6). The increased dopamine release may be caused by the increase in the serotonergic system.

4 GABA receptors

GABA is the major inhibitory transmitter in the mammalian brain. GABAergic transmission plays an important role in inhibitory modulation of pyramidal cell and interneuron firing in both the mnemonic and sensorimotor phases of the working memory process and in the construction of spatial tuning (Rao et al., 2000; Constantinidis et al., 2002; Parameshwaran et al., 2008). Detrimental effects of Aβ fragments on GABAergic interneurons have been described (Pakaski et al., 1998). Significant reductions in cortical GABA concentrations were also observed in AD brains (Ellison et al., 1986). However, other authors described the GABAergic system as relatively spared in AD compared to the glutamatergic and cholinergic systems (Rissman et al., 2007) and even be resistant to Aβ toxicity (Pike and Cotman, 1993).

This is in agreement with the lack of impairment of the antagonist binding sites of $GABA_A$ receptors and benzodiazepine binding sites in ***LRP1*, *tg5xFAD* and *tg5xFAD/LRP1*** mice in the current study. $GABA_B$ receptors were significant reduced only in the olfactory bulb of ***LRP1*** mice. ***Tg5xAFD* and *tg5xFAD/LRP1*** mice showed a significant downregulation of the agonistic binding sites of $GABA_A$ receptors only in the stratum moleculare/granulosum (for discussion of this finding, see discussion of the *tgArcAβ* mice below).

In contrast, the ***tgArcAβ*** mouse was affected. The agonistic binding sites of $GABA_A$ receptors were downregulated in the olfactory bulb, the striatum and the mossy fiber terminal fields/hilus. $GABA_B$ receptors and benzodiazepine binding sites were not affected.

As described in chapter 1, Aβ can lead to accumulation of glutamate and thus to neuronal depolarization. GABA stimulates $GABA_A$ receptors, leading to influx of Cl^- and hyperpolarization. $GABA_B$ receptors, which are coupled to G protein and activate K^+

conductance, cause hyperpolarization of the membrane. Thus, activation of GABA receptors counteracts the depolarization caused by the activation of glutamate receptors. Taurine, a naturally occurring β-amino acid in the mammalian brain, is involved in several physiological processes, e.g. calcium ion regulation amongst others (Huxtable, 1992). Interestingly, taurine activates $GABA_A$ receptors, and therefore enhances the Cl^- conductance of the membrane (Okamoto et al., 1983; del Olmo et al., 2000). Furthermore, taurine, GABA and Muscimol, a GABA agonist, are able to block the neurotoxicity of Aβ to cortical and hippocampal neurons (Paula-Lima et al., 2005). Similar findings were also made by Lee and colleagues (Lee et al., 2005).

Treatment of cortical neurons with Muscimol protected neurons against apoptosis, inhibited both the increase of calcium influx and the elevation of glutamate release as well as the generation of reactive oxygen species, all processes induced by Aβ. Further evidence of GABA receptors and taurine as factors in the generation of AD rises from the findings that GABA (Grachev and Apkarian, 2001) and taurine (Benedetti et al., 1991) levels are decreased in the brain of aged humans and rats as well as in the brain of AD patients (Paula-Lima et al., 2005). Decrease of GABA and taurine in the brain of the mouse models could occur during ageing and accumulation of glutamate would aggravate this effect. Downregulation of GABA receptors might indicate loss of this protective effect in the *tgArcAβ* mice. Since our *tgArcAβ* mice were 2 -4 months older than the other mouse models, this downregulation of GABA receptors was not found in the latter mice strains with the exception of a downregulation of the agonistic binding sites of $GABA_A$ receptors in the stratum moleculare/granulosum of *tg5xAFD* and *tg5xFAD/LRP1* mice and a downregulation of $GABA_B$ in the olfactory bub of *LRP1* mice.

5 Noradrenaline receptors

Adrenergic receptors belong to the group of G protein coupled receptors. They are divided into two main groups, α and β, which can be subdivided further into α_1 and α_2 and β_1, β_2 and β_3. The corresponding neurotransmitter and hormones are adrenaline and noradrenaline, which are produced in the adrenal medulla and the locus coeruleus (LC), respectively. The adrenergic system is supposed to have a role in learning and memory, sleep-wake cycle

regulation, affective psychosis and regulation of aggression (Russo-Neustadt and Cotman, 1997).

In the current study, the adrenergic system was affected in all mouse models, the strongest effect was found in *LRP1*, *tg5xFAD* and *tg5xFAD/LRP1* mice.

***LRP1* mice:** The density of α_2 receptors was significantly enhanced in all regions, with exception of the stratum granulosum/moleculare and the piriform cortex. In the piriform cortex, LRP1 mice showed a trend towards upregulation. Significantly reduced levels of α_1 receptors were found in the olfactory bulb, the somatosensory and the piriform cortex. Furthermore, *LRP1* showed reduced, though not significant, levels of α_1 receptors in all other regions analyzed, particularly in the olfactory bulb.

***tg5xFAD* and *tg5xFAD/LRP1* mice:** In all regions, the α_2 receptor density was significantly increased, with exception of the stratum granulosum/moleculare of *tg5xFAD/LRP1* mice. Still, *tg5xFAD/LRP1* mice revealed a trend toward upregulation in stratum granulosum/moleculare. In *tg5xFAD* and *tg5xFAD/LRP1* mice, a trend towards downregulation of α_1 receptors in all brain regions was observed as well. This implicates that lower levels of α_1 receptors are linked especially to the knockout of LRP1 and PS1 mutations. A possible explanation for the fact that most reductions were not significant could be the age of the mice. Since AD is a disease of age, the observed modulations where only visible as trend and may aggravate over time.

Reduction of α_1 receptors indicates that noradrenaline may be reduced in the brain of the used mouse models. Moreover, α_2 receptors proved to be strongly upregulated in nearly all brain regions. Activation of α_2 receptors by noradrenaline and adrenaline leads to decreased release of neurotransmitters, caused by negative feedback. Therefore, it seems that those adrenergic neurotransmitters are reduced in the investigated mouse models. This is interesting since the cholinergic system is affected as well. Release of adrenaline and noradrenaline from the adrenal medulla is exclusively regulated by cholinergic synapses. Cholinergic receptors are reduced in *LRP1*, *tg5xFAD* and *tg5xFAD/LRP1* mice, with the exception of the M_2 antagonist binding site in the striatum of *LRP1* and of the M_3 receptor in the CA1 region of *tg5xFAD* mice. This could at least partly account to a low level of adrenergic transmitters.

Furthermore, noradrenaline seems to exert anti-inflammatory and anti-oxidative mechanisms within the CNS (Feinstein et al., 2002; Heneka et al., 2002; Jardanhazi-Kurutz et al., 2011), both being associated with AD. Reduction of noradrenaline by the neurotoxin N-(2-chloroethyl)-N-ethyl-2 bromobenzylamine (DSP4) caused increased cortical inflammatory reaction in response to injection of aggregated Aβ (Heneka et al., 2002). Antagonists of α_2 receptors exert a positive effect regarding neuroprotection. They increase growth factor expression and on the contrary reduce apoptosis (Bauer et al., 2003; Debeir et al., 2004). Noradrenaline release is increased as well. Kalinin et al. (2006) proved that injection of Aβ caused expression of the nitric oxide synthase NOS2 in cortical neurons if the noradrenaline level was reduced first (Kalinin et al., 2006). Likewise, disruption of LC increases Aβ burden, neuronal damage and behavioral deficits in tgAPP mice (Heneka et al., 2006).

***tgArcAβ* mice:** In the *tgArcAβ* mouse model increased density of α_2 receptors was observed in fewer regions compared to the other AD models, but was affected in the olfactory bulb, the piriform cortex and the hippocampus. Additionally, α_1 receptor density was increased in the striatum. Increased density of α_2 receptors was already explained above (see *LRP1*, *tg5xFAD* and *tg5xFAD/LRP1* mice). The increase of the α_1 receptor in this strain needs further examination.

Due to its neuroprotective actions, the adrenergic system might be considered as a novel therapeutic target. Since the α_2 receptor reduces the release of noradrenaline, and increased receptors may further aggravate this effect, a reduction of this α_2 receptor may improve cognitive abilities. This has been shown using a chronic treatment with the α_2 receptors antagonist fluparoxan. This procedure prevented memory deficits in APP/PS1 mice in cognitive tests where noradrenaline plays an integral role in (Scullion et al., 2011).

6 Dopamine receptors

Dopamine is synthesized in midbrain neurons, i.e. in the ventral tegmental area and the substantia nigra, and contributes importantly to synaptic plasticity, thereby innervating the hippocampus, neocortex and basal ganglia (Martorana et al., 2013). The five dopamine receptors are differentiated in two main subclasses, the D_1-like (comprising the D_1 and D_5

receptors) and D_2-like (comprising the D_2, D_3 and D_4 receptors). All are coupled to a G-protein and influence cyclic adenosine monophosphate (cAMP), D_1-like by activating adenylate cyclase and D_2-like by inhibiting cAMP. Dopaminergic control of cortical activity is performed particularly by D_2 and D_3 receptors. Binding of dopamine to D_2 receptors causes reduced excitability (Gulledge and Jaffe, 1998; Tseng and O'Donnell, 2007), while D_3 receptors innervate cortical acetylcholine release (Millan et al., 2007). However, the role of dopamine in AD is still not quite well understood.

In the present study, the density of D_2 receptors was increased significantly only in ***tg5xFAD*** mice. Analysis of $D_{2/3}$ receptor density revealed a trend towards upregulation. A trend towards increase was also observed in the ***LRP1*** and ***tg5xFAD/LRP1*** mouse model in the D_2 receptor and $D_{2/3}$ receptor density. In the ***tgArcAβ*** mouse model a trend towards upregulation of the $D_{2/3}$ receptor density was shown.

The enhanced level of D_2 receptors may play an important role in the reduction of the cholinergic system, due to its close interaction with each other. Increased D_2 receptors density may also contribute to modification of motor behavior, although the mouse models do not show any motor symptoms. An exception is the *LRP1* mouse model, which shows muscle tremor and dystonia (May et al., 2004). However, it is well known that rodents are able to compensate even large alterations in their brain.

In the current study, D_2 receptors were only investigated in the striatum. In recent studies, abnormalities in the ventral striatum, i.e. rostral medial caudate head and the ventral lateral putamen, have been found in AD patients. Moreover, cognitive impairment was associated with the degree of surface alterations in the ventral areas of the caudate and putamen as well as the accumbens area (de Jong et al., 2011). It seems that the volume reduction of the putamen and the nucleus accumbens are closely related to cognitive decline (de Jong et al., 2012). Former studies indicate a functional interaction between the prefrontal cortex and the nucleus accumbens, thus having great importance in cognitive and motor behavior (Ongur and Price, 2000; Tzschentke, 2001). Likewise, the stimulation of prefrontal D_2 receptors decreased the extracellular level of dopamine and acetylcholine in the nucleus accumbens. Moreover, stimulation of D_2 receptors in nucleus accumbens caused reduction in the release of acetylcholine (Brooks et al., 2007; Del Arco et al., 2007).

Furthermore, in *tg5xFAD* mice, the glutamatergic receptors are reduced together with enhanced D_2 receptor density. Whether the reduction in the glutamatergic system is linked to the reduced excitability caused by D_2 receptors as mentioned above cannot be answered in this study.

7 Correlations between behavior, transmitter and receptor alterations

Beside the cognitive impairment, the most frequent symptoms of AD are apathy (45%), depression (44%) and aggression (40%) (Lyketsos et al., 2002). There is evidence that alteration in neurotransmitter systems, especially in the **cholinergic system**, contribute to these changes (Cummings and Kaufer, 1996; Lanari et al., 2006). Deficits in the cholinergic system of the basal forebrain correlate positively with behavioral disturbance. For instance, ChAT activity was reduced in brains of AD patients, which showed hyperactivity, compared to controls (Minger et al., 2000). Liu et al. reported that 18 months old *LRP1* mice traveled significantly longer distance than control mice, indicating that LRP1 deletion causes hyperactivity in mice (Liu et al., 2010). Since M_2 receptor density was decreased in hippocampal areas, it may at least partly explain the hyperactivity found in *LRP1* mice.
Hyperactivity was also observed in *tgArcAβ* mice in the first three months. However, only a slight increase of M_2 receptors was found in the present study. This correlates with the results of Knobloch et al. (2006), who observed hyperactivity in *tgArcAβ* mice during the first three months. With age, hyperactivity disappeared and changed to hypoactivity between 6 and 9 months of age. In the present study, t*gArcAβ* mice were 8 months old, thus starting to change to hypoactivity.

Besides the cholinergic system, the **adrenergic system** seems to be involved in mood alteration. Several studies have found LC neuron loss in AD patients with depression (Zubenko and Moossy, 1988; Zweig et al., 1988; Förstl et al., 1992). As already mentioned in chapter 5, noradrenaline is produced in the LC. Therefore, less noradrenaline might be present due to LC neuron loss. Among the most common symptoms of AD are aggression, irritability and agitation, causing great problems in the care of the patients (Russo-Neustadt and Cotman, 1997). Enhanced density of α_2 receptors in the cerebellum has been found to correlate with aggressive behavior in AD patients (Russo-Neustadt and Cotman, 1997). In the

present study, the cerebellum was not investigated. However, in all mouse models used and all regions analyzed in this study, α2 receptors were increased. As a result, an involvement of the adrenergic system in behavioral changes seems plausible.

Antidepressant drugs directly or indirectly reduce **NMDA** receptor function (Zarate et al., 2003) and seem to raise **GABA** levels (Krystal et al., 2002). This is in agreement with the findings according to the *tgArcAβ* mouse model, in which NMDA receptors are upregulated while in the GABAergic system a downregulation could be observed.

Dysfunction of the **dopaminergic** system is also often associated with behavioral alteration. Common therapy for schizophrenic symptoms in AD are D_2 receptor antagonists (Lanari et al., 2006). Enhanced levels of striatal D_2 receptors were reported in AD patients showing delusional symptoms (Reeves et al., 2009). Likely, attention performance was poor when density of dopaminergic D_2 receptors was increased (Reeves et al., 2010). Notably, an increased D_2 receptor density was found in the 5xFAD model of the present study.

8 Olfactory function

One of the greatest problems in the treatment of AD is an early clinical diagnosis. At the time when AD is first diagnosed, neurodegeneration has already started. Therefore, therapies should start as early as possible, prior clinical manifestation, and an early marker is required to identify AD as early as possible.

Deficits in olfactory functioning, with respect to odor detection, discrimination, recognition identification and naming are a well-known hallmarks of AD (Cassano et al., 2011), and occur early in the pathogenesis of dementia (Hawkes, 2003). About 90% of all patients suffering from FAD exhibit severe olfactory dysfunction (Hawkes, 2003). Olfactory processing involves several steps, from sensory neuron input to the olfactory bulb, decoding and plasticity in the piriform cortex and downstream neurons in the hippocampus (Brennan and Keverne, 1997; Cassano et al., 2011).

The patterns of neurotransmitter receptor changes in the olfactory bulb and piriform cortex were most similar between *tg5xFAD* and *tg5xFAD/LRP1* mice. Both mouse models revealed

altered levels of neurotransmitter receptors in the glutamatergic, cholinergic and adrenergic system compared to control mice. *LRP1* mice proved similar regulation, with reduced density in the glutamatergic system and increased density in the adrenergic α2 receptor. Furthermore, they exhibited significantly enhanced levels of $GABA_B$ in the olfactory bulb. Only minor changes were revealed in the olfactory bulb and piriform cortex of *tgArcAβ* mice. The transmitter systems affected were the glutamatergic, adrenergic and GABAergic system. The NMDA receptor density was increased in the piriform cortex, while in the adrenergic system the α_2 receptor was enhanced in the olfactory bulb as well as in the piriform cortex. Changes are summarized in Figure 43 and Figure 78.

Besides the different degree of changes, the glutamatergic and adrenergic system seems to be impaired in all mouse models investigated. However, while in *LRP1*, *tg5xFAD* and *tg5xFAD/LRP1* mice the glutamate receptors are decreased, NMDA receptor density is increased in the *tgArcAβ* model, implicating a diverse mechanism of involvement. In all models, the adrenergic system was altered, suggesting an association of this system with olfactory deficits found in former studies. Noradrenergic neurons have been shown to intensely innervate the olfactory bulb in rodents. 40% of efferent LC neurons, where noradrenaline is produced, project to different layers of the olfactory bulb (Shipley et al., 1985). Treatment of APP/PS1 mice with the neurotoxin DSP4 caused impaired short term olfactory memory and discrete weakening of olfactory discrimination abilities (Rey et al., 2012). Moreover, noradrenaline modulates olfactory discrimination ability (Doucette et al., 2007) and odor habituation and discrimination after LC lesion can be restored by infusion of noradrenaline (Guerin et al., 2008).

Little is known about the role of Aβ in olfactory dysfunction. Evidence that Aβ seems to influence the olfactory processing comes from Wesson et al. (2010), who revealed a correlation between perceptual olfactory function and temporal-spatial pattern of Aβ in a mouse model of AD. Although the alteration in neurotransmitter receptors were found in the olfactory bulb and piriform cortex, plaques were observed in the mouse models neither in the olfactory bulb nor in the piriform cortex. However, olfactory testing was not performed with the mice used in the present study. Therefore, it is possible that the mice already showed alterations of receptor density in the olfactory bulb and piriform cortex preceding impairments in olfactory performance caused by plaque formation.

9 Conclusion

In all models, the glutamatergic, the cholinergic, the GABAergic and the adrenergic systems were affected. Additionally, the serotonergic system revealed differences in the *tgArcAβ* and *tg5xFAD/LRP1* mice compared to controls, while the dopaminergic system was affected in the *tg5xFAD* mice. Furthermore, a trend towards upregulation of the dopaminergic D_2 receptors was observed in *LRP1* and *tg5xFAD/LRP1* mice. NMDA receptor density was increased in *tgArcAβ* and *LRP1* mice, while it was reduced in *tg5xFAD* and *tg5xFAD/LRP1* mice, therefore pointing to different alterations in the course of AD.

tgArcAβ, tg5xFAD and *tg5xFAD/LRP1* mice all reflect mutations found in cases of FAD. All these mutations cause increased levels of Aβ. Since alterations of neurotransmitter receptors are similar in most cases, Aβ seems to play an important role in receptor alterations. The presence of mutations in the *PS1* gene causes a shift in the ratio of Aβ40/ Aβ42, which is believed to be more neurotoxic. Furthermore, the *tg5xFAD* mouse model is known to suffer from a very aggressive plaque generation. Indeed, numerous differences were observed in *tg5xFAD* and *tg5xFAD/LRP1* mice, although they were only between four and six months of age and therefore much younger than *tgArcAβ* mice.

LRP1 mice, however, reflect the loss of LRP1 protein that interacts with two factors that are connected to sporadic AD. Receptor alterations of *LRP1* mice did not differ from mouse models expressing mutations associated with FAD, with exception of the serotonergic and dopaminergic system. Extracellular plaques were only observed in *tg5xFAD* and *tg5xFAD/LRP1* mice. In *LRP1* mice, plaques were not found, although a beginning aggregation of Aβ seemed to be present in the motor cortex and hippocampus. However, this has to be confirmed using additional staining, such as Thioflavin S. Intracellular accumulation of Aβ was observed in the *tgArcAβ* mouse model. It is striking that several regions and neurotransmitter receptors were affected in all mouse models. Changes occurred also in regions and mouse models, which did not express plaques. For example, *LRP1* mice revealed the strongest reduction of kainate receptors of all mouse models and strong alterations in the cholinergic system without plaques generation. Impaired synaptic plasticity might contribute to the changes in the receptor systems. The uptake of cholesterol into neurons by apoE is mediated by LRP1. Cholesterol, however, is important for synaptic

plasticity. Mutations causing enhanced levels of Aβ also lead to altered receptor density. It seems that Aβ as well as impairment of cholesterol metabolism has an effect on receptor systems. Furthermore, γ-secretase-dependent APP processing seems to be involved in the regulation of brain cholesterol by transcriptional repression of LRP1. Increased APP processing by γ-secretase, as it was found in mice harboring FAD mutations, might lead to reduced levels of LRP1. In summary, these results indicate similar receptor changes, although the mechanism behind the plaque generation is different in FAD and sporadic AD.

V. Summary

The aim of the study was to analyze the distribution and density of neurotransmitter receptors of the glutamatergic, cholinergic, GABAergic, serotonergic, adrenergic, dopaminergic and adenosinergic system in several mouse models of AD. The *tgArcAβ* und *tg5xFAD* mouse models mirror mutations found in familiar AD (FAD), while *LRP1* mice reflect a risk factor found in sporadic AD. *tg5xFAD/LRP1* mice combine both factors. Using quantitative receptor autoradiography, eight brain regions were investigated, i.e. the olfactory bulb, the motor, somatosensory and piriform cortex, the hippocampal regions CA1, mossy fiber termination regions/hilus and stratum moleculare/granulosum. Presence of Aβ, a hallmark of AD, was tested by the use of immunohistochemistry.

In all models, the glutamatergic, cholinergic, GABAergic and adrenergic system was affected. The cholinergic and GABAergic system revealed reduced receptor density, while the adrenergic receptors were increased in several regions. This indicates a similar mechanism in AD regarding these receptor systems. The glutamatergic kainate and mGlu2/3 receptors were reduced in all mouse models, with exception of increased kainate receptor density *tg5xFAD/LRP1* mice. NMDA receptor density was increased in in *tgArcAβ* and *LRP1* mice, while it was reduced in *tg5xFAD* and *tg5xFAD/LRP1* mice, pointing to different alterations in the course of AD. The serotonergic receptors revealed differences in the *tgArcAβ* and *tg5xFAD/LRP1* mice compared to controls, while the dopaminergic system was significantly affected only in the *tg5xFAD* mice.

In conclusion, comparison of the neurotransmitter receptor changes of all mouse models revealed similar changes. *tgArcAβ, tg5xFAD* and *tg5xFAD/LRP1* mice mirrored the effects of mutation associated with FAD, generating increased Aβ. Aβ seems to repress LRP1, causing impaired cholesterol transport into neurons. LRP1, however, interacts with two risk factors of sporadic AD, i.e. apoE and α2M. *LRP1* mice reflect impaired LRP1 metabolism, which may be also a possible cause of AD. In summary, these results indicate similar receptor changes, although the mechanisms behind the plaque generation is different in FAD and sporadic AD.

VI. Bibliography

Andersen OM, Willnow TE (2006) Lipoprotein receptors in Alzheimer's disease. Trends in Neurosciences 29:687-694.

Anderson JP, Esch FS, Keim PS, Sambamurti K, Lieberburg I, Robakis NK (1991) Exact cleavage site of Alzheimer amyloid precursor in neuronal PC-12 cells. Neuroscience Letters 128:126-128.

Araujo DM, Lapchak PA, Robitaille Y, Gauthier S, Quirion R (1988) Differential alteration of various cholinergic markers in cortical and subcortical regions of human brain in Alzheimer's disease. Journal of Neurochemistry 50:1914-1923.

Auld DS, Kornecook TJ, Bastianetto S, Quirion R (2002) Alzheimer's disease and the basal forebrain cholinergic system: relations to beta-amyloid peptides, cognition, and treatment strategies. Progress in Neurobiology 68:209-245.

Bauer S, Moyse E, Jourdan F, Colpaert F, Martel JC, Marien M (2003) Effects of the alpha 2-adrenoreceptor antagonist dexefaroxan on neurogenesis in the olfactory bulb of the adult rat in vivo: selective protection against neuronal death. Neuroscience 117:281-291.

Benedetti MS, Russo A, Marrari P, Dostert P (1991) Effects of ageing on the content in sulfur-containing amino acids in rat brain. Journal of Neural Transmission General Section 86:191-203.

Berezovska O, Lleo A, Herl LD, Frosch MP, Stern EA, Bacskai BJ, Hyman BT (2005) Familial Alzheimer's disease presenilin 1 mutations cause alterations in the conformation of presenilin and interactions with amyloid precursor protein. The Journal of Neuroscience : the Official Journal of the Society for Neuroscience 25:3009-3017.

Bernareggi A, Duenas Z, Reyes-Ruiz JM, Ruzzier F, Miledi R (2007) Properties of glutamate receptors of Alzheimer's disease brain transplanted to frog oocytes. Proceedings of the National Academy of Sciences of the United States of America 104:2956-2960.

Bitan G, Kirkitadze MD, Lomakin A, Vollers SS, Benedek GB, Teplow DB (2003) Amyloid beta -protein (Abeta) assembly: Abeta 40 and Abeta 42 oligomerize through distinct pathways. Proceedings of the National Academy of Sciences of the United States of America 100:330-335.

Blacker D, Wilcox MA, Laird NM, Rodes L, Horvath SM, Go RC, Perry R, Watson B, Jr., Bassett SS, McInnis MG, Albert MS, Hyman BT, Tanzi RE (1998) Alpha-2 macroglobulin is genetically associated with Alzheimer disease. Nature Genetics 19:357-360.

Blin J, Baron JC, Dubois B, Crouzel C, Fiorelli M, Attar-Levy D, Pillon B, Fournier D, Vidailhet M, Agid Y (1993) Loss of brain 5-HT2 receptors in Alzheimer's disease. In vivo assessment with positron emission tomography and [18F]setoperone. Brain : a Journal of Neurology 116 (Pt 3):497-510.

Boer S, Sanchez D, Reinieren I, van den Boom T, Udawela M, Scarr E, Ganfornina MD, Dean B (2010) Decreased kainate receptors in the hippocampus of apolipoprotein D knockout mice. Progress inNneuropsychopharmacology & Biological Psychiatry 34:271-278.

Borchelt DR, Thinakaran G, Eckman CB, Lee MK, Davenport F, Ratovitsky T, Prada CM, Kim G, Seekins S, Yager D, Slunt HH, Wang R, Seeger M, Levey AI, Gandy SE, Copeland NG, Jenkins NA, Price DL, Younkin SG, Sisodia SS (1996) Familial Alzheimer's disease-linked presenilin 1 variants elevate Abeta1-42/1-40 ratio in vitro and in vivo. Neuron 17:1005-1013.

Braak H, Braak E (1991) Neuropathological stageing of Alzheimer-related changes. Acta neuropathologica 82:239-259.

Bracco L, Gallato R, Grigoletto F, Lippi A, Lepore V, Bino G, Lazzaro MP, Carella F, Piccolo T, Pozzilli C, et al. (1994) Factors affecting course and survival in Alzheimer's disease. A 9-year longitudinal study. Archives of Neurology 51:1213-1219.

Brennan PA, Keverne EB (1997) Neural mechanisms of mammalian olfactory learning. Progress in Neurobiology 51:457-481.

Brionne TC, Tesseur I, Masliah E, Wyss-Coray T (2003) Loss of TGF-beta 1 leads to increased neuronal cell death and microgliosis in mouse brain. Neuron 40:1133-1145.

Brooks JM, Sarter M, Bruno JP (2007) D2-like receptors in nucleus accumbens negatively modulate acetylcholine release in prefrontal cortex. Neuropharmacology 53:455-463.

Bruno V, Battaglia G, Copani A, Giffard RG, Raciti G, Raffaele R, Shinozaki H, Nicoletti F (1995) Activation of class II or III metabotropic glutamate receptors protects cultured cortical neurons against excitotoxic degeneration. The European Journal of Neuroscience 7:1906-1913.

Bruno V, Battaglia G, Copani A, D'Onofrio M, Di Iorio P, De Blasi A, Melchiorri D, Flor PJ, Nicoletti F (2001) Metabotropic glutamate receptor subtypes as targets for neuroprotective drugs. Journal of Cerebral Blood Flow and Metabolism : official journal of the International Society of Cerebral Blood Flow and Metabolism 21:1013-1033.

Bu G (2009) Apolipoprotein E and its receptors in Alzheimer's disease: pathways, pathogenesis and therapy. Nature Reviews Neuroscience 10:333-344.

Bu G, Maksymovitch EA, Nerbonne JM, Schwartz AL (1994) Expression and function of the low density lipoprotein receptor-related protein (LRP) in mammalian central neurons. The Journal of Biological Chemistry 269:18521-18528.

Burdick D, Soreghan B, Kwon M, Kosmoski J, Knauer M, Henschen A, Yates J, Cotman C, Glabe C (1992) Assembly and aggregation properties of synthetic Alzheimer's A4/beta amyloid peptide analogs. The Journal of Biological Chemistry 267:546-554.

Cai XD, Golde TE, Younkin SG (1993) Release of excess amyloid beta protein from a mutant amyloid beta protein precursor. Science 259:514-516.

Caille I, Allinquant B, Dupont E, Bouillot C, Langer A, Muller U, Prochiantz A (2004) Soluble form of amyloid precursor protein regulates proliferation of progenitors in the adult subventricular zone. Development 131:2173-2181.

Cam JA, Bu G (2006) Modulation of beta-amyloid precursor protein trafficking and processing by the low density lipoprotein receptor family. Molecular Neurodegeneration 1:8.

Caraci F, Spampinato S, Sortino MA, Bosco P, Battaglia G, Bruno V, Drago F, Nicoletti F, Copani A (2012) Dysfunction of TGF-beta1 signaling in Alzheimer's disease: perspectives for neuroprotection. Cell and Tissue research 347:291-301.

Cassano T, Romano A, Macheda T, Colangeli R, Cimmino CS, Petrella A, LaFerla FM, Cuomo V, Gaetani S (2011) Olfactory memory is impaired in a triple transgenic model of Alzheimer disease. Behavioural Brain Research 224:408-412.

Chen YR, Glabe CG (2006) Distinct early folding and aggregation properties of Alzheimer amyloid-beta peptides Abeta40 and Abeta42: stable trimer or tetramer formation by Abeta42. The Journal of Biological Chemistry 281:24414-24422.

Citron M, Oltersdorf T, Haass C, McConlogue L, Hung AY, Seubert P, Vigo-Pelfrey C, Lieberburg I, Selkoe DJ (1992) Mutation of the beta-amyloid precursor protein in familial Alzheimer's disease increases beta-protein production. Nature 360:672-674.

Citron M, Eckman CB, Diehl TS, Corcoran C, Ostaszewski BL, Xia W, Levesque G, St George Hyslop P, Younkin SG, Selkoe DJ (1998) Additive effects of PS1 and APP mutations on secretion of the 42-residue amyloid beta-protein. Neurobiology of Disease 5:107-116.

Citron M et al. (1997) Mutant presenilins of Alzheimer's disease increase production of 42-residue amyloid beta-protein in both transfected cells and transgenic mice. Nature Medicine 3:67-72.

Cleary JP, Walsh DM, Hofmeister JJ, Shankar GM, Kuskowski MA, Selkoe DJ, Ashe KH (2005) Natural oligomers of the amyloid-beta protein specifically disrupt cognitive function. Nature Neuroscience 8:79-84.

Constantinidis C, Williams GV, Goldman-Rakic PS (2002) A role for inhibition in shaping the temporal flow of information in prefrontal cortex. Nature Neuroscience 5:175-180.

Corder EH, Saunders AM, Strittmatter WJ, Schmechel DE, Gaskell PC, Small GW, Roses AD, Haines JL, Pericak-Vance MA (1993) Gene dose of apolipoprotein E type 4 allele and the risk of Alzheimer's disease in late onset families. Science 261:921-923.

Coutinho V, Knopfel T (2002) Metabotropic glutamate receptors: electrical and chemical signaling properties. The Neuroscientist 8:551-561.

Coyle JT, Price DL, DeLong MR (1983) Alzheimer's disease: a disorder of cortical cholinergic innervation. Science 219:1184-1190.

Cummings JL, Kaufer D (1996) Neuropsychiatric aspects of Alzheimer's disease: the cholinergic hypothesis revisited. Neurology 47:876-883.

D'Onofrio M, Cuomo L, Battaglia G, Ngomba RT, Storto M, Kingston AE, Orzi F, De Blasi A, Di Iorio P, Nicoletti F, Bruno V (2001) Neuroprotection mediated by glial group-II metabotropic glutamate receptors requires the activation of the MAP kinase and the phosphatidylinositol-3-kinase pathways. Journal of Neurochemistry 78:435-445.

De Felice FG, Velasco PT, Lambert MP, Viola K, Fernandez SJ, Ferreira ST, Klein WL (2007) Abeta oligomers induce neuronal oxidative stress through an N-methyl-D-aspartate receptor-dependent mechanism that is blocked by the Alzheimer drug memantine. The Journal of Biological Chemistry 282:11590-11601.

de Jong LW, Wang Y, White LR, Yu B, van Buchem MA, Launer LJ (2012) Ventral striatal volume is associated with cognitive decline in older people: a population based MR-study. Neurobiology of Aging 33:424 e421-410.

de Jong LW, Ferrarini L, van der Grond J, Milles JR, Reiber JH, Westendorp RG, Bollen EL, Middelkoop HA, van Buchem MA (2011) Shape abnormalities of the striatum in Alzheimer's disease. Journal of Alzheimer's Disease : JAD 23:49-59.

Deane R, Wu Z, Sagare A, Davis J, Du Yan S, Hamm K, Xu F, Parisi M, LaRue B, Hu HW, Spijkers P, Guo H, Song X, Lenting PJ, Van Nostrand WE, Zlokovic BV (2004) LRP/amyloid beta-peptide interaction mediates differential brain efflux of Abeta isoforms. Neuron 43:333-344.

Debeir T, Marien M, Ferrario J, Rizk P, Prigent A, Colpaert F, Raisman-Vozari R (2004) In vivo upregulation of endogenous NGF in the rat brain by the alpha2-adrenoreceptor antagonist dexefaroxan: potential role in the protection of the basalocortical cholinergic system during neurodegeneration. Experimental Neurology 190:384-395.

Del Arco A, Mora F, Mohammed AH, Fuxe K (2007) Stimulation of D2 receptors in the prefrontal cortex reduces PCP-induced hyperactivity, acetylcholine release and dopamine metabolism in the nucleus accumbens. Journal of Neural Transmission 114:185-193.

del Olmo N, Bustamante J, del Rio RM, Solis JM (2000) Taurine activates GABA(A) but not GABA(B) receptors in rat hippocampal CA1 area. Brain Research 864:298-307.

Doucette W, Milder J, Restrepo D (2007) Adrenergic modulation of olfactory bulb circuitry affects odor discrimination. Learning & Memory 14:539-547.

Duff K, Eckman C, Zehr C, Yu X, Prada CM, Perez-tur J, Hutton M, Buee L, Harigaya Y, Yager D, Morgan D, Gordon MN, Holcomb L, Refolo L, Zenk B, Hardy J, Younkin S (1996) Increased amyloid-beta42(43) in brains of mice expressing mutant presenilin 1. Nature 383:710-713.

Eckman CB, Mehta ND, Crook R, Perez-tur J, Prihar G, Pfeiffer E, Graff-Radford N, Hinder P, Yager D, Zenk B, Refolo LM, Prada CM, Younkin SG, Hutton M, Hardy J (1997) A new pathogenic mutation in the APP gene (I716V) increases the relative proportion of A beta 42(43). Human Molecular Genetics 6:2087-2089.

Everitt BJ, Robbins TW (1997) Central cholinergic systems and cognition. Annual Review of Psychology 48:649-684.

Feinstein DL, Heneka MT, Gavrilyuk V, Dello Russo C, Weinberg G, Galea E (2002) Noradrenergic regulation of inflammatory gene expression in brain. Neurochemistry International 41:357-365.

Förstl H, Kurz A (1999) Clinical features of Alzheimer's disease. European Archives of Psychiatry and Clinical Neuroscience 249:288-290.

Förstl H, Burns A, Luthert P, Cairns N, Lantos P, Levy R (1992) Clinical and europathological correlates of depression in Alzheimer's disease. Psychological Medicine 22:877-884.

Frank C, Rufini S, Tancredi V, Forcina R, Grossi D, D'Arcangelo G (2008) Cholesterol depletion inhibits synaptic transmission and synaptic plasticity in rat hippocampus. Experimental Neurology 212:407-414.

Frisardi V, Panza F, Farooqui AA (2011) Late-life depression and Alzheimer's disease: the glutamatergic system inside of this mirror relationship. Brain Research Reviews 67:344-355.

Furukawa K, Barger SW, Blalock EM, Mattson MP (1996) Activation of K+ channels and suppression of neuronal activity by secreted beta-amyloid-precursor protein. Nature 379:74-78.

Gakhar-Koppole N, Hundeshagen P, Mandl C, Weyer SW, Allinquant B, Muller U, Ciccolini F (2008) Activity requires soluble amyloid precursor protein alpha to promote neurite outgrowth in neural stem cell-derived neurons via activation of the MAPK pathway. The European Journal of Neuroscience 28:871-882.

Gao SF, Bao AM (2011) Corticotropin-releasing hormone, glutamate, and gamma-aminobutyric acid in depression. The Neuroscientist 17:124-144.

Geddes JW, Monaghan DT, Cotman CW, Lott IT, Kim RC, Chui HC (1985) Plasticity of hippocampal circuitry in Alzheimer's disease. Science 230:1179-1181.

Gerhardt CC, van Heerikhuizen H (1997) Functional characteristics of heterologously expressed 5-HT receptors. European Journal of Pharmacology 334:1-23.

Glabe C (2001) Intracellular mechanisms of amyloid accumulation and pathogenesis in Alzheimer's disease. Journal of Molecular Neuroscience : MN 17:137-145.

Glenner GG, Wong CW (1984) Alzheimer's disease: initial report of the purification and characterization of a novel cerebrovascular amyloid protein. Biochemical and Biophysical Research Communications 120:885-890.

Goate A, Chartier-Harlin MC, Mullan M, Brown J, Crawford F, Fidani L, Giuffra L, Haynes A, Irving N, James L, et al. (1991) Segregation of a missense mutation in the amyloid precursor protein gene with familial Alzheimer's disease. Nature 349:704-706.

Goldgaber D, Lerman MI, McBride OW, Saffiotti U, Gajdusek DC (1987) Characterization and chromosomal localization of a cDNA encoding brain amyloid of Alzheimer's disease. Science 235:877-880.

Grachev ID, Apkarian AV (2001) Aging alters regional multichemical profile of the human brain: an in vivo 1H-MRS study of young versus middle-aged subjects. Journal of Neurochemistry 76:582-593.

Guerin D, Peace ST, Didier A, Linster C, Cleland TA (2008) Noradrenergic neuromodulation in the olfactory bulb modulates odor habituation and spontaneous discrimination. Behavioral Neuroscience 122:816-826.

Gulledge AT, Jaffe DB (1998) Dopamine decreases the excitability of layer V pyramidal cells in the rat prefrontal cortex. The Journal of Neuroscience : the Official Journal of the Society for Neuroscience 18:9139-9151.

Haass C, Selkoe DJ (1993) Cellular processing of beta-amyloid precursor protein and the genesis of amyloid beta-peptide. Cell 75:1039-1042.

Haass C, Steiner H (2002) Alzheimer disease gamma-secretase: a complex story of GxGD-type presenilin proteases. Trends in Cell Biology 12:556-562.

Haass C, Selkoe DJ (2007) Soluble protein oligomers in neurodegeneration: lessons from the Alzheimer's amyloid beta-peptide. Nature Reviews Molecular Cell Biology 8:101-112.

Haass C, Kaether C, Thinakaran G, Sisodia S (2012) Trafficking and proteolytic processing of APP. Cold Spring Harbor Perspectives in Medicine 2:a006270.

Haass C, Hung AY, Schlossmacher MG, Oltersdorf T, Teplow DB, Selkoe DJ (1993) Normal cellular processing of the beta-amyloid precursor protein results in the secretion of the amyloid beta peptide and related molecules. Annals of the New York Academy of Sciences 695:109-116.

Haass C, Schlossmacher MG, Hung AY, Vigo-Pelfrey C, Mellon A, Ostaszewski BL, Lieberburg I, Koo EH, Schenk D, Teplow DB, et al. (1992) Amyloid beta-peptide is produced by cultured cells during normal metabolism. Nature 359:322-325.

Hardy J, Selkoe DJ (2002) The amyloid hypothesis of Alzheimer's disease: progress and problems on the road to therapeutics. Science 297:353-356.

Hardy J, Duff K, Hardy KG, Perez-Tur J, Hutton M (1998) Genetic dissection of Alzheimer's disease and related dementias: amyloid and its relationship to tau. Nature Neuroscience 1:355-358.

Harkany T, Dijkstra IM, Oosterink BJ, Horvath KM, Abraham I, Keijser J, Van der Zee EA, Luiten PG (2000) Increased amyloid precursor protein expression and serotonergic sprouting following excitotoxic lesion of the rat magnocellular nucleus basalis: neuroprotection by Ca(2+) antagonist nimodipine. Neuroscience 101:101-114.

Harkany T, O'Mahony S, Keijser J, Kelly JP, Konya C, Borostyankoi ZA, Gorcs TJ, Zarandi M, Penke B, Leonard BE, Luiten PG (2001) Beta-amyloid(1-42)-induced cholinergic lesions in rat nucleus basalis bidirectionally modulate serotonergic innervation of the basal forebrain and cerebral cortex. Neurobiology of Disease 8:667-678.

Hawkes C (2003) Olfaction in neurodegenerative disorder. Movement Disorders : Official Journal of the Movement Disorder Society 18:364-372.

Heneka MT, Galea E, Gavriluyk V, Dumitrescu-Ozimek L, Daeschner J, O'Banion MK, Weinberg G, Klockgether T, Feinstein DL (2002) Noradrenergic depletion potentiates beta -amyloid-induced cortical inflammation: implications for Alzheimer's disease. The Journal of Neuroscience : the Official Journal of the Society for Neuroscience 22:2434-2442.

Heneka MT, Ramanathan M, Jacobs AH, Dumitrescu-Ozimek L, Bilkei-Gorzo A, Debeir T, Sastre M, Galldiks N, Zimmer A, Hoehn M, Heiss WD, Klockgether T, Staufenbiel M (2006) Locus ceruleus degeneration promotes Alzheimer pathogenesis in amyloid precursor protein 23 transgenic mice. The Journal of Neuroscience : the Official Journal of the Society for Neuroscience 26:1343-1354.

Henze DA, Urban NN, Barrionuevo G (2000) The multifarious hippocampal mossy fiber pathway: a review. Neuroscience 98:407-427.

Hering H, Lin CC, Sheng M (2003) Lipid rafts in the maintenance of synapses, dendritic spines, and surface AMPA receptor stability. The Journal of Neuroscience : the official journal of the Society for Neuroscience 23:3262-3271.

Herz J, Strickland DK (2001) LRP: a multifunctional scavenger and signaling receptor. The Journal of Clinical Investigation 108:779-784.

Holm P, Ettrup A, Klein AB, Santini MA, El-Sayed M, Elvang AB, Stensbol TB, Mikkelsen JD, Knudsen GM, Aznar S (2010) Plaque deposition dependent decrease in 5-HT2A serotonin receptor in AbetaPPswe/PS1dE9 amyloid overexpressing mice. Journal of Alzheimer's Disease : JAD 20:1201-1213.

Hoshi M, Takashima A, Murayama M, Yasutake K, Yoshida N, Ishiguro K, Hoshino T, Imahori K (1997) Nontoxic amyloid beta peptide 1-42 suppresses acetylcholine synthesis. Possible role in cholinergic dysfunction in Alzheimer's disease. The Journal of Biological Chemistry 272:2038-2041.

Hoyer D, Martin G (1997) 5-HT receptor classification and nomenclature: towards a harmonization with the human genome. Neuropharmacology 36:419-428.

Hung AY, Haass C, Nitsch RM, Qiu WQ, Citron M, Wurtman RJ, Growdon JH, Selkoe DJ (1993) Activation of protein kinase C inhibits cellular production of the amyloid beta-protein. The Journal of Biological Chemistry 268:22959-22962.

Huxtable RJ (1992) Physiological actions of taurine. Physiological Reviews 72:101-163.

Hynd MR, Scott HL, Dodd PR (2004) Glutamate-mediated excitotoxicity and neurodegeneration in Alzheimer's disease. Neurochemistry International 45:583-595.

Jardanhazi-Kurutz D, Kummer MP, Terwel D, Vogel K, Thiele A, Heneka MT (2011) Distinct adrenergic system changes and neuroinflammation in response to induced locus ceruleus degeneration in APP/PS1 transgenic mice. Neuroscience 176:396-407.

Jarrett JT, Berger EP, Lansbury PT, Jr. (1993a) The C-terminus of the beta protein is critical in amyloidogenesis. Annals of the New York Academy of Sciences 695:144-148.

Jarrett JT, Berger EP, Lansbury PT, Jr. (1993b) The carboxy terminus of the beta amyloid protein is critical for the seeding of amyloid formation: implications for the pathogenesis of Alzheimer's disease. Biochemistry 32:4693-4697.

Johansson AS, Berglind-Dehlin F, Karlsson G, Edwards K, Gellerfors P, Lannfelt L (2006) Physiochemical characterization of the Alzheimer's disease-related peptides A beta 1-42Arctic and A beta 1-42wt. The FEBS Journal 273:2618-2630.

Kaether C, Schmitt S, Willem M, Haass C (2006) Amyloid precursor protein and Notch intracellular domains are generated after transport of their precursors to the cell surface. Traffic 7:408-415.

Kalinin, S., Polak, P. E., Madrigal, J. L., Gavrilyuk, V., Sharp, A., Chauhan, N., Marien, M., Colpaert, F. & Feinstein, D. L. (2006). Beta-amyloid-dependent expression of NOS2 in neurons: prevention by an alpha2-adrenergic antagonist. *Antioxid Redox Signal* **8**, 873-83.

Kanekiyo T, Zhang J, Liu Q, Liu CC, Zhang L, Bu G (2011) Heparan sulphate proteoglycan and the low-density lipoprotein receptor-related protein 1 constitute major pathways for

neuronal amyloid-beta uptake. The Journal of Neuroscience : the Official Journal of the Society for Neuroscience 31:1644-1651.

Kang DE, Pietrzik CU, Baum L, Chevallier N, Merriam DE, Kounnas MZ, Wagner SL, Troncoso JC, Kawas CH, Katzman R, Koo EH (2000) Modulation of amyloid beta-protein clearance and Alzheimer's disease susceptibility by the LDL receptor-related protein pathway. The Journal of Clinical Investigation 106:1159-1166.

Kang J, Lemaire HG, Unterbeck A, Salbaum JM, Masters CL, Grzeschik KH, Multhaup G, Beyreuther K, Muller-Hill B (1987) The precursor of Alzheimer's disease amyloid A4 protein resembles a cell-surface receptor. Nature 325:733-736.

Kar S, Seto D, Gaudreau P, Quirion R (1996) Beta-amyloid-related peptides inhibit potassium-evoked acetylcholine release from rat hippocampal slices. The Journal of Neuroscience : the Official Journal of the Society for Neuroscience 16:1034-1040.

Kimberly WT, Esler WP, Ye W, Ostaszewski BL, Gao J, Diehl T, Selkoe DJ, Wolfe MS (2003) Notch and the amyloid precursor protein are cleaved by similar gamma-secretase(s). Biochemistry 42:137-144.

Kinoshita A, Fukumoto H, Shah T, Whelan CM, Irizarry MC, Hyman BT (2003) Demonstration by FRET of BACE interaction with the amyloid precursor protein at the cell surface and in early endosomes. Journal of Cell Science 116:3339-3346.

Knobloch M, Konietzko U, Krebs DC, Nitsch RM (2007) Intracellular Abeta and cognitive deficits precede beta-amyloid deposition in transgenic arcAbeta mice. Neurobiology of Aging 28:1297-1306.

Krieglstein K, Miyazono K, ten Dijke P, Unsicker K (2012) TGF-beta in aging and disease. Cell and Tissue Research 347:5-9.

Krystal JH, Sanacora G, Blumberg H, Anand A, Charney DS, Marek G, Epperson CN, Goddard A, Mason GF (2002) Glutamate and GABA systems as targets for novel antidepressant and mood-stabilizing treatments. Molecular Psychiatry 7 Suppl 1:S71-80.

Lacor PN, Buniel MC, Chang L, Fernandez SJ, Gong Y, Viola KL, Lambert MP, Velasco PT, Bigio EH, Finch CE, Krafft GA, Klein WL (2004) Synaptic targeting by Alzheimer's-related amyloid beta oligomers. The Journal of Neuroscience : the Official Journal of the Society for Neuroscience 24:10191-10200.

LaFerla FM, Green KN, Oddo S (2007) Intracellular amyloid-beta in Alzheimer's disease. Nature Reviews Neuroscience 8:499-509.

Lamb BT, Sisodia SS, Lawler AM, Slunt HH, Kitt CA, Kearns WG, Pearson PL, Price DL, Gearhart JD (1993) Introduction and expression of the 400 kilobase amyloid precursor protein gene in transgenic mice [corrected]. Nature Genetics 5:22-30.

Lambert MP, Barlow AK, Chromy BA, Edwards C, Freed R, Liosatos M, Morgan TE, Rozovsky I, Trommer B, Viola KL, Wals P, Zhang C, Finch CE, Krafft GA, Klein WL (1998) Diffusible, nonfibrillar ligands derived from Abeta1-42 are potent central nervous system neurotoxins. Proceedings of the National Academy of Sciences of the United States of America 95:6448-6453.

Lanari A, Amenta F, Silvestrelli G, Tomassoni D, Parnetti L (2006) Neurotransmitter deficits in behavioural and psychological symptoms of Alzheimer's disease. Mechanisms of Ageing and Development 127:158-165.

Lanctot KL, Herrmann N, Mazzotta P (2001) Role of serotonin in the behavioral and psychological symptoms of dementia. The Journal of Neuropsychiatry and Clinical Neurosciences 13:5-21.

Lee HG, Castellani RJ, Zhu X, Perry G, Smith MA (2005) Amyloid-beta in Alzheimer's disease: the horse or the cart? Pathogenic or protective? International Journal of Experimental Pathology 86:133-138.

Lee J, Retamal C, Cuitino L, Caruano-Yzermans A, Shin JE, van Kerkhof P, Marzolo MP, Bu G (2008) Adaptor protein sorting nexin 17 regulates amyloid precursor protein trafficking and processing in the early endosomes. The Journal of Biological Chemistry 283:11501-11508.

Levy-Lahad E, Wasco W, Poorkaj P, Romano DM, Oshima J, Pettingell WH, Yu CE, Jondro PD, Schmidt SD, Wang K, et al. (1995) Candidate gene for the chromosome 1 familial Alzheimer's disease locus. Science 269:973-977.

Li MO, Wan YY, Sanjabi S, Robertson AK, Flavell RA (2006) Transforming growth factor-beta regulation of immune responses. Annual Review of Immunology 24:99-146.

Lin L, Georgievska B, Mattsson A, Isacson O (1999) Cognitive changes and modified processing of amyloid precursor protein in the cortical and hippocampal system after cholinergic synapse loss and muscarinic receptor activation. Proceedings of the National Academy of Sciences of the United States of America 96:12108-12113.

Ling Y, Morgan K, Kalsheker N (2003) Amyloid precursor protein (APP) and the biology of proteolytic processing: relevance to Alzheimer's disease. The International Journal of Biochemistry & Cell Biology 35:1505-1535.

Liu Q, Zerbinatti CV, Zhang J, Hoe HS, Wang B, Cole SL, Herz J, Muglia L, Bu G (2007) Amyloid precursor protein regulates brain apolipoprotein E and cholesterol metabolism through lipoprotein receptor LRP1. Neuron 56:66-78.

Liu Q, Trotter J, Zhang J, Peters MM, Cheng H, Bao J, Han X, Weeber EJ, Bu G (2010) Neuronal LRP1 knockout in adult mice leads to impaired brain lipid metabolism and progressive, age-dependent synapse loss and neurodegeneration. The Journal of Neuroscience : the Official Journal of the Society for Neuroscience 30:17068-17078.

Lopez-Gimenez JF, Vilaro MT, Palacios JM, Mengod G (1998) [3H]MDL 100,907 labels 5-HT2A serotonin receptors selectively in primate brain. Neuropharmacology 37:1147-1158.

Lord A, Kalimo H, Eckman C, Zhang XQ, Lannfelt L, Nilsson LN (2006) The Arctic Alzheimer mutation facilitates early intraneuronal Abeta aggregation and senile plaque formation in transgenic mice. Neurobiology of Aging 27:67-77.

Lyketsos CG, Lopez O, Jones B, Fitzpatrick AL, Breitner J, DeKosky S (2002) Prevalence of neuropsychiatric symptoms in dementia and mild cognitive impairment: results from the cardiovascular health study. JAMA : the Journal of the American Medical Association 288:1475-1483.

Martorana A, Di Lorenzo F, Esposito Z, Lo Giudice T, Bernardi G, Caltagirone C, Koch G (2013) Dopamine D(2)-agonist rotigotine effects on cortical excitability and central cholinergic transmission in Alzheimer's disease patients. Neuropharmacology 64:108-113.

Mattson MP, Furukawa K (1998) Signaling events regulating the neurodevelopmental triad. Glutamate and secreted forms of beta-amyloid precursor protein as examples. Perspectives on Developmental Neurobiology 5:337-352.

Mattson MP, Cheng B, Culwell AR, Esch FS, Lieberburg I, Rydel RE (1993) Evidence for excitoprotective and intraneuronal calcium-regulating roles for secreted forms of the beta-amyloid precursor protein. Neuron 10:243-254.

Mauch DH, Nagler K, Schumacher S, Goritz C, Muller EC, Otto A, Pfrieger FW (2001) CNS synaptogenesis promoted by glia-derived cholesterol. Science 294:1354-1357.

May P, Rohlmann A, Bock HH, Zurhove K, Marth JD, Schomburg ED, Noebels JL, Beffert U, Sweatt JD, Weeber EJ, Herz J (2004) Neuronal LRP1 functionally associates with postsynaptic proteins and is required for normal motor function in mice. Molecular and Cellular Biology 24:8872-8883.

McLean CA, Cherny RA, Fraser FW, Fuller SJ, Smith MJ, Beyreuther K, Bush AI, Masters CL (1999) Soluble pool of Abeta amyloid as a determinant of severity of neurodegeneration in Alzheimer's disease. Annals of Neurology 46:860-866.

Meltzer CC, Smith G, DeKosky ST, Pollock BG, Mathis CA, Moore RY, Kupfer DJ, Reynolds CF, 3rd (1998) Serotonin in aging, late-life depression, and Alzheimer's disease: the emerging role of functional imaging. Neuropsychopharmacology : Official Publication of the American College of Neuropsychopharmacology 18:407-430.

Meltzer HY (1992) The importance of serotonin-dopamine interactions in the action of clozapine. The British Journal of Psychiatry Supplement:22-29.

Merker B (1983) Silver staining of cell bodies by means of physical development. Journal of Neuroscience Methods 9:235-241.

Millan MJ, Di Cara B, Dekeyne A, Panayi F, De Groote L, Sicard D, Cistarelli L, Billiras R, Gobert A (2007) Selective blockade of dopamine D(3) versus D(2) receptors enhances frontocortical cholinergic transmission and social memory in rats: a parallel neurochemical and behavioural analysis. Journal of Neurochemistry 100:1047-1061.

Minger SL, Esiri MM, McDonald B, Keene J, Carter J, Hope T, Francis PT (2000) Cholinergic deficits contribute to behavioral disturbance in patients with dementia. Neurology 55:1460-1467.

Mullan M, Crawford F, Axelman K, Houlden H, Lilius L, Winblad B, Lannfelt L (1992) A pathogenic mutation for probable Alzheimer's disease in the APP gene at the N-terminus of beta-amyloid. Nature Genetics 1:345-347.

Murakami K, Irie K, Morimoto A, Ohigashi H, Shindo M, Nagao M, Shimizu T, Shirasawa T (2002) Synthesis, aggregation, neurotoxicity, and secondary structure of various A beta 1-42 mutants of familial Alzheimer's disease at positions 21-23. Biochemical and Biophysical Research Communications 294:5-10.

Nilsberth C, Westlind-Danielsson A, Eckman CB, Condron MM, Axelman K, Forsell C, Stenh C, Luthman J, Teplow DB, Younkin SG, Naslund J, Lannfelt L (2001) The 'Arctic' APP mutation (E693G) causes Alzheimer's disease by enhanced Abeta protofibril formation. Nature Neuroscience 4:887-893.

Nilsson L, Nordberg A, Hardy J, Wester P, Winblad B (1986) Physostigmine restores 3H-acetylcholine efflux from Alzheimer brain slices to normal level. Journal of Neural Transmission 67:275-285.

Nitsch RM, Slack BE, Wurtman RJ, Growdon JH (1992) Release of Alzheimer amyloid precursor derivatives stimulated by activation of muscarinic acetylcholine receptors. Science 258:304-307.

Noristani HN, Meadows RS, Olabarria M, Verkhratsky A, Rodriguez JJ (2011) Increased hippocampal CA1 density of serotonergic terminals in a triple transgenic mouse model of Alzheimer's disease: an ultrastructural study. Cell Death & Disease 2:e210.

Nyakas C, Granic I, Halmy LG, Banerjee P, Luiten PG (2011) The basal forebrain cholinergic system in aging and dementia. Rescuing cholinergic neurons from neurotoxic amyloid-beta42 with memantine. Behavioural Brain Research 221:594-603.

O'Brien RJ, Wong PC (2011) Amyloid precursor protein processing and Alzheimer's disease. Annual Review of Neuroscience 34:185-204.

Oakley H, Cole SL, Logan S, Maus E, Shao P, Craft J, Guillozet-Bongaarts A, Ohno M, Disterhoft J, Van Eldik L, Berry R, Vassar R (2006) Intraneuronal beta-amyloid aggregates, neurodegeneration, and neuron loss in transgenic mice with five familial Alzheimer's disease mutations: potential factors in amyloid plaque formation. The Journal of Neuroscience : the Official Journal of the Society for Neuroscience 26:10129-10140.

Oddo S, Caccamo A, Shepherd JD, Murphy MP, Golde TE, Kayed R, Metherate R, Mattson MP, Akbari Y, LaFerla FM (2003) Triple-transgenic model of Alzheimer's disease with plaques and tangles: intracellular Abeta and synaptic dysfunction. Neuron 39:409-421.

Okamoto K, Kimura H, Sakai Y (1983) Taurine-induced increase of the Cl-conductance of cerebellar Purkinje cell dendrites in vitro. Brain Research 259:319-323.

Ongur D, Price JL (2000) The organization of networks within the orbital and medial prefrontal cortex of rats, monkeys and humans. Cerebral Cortex 10:206-219.

Pakaski M, Farkas Z, Kasa P, Jr., Forgon M, Papp H, Zarandi M, Penke B, Kasa P, Sr. (1998) Vulnerability of small GABAergic neurons to human beta-amyloid pentapeptide. Brain Research 796:239-246.

Palomero-Gallagher N, Bidmon HJ, Zilles K (2003) AMPA, kainate, and NMDA receptor densities in the hippocampus of untreated male rats and females in estrus and diestrus. The Journal of Comparative Neurology 459:468-474.

Parameshwaran K, Dhanasekaran M, Suppiramaniam V (2008) Amyloid beta peptides and glutamatergic synaptic dysregulation. Experimental Neurology 210:7-13.

Paula-Lima AC, De Felice FG, Brito-Moreira J, Ferreira ST (2005) Activation of GABA(A) receptors by taurine and muscimol blocks the neurotoxicity of beta-amyloid in rat hippocampal and cortical neurons. Neuropharmacology 49:1140-1148.

Pierrot N, Ghisdal P, Caumont AS, Octave JN (2004) Intraneuronal amyloid-beta1-42 production triggered by sustained increase of cytosolic calcium concentration induces neuronal death. Journal of Neurochemistry 88:1140-1150.

Pike CJ, Cotman CW (1993) Cultured GABA-immunoreactive neurons are resistant to toxicity induced by beta-amyloid. Neuroscience 56:269-274.

Price DL, Tanzi RE, Borchelt DR, Sisodia SS (1998) Alzheimer's disease: genetic studies and transgenic models. Annual Review of Genetics 32:461-493.

Price JL, Morris JC (1999) Tangles and plaques in nondemented aging and "preclinical" Alzheimer's disease. Annals of Neurology 45:358-368.

Qiu Z, Strickland DK, Hyman BT, Rebeck GW (2002) alpha 2-Macroglobulin exposure reduces calcium responses to N-methyl-D-aspartate via low density lipoprotein receptor-related protein in cultured hippocampal neurons. The Journal of Biological Chemistry 277:14458-14466.

Racchi M, Govoni S (2003) The pharmacology of amyloid precursor protein processing. Experimental Gerontology 38:145-157.

Rajendran L, Annaert W (2012) Membrane trafficking pathways in Alzheimer's disease. Traffic 13:759-770.

Rajendran L, Knobloch M, Geiger KD, Dienel S, Nitsch R, Simons K, Konietzko U (2007) Increased Abeta production leads to intracellular accumulation of Abeta in flotillin-1-positive endosomes. Neurodegenerative diseases 4:164-170.

Rao SG, Williams GV, Goldman-Rakic PS (2000) Destruction and creation of spatial tuning by disinhibition: GABA(A) blockade of prefrontal cortical neurons engaged by working

memory. The Journal of Neuroscience : the Official Journal of the Society for Neuroscience 20:485-494.

Reeves S, Brown R, Howard R, Grasby P (2009) Increased striatal dopamine (D2/D3) receptor availability and delusions in Alzheimer disease. Neurology 72:528-534.

Reeves S, Mehta M, Howard R, Grasby P, Brown R (2010) The dopaminergic basis of cognitive and motor performance in Alzheimer's disease. Neurobiology of Disease 37:477-482.

Rey NL, Jardanhazi-Kurutz D, Terwel D, Kummer MP, Jourdan F, Didier A, Heneka MT (2012) Locus coeruleus degeneration exacerbates olfactory deficits in APP/PS1 transgenic mice. Neurobiology of Aging 33:426 e421-411.

Ring S, Weyer SW, Kilian SB, Waldron E, Pietrzik CU, Filippov MA, Herms J, Buchholz C, Eckman CB, Korte M, Wolfer DP, Muller UC (2007) The secreted beta-amyloid precursor protein ectodomain APPs alpha is sufficient to rescue the anatomical, behavioral, and electrophysiological abnormalities of APP-deficient mice. The Journal of Neuroscience : the Official Journal of the Society for Neuroscience 27:7817-7826.

Rissman RA, De Blas AL, Armstrong DM (2007) GABA(A) receptors in aging and Alzheimer's disease. Journal of Neurochemistry 103:1285-1292.

Russo-Neustadt A, Cotman CW (1997) Adrenergic receptors in Alzheimer's disease brain: selective increases in the cerebella of aggressive patients. The Journal of Neuroscience : the Official Journal of the Society for Neuroscience 17:5573-5580.

Sandbrink R, Masters CL, Beyreuther K (1994) Similar alternative splicing of a non-homologous domain in beta A4-amyloid protein precursor-like proteins. The Journal of Biological Chemistry 269:14227-14234.

Scheuner D et al. (1996) Secreted amyloid beta-protein similar to that in the senile plaques of Alzheimer's disease is increased in vivo by the presenilin 1 and 2 and APP mutations linked to familial Alzheimer's disease. Nature Medicine 2:864-870.

Scullion GA, Kendall DA, Marsden CA, Sunter D, Pardon MC (2011) Chronic treatment with the alpha2-adrenoceptor antagonist fluparoxan prevents age-related deficits in spatial working memory in APPxPS1 transgenic mice without altering beta-amyloid plaque load or astrocytosis. Neuropharmacology 60:223-234.

Selkoe DJ (1994) Cell biology of the amyloid beta-protein precursor and the mechanism of Alzheimer's disease. Annual Review of Cell Biology 10:373-403.

Selkoe DJ (1996) Amyloid beta-protein and the genetics of Alzheimer's disease. The Journal of Biological Chemistry 271:18295-18298.

Selkoe DJ (1999) Translating cell biology into therapeutic advances in Alzheimer's disease. Nature 399:A23-31.

Selkoe DJ (2001a) Alzheimer's disease: genes, proteins, and therapy. Physiological Reviews 81:741-766.

Selkoe DJ (2001b) Alzheimer's disease results from the cerebral accumulation and cytotoxicity of amyloid beta-protein. Journal of Alzheimer's Disease : JAD 3:75-80.

Selkoe DJ (2002) Alzheimer's disease is a synaptic failure. Science 298:789-791.

Seubert P, Vigo-Pelfrey C, Esch F, Lee M, Dovey H, Davis D, Sinha S, Schlossmacher M, Whaley J, Swindlehurst C, et al. (1992) Isolation and quantification of soluble Alzheimer's beta-peptide from biological fluids. Nature 359:325-327.

Shankar GM, Li S, Mehta TH, Garcia-Munoz A, Shepardson NE, Smith I, Brett FM, Farrell MA, Rowan MJ, Lemere CA, Regan CM, Walsh DM, Sabatini BL, Selkoe DJ (2008) Amyloid-beta protein dimers isolated directly from Alzheimer's brains impair synaptic plasticity and memory. Nature Medicine 14:837-842.

Sherrington R et al. (1996) Alzheimer's disease associated with mutations in presenilin 2 is rare and variably penetrant. Human Molecular Genetics 5:985-988.

Shibata M, Yamada S, Kumar SR, Calero M, Bading J, Frangione B, Holtzman DM, Miller CA, Strickland DK, Ghiso J, Zlokovic BV (2000) Clearance of Alzheimer's amyloid-ss(1-40) peptide from brain by LDL receptor-related protein-1 at the blood-brain barrier. The Journal of Clinical Investigation 106:1489-1499.

Shipley MT, Halloran FJ, de la Torre J (1985) Surprisingly rich projection from locus coeruleus to the olfactory bulb in the rat. Brain Research 329:294-299.

Siever LJ, Kahn RS, Lawlor BA, Trestman RL, Lawrence TL, Coccaro EF (1991) Critical issues in defining the role of serotonin in psychiatric disorders. Pharmacological Reviews 43:509-525.

Sisodia SS (1992) Beta-amyloid precursor protein cleavage by a membrane-bound protease. Proceedings of the National Academy of Sciences of the United States of America 89:6075-6079.

Sitaram N, Weingartner H, Gillin JC (1978) Human serial learning: enhancement with arecholine and choline impairment with scopolamine. Science 201:274-276.

Spuch C, Ortolano S, Navarro C (2012) LRP-1 and LRP-2 receptors function in the membrane neuron. Trafficking mechanisms and proteolytic processing in Alzheimer's disease. Frontiers in Physiology 3:269.

Squire LR (1992) Memory and the hippocampus: a synthesis from findings with rats, monkeys, and humans. Psychological Review 99:195-231.

Struble RG, Cork LC, Whitehouse PJ, Price DL (1982) Cholinergic innervation in neuritic plaques. Science 216:413-415.

Suzuki N, Cheung TT, Cai XD, Odaka A, Otvos L, Jr., Eckman C, Golde TE, Younkin SG (1994) An increased percentage of long amyloid beta protein secreted by familial amyloid beta protein precursor (beta APP717) mutants. Science 264:1336-1340.

Taipale J, Saharinen J, Keski-Oja J (1998) Extracellular matrix-associated transforming growth factor-beta: role in cancer cell growth and invasion. Advances in Cancer Research 75:87-134.

Tamaoka A, Odaka A, Ishibashi Y, Usami M, Sahara N, Suzuki N, Nukina N, Mizusawa H, Shoji S, Kanazawa I, et al. (1994) APP717 missense mutation affects the ratio of amyloid beta protein species (A beta 1-42/43 and a beta 1-40) in familial Alzheimer's disease brain. The Journal of Biological Chemistry 269:32721-32724.

Taylor CJ, Ireland DR, Ballagh I, Bourne K, Marechal NM, Turner PR, Bilkey DK, Tate WP, Abraham WC (2008) Endogenous secreted amyloid precursor protein-alpha regulates hippocampal NMDA receptor function, long-term potentiation and spatial memory. Neurobiology of Disease 31:250-260.

Terry RD, Masliah E, Salmon DP, Butters N, DeTeresa R, Hill R, Hansen LA, Katzman R (1991) Physical basis of cognitive alterations in Alzheimer's disease: synapse loss is the major correlate of cognitive impairment. Annals of Neurology 30:572-580.

Tesseur I, Zou K, Esposito L, Bard F, Berber E, Can JV, Lin AH, Crews L, Tremblay P, Mathews P, Mucke L, Masliah E, Wyss-Coray T (2006) Deficiency in neuronal TGF-beta signaling promotes neurodegeneration and Alzheimer's pathology. The Journal of Clinical Investigation 116:3060-3069.

Truchot L, Costes SN, Zimmer L, Laurent B, Le Bars D, Thomas-Anterion C, Croisile B, Mercier B, Hermier M, Vighetto A, Krolak-Salmon P (2007) Up-regulation of hippocampal serotonin metabolism in mild cognitive impairment. Neurology 69:1012-1017.

Tseng KY, O'Donnell P (2007) D2 dopamine receptors recruit a GABA component for their attenuation of excitatory synaptic transmission in the adult rat prefrontal cortex. Synapse 61:843-850.

Twamley EW, Ropacki SA, Bondi MW (2006) Neuropsychological and neuroimaging changes in preclinical Alzheimer's disease. Journal of the International Neuropsychological Society : JINS 12:707-735.

Tzschentke TM (2001) Pharmacology and behavioral pharmacology of the mesocortical dopamine system. Progress in Neurobiology 63:241-320.

Vance JE, Karten B, Hayashi H (2006) Lipid dynamics in neurons. Biochemical Society Transactions 34:399-403.

Vivien D, Ali C (2006) Transforming growth factor-beta signalling in brain disorders. Cytokine & Growth Factor Reviews 17:121-128.

Walsh DM, Klyubin I, Fadeeva JV, Cullen WK, Anwyl R, Wolfe MS, Rowan MJ, Selkoe DJ (2002) Naturally secreted oligomers of amyloid beta protein potently inhibit hippocampal long-term potentiation in vivo. Nature 416:535-539.

Weidemann A, Konig G, Bunke D, Fischer P, Salbaum JM, Masters CL, Beyreuther K (1989) Identification, biogenesis, and localization of precursors of Alzheimer's disease A4 amyloid protein. Cell 57:115-126.

Wesson DW, Levy E, Nixon RA, Wilson DA (2010) Olfactory dysfunction correlates with amyloid-beta burden in an Alzheimer's disease mouse model. The Journal of Neuroscience : the Official Journal of the Society for Neuroscience 30:505-514.

Whitehouse PJ, Price DL, Struble RG, Clark AW, Coyle JT, Delon MR (1982) Alzheimer's disease and senile dementia: loss of neurons in the basal forebrain. Science 215:1237-1239.

Wirths O, Multhaup G, Bayer TA (2004) A modified beta-amyloid hypothesis: intraneuronal accumulation of the beta-amyloid peptide--the first step of a fatal cascade. Journal of Neurochemistry 91:513-520.

Wolfe MS, Guenette SY (2007) APP at a glance. Journal of Cell Science 120:3157-3161.

Wong TP, Debeir T, Duff K, Cuello AC (1999) Reorganization of cholinergic terminals in the cerebral cortex and hippocampus in transgenic mice carrying mutated presenilin-1 and amyloid precursor protein transgenes. The Journal of Neuroscience : the Official Journal of the Society for Neuroscience 19:2706-2716.

Xu Y, Yan J, Zhou P, Li J, Gao H, Xia Y, Wang Q (2012) Neurotransmitter receptors and cognitive dysfunction in Alzheimer's disease and Parkinson's disease. Progress in Neurobiology 97:1-13.

Yoo AS, Cheng I, Chung S, Grenfell TZ, Lee H, Pack-Chung E, Handler M, Shen J, Xia W, Tesco G, Saunders AJ, Ding K, Frosch MP, Tanzi RE, Kim TW (2000) Presenilin-mediated modulation of capacitative calcium entry. Neuron 27:561-572.

Zagorski MG, Barrow CJ (1992) NMR studies of amyloid beta-peptides: proton assignments, secondary structure, and mechanism of an alpha-helix----beta-sheet conversion for a homologous, 28-residue, N-terminal fragment. Biochemistry 31:5621-5631.

Zarate CA, Jr., Du J, Quiroz J, Gray NA, Denicoff KD, Singh J, Charney DS, Manji HK (2003) Regulation of cellular plasticity cascades in the pathophysiology and treatment of mood disorders: role of the glutamatergic system. Annals of the New York Academy of Sciences 1003:273-291.

Zilles K, Schleicher A (1991) Quantitative receptor autoradiography and image analysis. Bulletin de l'Association des Anatomistes 75:117-121.

Zilles K, Schleicher A (1995) Correlative imaging of transmitter receptor distributions in human cortex. In: Autoradiography and Correlative Imaging (Stumpf WE. SH, ed), pp 277-307: Academic Press Inc.

Zilles K, Palomero-Gallagher N, Schleicher A (2004) Transmitter receptors and functional anatomy of the cerebral cortex. Journal of Anatomy 205:417-432.

Zilles K, Schleicher A, Palomero-Gallagher N, Amunts K (2002a) Quantitative Analysis of Cyto- and Receptor Architecture of the Human Brain. In: Brain Mapping: The Methods (Toga AW, Mazziotta JC, eds), pp 573-602: Elsevier Inc.

Zilles K, Palomero-Gallagher N, Grefkes C, Scheperjans F, Boy C, Amunts K, Schleicher A (2002b) Architectonics of the human cerebral cortex and transmitter receptor fingerprints: reconciling functional neuroanatomy and neurochemistry. European Neuropsychopharmacology 12:587-599.

Zubenko GS, Moossy J (1988) Major depression in primary dementia. Clinical and neuropathologic correlates. Archives of Neurology 45:1182-1186.

Zweig RM, Ross CA, Hedreen JC, Steele C, Cardillo JE, Whitehouse PJ, Folstein MF, Price DL (1988) The neuropathology of aminergic nuclei in Alzheimer's disease. Annals of Neurology 24:233-242.

VII. Appendix

1 Chemicals, solutions and technical equipment

Preparation of slices

- Cryostat Leica CM3050 (Leica Instruments GmbH, Wetzlar, Germany)
- Paraformaldehyde (Sigma-Aldrich Chemie GmbH, Steinheim, Germany)
- Phosphate buffered saline (PBS) (Invitrogen, Life Technologies GmbH, Darmstadt, Germany)
- Silan-coated slides (Paul Marienfeld GmbH & Co. KG, Lauda-Königshofen, Germany)

[3H]-receptor autoradiography

- Liquid Scintillation Analyzer Tri-Carb 2100 TR (Packard BioScience, PerkinElmer, Rodgau, Germany)
- Liquid Scintillation Cocktail Ultima Gold XR (PerkinElmer, Rodgau, Germany)

- [3H]-ligands:
  - AF-DX 384 (Perkin Elmer, Rodgau, Germany)
  - AMPA (Perkin Elmer, Rodgau, Germany)
  - CGP 54626 (Biotrend Chemikalien GmbH, Köln, Germany)
  - 4-DAMP (Perkin Elmer, Rodgau, Germany)
  - Fallyprid (Institute for Nuclear Chemistry, Johannes Gutenberg Universität Mainz, Mainz, Germany)
  - Flumazenil (Perkin Elmer, Rodgau, Germany)
  - Kainate (Perkin Elmer, Rodgau, Germany)
  - Ketanserin (Perkin Elmer, Rodgau, Germany)
  - LY 341,495 (Biotrend Chemikalien GmbH, Köln, Germany)
  - MK 801 (Perkin Elmer, Rodgau, Germany)
  - Muscimol (Perkin Elmer, Rodgau, Germany)
  - 8-OH-DPAT (Perkin Elmer, Rodgau, Germany)
  - Oxotremorine-M (Perkin Elmer, Rodgau, Germany)
  - Pirenzepine (Perkin Elmer, Rodgau, Germany)
  - Prazosin (Perkin Elmer, Rodgau, Germany)

- Raclopride (Perkin Elmer, Rodgau, Germany)
- SCH 23390 (Perkin Elmer, Rodgau, Germany)
- SR 95531 (Perkin Elmer, Rodgau, Germany)
- UK14,304 (Perkin Elmer, Rodgau, Germany)
- ZM 241 385 (Biotrend Chemikalien GmbH, Köln, Germany)

- **Displacer:**
  - Atropine sulphate (Sigma-Aldrich Chemie GmbH, Steinheim, Germany)
  - Butaclamol hydrochloride (Sigma-Aldrich Chemie GmbH, Steinheim, Germany)
  - Carbachol (Sigma-Aldrich Chemie GmbH, Steinheim, Germany)
  - CGP 55845 (Biotrend Chemikalien GmbH, Köln, Germany)
  - 2-Chloroadenosine (Sigma-Aldrich Chemie GmbH, Steinheim, Germany)
  - Clonazepam (Sigma-Aldrich Chemie GmbH, Steinheim, Germany)
  - GABA (Biotrend Chemikalien GmbH, Köln, Germany)
  - Haloperidol (Sigma-Aldrich Chemie GmbH, Steinheim, Germany)
  - L-Glutamate (Sigma-Aldrich Chemie GmbH, Steinheim, Germany)
  - Mianserin (Sigma-Aldrich Chemie GmbH, Steinheim, Germany)
  - MK 801 (Biotrend Chemikalien GmbH, Köln, Germany)
  - Nicotine-di-d-tartrate (Sigma-Aldrich Chemie GmbH, Steinheim, Germany
  - Phentolamine mesylate (Biotrend Chemikalien GmbH, Köln, Germany)
  - Pirenzepine dehydrate (Sigma-Aldrich Chemie GmbH, Steinheim, Germany)
  - Serotonin (Sigma-Aldrich Chemie GmbH, Steinheim, Germany)
  - SKF 83566 (Sigma-Aldrich Chemie GmbH, Steinheim, Germany)
  - SYM 2081 (Sigma-Aldrich Chemie GmbH, Steinheim, Germany)
  - Quisqualate (Biotrend Chemikalien GmbH, Köln, Germany)
- **Buffers and solutions:**
  - Adenosine deaminase (Sigma-Aldrich Chemie GmbH, Steinheim, Germany)
  - Ascorbate (Sigma-Aldrich Chemie GmbH, Steinheim, Germany)
  - Acetone (VWR International, Langenfeld, Germany)
  - Calcium acetate (Sigma-Aldrich Chemie GmbH, Steinheim, Germany)
  - Calcium chloride (CaCl2) (Merck KGaA, Darmstadt, Germany)
  - D-Glucose (Merck KGaA, Darmstadt, Germany)

- Ethylenediaminetetraacetic acid (EDTA) dihydrat (Sigma-Aldrich Chemie GmbH, Steinheim, Germany)
- Glutamate (Sigma-Aldrich Chemie GmbH, Steinheim, Germany)
- Glutaraldehyde (Sigma-Aldrich Chemie GmbH, Steinheim, Germany)
- Glycine (Sigma-Aldrich Chemie GmbH, Steinheim, Germany)
- HEPES (Sigma-Aldrich Chemie GmbH, Steinheim, Germany)
- Magnesium chloride (MgCl2) (Merck KGaA, Darmstadt, Germany)
- Magnesium sulfate (MgSO4) (Sigma-Aldrich Chemie GmbH, Steinheim, Germany)
- Manganese(II) chloride (MnCl2) (Sigma-Aldrich Chemie GmbH, Steinheim, Germany)
- Mianserin (Sigma-Aldrich Chemie GmbH, Steinheim, Germany)
- Phenylmethanesulfonyl fluoride (PMSF) (Sigma-Aldrich Chemie GmbH, Steinheim, Germany)
- Potassium bromide (KBr) (Sigma-Aldrich Chemie GmbH, Steinheim, Germany)
- Potassium chloride (KCl) (Sigma-Aldrich Chemie GmbH, Steinheim, Germany)
- Potassium phosphate monobasic (KH2PO4) (Merck KGaA, Darmstadt, Germany)
- Potassium thiocyanate (KSCN) (Sigma-Aldrich Chemie GmbH, Steinheim, Germany)
- Sodium bicarbonate (NaHCO3) (Merck KGaA, Darmstadt, Germany)
- Sodium chloride (NaCl) (Merck KGaA, Darmstadt, Germany)
- Sodium phosphate dibasic dihydrate (Na2HPO4 x 2H2O) (Merck KGaA, Darmstadt, Germany)
- Spermidine (Sigma-Aldrich Chemie GmbH, Steinheim, Germany)
- Tris-acetate (Sigma-Aldrich Chemie GmbH, Steinheim, Germany)
- Tris-citrate (Sigma-Aldrich Chemie GmbH, Steinheim, Germany)
- Tris-HCl (Sigma-Aldrich Chemie GmbH, Steinheim, Germany)

Film exposition and development

- BioMax MR β^--sensitive films (Kodak, Sigma-Aldrich Chemie GmbH, Steinheim, Germany)
- GBX-Developer (Kodak, Sigma-Aldrich Chemie GmbH, Steinheim, Germany)
- GBX-Fixer (Kodak, Sigma-Aldrich Chemie GmbH, Steinheim, Germany)

- Hyperprocessor SRX-101A (Amersham Biosciences, GE Healthcare Europe GmbH, Europe)
- Radioactive standards (GE Healthcare GmbH, München, Germany)

Digital processing of autoradiographic films

- AxioVision image analyzing software Rel. 4.8.2 (Zeiss, Carl Zeiss MikroImaging GmbH, Göttingen, Germany)
- Digital camera AxioCam HRm (Zeiss, Carl Zeiss MikroImaging GmbH, Göttingen, Germany)

Histological staining

- Acetic acid (Merck KGaA, Darmstadt, Germany)
- Ammonium nitrate (Merck KGaA, Darmstadt, Germany)
- DPX mountant for histology (Fluka, Sigma-Aldrich Chemie GmbH, Steinheim, Germany)
- Formaldehyde solution (Merck KGaA, Darmstadt, Germany)
- Formic acid (Milipore, Schwalbach, Germany)
- Hydrogen peroxide (Milipore, Schwalbach, Germany)
- 2-Propanol (Merck KGaA, Darmstadt, Germany)
- Silver nitrate (Merck KGaA, Darmstadt, Germany)
- Sodium carbonate (Millipore, Schwalbach, Germany)
- Tungstosilicic acid (Sigma-Aldrich Chemie GmbH, Steinheim, Germany)
- XEM 200 (DiaTec, Diagostische System-Technik, Bamberg, Germany)

9.7. Immunohistochemistry

- Aqua Poly/Mont (DAKO, Agilant Technologies, Hamburg, Germany)
- DAPI (Sigma-Aldrich Chemie GmbH, Steinheim, Germany)
- Formic acid (Millipore, Schwalbach, Germany)
- G2-10 (Millipore, Schwalbach, Germany)
- G-M A488 (Life Technologies GmbH, Darmstadt, Germany)
- G-R A568 (Life Technologies GmbH, Darmstadt, Germany)
- M.O.M. (Vector Labs, Burlingame, USA)

- NaCl (VWR International, Langenfeld, Germany)
- Paraformaldehyde (Sigma-Aldrich Chemie GmbH, Steinheim, Germany)
- Tris (AppliChem, Darmstadt, Germany)
- Triton X (AppliChem, Darmstadt, Germany)
- 1-11-3 (Covance, Munich, Germany)

2 Raw data

Table 4: Receptor density of kainate (fmol/mg protein) of brain regions investigated of *LRP1* mice. Mean density ± standard deviation quoted

animal	Group	OB	M1	S1	Pir	CPu	CA1	MosHil	MGr
1	wt	1592	1078	905	755	1495	569	1485	1340
2	wt	1463	1480	1346	1075	1915	640	1739	1428
3	wt	1705	1239	1107	908	1767	578	1876	1454
4	wt	1492	1052	888	885	1535	572	1894	1519
5	wt	1287	1261	1315	860	1480	568	1525	1245
20	wt	1533	1484	1300	911	1874	650	1500	1366
	mean	1512	1266	1143	899	1678	596	1670	1392
	SD	140	187	209	104	198	38	191	96
6	LRP1	1160	1178	1241	755	2123	592	1732	1290
7	LRP1	1133	929	847	685	1140	419	1484	946
8	LRP1	1024	995	911	664	1307	476	1398	1030
9	LRP1	1031	1185	1104	632	1468	489	1632	1065
	mean	1087	1072	1026	684	1509	494	1562	1083
	SD	69	130	180	52	430	72	149	147

Table 5: Receptor density of NMDA (fmol/mg protein) of brain regions investigated of *LRP1* mice. Mean density ± standard deviation quoted

animal	Group	OB	M1	S1	Pir	CPu	CA1	MosHil	MGr
1	wt	853	1308	1233	1215	807	3854	1160	3441
2	wt	955	1458	1412	1933	1008	3634	1197	3613
3	wt	1082	1781	1654	1705	1100	4458	1496	3952
4	wt	981	1536	1444	1558	944	3921	1355	3614
5	wt	831	1420	1278	1817	893	3674	1332	3254
20	wt	916	1650	1594	1653	1059	4849	1293	4115
	mean	936	1525	1436	1647	968	4065	1306	3665
	SD	92	170	167	248	109	485	120	319
6	LRP1	1050	1876	1746	1718	1256	4685	1468	3998
7	LRP1	863	1370	1451	1424	789	4751	1405	4238
8	LRP1	902	1638	1543	1534	954	4786	1317	4261
9	LRP1	759	1547	1436	1571	839	4598	1309	3912
	mean	893	1608	1544	1562	959	4705	1375	4102
	SD	120	210	143	121	210	83	76	174

Table 6: Receptor density of mGlu2/3 (fmol/mg protein) of brain regions investigated of *LRP1* mice. Mean density ± standard deviation quoted

animal	Group	OB	M1	S1	Pir	CPu	CA1	MosHil	MGr
1	wt	3484	7346	7816	8929	5854	3912	3343	7817
2	wt	4664	10968	11807	16575	9079	6414	4890	11436
3	wt	3176	7862	8443	10081	7613	4047	3967	10460
4	wt	4989	11563	11755	14716	10242	6690	5470	11806
5	wt	2830	9800	9862	14717	10411	5033	4206	11073
20	wt	2267	8442	9488	9699	8170	4721	4204	10481
	mean	3568	9330	9862	12453	8562	5136	4347	10512
	SD	1060	1719	1656	3252	1726	1176	742	1422

6	LRP1	2646	10942	10826	8760	8976	3378	3497	10338
7	LRP1	3427	7704	7684	9451	6208	3258	4173	10131
8	LRP1	1979	9367	9856	9952	8381	2909	3747	7504
9	LRP1	3195	10358	9942	8979	8131	3714	4479	9566
	mean	2812	9593	9577	9286	7924	3315	3974	9385
	SD	644	1417	1336	530	1198	332	437	1296

Table 7: Receptor density of M_1 (fmol/mg protein) of brain regions investigated of *LRP1* mice. Mean density ± standard deviation quoted

animal	Group	OB	M1	S1	Pir	CPu	CA1	MosHil	MGr
1	wt	1560	2349	2211	2331	3562	4127	2301	4201
2	wt	2474	4188	4233	4701	7843	7546	4078	8215
3	wt	1632	2462	2343	2488	4589	4068	2268	4108
4	wt	1565	2449	2263	2742	4269	4259	3301	4674
5	wt	1517	2601	2695	3358	4782	4699	2622	4762
20	wt	1631	3461	3614	2894	6336	6475	2948	5993
	mean	1730	2918	2893	3086	5230	5196	2920	5325
	SD	367	743	839	868	1573	1463	690	1567
6	LRP1	1221	2276	2148	2055	4607	3637	1995	3508
7	LRP1	1810	2841	2757	3320	7163	6718	3568	5785
8	LRP1	1521	2509	2520	2592	5717	4506	2610	4584
9	LRP1	2003	2970	3132	3307	7472	5971	3586	6399
	mean	1639	2649	2639	2819	6240	5208	2940	5069
	SD	342	315	413	612	1331	1393	778	1285

Table 8: Receptor density of $M_{2\,AG}$ (fmol/mg protein) of brain regions investigated of *LRP1* mice. Mean density ± standard deviation quoted

animal	Group	OB	M1	S1	Pir	CPu	CA1	MosHil	MGr
1	wt	2993	998	1299	490	1373	613	624	447
2	wt	3074	1168	1696	540	1637	792	752	540
3	wt	2816	1105	1461	544	1586	645	735	433
4	wt	2945	988	1282	484	1237	787	718	456
5	wt	2570	1135	1322	609	1647	650	638	464
20	wt	2328	1151	1621	503	1593	611	632	381
	mean	2788	1091	1447	528	1512	683	683	453
	SD	286	78	177	47	168	84	58	52
6	LRP1	2717	1092	1732	515	1819	605	611	485
7	LRP1	2683	943	1493	322	1183	387	442	166
8	LRP1	2611	1125	1673	366	1742	349	420	212
9	LRP1	2793	1298	1922	501	1837	423	426	233
	mean	2701	1115	1705	426	1645	441	475	274
	SD	76	146	177	97	311	113	91	144

Table 9: Receptor density of $M_{2\,ANT}$ (fmol/mg protein) of brain regions investigated of *LRP1* mice. Mean density ± standard deviation quoted

animal	Group	OB	M1	S1	Pir	CPu	CA1	MosHil	MGr
1	wt	3602	1745	2237	1041	4553	1442	889	1034
2	wt	2620	1812	2281	1028	4293	1409	795	875
3	wt	3322	1707	2095	744	4565	1282	716	890

4	wt	4006	1882	2356	912	4840	1510	779	1047
5	wt	2255	2035	2276	1169	5228	1282	694	920
20	wt	2793	1819	2477	888	4961	1308	618	850
	mean	3100	1833	2287	964	4740	1372	749	936
	SD	657	116	127	147	335	96	94	84
6	LRP1	3392	1919	2841	1115	5839	1384	832	875
7	LRP1	3037	1682	2264	841	5619	1040	552	700
8	LRP1	3169	1556	2375	569	4992	1021	553	757
9	LRP1	3429	1962	2805	1023	5766	1115	633	822
	mean	3257	1780	2571	887	5554	1140	642	789
	SD	186	193	294	241	386	168	132	76

Table 10: Receptor density of M_3 (fmol/mg protein) of brain regions investigated of *LRP1* mice. Mean density ± standard deviation quoted

animal	Group	OB	M1	S1	Pir	CPu	CA1	MosHil	MGr
1	wt	3812	4743	4364	3599	6687	7705	4977	6765
2	wt	3148	5136	5417	5058	8053	7770	4320	7297
3	wt	2335	4413	4116	3353	7304	6597	3777	6174
4	wt	3061	4422	4452	3908	6874	6530	3455	6006
5	wt	2735	4568	4259	4372	7724	7776	4102	7097
20	wt	2131	5297	5389	3491	7541	7940	4388	7315
	mean	2870	4763	4666	3963	7364	7386	4170	6776
	SD	609	374	581	647	517	643	527	569
6	LRP1	2383	3885	4137	3151	7082	7245	3590	6484
7	LRP1	2649	3923	3824	3229	7879	6419	4015	7808
8	LRP1	2359	4515	4605	3787	7377	6834	4087	6849
9	LRP1	2620	4343	4432	4353	8246	6953	3956	6616
	mean	2503	4167	4250	3630	7646	6862	3912	6939
	SD	153	311	343	559	518	343	221	598

Table 11: Receptor density of 5-HT_{2A} (fmol/mg protein) of brain regions investigated of *LRP1* mice. Mean density ± standard deviation quoted

animal	Group	OB	M1	S1	Pir	CPu	CA1	MosHil	MGr
1	wt	180	430	402	279	754	175	212	140
2	wt	154	474	436	220	755	184	162	138
3	wt	178	537	485	351	892	200	181	216
4	wt	182	503	450	343	806	191	156	203
5	wt	174	555	468	289	1113	247	214	289
20	wt	242	628	542	354	887	345	337	231
	mean	185	521	464	306	868	224	210	203
	SD	30	69	48	53	134	65	67	58
6	LRP1	186	693	518	309	997	269	232	271
7	LRP1	198	490	493	329	912	184	229	178
8	LRP1	170	442	457	256	894	207	209	193
9	LRP1	151	397	400	306	817	179	177	186
	mean	176	506	467	300	905	210	212	207
	SD	20	131	51	31	74	41	25	43

Table 12: Receptor density of $GABA_{A\,AG}$ (fmol/mg protein) of brain regions investigated of *LRP1* mice. Mean density ± standard deviation quoted

animal	Group	OB	M1	S1	Pir	CPu	CA1	MosHil	MGr
1	wt	1738	1820	2000	1389	1208	1540	1022	2333
2	wt	2281	2249	2430	1733	1498	1854	1458	3372
3	wt	2405	1882	2445	1814	1351	1647	1127	2706
4	wt	2716	1572	2362	1843	1113	1507	1207	2777
5	wt	1745	1262	1497	1550	1106	1284	868	2447
20	wt	1973	2372	2753	1960	1751	2009	1301	2767
	mean	2143	1860	2248	1715	1338	1640	1164	2734
	SD	392	414	439	210	252	259	208	361
6	LRP1	2024	1846	1978	1712	1700	1917	1246	3295
7	LRP1	1361	1272	1538	1403	1347	876	848	1965
8	LRP1	1928	1451	1717	1639	1628	1194	860	2213
9	LRP1	1740	1619	1767	1813	1520	1314	1044	2151
	mean	1763	1547	1750	1642	1549	1325	999	2406
	SD	293	244	181	174	153	436	187	602

Table 13: Receptor density of $GABA_{A\,ANT}$ (fmol/mg protein) of brain regions investigated of *LRP1* mice. Mean density ± standard deviation quoted

animal	Group	OB	M1	S1	Pir	CPu	CA1	MosHil	MGr
1	wt	1925	2039	1825	1403	1223	3270	2167	3906
2	wt	2258	1857	1733	1780	1219	3903	2538	4361
3	wt	1917	2056	1983	1877	1347	3380	2367	4177
4	wt	2242	2002	1986	1827	1212	3352	2153	3979
5	wt	1820	1928	1703	1600	1053	3466	2114	3396
20	wt	1417	2641	2733	2305	1293	3930	2386	3656
	mean	1930	2087	1994	1799	1224	3550	2287	3912
	SD	310	281	382	303	99	291	168	349
6	LRP1	2294	1824	1831	1456	917	2583	1587	2960
7	LRP1	3240	1960	2144	1956	1374	3486	2490	3689
8	LRP1	1789	2422	2206	1768	1471	3473	2484	4364
9	LRP1	986	1904	1815	1530	1123	3118	1973	3022
	mean	2077	2027	1999	1677	1221	3165	2133	3508
	SD	944	269	205	229	250	424	437	659

Table 14: Receptor density of BZ (fmol/mg protein) of brain regions investigated of *LRP1* mice. Mean density ± standard deviation quoted

animal	Group	OB	M1	S1	Pir	CPu	CA1	MosHil	MGr
1	wt	4232	4021	4771	3479	1426	5946	3157	6688
2	wt	6885	4999	6064	2156	1779	5547	3291	6623
3	wt	5587	4407	5874	4223	1794	4521	2977	5392
4	wt	6741	4259	4680	3943	1430	4230	2989	5346
5	wt	5002	4334	4687	3284	1439	5085	2812	5022
20	wt	4952	4708	5864	4406	1649	6170	2739	6182
	mean	5566	4455	5323	3582	1586	5250	2994	5875
	SD	1058	347	674	819	177	777	206	715
6	LRP1	6038	4151	5054	3948	1418	5269	2812	5521
7	LRP1	6089	4772	5396	3873	1726	4843	2702	5766
8	LRP1	6550	4796	5550	4076	1959	4984	3217	6327

9	LRP1	4907	4364	5094	3815	1623	4899	2914	5114
	mean	5896	4521	5273	3928	1682	4999	2912	5682
	SD	698	316	239	113	225	189	222	507

Table 15: Receptor density of $GABA_B$ (fmol/mg protein) of brain regions investigated of *LRP1* mice. Mean density ± standard deviation quoted

animal	Group	OB	M1	S1	Pir	CPu	CA1	MosHil	MGr
1	wt	2857	8318	7268	7728	3777	7114	5086	9726
2	wt	3445	10535	10151	8971	6426	11326	7480	15183
3	wt	3043	8673	9741	8705	4841	7174	5190	10040
4	wt	2802	9748	9300	8743	5222	9299	7313	11894
5	wt	2442	7241	6527	6488	3754	7158	5508	10222
20	wt	3246	8782	8578	7818	3678	8055	4951	9860
	mean	2973	8883	8594	8075	4616	8354	5921	11154
	SD	354	1144	1433	933	1098	1684	1158	2126
6	LRP1	2922	10098	8460	8696	4287	7988	5770	11417
7	LRP1	1956	6233	5758	5598	3086	4428	3344	5975
8	LRP1	2274	7619	7166	6872	3794	6457	5108	9914
9	LRP1	2275	8754	7399	8154	3989	5994	4206	7907
	mean	2357	8176	7196	7330	3789	6217	4607	8803
	SD	406	1644	1112	1385	511	1466	1058	2371

Table 16: Receptor density of α_1 (fmol/mg protein) of brain regions investigated of *LRP1* mice. Mean density ± standard deviation quoted

animal	Group	OB	M1	S1	Pir	CPu	CA1	MosHil	MGr
1	wt	845	1230	737	572	361	366	345	467
2	wt	818	1018	654	486	273	200	218	286
3	wt	663	561	401	420	151	143	111	196
4	wt	687	700	407	370	133	124	129	196
5	wt	637	738	461	324	139	170	140	211
20	wt	891	853	532	518	168	212	161	275
	mean	757	850	532	448	204	203	184	272
	SD	107	241	138	93	92	87	87	103
6	LRP1	684	580	361	375	96	105	95	154
7	LRP1	468	580	344	345	102	121	118	184
8	LRP1	624	653	381	313	108	141	127	203
9	LRP1	543	635	374	290	113	149	113	205
	mean	580	612	365	331	105	129	113	186
	SD	95	37	16	37	7	20	14	24

Table 17: Receptor density of α_2 (fmol/mg protein) of brain regions investigated of *LRP1* mice. Mean density ± standard deviation quoted

animal	Group	OB	M1	S1	Pir	CPu	CA1	MosHil	MGr
1	wt	221	282	221	223	104	104	83	284
2	wt	202	173	153	79	82	120	107	333
3	wt	161	229	206	394	105	129	125	364
4	wt	175	184	155	342	84	108	100	294
5	wt	142	195	195	298	81	118	98	285
20	wt	163	199	194	267	107	153	120	368

	mean	177	210	187	267	94	122	105	321
	SD	29	40	27	110	13	18	15	39
6	LRP1	177	228	240	290	152	136	142	305
7	LRP1	377	274	272	336	163	174	141	338
8	LRP1	279	357	340	403	214	185	160	357
9	LRP1	277	259	250	345	180	169	154	314
	mean	277	280	275	344	177	166	149	328
	SD	82	55	45	47	27	21	10	24

Table 18: Receptor density of D_1 (fmol/mg protein) of brain regions investigated of *LRP1* mice. Mean density ± standard deviation quoted

animal	**Group**	**OB**	**M1**	**S1**	**Pir**	**CPu**	**CA1**	**MosHil**	**MGr**
1	wt					3643			
2	wt					2975			
3	wt					3483			
4	wt					3207			
5	wt					4307			
20	wt					3231			
	mean					3474			
	SD					469			
6	LRP1					4266			
7	LRP1					3133			
8	LRP1					2576			
9	LRP1					4121			
	mean					3524			
	SD					808			

Table 19: Receptor density of D_2 (fmol/mg protein) of brain regions investigated of *LRP1* mice. Mean density ± standard deviation quoted

animal	**Group**	**OB**	**M1**	**S1**	**Pir**	**CPu**	**CA1**	**MosHil**	**MGr**
1	wt					321			
2	wt					319			
3	wt					406			
4	wt					392			
5	wt					385			
20	wt					465			
	mean					381			
	SD					55			
6	LRP1					560			
7	LRP1					377			
8	LRP1					490			
9	LRP1					565			
	mean					498			
	SD					88			

Table 20: Receptor density of $D_{2/3}$ (fmol/mg protein) of brain regions investigated of *LRP1* mice. Mean density ± standard deviation quoted

animal	Group	OB	M1	S1	Pir	CPu	CA1	MosHil	MGr
1	wt					2083			
2	wt					2267			
3	wt					2095			
4	wt					2236			
5	wt					2214			
20	wt					2423			
	mean					2220			
	SD					125			
6	LRP1					2566			
7	LRP1					2302			
8	LRP1					2307			
9	LRP1					2471			
	mean					2412			
	SD					129			

Table 21: Receptor density of A_2 (fmol/mg protein) of brain regions investigated of *LRP1* mice. Mean density ± standard deviation quoted

animal	Group	OB	M1	S1	Pir	CPu	CA1	MosHil	MGr
1	wt					3746			
2	wt					2972			
3	wt					3242			
4	wt					3046			
5	wt					2771			
20	wt					3538			
	mean					3219			
	SD					367			
6	LRP1					3681			
7	LRP1					2748			
8	LRP1					2909			
9	LRP1					3438			
	mean					3194			
	SD					439			

Table 22: Receptor density of kainate (fmol/mg protein) of brain regions investigated of *tg5xFAD* mice. Mean density ± standard deviation quoted

animal	Group	OB	M1	S1	Pir	CPu	CA1	MosHil	MGr
1	wt	1592	1078	905	755	1495	569	1485	1340
2	wt	1463	1480	1346	1075	1915	640	1739	1428
3	wt	1705	1239	1107	908	1767	578	1876	1454
4	wt	1492	1052	888	885	1535	572	1894	1519
5	wt	1287	1261	1315	860	1480	568	1525	1245
20	wt	1533	1484	1300	911	1874	650	1500	1366
	mean	1512	1266	1143	899	1678	596	1670	1392
	SD	140	187	209	104	198	38	191	96
10	5xFAD	824	1403	1134	908	1691	630	2090	1345
11	5xFAD	1264	1168	1038	845	1493	719	2314	1408
12	5xFAD	1013	1176	1156	706	1543	566	1885	1174

13	5xFAD	1213	974	996	617	1524	595	1731	1113
14	5xFAD	1594	1058	1112	739	1587	631	1761	1448
21	5xFAD	1110	867	754	643	1290	501	1469	1157
	mean	1170	1108	1032	743	1521	607	1875	1274
	SD	260	186	149	114	133	73	296	143

Table 23: Receptor density of NMDA (fmol/mg protein) of brain regions investigated of *tg5xFAD* mice. Mean density ± standard deviation quoted

animal	**Group**	**OB**	**M1**	**S1**	**Pir**	**CPu**	**CA1**	**MosHil**	**MGr**
1	wt	853	1308	1233	1215	807	3854	1160	3441
2	wt	955	1458	1412	1933	1008	3634	1197	3613
3	wt	1082	1781	1654	1705	1100	4458	1496	3952
4	wt	981	1536	1444	1558	944	3921	1355	3614
5	wt	831	1420	1278	1817	893	3674	1332	3254
20	wt	916	1650	1594	1653	1059	4849	1293	4115
	mean	936	1525	1436	1647	968	4065	1306	3665
	SD	92	170	167	248	109	485	120	319
10	5xFAD	663	1457	1302	1465	786	3883	1129	3368
11	5xFAD	837	1381	1341	1395	815	4706	1288	4116
12	5xFAD	760	2081	1186	1144	1055	4295	1331	3800
13	5xFAD	730	1186	1102	1074	717	4364	1185	3544
14	5xFAD	710	1170	1145	968	786	3546	1011	2885
21	5xFAD	781	1359	1257	1326	813	4058	1131	3690
	mean	747	1439	1222	1229	829	4142	1179	3567
	SD	60	334	93	196	117	405	117	418

Table 24: Receptor density of mGlu2/3 (fmol/mg protein) of brain regions investigated of *tg5xFAD* mice. Mean density ± standard deviation quoted

animal	**Group**	**OB**	**M1**	**S1**	**Pir**	**CPu**	**CA1**	**MosHil**	**MGr**
1	wt	3484	7346	7816	8929	5854	3912	3343	7817
2	wt	4664	10968	11807	16575	9079	6414	4890	11436
3	wt	3176	7862	8443	10081	7613	4047	3967	10460
4	wt	4989	11563	11755	14716	10242	6690	5470	11806
5	wt	2830	9800	9862	14717	10411	5033	4206	11073
20	wt	2267	8442	9488	9699	8170	4721	4204	10481
	mean	3568	9330	9862	12453	8562	5136	4347	10512
	SD	1060	1719	1656	3252	1726	1176	742	1422
10	5xFAD	1010	8622	10723	9467	8244	3445	3845	9154
11	5xFAD	3201	8823	9398	9719	7460	3124	3773	9729
12	5xFAD	2210	7591	8187	8591	7170	3423	3592	8266
13	5xFAD	2405	11342	11119	10584	9249	3596	3583	10540
14	5xFAD	1907	9025	8224	11445	8337	4163	3908	10155
21	5xFAD	2563	9308	11580	13514	8220	4214	4845	9876
	mean	2216	9119	9872	10553	8113	3661	3924	9620
	SD	732	1238	1482	1749	733	437	470	807

Table 25: Receptor density of M_1 (fmol/mg protein) of brain regions investigated of *tg5xFAD* mice. Mean density ± standard deviation quoted

animal	Group	OB	M1	S1	Pir	CPu	CA1	MosHil	MGr
1	wt	1560	2349	2211	2331	3562	4127	2301	4201
2	wt	2474	4188	4233	4701	7843	7546	4078	8215
3	wt	1632	2462	2343	2488	4589	4068	2268	4108
4	wt	1565	2449	2263	2742	4269	4259	3301	4674
5	wt	1517	2601	2695	3358	4782	4699	2622	4762
20	wt	1631	3461	3614	2894	6336	6475	2948	5993
	mean	1730	2918	2893	3086	5230	5196	2920	5325
	SD	367	743	839	868	1573	1463	690	1567
10	5xFAD	1047	1514	1572	1803	2386	2596	1484	2302
11	5xFAD	1202	2135	2072	2448	4703	6609	2241	5421
12	5xFAD	1031	1489	1468	1485	2442	2815	1520	2527
13	5xFAD	1206	1837	1848	1683	4126	4776	2013	4280
14	5xFAD	1765	3162	3116	3063	6179	7811	3064	6496
21	5xFAD	1756	2773	2548	2502	4770	5334	2728	5437
	mean	1334	2152	2104	2164	4101	4990	2175	4411
	SD	338	686	628	604	1471	2059	638	1699

Table 26: Receptor density of $M_{2\,AG}$ (fmol/mg protein) of brain regions investigated of *tg5xFAD* mice. Mean density ± standard deviation quoted

animal	Group	OB	M1	S1	Pir	CPu	CA1	MosHil	MGr
1	wt	2993	998	1299	490	1373	613	624	447
2	wt	3074	1168	1696	540	1637	792	752	540
3	wt	2816	1105	1461	544	1586	645	735	433
4	wt	2945	988	1282	484	1237	787	718	456
5	wt	2570	1135	1322	609	1647	650	638	464
20	wt	2328	1151	1621	503	1593	611	632	381
	mean	2788	1091	1447	528	1512	683	683	453
	SD	286	78	177	47	168	84	58	52
10	5xFAD	2566	1139	1686	514	1701	675	440	360
11	5xFAD	2502	1110	1481	533	1723	607	547	314
12	5xFAD	2271	1123	1649	609	2009	621	511	295
13	5xFAD	2107	1158	1191	322	1335	531	384	213
14	5xFAD	2740	1124	1534	505	1563	675	607	407
21	5xFAD	2546	1241	1661	512	1478	735	712	476
	mean	2456	1149	1534	499	1635	641	533	344
	SD	228	48	186	95	233	71	118	92

Table 27: Receptor density of $M_{2\,ANT}$ (fmol/mg protein) of brain regions investigated of *tg5xFAD* mice. Mean density ± standard deviation quoted

animal	Group	OB	M1	S1	Pir	CPu	CA1	MosHil	MGr
1	wt	3602	1745	2237	1041	4553	1442	889	1034
2	wt	2620	1812	2281	1028	4293	1409	795	875
3	wt	3322	1707	2095	744	4565	1282	716	890
4	wt	4006	1882	2356	912	4840	1510	779	1047
5	wt	2255	2035	2276	1169	5228	1282	694	920
20	wt	2793	1819	2477	888	4961	1308	618	850
	mean	3100	1833	2287	964	4740	1372	749	936
	SD	657	116	127	147	335	96	94	84
10	5xFAD	3452	1881	2583	859	4599	1301	575	809
11	5xFAD	3188	1899	2185	1029	4657	1596	817	995

12	5xFAD	2558	1841	2535	1093	5184	1351	657	929
13	5xFAD	2559	1749	2342	1071	4852	1415	603	816
14	5xFAD	3531	1993	2724	797	5095	1555	671	948
21	5xFAD	2121	1393	1852	799	3763	1025	612	708
	mean	2901	1793	2370	941	4691	1374	656	867
	SD	570	212	317	138	511	205	87	108

Table 28: Receptor density of M_3 (fmol/mg protein) of brain regions investigated of *tg5xFAD* mice. Mean density ± standard deviation quoted

animal	**Group**	**OB**	**M1**	**S1**	**Pir**	**CPu**	**CA1**	**MosHil**	**MGr**
1	wt	3812	4743	4364	3599	6687	7705	4977	6765
2	wt	3148	5136	5417	5058	8053	7770	4320	7297
3	wt	2335	4413	4116	3353	7304	6597	3777	6174
4	wt	3061	4422	4452	3908	6874	6530	3455	6006
5	wt	2735	4568	4259	4372	7724	7776	4102	7097
20	wt	2131	5297	5389	3491	7541	7940	4388	7315
	mean	2870	4763	4666	3963	7364	7386	4170	6776
	SD	609	374	581	647	517	643	527	569
10	5xFAD	2409	5742	5840	4987	8189	8724	4144	7204
11	5xFAD	2575	5105	4695	4347	7748	8446	3676	7319
12	5xFAD	2547	5581	5322	3710	8749	9234	4305	7922
13	5xFAD	2594	4757	5036	4318	8408	8289	4009	7228
14	5xFAD	3149	4796	5456	4041	7639	9540	3887	7978
21	5xFAD	2228	3202	3211	2584	6289	6915	3230	5944
	mean	2584	4864	4927	3998	7837	8525	3875	7266
	SD	310	908	925	811	863	919	383	734

Table 29: Receptor density of 5-HT_{2A} (fmol/mg protein) of brain regions investigated of *tg5xFAD* mice. Mean density ± standard deviation quoted

animal	**Group**	**OB**	**M1**	**S1**	**Pir**	**CPu**	**CA1**	**MosHil**	**MGr**
1	wt	180	430	402	279	754	175	212	140
2	wt	154	474	436	220	755	184	162	138
3	wt	178	537	485	351	892	200	181	216
4	wt	182	503	450	343	806	191	156	203
5	wt	174	555	468	289	1113	247	214	289
20	wt	242	628	542	354	887	345	337	231
	mean	185	521	464	306	868	224	210	203
	SD	30	69	48	53	134	65	67	58
10	5xFAD	142	626	394	336	749	253	179	181
11	5xFAD	174	427	386	279	713	241	199	158
12	5xFAD	183	486	436	303	849	259	231	200
13	5xFAD	184	456	454	338	820	277	275	195
14	5xFAD	252	481	468	414	1049	325	277	240
21	5xFAD	170	437	433	274	858	229	252	172
	mean	184	485	429	324	840	264	235	191
	SD	36	72	32	52	117	34	40	29

Table 30: Receptor density of $GABA_{A\,AG}$ (fmol/mg protein) of brain regions investigated of *tg5xFAD* mice. Mean density ± standard deviation quoted

animal	Group	OB	M1	S1	Pir	CPu	CA1	MosHil	MGr
1	wt	1738	1820	2000	1389	1208	1540	1022	2333
2	wt	2281	2249	2430	1733	1498	1854	1458	3372
3	wt	2405	1882	2445	1814	1351	1647	1127	2706
4	wt	2716	1572	2362	1843	1113	1507	1207	2777
5	wt	1745	1262	1497	1550	1106	1284	868	2447
20	wt	1973	2372	2753	1960	1751	2009	1301	2767
	mean	2143	1860	2248	1715	1338	1640	1164	2734
	SD	392	414	439	210	252	259	208	361
10	5xFAD	1321	1983	2105	1635	1241	1504	1063	2220
11	5xFAD	1887	1664	1954	1684	1400	1758	1118	2191
12	5xFAD	1976	2071	2223	1558	1423	1659	990	2364
13	5xFAD	1393	1776	1907	1586	1349	1156	930	1833
14	5xFAD	2031	1649	1837	1481	1110	1205	883	1901
21	5xFAD	1688	1564	1940	1388	1206	1326	915	1988
	mean	1716	1784	1994	1555	1288	1435	983	2083
	SD	302	201	143	107	123	246	92	207

Table 31: Receptor density of $GABA_{A\ ANT}$ (fmol/mg protein) of brain regions investigated of *tg5xFAD* mice. Mean density ± standard deviation quoted

animal	Group	OB	M1	S1	Pir	CPu	CA1	MosHil	MGr
1	wt	1925	2039	1825	1403	1223	3270	2167	3906
2	wt	2258	1857	1733	1780	1219	3903	2538	4361
3	wt	1917	2056	1983	1877	1347	3380	2367	4177
4	wt	2242	2002	1986	1827	1212	3352	2153	3979
5	wt	1820	1928	1703	1600	1053	3466	2114	3396
20	wt	1417	2641	2733	2305	1293	3930	2386	3656
	mean	1930	2087	1994	1799	1224	3550	2287	3912
	SD	310	281	382	303	99	291	168	349
10	5xFAD	1060	1060	1060	1060	1060	1060	2419	1060
11	5xFAD	1655	1655	1655	1655	1655	1655	2272	1655
12	5xFAD	1094	1094	1094	1094	1094	1094	1837	1094
13	5xFAD	1218	1218	1218	1218	1218	1218	1657	1218
14	5xFAD	2422	2422	2422	2422	2422	2422	2536	2422
21	5xFAD	1753	1753	1753	1753	1753	1753	2207	1753
	mean	1534	1534	1534	1534	1534	1534	2155	1534
	SD	523	523	523	523	523	523	341	523

Table 32: Receptor density of BZ (fmol/mg protein) of brain regions investigated of *tg5xFAD* mice. Mean density ± standard deviation quoted

animal	Group	OB	M1	S1	Pir	CPu	CA1	MosHil	MGr
1	wt	4232	4021	4771	3479	1426	5946	3157	6688
2	wt	6885	4999	6064	2156	1779	5547	3291	6623
3	wt	5587	4407	5874	4223	1794	4521	2977	5392
4	wt	6741	4259	4680	3943	1430	4230	2989	5346
5	wt	5002	4334	4687	3284	1439	5085	2812	5022
20	wt	4952	4708	5864	4406	1649	6170	2739	6182
	mean	5566	4455	5323	3582	1586	5250	2994	5875
	SD	1058	347	674	819	177	777	206	715
10	5xFAD	5839	5366	6120	4457	1660	6890	3292	7182
11	5xFAD	6550	5553	6107	4627	1545	6233	3474	6514

12	5xFAD	5074	4882	5691	4130	1686	6411	3198	6679
13	5xFAD	5135	4209	5098	3789	1513	5289	2478	5825
14	5xFAD	5464	3623	4132	3542	1508	4026	2484	4641
21	5xFAD	6870	4131	4742	3639	1489	5449	2776	5905
	mean	5822	4627	5315	4031	1567	5716	2951	6124
	SD	747	761	799	447	85	1023	430	885

Table 33: Receptor density of $GABA_B$ (fmol/mg protein) of brain regions investigated of *tg5xFAD* mice. Mean density ± standard deviation quoted

animal	**Group**	**OB**	**M1**	**S1**	**Pir**	**CPu**	**CA1**	**MosHil**	**MGr**
1	wt	2857	8318	7268	7728	3777	7114	5086	9726
2	wt	3445	10535	10151	8971	6426	11326	7480	15183
3	wt	3043	8673	9741	8705	4841	7174	5190	10040
4	wt	2802	9748	9300	8743	5222	9299	7313	11894
5	wt	2442	7241	6527	6488	3754	7158	5508	10222
20	wt	3246	8782	8578	7818	3678	8055	4951	9860
	mean	2973	8883	8594	8075	4616	8354	5921	11154
	SD	354	1144	1433	933	1098	1684	1158	2126
10	5xFAD	1379	9371	8832	7349	3792	7215	4837	9280
11	5xFAD	2923	7527	7383	11492	3475	9849	7364	12462
12	5xFAD	2313	8300	7713	5550	3257	7410	5670	9621
13	5xFAD	2218	8367	8003	7024	3297	8046	5685	10781
14	5xFAD	2617	9685	9383	5779	3983	10156	6496	12549
21	5xFAD	2384	8758	7699	8790	4020	7231	5425	9430
	mean	2306	8668	8169	7664	3637	8318	5913	10687
	SD	520	783	773	2211	339	1343	889	1505

Table 34: Receptor density of α_1 (fmol/mg protein) of brain regions investigated of *tg5xFAD* mice. Mean density ± standard deviation quoted

animal	**Group**	**OB**	**M1**	**S1**	**Pir**	**CPu**	**CA1**	**MosHil**	**MGr**
1	wt	845	1230	737	572	361	366	345	467
2	wt	818	1018	654	486	273	200	218	286
3	wt	663	561	401	420	151	143	111	196
4	wt	687	700	407	370	133	124	129	196
5	wt	637	738	461	324	139	170	140	211
20	wt	891	853	532	518	168	212	161	275
	mean	757	850	532	448	204	203	184	272
	SD	107	241	138	93	92	87	87	103
10	5xFAD	559	749	441	439	142	163	125	228
11	5xFAD	690	833	449	318	126	157	137	246
12	5xFAD	584	668	384	331	117	122	114	227
13	5xFAD	649	587	389	340	120	125	114	194
14	5xFAD	689	569	391	365	123	121	111	184
21	5xFAD	828	783	471	453	180	179	168	257
	mean	667	698	421	374	135	145	128	223
	SD	96	108	37	58	24	25	22	29

Table 35: Receptor density of α_2 (fmol/mg protein) of brain regions investigated of *tg5xFAD* mice. Mean density ± standard deviation quoted

animal	Group	OB	M1	S1	Pir	CPu	CA1	MosHil	MGr
1	wt	221	282	221	223	104	104	83	284
2	wt	202	173	153	79	82	120	107	333
3	wt	161	229	206	394	105	129	125	364
4	wt	175	184	155	342	84	108	100	294
5	wt	142	195	195	298	81	118	98	285
20	wt	163	199	194	267	107	153	120	368
	mean	177	210	187	267	94	122	105	321
	SD	29	40	27	110	13	18	15	39
10	5xFAD	216	288	248	329	139	184	151	387
11	5xFAD	251	242	235	429	142	185	153	384
12	5xFAD	212	271	227	337	150	183	166	407
13	5xFAD	259	287	263	417	153	176	158	363
14	5xFAD	197	300	248	359	143	178	154	492
21	5xFAD	211	326	258	412	143	232	163	436
	mean	224	286	246	381	145	190	157	411
	SD	25	28	14	44	5	21	6	47

Table 36: Receptor density of D_1 (fmol/mg protein) of brain regions investigated of *tg5xFAD* mice. Mean density ± standard deviation quoted

animal	Group	OB	M1	S1	Pir	CPu	CA1	MosHil	MGr
1	wt					3643			
2	wt					2975			
3	wt					3483			
4	wt					3207			
5	wt					4307			
20	wt					3231			
	mean					3474			
	SD					469			
10	5xFAD					3287			
11	5xFAD					3122			
12	5xFAD					3686			
13	5xFAD					2552			
14	5xFAD					3848			
21	5xFAD					2787			
	mean					3214			
	SD					502			

Table 37: Receptor density of D_2 (fmol/mg protein) of brain regions investigated of *tg5xFAD* mice. Mean density ± standard deviation quoted

animal	Group	OB	M1	S1	Pir	CPu	CA1	MosHil	MGr
1	wt					321			
2	wt					319			
3	wt					406			
4	wt					392			
5	wt					385			
20	wt					465			
	mean					381			
	SD					55			
10	5xFAD					495			
11	5xFAD					488			

12	5xFAD					525			
13	5xFAD					484			
14	5xFAD					417			
21	5xFAD					480			
	mean					481			
	SD					35			

Table 38: Receptor density of $D_{2/3}$ (fmol/mg protein) of brain regions investigated of *tg5xFAD* mice. Mean density ± standard deviation quoted

animal	Group	OB	M1	S1	Pir	CPu	CA1	MosHil	MGr
1	wt					2083			
2	wt					2267			
3	wt					2095			
4	wt					2236			
5	wt					2214			
20	wt					2423			
	mean					2220			
	SD					125			
10	5xFAD					2376			
11	5xFAD					2488			
12	5xFAD					2483			
13	5xFAD					2449			
14	5xFAD					2196			
21	5xFAD					2179			
	mean					2362			
	SD					141			
						2376			

Table 39: Receptor density of A_2 (fmol/mg protein) of brain regions investigated of *tg5xFAD* mice. Mean density ± standard deviation quoted

animal	Group	OB	M1	S1	Pir	CPu	CA1	MosHil	MGr
1	wt					3746			
2	wt					2972			
3	wt					3242			
4	wt					3046			
5	wt					2771			
20	wt					3538			
	mean					3219			
	SD					367			
10	5xFAD					2713			
11	5xFAD					3243			
12	5xFAD					2960			
13	5xFAD					2862			
14	5xFAD					2996			
21	5xFAD					3065			
	mean					2973			
	SD					180			

Table 40: Receptor density of kainate (fmol/mg protein) of brain regions investigated of *tg5xFAD/LRP1* mice. Mean density ± standard deviation quoted

animal	Group	OB	M1	S1	Pir	CPu	CA1	MosHil	MGr
1	wt	1592	1078	905	755	1495	569	1485	1340
2	wt	1463	1480	1346	1075	1915	640	1739	1428
3	wt	1705	1239	1107	908	1767	578	1876	1454
4	wt	1492	1052	888	885	1535	572	1894	1519
5	wt	1287	1261	1315	860	1480	568	1525	1245
20	wt	1533	1484	1300	911	1874	650	1500	1366
	mean	1512	1266	1143	899	1678	596	1670	1392
	SD	140	187	209	104	198	38	191	96
15	5xFAD/ LRP1	1337	1589	1523	885	1868	640	1992	1309
16		1158	1463	1360	693	1886	693	2355	1495
17		1243	1210	1061	774	1829	699	2000	1374
35		1341	956	1005	621	1537	565	1681	1318
36		1217	990	1004	726	1496	581	1937	1230
37		1378	1143	1061	758	1690	504	1643	1198
38		1007	1455	1379	937	1780	594	1930	1306
39		1289	986	1048	648	1750	605	1928	1382
40		1629	1273	1182	823	1760	588	1869	1471
	mean	1160	1229	1180	763	1733	608	1926	1343
	SD	438	233	193	105	137	62	205	99

Table 41: Receptor density of NMDA (fmol/mg protein) of brain regions investigated of *tg5xFAD/LRP1* mice. Mean density ± standard deviation quoted

animal	Group	OB	M1	S1	Pir	CPu	CA1	MosHil	MGr
1	wt	853	1308	1233	1215	807	3854	1160	3441
2	wt	955	1458	1412	1933	1008	3634	1197	3613
3	wt	1082	1781	1654	1705	1100	4458	1496	3952
4	wt	981	1536	1444	1558	944	3921	1355	3614
5	wt	831	1420	1278	1817	893	3674	1332	3254
20	wt	916	1650	1594	1653	1059	4849	1293	4115
	mean	936	1525	1436	1647	968	4065	1306	3665
	SD	92	170	167	248	109	485	120	319
15	5xFAD/ LRP1	653	1436	1278	1381	924	4207	1382	3207
16		818	1343	1351	1331	920	4615	1760	3621
17		874	1841	1678	1756	987	5103	1516	3793
35		821	1332	1223	1305	858	4575	1288	3587
36		748	1461	1372	1511	855	4205	1490	3372
37		837	1533	1395	1652	941	4424	1475	3498
38		794	1605	1494	1562	927	4483	1669	3591
39		897	1437	1453	1518	923	4447	1469	3559
40		982	1627	1535	1526	967	4225	1402	3554
	mean	743	1513	1420	1505	922	4476	1495	3531
	SD	275	160	138	147	44	282	144	164

Table 42: Receptor density of mGlu2/3 (fmol/mg protein) of brain regions investigated of *tg5x FAD/LRP1* mice. Mean density ± standard deviation quoted

animal	Group	OB	M1	S1	Pir	CPu	CA1	MosHil	MGr

1	wt	3484	7346	7816	8929	5854	3912	3343	7817
2	wt	4664	10968	11807	16575	9079	6414	4890	11436
3	wt	3176	7862	8443	10081	7613	4047	3967	10460
4	wt	4989	11563	11755	14716	10242	6690	5470	11806
5	wt	2830	9800	9862	14717	10411	5033	4206	11073
20	wt	2267	8442	9488	9699	8170	4721	4204	10481
	mean	3568	9330	9862	12453	8562	5136	4347	10512
	SD	1060	1719	1656	3252	1726	1176	742	1422
15	5xFAD/ LRP1	3511	8406	9515	11455	6525	4164	4718	11680
16		3447	9787	10840	11785	7523	3491	4001	9112
17		3324	9203	9437	13281	7330	3106	3694	9329
35		2901	7855	8952	8900	6614	2995	3573	9697
36		2657	9216	10861	9492	8400	3150	3808	9966
37		3239	9523	10131	12374	7585	3596	3841	10326
38		2671	6485	7243	8893	6335	3827	3999	9253
39		3050	7574	8322	12250	7128	3443	4410	10311
40		3036	9782	11187	13506	7732	4297	4421	12097
	mean	2783	8648	9610	11326	7241	3563	4052	10197
	SD	1022	1146	1302	1800	664	460	383	1058

Table 43: Receptor density of M_1 (fmol/mg protein) of brain regions investigated of *tg5xFAD/LRP1* mice. Mean density ± standard deviation quoted

animal	**Group**	**OB**	**M1**	**S1**	**Pir**	**CPu**	**CA1**	**MosHil**	**MGr**
1	wt	1560	2349	2211	2331	3562	4127	2301	4201
2	wt	2474	4188	4233	4701	7843	7546	4078	8215
3	wt	1632	2462	2343	2488	4589	4068	2268	4108
4	wt	1565	2449	2263	2742	4269	4259	3301	4674
5	wt	1517	2601	2695	3358	4782	4699	2622	4762
20	wt	1631	3461	3614	2894	6336	6475	2948	5993
	mean	1730	2918	2893	3086	5230	5196	2920	5325
	SD	367	743	839	868	1573	1463	690	1567
15	5xFAD/ LRP1	1645	2707	2634	2529	5109	5663	2565	4850
16		1642	3071	2755	3429	5523	6959	2801	5777
17		1474	3182	2913	2907	5807	6577	2840	5811
35		1417	2027	2064	2245	4209	6099	2483	4916
36		1584	2870	2823	2861	6094	5876	2825	5296
37		1306	2611	2596	2557	4776	4936	2370	4494
38		1687	3333	3063	2553	5519	6997	3249	6397
39		1684	3608	3452	3660	6251	7292	3245	6505
40		1880	3312	3408	3156	5223	7063	3170	6579
	mean	1432	2969	2856	2877	5390	6385	2839	5625
	SD	528	475	427	464	644	790	329	777

Table 44: Receptor density of $M_{2\ AG}$ (fmol/mg protein) of brain regions investigated of *tg5xFAD/LRP1* mice. Mean density ± standard deviation quoted

animal	**Group**	**OB**	**M1**	**S1**	**Pir**	**CPu**	**CA1**	**MosHil**	**MGr**
1	wt	2993	998	1299	490	1373	613	624	447
2	wt	3074	1168	1696	540	1637	792	752	540
3	wt	2816	1105	1461	544	1586	645	735	433
4	wt	2945	988	1282	484	1237	787	718	456
5	wt	2570	1135	1322	609	1647	650	638	464

20	wt	2328	1151	1621	503	1593	611	632	381
	mean	2788	1091	1447	528	1512	683	683	453
	SD	286	78	177	47	168	84	58	52
15	5xFAD/ LRP1	2530	1069	1266	666	1595	680	696	359
16		2630	1137	1520	604	1567	706	732	400
17		2261	1135	1439	672	1687	650	589	443
35		2261	970	1259	475	1445	641	551	447
36		1961	879	1187	354	1037	692	630	448
37		2223	1131	1580	549	1372	714	615	532
38		1630	1152	1814	556	1632	623	486	402
39		2393	1182	1798	557	1604	734	667	501
40		2963	1239	1594	607	1577	835	785	541
	mean	2085	1099	1495	560	1502	697	639	453
	SD	817	111	228	98	199	63	93	62

Table 45: Receptor density of $M_{2\ ANT}$ (fmol/mg protein) of brain regions investigated of *tg5xFAD/LRP1* mice. Mean density ± standard deviation quoted

animal	**Group**	**OB**	**M1**	**S1**	**Pir**	**CPu**	**CA1**	**MosHil**	**MGr**
1	wt	3602	1745	2237	1041	4553	1442	889	1034
2	wt	2620	1812	2281	1028	4293	1409	795	875
3	wt	3322	1707	2095	744	4565	1282	716	890
4	wt	4006	1882	2356	912	4840	1510	779	1047
5	wt	2255	2035	2276	1169	5228	1282	694	920
20	wt	2793	1819	2477	888	4961	1308	618	850
	mean	3100	1833	2287	964	4740	1372	749	936
	SD	657	116	127	147	335	96	94	84
15	5xFAD/ LRP1	1898	1540	1802	990	4649	1678	821	1012
16		2756	1669	1955	917	4571	1392	833	917
17		2119	1645	2023	798	4567	1433	652	793
35		2307	1446	1828	969	3951	1376	668	822
36		2566	1468	1903	816	3984	1448	742	855
37		2601	1438	1989	3279	3567	1165	560	741
38		2616	1985	2543	1137	4391	1533	689	1042
39		2395	1455	2036	915	3733	1292	549	798
40		2669	1607	2009	807	4289	1329	627	855
	mean	2193	1584	2010	1181	4189	1405	682	871
	SD	815	175	217	794	394	146	101	101

Table 46: Receptor density of M_3 (fmol/mg protein) of brain regions investigated of *tg5xFAD/LRP1* mice. Mean density ± standard deviation quoted

animal	**Group**	**OB**	**M1**	**S1**	**Pir**	**CPu**	**CA1**	**MosHil**	**MGr**
1	wt	3812	4743	4364	3599	6687	7705	4977	6765
2	wt	3148	5136	5417	5058	8053	7770	4320	7297
3	wt	2335	4413	4116	3353	7304	6597	3777	6174
4	wt	3061	4422	4452	3908	6874	6530	3455	6006
5	wt	2735	4568	4259	4372	7724	7776	4102	7097
20	wt	2131	5297	5389	3491	7541	7940	4388	7315
	mean	2870	4763	4666	3963	7364	7386	4170	6776
	SD	609	374	581	647	517	643	527	569
15	5xFAD/ LRP1	2669	4708	5028	4544	6562	7060	3694	5347
16		2572	4209	4434	2731	7656	7981	3922	6053

17		2133	4332	4504	3620	6328	7087	3483	5983
35		2542	4283	4226	3747	7551	8312	4272	7216
36		2189	4293	4356	2932	6528	7183	3774	6025
37		2079	4452	4486	3053	7360	7059	3462	5985
38		2295	4409	4574	4590	6321	6671	3750	5896
39		2579	4861	5250	3794	6981	7907	3908	6361
40		2520	5832	5934	4368	8020	9261	3915	7078
	mean	2158	4598	4755	3709	7034	7613	3798	6216
	SD	787	509	550	700	635	820	248	591

Table 47: Receptor density of 5-HT_{2A} (fmol/mg protein) of brain regions investigated of *tg5xFAD/LRP1* mice. Mean density ± standard deviation quoted

animal	**Group**	**OB**	**M1**	**S1**	**Pir**	**CPu**	**CA1**	**MosHil**	**MGr**
1	wt	180	430	402	279	754	175	212	140
2	wt	154	474	436	220	755	184	162	138
3	wt	178	537	485	351	892	200	181	216
4	wt	182	503	450	343	806	191	156	203
5	wt	174	555	468	289	1113	247	214	289
20	wt	242	628	542	354	887	345	337	231
	mean	185	521	464	306	868	224	210	203
	SD	30	69	48	53	134	65	67	58
15	5xFAD/ LRP1	236	607	617	446	1108	331	275	213
16		237	593	619	284	1141	347	370	234
17		223	555	517	362	996	344	316	237
35		197	438	398	290	952	266	214	168
36		199	605	453	344	1102	270	267	216
37		200	507	483	371	1189	280	234	181
38		170	507	376	305	752	252	175	169
39		172	465	473	310	964	285	263	238
40		184	465	487	389	1012	263	268	172
	mean	182	527	492	345	1024	293	265	203
	SD	68	65	84	53	131	37	56	31

Table 48: Receptor density of $GABA_{A\,AG}$ (fmol/mg protein) of brain regions investigated of *tg5xFAD/LRP1* mice. Mean density ± standard deviation quoted

animal	**Group**	**OB**	**M1**	**S1**	**Pir**	**CPu**	**CA1**	**MosHil**	**MGr**
1	wt	1738	1820	2000	1389	1208	1540	1022	2333
2	wt	2281	2249	2430	1733	1498	1854	1458	3372
3	wt	2405	1882	2445	1814	1351	1647	1127	2706
4	wt	2716	1572	2362	1843	1113	1507	1207	2777
5	wt	1745	1262	1497	1550	1106	1284	868	2447
20	wt	1973	2372	2753	1960	1751	2009	1301	2767
	mean	2143	1860	2248	1715	1338	1640	1164	2734
	SD	392	414	439	210	252	259	208	361
15	5xFAD/ LRP1	1523	1854	1823	1938	1457	1746	1201	2375
16		1792	1718	1935	1757	1341	1281	872	1853
17		1990	1951	2121	1888	1461	1478	1341	2533
35		1971	1550	1753	1596	1174	1286	899	1985
36		1945	1655	1918	1370	1154	1271	956	2196
37		1370	1598	1749	1402	997	1440	894	2072
38		2209	1766	2292	1975	1275	1457	874	1899

39		1903	2130	2480	1832	1452	2116	1358	2811
40		1726	1827	2107	1422	969	1496	1020	2222
	mean	1643	1783	2020	1687	1253	1508	1046	2216
	SD	626	182	251	243	192	272	200	314

Table 49: Receptor density of $GABA_{A\,ANT}$ (fmol/mg protein) of brain regions investigated of *tg5xFAD/LRP1* mice. Mean density ± standard deviation quoted

animal	Group	OB	M1	S1	Pir	CPu	CA1	MosHil	MGr
1	wt	1925	2039	1825	1403	1223	3270	2167	3906
2	wt	2258	1857	1733	1780	1219	3903	2538	4361
3	wt	1917	2056	1983	1877	1347	3380	2367	4177
4	wt	2242	2002	1986	1827	1212	3352	2153	3979
5	wt	1820	1928	1703	1600	1053	3466	2114	3396
20	wt	1417	2641	2733	2305	1293	3930	2386	3656
	mean	1930	2087	1994	1799	1224	3550	2287	3912
	SD	310	281	382	303	99	291	168	349
15	5xFAD/ LRP1	1610	2686	2376	2442	1424	3529	2233	3267
16		1550	2351	2127	2176	1524	3680	2801	4479
17		1829	2505	2159	2221	1371	3436	2505	3542
35		1758	1260	1364	1782	840	2281	1583	2507
36		1343	2073	1881	1464	1183	3510	2399	3981
37		1942	1790	1798	1675	1153	3836	2257	4439
38		1785	2207	1935	1712	1230	3977	2270	4130
39		1135	2163	2299	1713	1154	4147	2521	4307
40		1763	2514	2343	2008	1355	3658	2477	4169
	mean	1471	2172	2031	1910	1248	3562	2339	3869
	SD	571	435	325	318	201	533	334	650

Table 50: Receptor density of BZ (fmol/mg protein) of brain regions investigated of *tg5xFAD/LRP1* mice. Mean density ± standard deviation quoted

animal	Group	OB	M1	S1	Pir	CPu	CA1	MosHil	MGr
1	wt	4232	4021	4771	3479	1426	5946	3157	6688
2	wt	6885	4999	6064	2156	1779	5547	3291	6623
3	wt	5587	4407	5874	4223	1794	4521	2977	5392
4	wt	6741	4259	4680	3943	1430	4230	2989	5346
5	wt	5002	4334	4687	3284	1439	5085	2812	5022
20	wt	4952	4708	5864	4406	1649	6170	2739	6182
	mean	5566	4455	5323	3582	1586	5250	2994	5875
	SD	1058	347	674	819	177	777	206	715
15	5xFAD/ LRP1	5465	3703	4394	3578	1482	3562	2376	3862
16		6322	4054	4625	3123	1644	5005	3037	5609
17		5588	4249	4370	4184	1648	5034	2845	5984
35		5628	4209	4669	3553	1372	5372	2753	6159
36		5391	4035	4383	3779	1546	5080	2978	5567
37		5417	5665	5613	4176	2469	6692	3311	7487
38		6535	5325	6307	4443	1532	6466	2907	6794
39		4427	4063	4809	3438	1329	5366	2717	5746
40		6682	4630	5422	4081	1502	6503	3300	6407
	mean	5146	4437	4955	3817	1614	5453	2914	5957
	SD	1924	653	678	430	338	985	293	1000

Table 51: Receptor density of $GABA_B$ (fmol/mg protein) of brain regions investigated of *tg5xFAD/LRP1* mice. Mean density ± standard deviation quoted

animal	Group	OB	M1	S1	Pir	CPu	CA1	MosHil	MGr
1	wt	2857	8318	7268	7728	3777	7114	5086	9726
2	wt	3445	10535	10151	8971	6426	11326	7480	15183
3	wt	3043	8673	9741	8705	4841	7174	5190	10040
4	wt	2802	9748	9300	8743	5222	9299	7313	11894
5	wt	2442	7241	6527	6488	3754	7158	5508	10222
20	wt	3246	8782	8578	7818	3678	8055	4951	9860
	mean	2973	8883	8594	8075	4616	8354	5921	11154
	SD	354	1144	1433	933	1098	1684	1158	2126
15	5xFAD/ LRP1	1963	11458	10794	11257	5491	11936	8489	15243
16		2570	11561	11505	2397	3895	12373	8861	15305
17		3005	11958	11170	11686	4498	11313	7373	14270
35		2718	8305	7266	7515	3311	8975	5301	10218
36		2690	8121	7555	5696	3019	7475	5077	9515
37		2666	9804	9093	7313	4283	10466	6854	13334
38		2551	7944	7534	7173	3665	9215	5495	11309
39		2174	7006	6724	5273	2719	6683	4379	7915
40		3128	8690	8178	8040	3589	6785	5280	8700
	mean	2347	9428	8869	7372	3830	9469	6345	11757
	SD	893	1830	1842	2876	841	2184	1607	2856

Table 52: Receptor density of α_1 (fmol/mg protein) of brain regions investigated of *tg5xFAD/LRP1* mice. Mean density ± standard deviation quoted

animal	Group	OB	M1	S1	Pir	CPu	CA1	MosHil	MGr
1	wt	845	1230	737	572	361	366	345	467
2	wt	818	1018	654	486	273	200	218	286
3	wt	663	561	401	420	151	143	111	196
4	wt	687	700	407	370	133	124	129	196
5	wt	637	738	461	324	139	170	140	211
20	wt	891	853	532	518	168	212	161	275
	mean	757	850	532	448	204	203	184	272
	SD	107	241	138	93	92	87	87	103
15	5xFAD/ LRP1	747	663	448	339	120	138	120	221
16		728	818	448	338	145	136	141	235
17		696	764	472	469	137	159	132	239
35		674	758	433	309	162	170	160	265
36		711	749	485	427	166	162	167	260
37		771	783	478	416	176	152	149	265
38		571	764	462	244	165	149	151	241
39		511	761	470	391	166	166	152	219
40		871	831	484	568	158	164	146	252
	mean	628	766	465	389	155	155	146	244
	SD	242	48	18	96	18	12	14	17

Table 53: Receptor density of α_2 (fmol/mg protein) of brain regions investigated of *tg5xFAD/LRP1* mice. Mean density ± standard deviation quoted

animal	Group	OB	M1	S1	Pir	CPu	CA1	MosHil	MGr
1	wt	221	282	221	223	104	104	83	284

2	wt	202	173	153	79	82	120	107	333
3	wt	161	229	206	394	105	129	125	364
4	wt	175	184	155	342	84	108	100	294
5	wt	142	195	195	298	81	118	98	285
20	wt	163	199	194	267	107	153	120	368
	mean	177	210	187	267	94	122	105	321
	SD	29	40	27	110	13	18	15	39
15	5xFAD/ LRP1	217	305	264	467	160	181	135	338
16		236	250	220	388	138	168	141	310
17		231	259	215	443	130	155	137	296
35		274	272	260	371	162	188	181	392
36		243	372	362	437	184	200	183	366
37		259	379	319	472	204	205	192	389
38		268	361	325	404	184	201	193	439
39		235	295	301	382	178	211	200	453
40		232	341	317	404	190	170	177	369
	mean	220	315	287	419	170	187	171	373
	SD	79	50	50	37	25	19	26	53

Table 54: Receptor density of D_1 (fmol/mg protein) of brain regions investigated of *tg5xFAD/LRP1* mice. Mean density ± standard deviation quoted

animal	**Group**	**OB**	**M1**	**S1**	**Pir**	**CPu**	**CA1**	**MosHil**	**MGr**
1	wt					3643			
2	wt					2975			
3	wt					3483			
4	wt					3207			
5	wt					4307			
20	wt					3231			
	mean					3474			
	SD					469			
15	5xFAD/ LRP1					3984			
16						3417			
17						3226			
35						2865			
36						2788			
37						3314			
38						3287			
39						2549			
40						2499			
	mean					3103			
	SD					474			

Table 55: Receptor density of D_2 (fmol/mg protein) of brain regions investigated of *tg5xFAD/LRP1* mice. Mean density ± standard deviation quoted

animal	**Group**	**OB**	**M1**	**S1**	**Pir**	**CPu**	**CA1**	**MosHil**	**MGr**
1	wt					321			
2	wt					319			
3	wt					406			
4	wt					392			
5	wt					385			
20	wt					465			

	mean					381			
	SD					55			
15	5xFAD/ LRP1					578			
16						567			
17						576			
35						426			
36						378			
37						395			
38						468			
39						397			
40						498			
	mean					476			
	SD					83			

Table 56: Receptor density of $D_{2/3}$ (fmol/mg protein) of brain regions investigated of *tg5xFAD/LRP1* mice. Mean density ± standard deviation quoted

animal	**Group**	**OB**	**M1**	**S1**	**Pir**	**CPu**	**CA1**	**MosHil**	**MGr**
1	wt					2083			
2	wt					2267			
3	wt					2095			
4	wt					2236			
5	wt					2214			
20	wt					2423			
	mean					2220			
	SD					125			
15	5xFAD/ LRP1					2511			
16						2263			
17						2330			
35						2324			
36						2595			
37						2350			
38						2013			
39						1957			
40						2442			
	mean					2310			
	SD					211			

Table 57: Receptor density of A_2 (fmol/mg protein) of brain regions investigated of *tg5xFAD/LRP1* mice. Mean density ± standard deviation quoted

animal	**Group**	**OB**	**M1**	**S1**	**Pir**	**CPu**	**CA1**	**MosHil**	**MGr**
1	wt					3746			
2	wt					2972			
3	wt					3242			
4	wt					3046			
5	wt					2771			
20	wt					3538			
	mean					3219			
	SD					367			
15	5xFAD/ LRP1					3261			
16						3661			
17						3895			
35						2645			

36						2559			
37						2974			
38						2803			
39						3155			
40						3042			
	mean					3110			
	SD					445			

Table 58: Receptor density of AMPA (fmol/mg protein) of brain regions investigated of *tgArcAβ* mice. Mean density ± standard deviation quoted

animal	Group	OB	M1	S1	Pir	CPu	CA1	MosHil	MGr
8	wt	699	1028	973	1827	734	2017	1836	1909
9	wt	600	1114	1004	2193	848	1942	1506	1811
10	wt	931	1263	1185	1913	897	2317	2205	1957
11	wt	860	986	870	2057	699	2394	2099	2316
12	wt	740	765	824	1896	1170	2176	2106	1888
13	wt	779	1083	1052	1747	837	1994	2255	2016
14	wt	849	882	939	1808	830	1992	1854	1683
	mean	780	1017	978	1920	859	2119	1980	1940
	SD	111	162	120	155	153	179	264	197
1	ArcAβ	676	881	753	1552	679	2121	1577	1531
2	ArcAβ	813	1067	878	2050	877	2057	1895	1619
3	ArcAβ	1216	831	1023	1534	861	2286	2308	1891
4	ArcAβ	661	1147	1181	1955	931	2618	2351	2116
5	ArcAβ	657	1122	969	2126	885	2511	2227	2166
6	ArcAβ	885	1155	1198	2284	821	2478	2156	2016
7	ArcAβ	688	1019	837	1674	760	2057	1651	1586
	mean	799	1032	977	1882	831	2304	2024	1846
	SD	203	130	169	297	86	234	316	266

Table 59: Receptor density of kainate (fmol/mg protein) of brain regions investigated of *tgArcAβ* mice. Mean density ± standard deviation quoted

animal	Group	OB	M1	S1	Pir	CPu	CA1	MosHil	MGr
8	wt	2049	1868	1618	1327	2072	653	1898	1883
9	wt	2186	1954	1614	1022	2234	731	2213	1985
10	wt	2102	1967	1787	1014	2200	653	2022	1618
11	wt	2432	2018	1758	1272	2542	853	3029	1995
12	wt	2272	2341	1774	1194	2301	813	2427	1869
13	wt	2547	2003	1812	809	2335	789	2433	1841
14	wt	2484	2157	1923	1039	2417	833	2577	1909
	mean	2296	2044	1755	1097	2300	761	2371	1871
	SD	195	157	109	178	153	83	377	126
1	ArcAβ	2022	1414	1320	590	1769	713	1927	1859
2	ArcAβ	2093	1667	1693	1127	1953	806	2618	2071
3	ArcAβ	2029	2220	1763	916	1994	841	2819	1868
4	ArcAβ	2634	1574	1511	580	2103	761	2087	1891
5	ArcAβ	1852	1529	1525	773	1979	741	1882	2030
6	ArcAβ	2990	1785	1864	898	1998	756	2180	1882
7	ArcAβ	2100	1925	1600	1153	2056	843	2078	2207
	mean	2246	1730	1611	863	1979	780	2227	1973
	SD	409	274	181	231	105	50	355	133

Table 60: Receptor density of NMDA (fmol/mg protein) of brain regions investigated of *tgArcAβ* mice. Mean density ± standard deviation quoted

animal	Group	OB	M1	S1	Pir	CPu	CA1	MosHil	MGr
8	wt	813	813	1191	1398	825	3341	1467	3127
9	wt	682	682	707	608	433	2086	1016	2171
10	wt	781	781	1445	1269	1013	4288	1571	3476
11	wt	715	715	1319	1347	1072	3558	1420	3066
12	wt	764	764	1166	1300	959	3425	1780	3275
13	wt	984	984	1551	1566	949	2545	1234	1612
14	wt	751	751	1119	1298	848	2244	895	1926
	mean	784	784	1214	1255	871	3070	1340	2665
	SD	98	98	273	302	211	801	312	742
1	ArcAβ	748	1301	1065	1381	773	2998	1308	2724
2	ArcAβ	802	1559	1443	1626	1021	3973	1587	3293
3	ArcAβ	1182	1571	1373	1573	1048	3883	1641	3493
4	ArcAβ	988	1814	1614	1656	1110	4399	2240	3603
5	ArcAβ	807	1587	1383	1452	938	3029	1339	2939
6	ArcAβ	952	1778	1504	1693	962	3975	1418	3409
7	ArcAβ	905	1682	1461	1648	932	3473	1573	3533
	mean	912	1613	1406	1576	969	3676	1587	3285
	SD	147	171	171	116	108	526	316	331

Table 61: Receptor density of mGlu2/3 (fmol/mg protein) of brain regions investigated of *tgArcAβ* mice. Mean density ± standard deviation quoted

animal	Group	OB	M1	S1	Pir	CPu	CA1	MosHil	MGr
8	wt	1983	3896	3867	3535	3015	2464	2381	3922
9	wt	2127	2875	3180	3710	2041	2291	2261	4026
10	wt	2128	2972	2967	2487	2036	1711	1727	2919
11	wt	1915	3856	3854	3138	2599	2503	2461	4185
12	wt	1871	3125	2964	4124	2516	1949	2055	3313
13	wt	1988	3801	4101	4180	2442	2511	2042	3268
14	wt	2187	3045	3243	3928	2292	2074	2046	3684
	mean	2028	3367	3453	3586	2420	2215	2139	3616
	SD	120	460	474	603	342	312	249	464
1	ArcAβ	2739	2722	2658	2573	2074	1992	1924	3340
2	ArcAβ	1908	3297	3423	1790	2709	2321	2263	3804
3	ArcAβ	2258	3666	3815	2707	2537	2591	2440	4053
4	ArcAβ	1912	2977	3153	3211	2202	2339	1982	3735
5	ArcAβ	1858	3650	3292	2414	2775	2082	1980	3688
6	ArcAβ	2040	3571	3867	3822	2537	2061	2136	3799
7	ArcAβ	2092	3369	3344	3566	2646	2000	2277	3524
	mean	2115	3322	3365	2869	2497	2198	2143	3706
	SD	307	358	410	707	263	225	192	226

Table 62: Receptor density of M_1 (fmol/mg protein) of brain regions investigated of *tgArcAβ* mice. Mean density ± standard deviation quoted

animal	Group	OB	M1	S1	Pir	CPu	CA1	MosHil	MGr
8	wt	4216	6676	7061	7350	11172	11639	6661	13129
9	wt	3830	6327	6216	6224	10499	9824	6941	13075

10	wt	3071	6228	6224	6912	9379	10257	5044	9527
11	wt	4245	8084	7623	7424	12558	15122	7929	15932
12	wt	3126	8005	7821	8869	11432	8899	4794	9168
13	wt	3497	9991	9551	8789	14731	14617	9441	17413
14	wt	5463	8104	7989	7489	12561	11494	6941	12763
	mean	3921	7631	7498	7579	11762	11693	6821	13001
	SD	828	1337	1157	957	1723	2370	1603	3025
1	ArcAβ	4304	4527	4402	5284	7546	8262	4203	8111
2	ArcAβ	4853	7043	7205	7970	12443	12679	6714	12885
3	ArcAβ	3923	5484	5135	5856	8075	7189	4409	7650
4	ArcAβ	4534	7889	7195	7282	13248	13692	7107	14026
5	ArcAβ	4221	7132	7186	6901	12010	10545	5707	11259
6	ArcAβ	3467	7387	7006	7941	11884	13596	6685	13604
7	ArcAβ	4698	8262	7556	8948	14697	14615	7002	14640
	mean	4286	6818	6526	7169	11415	11511	5975	11739
	SD	476	1338	1230	1276	2642	2895	1228	2845

Table 63: Receptor density of M_2 (fmol/mg protein) of brain regions investigated of *tgArcAβ* mice. Mean density ± standard deviation quoted

animal	**Group**	**OB**	**M1**	**S1**	**Pir**	**CPu**	**CA1**	**MosHil**	**MGr**
8	wt	2994	1179	1586	613	1689	683	655	521
9	wt	2797	1223	1569	601	1793	692	622	550
10	wt	2421	1291	1661	604	2142	714	565	527
11	wt	2760	1358	1754	684	2202	668	711	531
12	wt	2781	1197	1442	523	1389	803	720	597
13	wt	3323	1482	2072	807	2611	862	748	714
14	wt	3143	1432	1956	747	2192	706	731	629
	mean	2888	1309	1720	654	2002	733	679	581
	SD	294	119	225	98	405	72	67	71
1	ArcAβ	2927	1350	1822	599	2047	558	545	467
2	ArcAβ	3011	1334	1953	495	2196	599	580	464
3	ArcAβ	2148	1291	1774	677	1705	692	723	565
4	ArcAβ	2867	1626	2143	506	2166	696	647	527
5	ArcAβ	2877	1392	2093	425	2137	716	1030	1785
6	ArcAβ	2803	1464	2197	654	2180	663	678	482
7	ArcAβ	2889	1312	1955	643	2076	611	610	460
	mean	2789	1396	1991	571	2073	648	688	679
	SD	289	116	160	96	171	59	162	490

Table 64: Receptor density of 5-HT_{1A} (fmol/mg protein) of brain regions investigated of *tgArcAβ* mice. Mean density ± standard deviation quoted

animal	**Group**	**OB**	**M1**	**S1**	**Pir**	**CPu**	**CA1**	**MosHil**	**MGr**
8	wt	35	152	133	54	17	699	89	141
9	wt	37	173	115	45	20	656	69	159
10	wt	45	157	164	35	20	992	107	280
11	wt	47	223	156	41	20	906	114	333
12	wt	49	179	111	53	20	798	67	136
13	wt	54	162	112	52	20	873	82	133
14	wt	48	145	115	53	21	644	75	116
	mean	45	170	129	48	20	795	86	185
	SD	7	26	22	7	1	134	18	85

1	ArcAβ	34	160	114	27	16	777	119	339
2	ArcAβ	34	123	115	33	17	864	84	174
3	ArcAβ	48	134	110	50	17	1004	91	329
4	ArcAβ	49	202	143	46	19	1078	96	203
5	ArcAβ	34	148	85	68	18	1070	121	242
6	ArcAβ	46	129	92	56	20	915	94	214
7	ArcAβ	46	143	120	54	23	982	94	176
	mean	42	148	111	48	18	956	100	240
	SD	7	27	19	14	2	110	14	68

Table 65: Receptor density of 5-HT_{2A} (fmol/mg protein) of brain regions investigated of *tgArcAβ* mice. Mean density ± standard deviation quoted

animal	**Group**	**OB**	**M1**	**S1**	**Pir**	**CPu**	**CA1**	**MosHil**	**MGr**
8	wt	522	1197	979	1008	1645	843	1016	697
9	wt	563	1231	977	995	1464	832	940	672
10	wt	562	1137	1080	1029	1762	922	883	808
11	wt	560	1108	971	907	1620	839	964	663
12	wt	490	1166	1088	715	1559	863	903	659
13	wt	528	1209	1012	919	1572	781	879	619
14	wt	577	1257	1046	998	1654	778	884	654
	mean	543	1186	1022	939	1611	837	924	682
	SD	31	52	50	109	93	49	52	60
1	ArcAβ	535	1486	1171	1196	1913	827	816	1026
2	ArcAβ	530	1285	1255	1106	1936	823	1010	755
3	ArcAβ	605	1278	1093	978	1699	848	897	702
4	ArcAβ	544	1364	1120	982	1709	762	823	680
5	ArcAβ	534	1257	1078	847	1814	840	919	727
6	ArcAβ	503	1214	1161	1041	1753	720	763	630
7	ArcAβ	497	1221	1005	945	1800	617	820	544
	mean	535	1301	1126	1014	1803	777	864	723
	SD	35	96	79	114	93	84	83	151

Table 66: Receptor density of $GABA_A$ (fmol/mg protein) of brain regions investigated of *tgArcAβ* mice. Mean density ± standard deviation quoted

animal	**Group**	**OB**	**M1**	**S1**	**Pir**	**CPu**	**CA1**	**MosHil**	**MGr**
8	wt	2243	2686	3090	2781	1853	2451	2039	3453
9	wt	2061	3371	3592	3056	2077	2527	2308	3881
10	wt	2397	2958	3120	2496	1733	2791	2237	3695
11	wt	2321	3200	3236	2801	1926	2780	2465	3918
12	wt	2167	2548	2469	1966	1677	2430	2280	3493
13	wt	2473	3054	3528	3039	1817	2485	2035	3497
14	wt	2110	2565	3133	2845	1552	2577	2349	3829
	mean	2253	2912	3167	2712	1805	2577	2245	3681
	SD	152	321	368	378	172	150	159	200
1	ArcAβ	2345	3029	3375	2804	1568	2903	2142	3668
2	ArcAβ	1522	2452	2821	2592	1436	2348	1836	2986
3	ArcAβ	1390	3021	3222	2437	1680	2244	1804	3063
4	ArcAβ	2152	2584	2825	1310	1604	2585	1905	3047
5	ArcAβ	1591	2688	3167	2705	1570	2817	2011	3808
6	ArcAβ	2124	3016	3917	2943	1707	2567	2046	3512
7	ArcAβ	1576	2950	2911	2151	1615	2827	2146	3693
	mean	1814	2820	3177	2421	1597	2613	1984	3397

	SD	379	241	389	553	88	252	139	353

Table 67: Receptor density of BZ (fmol/mg protein) of brain regions investigated of *tgArcAβ* mice. Mean density ± standard deviation quoted

animal	Group	OB	M1	S1	Pir	CPu	CA1	MosHil	MGr
8	wt	52273	36803	29886	38031	12678	22184	21989	52108
9	wt	39400	31950	23788	22116	12740	31972	22028	17142
10	wt	42739	41810	43349	14782	13850	26982	17674	17112
11	wt	48008	28962	31976	22203	10120	46791	26811	53050
12	wt	44200	43008	42117	35644	13331	24282	25799	45085
13	wt	48937	41214	31331	41264	13365	36553	24435	44478
14	wt	37919	36268	37142	27192	14604	39658	21509	45017
	mean	52273	36803	29886	38031	12678	22184	22892	39142
	SD	39400	31950	23788	22116	12740	31972	3079	15434
1	ArcAβ	44503	12365	25576	37100	12623	33657	15736	18422
2	ArcAβ	46523	31790	36627	19437	11170	42951	18699	44351
3	ArcAβ	32257	26638	39027	32689	12712	42413	23364	37652
4	ArcAβ	46652	36216	31160	31685	11413	30278	19754	43456
5	ArcAβ	41745	36960	37813	33435	7967	39748	21456	44794
6	ArcAβ	48090	38399	43030	36766	12006	37631	20443	43704
7	ArcAβ	35952	34883	41989	38035	5857	39321	12975	46318
	mean	42246	31036	36460	32735	10535	38000	18918	39814
	SD	6008	9124	6174	6348	2612	4608	3529	9818

Table 68: Receptor density of $GABA_B$ (fmol/mg protein) of brain regions investigated of *tgArcAβ* mice. Mean density ± standard deviation quoted

animal	Group	OB	M1	S1	Pir	CPu	CA1	MosHil	MGr
8	wt	2731	5158	4973	5412	2625	5202	4515	6517
9	wt	3027	6933	5866	5596	2997	6030	4714	7969
10	wt	3153	6422	6010	4902	2623	7195	5645	8425
11	wt	2808	6127	5871	6770	3087	5914	4831	7708
12	wt	3348	6392	6397	6239	3369	7322	5583	8659
13	wt	3000	6143	5911	6004	2943	5545	4847	6833
14	wt	3452	8042	7120	6031	3397	7766	6255	10690
	mean	3074	6460	6021	5851	3006	6425	5199	8115
	SD	265	879	646	607	313	990	636	1379
1	ArcAβ	2993	4872	4764	5358	2445	6051	4919	7735
2	ArcAβ	2902	6485	5709	5237	3077	5822	4721	7234
3	ArcAβ	2736	5841	5564	5463	2563	6995	5875	8976
4	ArcAβ	3411	5385	5642	6047	2794	6191	5726	7590
5	ArcAβ	2892	5996	5157	4930	2745	6100	4315	7771
6	ArcAβ	3250	6858	6100	6943	2948	6056	5191	7984
7	ArcAβ	2775	5480	5736	7080	2867	5206	4379	6837
	mean	2994	5845	5525	5865	2777	6060	5018	7732
	SD	249	677	436	852	218	529	615	669

Table 69: Receptor density of α_1 (fmol/mg protein) of brain regions investigated of *tgArcAβ* mice. Mean density ± standard deviation quoted

animal	Group	OB	M1	S1	Pir	CPu	CA1	MosHil	MGr
8	wt	546	540	401	458	154	198	169	235
9	wt	519	494	370	405	154	197	162	232
10	wt	488	422	330	356	151	188	167	227
11	wt	526	527	386	370	163	201	177	244
12	wt	517	533	367	369	152	202	190	243
13	wt	550	539	387	416	156	188	174	240
14	wt	554	597	397	375	156	203	179	250
	mean	528	522	377	393	155	197	174	239
	SD	23	54	24	36	4	6	9	8
1	ArcAβ	555	518	392	398	166	203	180	249
2	ArcAβ	509	542	393	368	169	205	180	244
3	ArcAβ	326	600	397	410	176	178	171	217
4	ArcAβ	514	540	409	423	184	211	202	281
5	ArcAβ	388	519	398	385	195	192	171	247
6	ArcAβ	537	617	417	391	180	212	200	262
7	ArcAβ	431	484	367	389	164	184	165	230
	mean	466	546	396	395	176	198	181	247
	SD	86	47	16	18	11	13	14	21

Table 70: Receptor density of α_2 (fmol/mg protein) of brain regions investigated of *tgArcAβ* mice. Mean density ± standard deviation quoted

animal	Group	OB	M1	S1	Pir	CPu	CA1	MosHil	MGr
8	wt	338	417	334	555	188	251	211	500
9	wt	346	297	261	422	175	207	148	408
10	wt	323	265	209	380	173	234	217	427
11	wt	303	327	267	465	177	233	328	397
12	wt	316	470	363	489	207	239	219	451
13	wt	324	334	289	433	206	237	224	483
14	wt	313	315	278	515	211	224	211	429
	mean	323	346	286	465	191	232	223	442
	SD	15	72	50	59	17	14	53	38
1	ArcAβ	379	304	243	567	155	219	177	491
2	ArcAβ	286	344	309	559	198	284	233	514
3	ArcAβ	423	309	246	572	174	193	178	448
4	ArcAβ	396	344	296	566	201	275	263	502
5	ArcAβ	379	413	342	661	209	217	217	535
6	ArcAβ	335	380	329	783	210	262	267	565
7	ArcAβ	420	370	363	603	241	255	218	518
	mean	374	352	304	616	198	244	222	510
	SD	49	39	46	82	28	34	36	36

Table 71: Receptor density of D_1 (fmol/mg protein) of brain regions investigated of *tgArcAβ* mice. Mean density ± standard deviation quoted

animal	Group	OB	M1	S1	Pir	CPu	CA1	MosHil	MGr
8	wt					5204			
9	wt					6139			
10	wt					6323			
11	wt					6487			
12	wt					5626			
13	wt					5775			
14	wt					5054			
	mean					5801			
	SD					548			
1	ArcAβ					4118			
2	ArcAβ					4927			
3	ArcAβ					4601			
4	ArcAβ					4646			
5	ArcAβ					5584			
6	ArcAβ					5499			
7	ArcAβ					4946			
	mean					4903			
	SD					516			

Table 72: Receptor density of D_2 (fmol/mg protein) of brain regions investigated of *tgArcAβ* mice. Mean density ± standard deviation quoted

animal	Group	OB	M1	S1	Pir	CPu	CA1	MosHil	MGr
8	wt					941			
9	wt					924			
10	wt					947			
11	wt					996			
12	wt					979			
13	wt					1004			
14	wt					1062			
	mean					979			
	SD					47			
1	ArcAβ					1013			
2	ArcAβ					932			
3	ArcAβ					973			
4	ArcAβ					1011			
5	ArcAβ					1010			
6	ArcAβ					1025			
7	ArcAβ					1052			
	mean					1002			
	SD					39			

Table 73: Receptor density of $D_{2/3}$ (fmol/mg protein) of brain regions investigated of *tgArcAβ* mice. Mean density ± standard deviation quoted

animal	Group	OB	M1	S1	Pir	CPu	CA1	MosHil	MGr
8	wt					3968			
9	wt					4174			
10	wt					4097			
11	wt					3933			
12	wt					3533			
13	wt					3916			
14	wt					4139			
	mean					3966			
	SD					217			
1	ArcAβ					4567			
2	ArcAβ					4049			
3	ArcAβ					4092			
4	ArcAβ					4673			
5	ArcAβ					4184			
6	ArcAβ					4562			
7	ArcAβ					4508			
	mean					4377			
	SD					259			

Table 74: Receptor density of A_2 (fmol/mg protein) of brain regions investigated of *tgArcAβ* mice. Mean density ± standard deviation quoted

animal	Group	OB	M1	S1	Pir	CPu	CA1	MosHil	MGr
8	wt					4309			
9	wt					4909			
10	wt					5880			
11	wt					5006			
12	wt					4063			
13	wt					5409			
14	wt					4637			
	mean					4888			
	SD					626			
1	ArcAβ					4001			
2	ArcAβ					4407			
3	ArcAβ					4683			
4	ArcAβ					4507			
5	ArcAβ					4206			
6	ArcAβ					4596			
7	ArcAβ					5225			
	mean					4518			
	SD					390			

Danksagung

Ich danke Prof. Dr. Zilles für die Möglichkeit, meine Arbeit an seinem Institut anzufertigen und die Bereitschaft, mich bei dieser Arbeit als Doktorvater zu unterstützen; des Weiteren für die hervorragende wissenschaftliche Betreuung und den vielfältigen konstruktiven Austausch. Auch möchte ich mich für die Freiheiten bedanken, die ich bei der Umsetzung der Arbeit hatte**.** Ebenfalls bedanken möchte ich mich bei Frau Prof. Dr. Amunts für die Möglichkeit, die Arbeit an Ihrem Institut fortzuführen und für vielfältige fachliche Anregungen.
Prof. Dr. von der Emde danke ich für Betreuung von Seiten der Universität Bonn, für die Übernahme des Zweitgutachtens, für Anregungen und für das Interesse, dass er meiner Arbeit entgegengebracht hat.

Herrn Dr. Schleicher und Frau Dr. Palomero-Gallagher danke ich für die Hilfe bei der statistischen Auswertung.

In so vielen kleinen und großen Dingen liegt der Erfolg einer Arbeit. Für eine tolle Arbeitsatmosphäre, großartige Hilfsbereitschaft, für die vielen Tipps, die den Umgang mit manchmal störrischen Geräten erleichtert haben und für viel Kuchen möchte ich mich besonders bei Markus Cremer, Jennifer Cremer, Sabrina Buller, Jessica Teske-Bausch, Christian Schramm, Sabine Wilms und Andrea Radermacher bedanken.

Frau Dr. Hack und Frau Dr. Willuweit danke ich für die Korrekturen und die Unterstützung bei den immunhistochemischen Versuchen. Zudem danke ich Frau Dr. Hack für die kreativen Versuche, für die „Speerspitze der deutschen Neuroforschung“, und Max Anstötz für den immerwährenden Kampf gegen das Mikroskop.

Ich danke meiner Familie und meinen Freunden, insbesondere meiner Schwester und meinem Schwager, für die nie nachlassende Unterstützung.
Bei Thomas Schmitges bedanke ich mich für die unerschütterliche Zuversicht, für die Geduld, für die Vergangenheit und die Zukunft.